Universidade de Aveiro Departamento de Química
2010

Cláudia Pereira Passos

Extracção supercrítica de óleo de grainha de uva combinada com pré-tratamentos enzimáticos

Universidade de Aveiro Departamento de Química
2010

Cláudia Pereira Passos

Extracção supercrítica de óleo de grainha de uva combinada com pré-tratamentos enzimáticos

dissertação apresentada à Universidade de Aveiro para cumprimento dos requisitos necessários à obtenção do grau de Doutor, realizada sob a orientação científica do Doutor Carlos Manuel Santos da Silva, Professor Auxiliar do Departamento de Química da Universidade de Aveiro.

Apoio financeiro da FCT e do FSE no âmbito do III Quadro Comunitário de Apoio.

Dedicatória

Dedico este trabalho aos meus pais por uma vida de incansável apoio.

o júri

Presidente

Professor José Joaquim de Almeida Grácio
Professor Catedrático da Universidade de Aveiro

Vogais

Professor José Joaquim Costa Cruz Pinto
Professor Catedrático da Universidade de Aveiro

Profª. Doutora Maria Gabriela Bernardo Gil
Professora Associada com Agregação do Instituto Técnico da Universidade Técnica de Lisboa

Prof. Doutor Manuel António Coimbra Rodrigues da Silva
Professor Associado com Agregação da Universidade de Aveiro

Prof. Doutor Francisco Miguel Portela da Gama
Professor Associado da Escola de Engenharia da Universidade do Minho

Prof. Doutor Carlos Manuel Santos da Silva
Professor Auxiliar da Universidade de Aveiro (Orientador)

agradecimentos

Ao meu orientador, Prof. Doutor Carlos Manuel Silva, e ao Prof. Doutor Manuel António Coimbra e Prof. Doutor Francisco Avelino da Silva, não só os conhecimentos transmitidos, mas também o apoio incondicional, o incentivo, o optimismo e acima de tudo a amizade. Para eles o meu profundo respeito e admiração.

Aos meus colaboradores, Prof[a]. Doutora Rosário Domingues, Doutora Susana Cardoso, e ao Doutor António Barros pela sua prestimosa colaboração.

À Estação Vitivinícola da Bairrada e Caves Messias, que gentilmente cederam as amostras de grainha necessárias para a concretização deste trabalho, e em particular ao Eng. António Dias Cardoso e Eng. José Carvalheira pela sempre pronta colaboração e simpatia.

Ao Departamento de Química da Universidade de Aveiro pelas condições para a realização deste trabalho, e a todos com os quais privei ao longo dos anos, professores e funcionários, pela ajuda e amizade.

Aos colegas e amigos dos laboratórios de Engenharia Química e de Bioquímica, pelo bom ambiente de trabalho e os bons momentos passados em conjunto com boa disposição e alegria. Agradeço também o apoio que sempre me demonstraram e a troca de ideias que muito contribuíram para a realização deste trabalho.

Um agradecimento sentido à Dra. Dulce Helena Teixeira pela pronta ajuda.

Ao colega Rui Silva pela preciosa rapidez e talento na montagem do Equipamento Supercrítico.

Um agradecimento especial às minhas colegas e amigas Alisa Rudnitskaya, Juliana Vinholes e Patrícia Lito pelo apoio e paciência com que me escutaram durante este ciclo.

Não esquecendo ainda as minhas colegas de casa Enoí Dagô e Cristina Maia pela força e carinho que sempre me deram durante os períodos mais difíceis.

Finalmente, um agradecimento muito especial aos meus pais e irmão a quem devo tudo aquilo que sou, por sempre me apoiarem e incentivarem a melhorar.

À FCT, pelo financiamento através de uma bolsa de doutoramento SFRH/BD/19072/2004.

palavras-chave

Extracção Supercrítica, grainha de uva, óleo, pré-tratamento enzimático, curva de extracção, espectroscopia, procianidinas, grau médio de polimerização, triacilglicerídeos, capacidade antioxidante, transferência de massa.

resumo

Neste trabalho estudou-se a extracção supercrítica do óleo de grainha de uva, usando dióxido de carbono, e combinou-se este processo com um pré-tratamento enzimático da semente para aumentar o rendimento global da extracção. A qualidade dos extractos obtidos foi avaliada pelo seu conteúdo em triacilglicerídeos, perfil de ácidos gordos e capacidade antioxidante. Realizaram-se também alguns estudos exploratórios sobre a aplicação de um pré-tratamento de alta pressão (HPP) à grainha da uva. Adicionalmente, efectuou-se o estudo da extracção, fraccionamento e caracterização estrutural das procianidinas da grainha da uva, bem como a avaliação da sua capacidade antioxidante.

A extracção de procianidinas da grainha da uva foi efectuada sequencialmente com metanol e acetona/água, tendo sido posteriormente fraccionadas por adição sucessiva de misturas metanol/clorofórmio progressivamente mais concentradas em clorofórmio. A caracterização das procianidinas foi feita por HPLC-UV e LC–MS, antes e depois de sujeitar as amostras a uma tiólise, e também por ESI-MS e ESI-MS/MS. Este estudo permitiu reportar, pela primeira vez, a ocorrência de procianidinas do tipo-A galoiladas na grainha da uva. Os resultados de HPLC-UV permitiram determinar o grau médio de polimerização das procianidinas e a sua composição monomérica em (+)-catequina, (-)-epicatequina e (-)-epicatequina-O-galato. Mostrou-se que a (+)-catequina é o flavan-3-ol terminal mais abundante e a (-)-epicatequina predomina largamente como unidade de extensão. No caso de procianidinas do tipo A, a ligação interflavânica C2-C7 encontra-se essencialmente nas unidades terminais. O grau médio de polimerização das diversas fracções varia entre 1.0 e 10.8. A sua capacidade antioxidante, medida pelo método espectrofotométrico de DPPH•, mostrou-se ser equivalente à de uma amostra comercial de (+)-catequina usada como referência. A partir dos graus médios de polimerização experimentais e das análises de FTIR das fracções correspondentes foi possível obter um modelo preditivo O-PLS com apenas uma variável latente.

O pré-tratamento enzimático justificou-se pelo conhecimento existente acerca do uso de enzimas específicas que destroem parcialmente as paredes celulares. Atendendo à composição das paredes celulares da grainha da uva preparou-se uma suspensão contendo protease, xilanase, pectinase e celulase. Para determinar as condições experimentais do pré-tratamento que maximizam o rendimento da extracção, estudou-se o efeito do tempo de reacção, temperatura, pH, diâmetro médio das partículas de grainha moída e a concentração das enzimas. Os incrementos do rendimento da extracção de óleo observados atingiram 163.2%.

O estudo da extracção supercrítica (SFE) do óleo da grainha de uva tratada e não-tratada permitiu obter as curvas de extracção correspondentes, bem com analisar a influência das condições operatórias sobre o seu andamento. Montou-se uma instalação laboratorial onde se realizaram experiências com dióxido de carbono a 160, 180, 200 e 220 bar e temperaturas de 313.15 e 323.15 K. Os rendimentos obtidos por SFE foram semelhantes aos de Soxhlet com *n*-hexano. As curvas de extracção medidas compreendem um primeiro período de extracção, onde se remove cerca de 92-97% do óleo disponível, e um segundo período, essencialmente difusional, com pouco impacto no rendimento final.

Os vários extractos recolhidos e o óleo global obtido foram caracterizados para avaliar a sua qualidade e relacioná-la com as condições operatórias de SFE. Determinaram-se o conteúdo total em triacilglicerídeos, o seu perfil de ácidos gordos e a capacidade antioxidante (AOC). Os resultados mostraram que a AOC aumenta com a elevação da pressão e, acentuadamente, com o acréscimo da temperatura. Ao longo da curva de extracção, a AOC é mais pronunciada nos extractos iniciais, nomeadamente nos primeiros 30 a 40% da extracção.

A modelação efectuada considerou que o óleo extractável se reparte entre células rompidas, predominantes na periferia da semente, e células intactas, mais interiores. Admitiu-se que o transporte de massa ocorre em série, i.e. das células intactas para as rompidas e destas para o solvente; mostrou-se que a dispersão axial era desprezável. Os balanços materiais à fase fluida e aos volumes de células rompidas e intactas, combinados com os fluxos interno, externo e a relação de equilíbrio foram resolvidos numericamente pelo método das linhas combinado com diferenças finitas atrasadas. O modelo reproduziu bem as curvas experimentais e permitiu simular curvas de eluição e os três perfis de concentração no leito.

Keywords

Supercritical fluid extraction, grape seed, oil, enzymatic pre-treatment, extraction curve, spectroscopy, procyanidins, average degree of polymerization, triacylglycerides, antioxidant capacity, mass transfer.

Abstract

The supercritical extraction of grape seed oil with carbon dioxide has been studied and combined with an enzymatic pre-treatment of the seed to enhance the global extraction yield. The quality of the attained extracts has been assessed by evaluating the content in triacylglycerides, fatty acids profile, and antioxidant capacity. An exploratory study with the application of a high pressure pre-treatment (HPP) to the seed has also been considered. Additionally, the extraction, fractionation, and structural characterization of grape seed procyanidins, as well as the evaluation of their antioxidant capacity, has been carried out.

The procyanidins were sequentially extracted with methanol and acetone/water from defatted seed, and further fractionated by precipitation in graded methanol/chloroform solutions. The procyanidins analysis included HPLC-UV and LC–MS, before and after thiolysis, as well ESI-MS e ESI-MS/MS. Such study allowed to report, for the first time, the occurrence of type-A galloylated procyanidins. The average degree of polymerization and the monomeric composition in (+)-catechin, (-)-epicatechin and (-)-epicatechin-O-gallate, were obtained using HPLC-UV. The results, showed (+)-catechin as the most abundant flavan-3-ol terminal unit, and the high predominance of (-)-epicatechin as the extension unit. In type-A procyanidins the C2-C7 interflavanic linkage appears essentially in the terminal units. The collected fractions presented an average degree of polymerization range from 1.0 to 10.8. Their antioxidant capacity, assessed by the DPPH• spectrophotometric method, presented a similar response to a commercial standard of (+)-catechin. A predictive O-PLS method, with one latent variable, was obtained using the experimental average degree of polymerization determined and combined with FTIR analyses.

The enzymatic pre-treatment approach was based on the knowledge that partial hydrolysis of the cell walls can occur by means of appropriate enzymes. With the given composition of grape seed walls four types of enzymes were considered, namely protease, xylanase, pectinase, and cellulase as the enzymatic cocktail.

The effect of reaction time, temperature, pH, grape seed average particle sizes and enzymes concentration were considered in the search for extraction yield improving conditions. The increments in the extraction yield attained 163.2%.

The supercritical fluid extraction (SFE) curves of grape seed oil for both treated and untreated seed were obtained and characterized on the influence of the operatory conditions on them. The supercritical extraction experiments were performed with carbon dioxide at 160, 180, 200, and 220 bar and 313.15 and 323.15 K in a semi-continuous apparatus built and assess at the University of Aveiro. The yields obtained by SFE were similar to those of Soxhlet using *n*-hexane. The extraction curves present a first period of extraction, where about 92-97% of the available oil is removed, and a second diffusional period, with no significant impact in the final yield.

The quality of the individual SFE extracts and global oil was evaluated and related to the SFE operating conditions. The total triacylglycerides content, fatty acids profile, and antioxidant capacity (AOC) of the extracts were measured. Results showed the AOC increases with increasing pressure and noticeably with rising temperature. Along extraction curves, the AOC is more pronounced on the oil collected during the first stages of the process, where 30-40% of the total oil is extracted.

The modelling assumed the hypothesis of the existence of broken (peripherical) and intact cell (core) fractions in the seed. A series mass transport was assumed, i.e., from intact cells to broken cells, and from those to the solvent; axial dispersion was shown to be neglectable. The resulting mass balances to the fluid phase, broken, and intact cells, combined with internal fluxes, and the equilibrium relationship were numerically solve by applying the method of lines combined with backward finite differences. The experimental extraction curves were well reproduced by the model which allowed the simulation of the elution curves and the three concentration profiles in the bed.

EXTRACÇÃO SUPERCRÍTICA DE ÓLEO DE GRAINHA DE UVA COMBINADA COM PRÉ-TRATAMENTOS ENZIMÁTICOS

TABLE OF CONTENTS

List of Tables

List of Figures

List of Schemes

Abbreviations

AOC	Antioxidant capacity;
DB-FFAP	Column with a stationary phase of nitroterephthalic acid modified polyethylene glycol
DPPH	Free radical α,α-diphenyl-β-picrylhydrazyl;
DTGS	Deuterated triglycine sulfate;
E	Extract;
ESI	Electrospray ionization;
FPR	Forward pressure regulator;
FTIR	Fourier transform infrared spectroscopy;
GC	Gas chromatography;
HPLC or LC	High performance liquid chromatography;
HPP	High Pressure Pre-treatment;
HRF	Heterocyclic-ring-fission fragmentation;
L	Linoleic acid;
LV	Latent variable;
M	Manometer;
MFM	Mass flow meter;
MS	Mass spectrometry;
MS/MS	Tandem mass spectrometry;
O	Oleic acid;
O-PLS	Orthogonal projections to latent structures;
P	Palmitic acid;
PCE	Procyanidin crude extract;
PCT	Principal component transform;
PLS	Partial least squares;
P_nG_m	Polymer with a total of n monomeric units of which *m* are epicatechin-*O*-gallate;
PUFA	Polyunsaturated fatty acids;
QM	Quinone-methide fragmentation;
RA	Red grape seeds extracted with acetone/water;
RDA	Retro-Diels-Alder fragmentation;
RM	Red grape seeds extracted with methanol;
RMSECV	Root mean square error of cross validation;
RMSEP	Root mean square error of prediction;
SC-CO_2	Supercritical carbon dioxide;
SCF	Supercritical fluid;
SFE	Supercritical fluid extraction;
SN	Supernatant after chloroform/methanol precipitations;
SNV	Standard normal variate;
SCP	Sequential methanol/chloroform precipitations;
SPE	Solid phase extraction;
TAG	Triacylglyceride;
V	Valve;
WA	White grape seeds extracted with acetone/water;
WM	White grape seeds extracted with methanol.

Nomenclature

a_0	$m^2 \cdot m^{-3}$	(Surface area per unit volume of extraction bed);
a_s	$m^2 \cdot m^{-3}$	(Surface area between the regions of intact and broken cells);
A	m^2	(Cross sectional area);
A_{sample}	-	(Absorbance after 30 min of reaction between "sample" and DPPH radical);
A_0	-	(Initial absorbance);
AAD	%	(Absolute average deviation);
C_1	-	(Internal parameter to the model);
C_2	-	(Internal parameter to the model);
co	$kg_{solute} \cdot kg_{seed}^{-1}$	(Solute content in the untreated solid);
d_E	m	(Extractor diameter);
d_p	m	(Average particle size);
d_{p_i}	m	(Average particle size for particles retain in sieve *i*);
D_{ax}	$m^2 s^{-1}$	(Axial dispersion);
DPn	-	(Average Degree of Polymerization);
D_{12}	$m^2 s^{-1}$	(Binary diffusion coefficient);
E	kg_{solute}	(Amount of extracted oil);
H	$\%,\ kg \cdot kg^{-1}$	(Water content);
IC_{50}	$g_{solute}\ L^{-1}_{solution}$	(Concentration of a compound required for 50% reduction of DPPH initial free radical concentration);
j_f	$kg_{solute} \cdot m^{-3}_{solid} s^{-1}$	(Mass transfer rate to the fluid phase);
J_f	-	(Dimensionless mass transfer rate to the fluid phase);
j_s	$kg_{solute} \cdot m^{-3}_{solid} s^{-1}$	(Mass transfer rate between the intact core cells and broken cells);
J_s	-	(Dimensionless mass transfer rate between the intact core cells and broken cells);
k_f	$m \cdot s^{-1}$	(Fluid-phase mass transfer coefficient);
$k_f a_0$	s^{-1}	(Fluid-phase mass transfer group);
k_s	$m \cdot s^{-1}$	(Solid-phase mass transfer coefficient);
$k_s a_s$	s^{-1}	(Solid-phase mass transfer group);
K	-	(Partition coefficient);
l	m	(Axial coordinate);
L	m	(Extraction bed length);
$\dot{m}$	$kg_{CO_2} \cdot s^{-1}$	(Solvent mass flow rate);
m_{co_2}	kg	(Amount of the passed solvent);
m_{seed}	kg	(Solid charge in the extractor, dried basis);
n	-	(Number of mixers in series assumed, grid number)
$N_{Pe,L}$	-	(Peclet number);
$N_{Pe,d}$	-	(Peclet number based on the particle diameter);
N_{Re}	-	(Reynolds number);
N_{Sc}	-	(Schmidt number);

N_{Sh}	-	(Sherwood number);
p	$kg^{-1} \cdot s^{-0.46}$	(Internal parameter to the model);
P	bar	(Pressure);
r	-	(Grinding efficiency, volumetric fraction of broken cells);
R^2	-	(Statistical variance);
$R^2\ \boldsymbol{X}$	%	(**X** variance);
$R^2\ \mathbf{y}$	%	(**y** variance);
t	s	(Time);
t_r	s	(Solvent residence time);
T	K	(Temperature);
u	$m \cdot s^{-1}$	(Interstitial fluid velocity);
U	$m \cdot s^{-1}$	(Superficial velocity);
V_{broken}	m^3	(Volumetric fraction of broken cells);
V_{intact}	m^3	(Volumetric fraction of close cells);
x	$kg_{solute} \cdot kg^{-1}_{insoluble\ solid}$	(Solute concentration in the solid);
x_t	$kg_{solute} \cdot kg^{-1}_{insoluble\ solid}$	(Transition concentration);
x_u	$kg_{solute} \cdot kg^{-1}_{insoluble\ solid}$	(Solute concentration in the untreated solid);
x_1	$kg_{solute} \cdot kg^{-1}_{insoluble\ solid}$	(Solute concentration in broken cells);
$x_{1,0}$	$kg_{solute} \cdot kg^{-1}_{insoluble\ solid}$	(Initial solute concentration in broken cells);
x_2	$kg_{solute} \cdot kg^{-1}_{insoluble\ solid}$	(Solute concentration in intact core cells);
$x_{2,0}$	$kg_{solute} \cdot kg^{-1}_{insoluble\ solid}$	(Initial concentration in intact core cells);
$\mathbf{X}$	-	(Independent variables data matrix, FTIR spectra for all the samples used);
X_{DPPH}	%	(Conversion of $DPPH \cdot$);
X_t	-	(Dimensionless, transition concentration);
X_1	-	(Dimensionless concentration in broken cells);
X_2	-	(Dimensionless concentration in core cells);
y	$kg_{solute} \cdot kg^{-1}_{CO_2}$	(Fluid phase concentration);
$\mathbf{y}$	-	(Dependent responses data vector, *DPn* determined by the reference method – HPLC);
y_{feed}	$kg_{solute} \cdot kg^{-1}_{CO_2}$	(Fluid phase concentration at the entrance of the extraction column);
y_s	$kg_{solute} \cdot kg^{-1}_{CO_2}$	(Solubility);
y_0	$kg_{solute} \cdot kg^{-1}_{CO_2}$	(Initial fluid phase concentration);
y^*	$kg_{solute} \cdot kg^{-1}_{CO_2}$	(Equilibrium fluid phase concentration);
Y	-	(Dimensionless, fluid phase concentration);
$\mathbf{Y}$	-	(Dependent responses data matrix);
Y^*	-	(Dimensionless, apparent solubility);
z	-	(Dimensionless, axial coordinate).

Greek letters

δ_{MTZ}	-	(Width of mass transfer zones);
ε	-	(Bed void fraction);
$(1-\varepsilon)$	-	(Biomass fraction);
ϕ	-	(Dimensionless extraction yield);
ϕ_c	-	(Dimensionless extraction yield at the transition point between the 1st and 2nd periods of extraction);
Γ	-	(Initial solid distribution between solvent and broken cells);
γ	-	(Solvent-to-matrix masses ratio in the bed);
η	$kg_{solute} \cdot kg_{seed}^{-1}$	(Dimensionless yield);
Θ_e	-	(Dimensionless external mass transfer resistance);
Θ_i	-	(Dimensionless internal mass transfer resistance);
ρ_f	$kg_{CO_2} \cdot m^{-3}$	(Solvent (SC-CO_2) density);
ρ_s	$kg_{\text{insoluble solid}} \cdot m^{-3}_{\text{solid phase}}$	(Solid density);
σ	-	(Statistical standard deviation);
τ	-	(Dimensionless time).
τ_c	-	(Dimensionless time at the transition point between the 1st and 2nd period of extraction);

0. Overview

Choose a job you love, and you will never have to work a day in your life.
[Confucius]

0. Overview

Grapes, the berries of *Vitis vinifera* L., are of worldwide interest for wine production, consumption, and also to produce extracts from their peel and seeds, which exhibits nutritional value. Grapes are approximately 25% (w/w) dry pomace, of which about 20-26% (w/w) is seed (Rice, 1976; Gómez *et al*., 1996). The seed contains typically between 7-20% (w/w) of oil (Gomez *et al.*, 1996; Passos *et al*., 2009b), and 10-20% (w/w) of polyphenolic compounds in dry basis (Bail *et al*. 2008; Passos *et al*., 2009a).

The annual availability of grape seeds was about 3 million tons in the 2004/2005 world campaign, and about 1.7 million tons just for Europe (IVV, 2008). Hence it is an appealing raw material due to its large availability as major wine industry by-product. Therefore, residues from the winemaking process, which have been traditionally presented as an economic and environmental problem as waste products, are becoming increasingly recognized as valuable commodities for the production of added value products.

Grape seeds are considered a rich source of phenolic compounds, which are notorious for their antioxidant properties, and considered as alternatives to synthetic antioxidants in the food, pharmaceutical, and cosmetic industries, aiming to the prevention of off-flavours and other objectionable compounds formation from lipids oxidation (Ho, 1992; Antolovich *et al.*, 2000). The range of compounds assumed as phenolics is however vast, as its classification embraces a considerable range of substances. It has been perceived that their degree of polymerization is an incontestable contributing factor for antioxidant capacity. In Chapter 1, an extensive study of the extraction, fractionation, and structural characterization of grape seed procyanidins is presented (Passos *et al.*, 2007), as well as their antioxidant capacity assessment.

In terms of applications, grape seed oil is becoming increasingly popular for culinary, pharmaceutical, cosmetics and medical purposes (Rozzi and Singh, 2002). The high level of polyunsaturated fatty acids is known for providing a beneficial lowering incidence of atherosclerosis and coronary heart diseases (Peschel *et al.*, 2006). Furthermore, an unusual high smoke point (about 463-503K) when compared to others such as olive oil (433-499K) and sunflower (380-505K) makes it suitable for cooking (Morin, 1996).

Most commercial extraction processes are concluded when just 90% of the oil has been removed. Beyond that limit, increased operating costs are not compensated by the corresponding extraction yield increment (e.g., del Valle and Galan, 2005). At this stage, other options such as the association of pre-treatments have become an advisable alternative. The most commonly used pre-

treatment is the mechanical one, however, a minimum particle size limit must not be passed over to avoid solvent channelling, high pressure drop, and lost of volatile compounds during the intensive grinding (Catchpole *et al.,* 1996b; Rozzi *et al.*, 2002, Rozzi and Singh 2002; Kaiser *et al.*, 2004; Reverchon and De Marco, 2006; Gomes *et al.*, 2007). In Chapter 2 the inclusion of two different seed pre-treatments, namely enzymatic and high pressure processing, is studied in order to partly destroy the seed internal structure and increase the ratio of broken-to-intact cells, to facilitate solvent penetration and diffusivity. The influence of the operating conditions upon extraction yield is evaluated.

The industrial processes commonly adopted for oil production include the extraction with organic solvents, giving rise to dark coloured and viscous extracts contaminated with solvent residues, which requires further refining and dictates the future commercial viability of the oil (Hanmoungjai *et al.,* 2000; Gomes *et al.*, 2007). Supercritical fluid technology is a rapidly growing alternative to conventional solvents, as it proceeds at reduced temperature in absence of light and oxygen, therefore reducing thermal degradation, decomposition of labile compounds, as well as other undesirable reactions such as hydrolysis and oxidation. Such conditions ensure as well the conservation of seed natural phytochemicals, such as antioxidants, ensuring oil quality preservation (Sanders, 1993; Bartley and Foley, 1994; Basile *et al.*, 1998; Palma *et al.*, 1999; Diaz-Reinoso *et al.*, 2006; Kornsteiner *et al.*, 2006; Rezaei *et al.*, 2007). In Chapter 3 the supercritical fluid extraction of grape seed oil is carried out, using not only untreated seed but also enzymatically (Passos *et al.*, 2009c) and high pressure pre-treated seed. Once more, the influence of the operating conditions is discussed.

The quality of the supercritical fluid extracted oil is assessed in Chapter 4 in terms of total triacylglycerides content, fatty acids profile, and antioxidant capacity expressed in tocopherol equivalents (Passos *et al.*, 2010). The relationship between these previous parameters and the supercritical operating conditions and seed pre-treatments has been investigated.

Modelling of the experimental data obtained in this work has been accomplished, and is reported in Chapter 5. Extraction and elution curves, and the oil concentration profiles in the bed, and in the seed have been correlated and/or predicted.

1. Phenolic Compounds

Pleasure in the job puts perfection in the work.
[Aristotle]

1. Phenolic Compounds

This chapter deals with extraction, separation and analysis of grape seed phenolics. Analysis and identification of phenolic compounds was carried out using high resolution techniques such as: High Performance Liquid Chromatography acoplated with UV-Vis detector (HPLC-UV) and/or acoplated with a Mass Spectrometry detector (LC-MS), Electrospray Ionization acoplated with a Mass Spectrometry detector (ESI-MS) and acoplated with a Tandem Mass Spectrometry detector (ESI-MS/MS) and Fourier Transform InfraRed spectroscopy (FTIR) associated with chemometric methods of analyses. The antioxidant capacity or activity (AOC) of these compounds was determined together with their average degree of polymerization that gives an insight to the structure-activity relationship for these compounds. A small discussion on the impact of storage on the antioxidant properties of these compounds is also presented.

1.1. Introduction

1.1.1. Phenolics – Definition and characterization

Phenolic compounds embrace a considerable range of substances possessing an aromatic ring bearing one or more hydroxyl substitutions (Ryan and Robards, 1998). They may be found as secondary metabolites of all plants (Macheix *et al.*, 1990). A convenient classification of the plant phenols distinguishes the number of constitutive carbon atoms in conjugation with the structure of the basic phenolic skeleton as shown in **Table 1.1** and illustrated in **Figure 1.1**. The range of known phenolics is thus vast, including polymeric lignins and condensed tannins (Antolovich *et al.*, 2000).

Table 1.1 – Classification of phenolic compounds (Antolovich *et al.*, 2000).

Basic skeleton	Class
C_6	Simple phenols, Benzoquinones
$C_6 - C_1$	Benzoic acids (**Figure 1.1b**)
$C_6 - C_2$	Phenylacetic acids
$C_6 - C_3$	Cinnamic acids (**Figure 1.1c**), Phenylpropenes, Coumarins, Chromones
$C_6 - C_4$	Naphthoquinones
$C_6 - C_1 - C_6$	Xanthones
$C_6 - C_2 - C_6$	Stilbenes, Anthraquinones
$C_6 - C_3 - C_6$	Flavonoids (**Figure 1.1a**), Flavones, Flavonols, Flavonol glycosides, Flavanonols, Flavanones, Flavanone, Glycosides, Anthocyanins, **Flavanols** (catechins), Chalcones
$(C_6 - C_3)_2$	Lignins
$(C_6 - C_3 - C_6)_2$	Biflavonoids

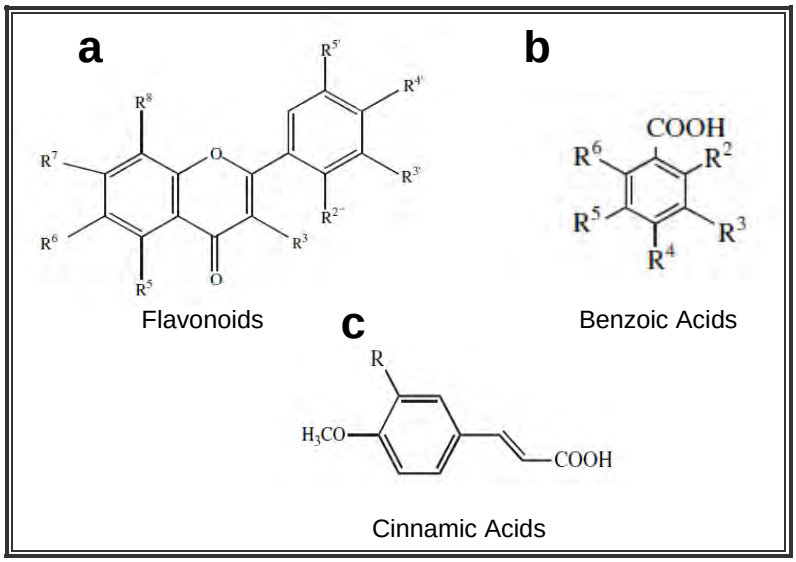

Figure 1.1 – Examples of phenolic compounds basic skeleton. (a) Flavonoids ($C_6 – C_3 – C_6$ skeleton); (b) benzoic acids (C_6-C_1); (c) cinnamic acids ($C_6 – C_3$).

Proanthocyanidins or condensed tannins are polyflavanoid in nature which can be divided into three main groups: procyanidins, prodelphinidins and propelargonidins. In grapes, the polyflavanoids differ in their quantity and structure depending on their localization in the tissues. While prodelphinidins are major grape skin proanthocyanidins, grape seed contains mainly procyanidins formed by mixtures of condensation units of the flavan-3-ol (-)-epicatechin and/or (+)-catechin (Monagas *et al.*, 2003). These procyanidins are linked mainly through C4-C8 bonds (**Figure 1.2a**) although C4-C6 linkages can also occur. Both structures are defined as type-B procyanidins, and may also be esterified through the (-)-epicatechin units forming 3-*O*-gallates (Escribano-Bailon *et al.*, 1992; Fuleki and Ricardo-da-Silva, 1997; de Freitas *et al.*, 1998; Gabetta *et al.*, 2000; Krueger *et al.*, 2000; Yang and Chien, 2000; Peng *et al.*, 2001; Saucier *et al.*, 2001; Flamini, 2003; Hayasaka *et al.*, 2003; Monagas *et al.*, 2003; Vivas *et al.*, 2004; Reed *et al.*, 2005). In addition to the C4-C8 bond, the flavan-3-ol units can be doubly-linked by a C2-C7 ether bond giving origin to type-A structures (**Figure 1.2b**) (Gu *et al.*, 2003a) that result from an oxidative intramolecular reaction (Kondo *et al.*, 2000).

1.1.2. Structural characterization methods

The main difficulty considering procyanidins structural characterization is to isolate them. Therefore, only mixtures containing more or less polymerized structures have been considered in previous studies. Several techniques have been applied for their separation and identification, including Thin Layer Chromatography, Nuclear Magnetic Resonance and high resolution chromatographic techniques, which have shown to be particularly suitable in the identification task (Antolovich *et al.*, 2000; Guyot *et al.*, 2001).

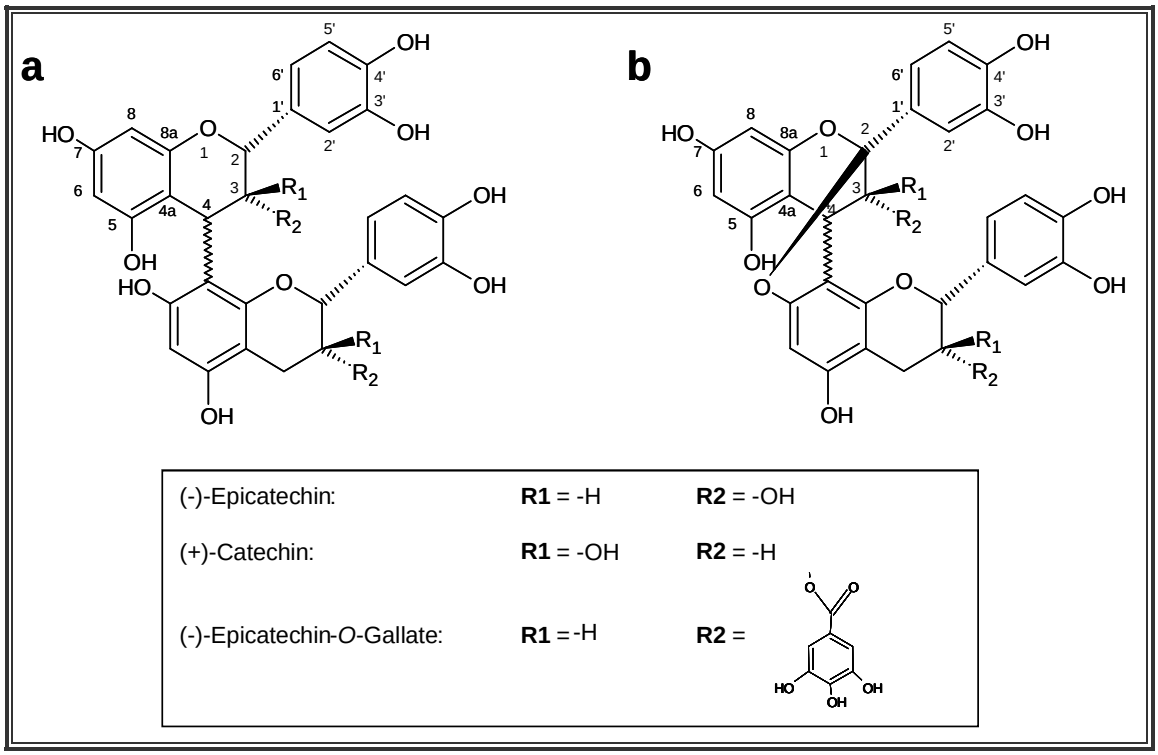

Figure 1.2 – Structure of procyanidin dimers. (a) Type-B, containing (C4-C8) interflavanic linkage; (b) Type-A, containing (C4-C8) and (C2-C7) interflavanic linkages.

HPLC. Derivatization steps prior to the analyses are generally mandatory when using Gas Chromatography (GC). In contrast, reversed-phase HPLC avoids the need for derivatization and therefore has been a method of choice for phenolic analysis. Isocratic elution has been used in some instances, but gradient elution was preferred owing to the diversity of phenols in most extracts. Different types of detectors can be used in conjunction with HPLC being the most commonly used in the detection of phenolic compounds the UV-Vis spectroscopic detector at the wavelength of 280 nm (Guyot *et al.*, 2001; Saucier *et al.*, 2001; Ferreira *et al.*, 2002; Naczk and Shahidi, 2004). If several compounds are eluted together in the given conditions, it may be possible to separate by HPLC and further identify them using standard compounds retention times or/and mass spectrometry.

ESI-MS. Electrospray ionization coupled with mass spectrometry detectors has been shown to be suitable for the analysis of polar compounds in aqueous solutions without any previous sample derivatization (Gaskell, 1997). Such conditions permit the identification of the molecular weight of procyanidins with different degrees of polymerization (Flamini, 2003). In addition, Tandem Mass Spectrometry (MS/MS) can elucidate more about the structural details of the different molecules. These techniques by themselves, due to their high accuracy and higher sensitivity, have been used for the conclusive identification of type-A procyanidins in a broad range of materials such as: fruits, cereals, nuts and spices (Gu *et al.*, 2002).

Grape seed procyanidins identification. The estimation of the average degree of polymerization (*DPn*) is useful to characterize the procyanidins present in a sample. Because the majority of procyanidin-rich samples contain molecules with different degrees of polymerization, fractionation steps can be used to improve their homogeneity (Le Bourvellec *et al.*, 2006). For the calculation of the *DPn* according to **Equation [1.1]** each polymer needs to be submitted to an acid-catalysed degradation process in the presence of nucleophilic agents such as in thiolysis, whose mechanism is schematically shown in **Figure 1.3**.

$$DPn = \frac{n^{\circ}(\text{Terminal Units}) + n^{\circ}(\text{Extension Units})}{n^{\circ}(\text{Terminal Units})} \qquad \textbf{[1.1]}$$

Such treatment promotes the formation of distinct monomers corresponding to one terminal and one-to-several extension units of the polymer (Guyot *et al.*, 2001; Saucier *et al.*, 2001; Ferreira *et al.*, 2002; Naczk and Shahidi, 2004). The example given by **Figure 1.3** exemplifies the mechanism for a procyanidin trimer. From one polymer initially composed of three procyanidin units it results (after being submitted to the thiolytic process): two extension units (one extension unit, from the initial sequence shown by **Figure 1.3a**, plus a second extension unit, from the second part of the mechanism shown in **Figure 1.3b**) and one terminal unit.

FTIR. Infrared spectroscopy is often suggested as an alternative to time consuming and expensive analytical techniques. FTIR is a versatile, cheap, and rapid method, which is of great interest for use in routine analysis or when no component identification is required. FTIR was also suggested for rapid evaluation of procyanidins' composition (Robb *et al.*, 2002; Jensen *et al.*, 2008). Nevertheless, resulting spectra are complex and non-selective, therefore chemometric analysis are necessary for extracting the information from the large and complex amount of data generated.

Chemometrics. Chemometric methods provide a better insight into the large and/or non-selective data sets and allow producing calibration models. Partial least squares (PLS) regression is one of the most used multivariate calibration methods (Wold and Wold, 1983; Martens and Naes, 1994; Wold *et al.*, 2001a, 2001b). The PLS algorithm is based on a bilinear model where the information contained in the **X** data matrix (independent variables, the FTIR spectra for all the samples used) is projected over a small number of latent variables known as PLS components. The **Y** data matrix is actively used for estimating the latent variables to ensure that the first components are the most relevant for predicting the **Y** variables (dependent responses, in this specific case will be the *DPn* determined by the reference method – HPLC). The interpretation of the relationships between the **X** and **Y** data is simplified to the relationships between the smaller number of PLS components (Barros and Rutledge, 2004; Guillen *et al.*, 2005).

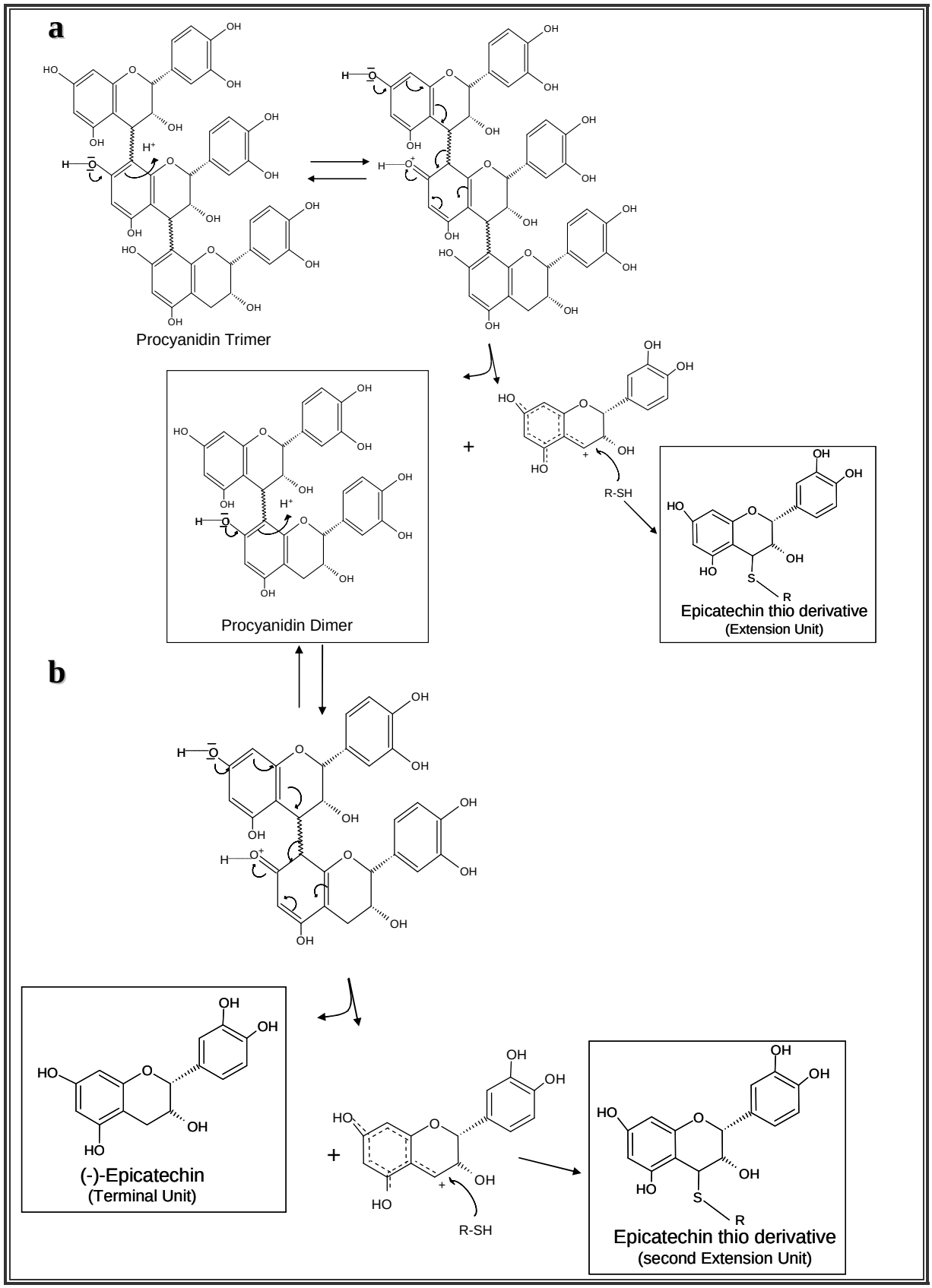

Figure 1.3 – Thiolysis mechanism using as example a procyanidin trimer with (-)-epicatechin composing units. (a) Formation of the first extension unit and a procyanidin dimer; (b) formation of the second extension unit and one terminal unit.

1.1.3. Antioxidant capacity (AOC)

Health benefits. Phenolic compounds are known for their antioxidant properties. Grape and grape-derived products in general have been further associated to anticarcinogenic, antiviral, antiallergic, altihepatotoxic, and anti-inflammatory effects (Facino *et al.*, 1998; Meyer *et al.*, 1998; de Gaulejac *et al.*, 1999; Kondo *et al.*, 2000). The benefits of phenolic compounds continue to be discovered within other potential pharmacological benefits associated to degenerative diseases as Parkinson and Ahlzeimer (Kaur and Kapoor, 2001). The procyanidins esterified with gallic acid, whose anti-inflammatory and antiallergenic properties have been reported to be higher than those of non-galloylated ones, are of special interest (Escribano-Bailon *et al.*, 1992). Although type-A procyanidins have lower antioxidant capacity when compared with type-B (Kondo *et al.*, 2000) they have shown a higher antiviral potential activity against herpes simplex virus (HSV) and human immunodeficiency virus (HIV) (de Bruyne *et al.*, 1999), and as a result have also become highly interesting. In terms of the AOC mechanism they may function: (a) as reducing agents, (b) as free radical scavengers, (c) as pro-oxidant metals complexers, and/or (d) as quenchers on the formation of singlet oxygen. Still, their major value for the food industry is their antioxidant activity in two distinct phases: as prevention or/and as lipoperoxidation terminator (Pincemail *et al.*, 1989).

Structure - activity relationship. It is assumed that the AOC of phenolics increases with the increasing number of hydroxyl groups and degree of polymerization. The results on the comparison of (-)-epicatechin with procyanidin B4 activities, which are a monomer and a dimer respectively, showed that the antioxidant power doubles with doubling number of hydroxyl groups in the B4 structure (Fan and Lou, 2004). In most cases, the AOC associated to these flavanols is related to the formation of quinones through the B-ring of the flavanol structure. These are called "*catechol type*" structures. However, there are other structures which do not yield to an *o*-quinone and still have high AOC. That is the case with "*pyrogallol type*" structures such as gallic acid. Gallic acid, a simpler structure with only three phenolic hydroxyl groups, showed a higher antioxidant power when compared to (-)-epicatechin, as the radical formed during the oxidation is highly stable. The existence of epicatechin-*O*-gallate in grape seeds, which contains both catechol and pyrogallol structures, seems even more interesting. Also, (-)-epicatechin was found to be a slightly more efficient antioxidant when compared to its isomer (+)-catechin, which was interpreted as a result of difference in structural configuration as (-)-epicatechin has a more significant area of charge delocalization (Freitas *et al.*, 1996). It is therefore evident that antioxidant activity of phenolics is defined by a range of factors. However, independently of how other factors may contribute to the final AOC of the compound, it has been perceived that DPn is an incontestable contributing factor.

1.2. Experimental Section

1.2.1. Samples conditioning

Plant material. The seeds used in this work were collected from grapes (*Vitis vinifera* L.) of the white variety 'Chardonnay' at technological maturity in Bairrada Appellation from an experimental vineyard (Estação Vitivinícola da Bairrada, Anadia, Portugal). A mixture of red grape varieties 'Touriga Nacional', 'Touriga Francesa' and 'Tinta Roriz' were also provided by wine producers of Adega Cooperativa de Pinhel (Portugal) during the year of 2004.

Seed preparation. The vinification process undergoes several stages after which the pulps, seeds, and other solid particles are disposed of the remaining liquid phase. The liquid phase continues in the vinification process, whereas the remaining solids are usually discarded. Collected solid particles were separated into three fractions by sieving through two sieves with mesh sizes of 5.0 and 2.0 mm. Only the fraction with middle size particles was used. Fractions with larger particles consisting mainly of agglomerated pulp, and with smaller particles consisting mainly of dust, were discarded. The remaining seed fraction was washed in several waters and air dried. The drying has lasted for three-to-five days depending on the atmospheric conditions. The total mass of obtained seeds was about 36 kg from the 100 kg of starting solid particles material.

Even after the separation and washing steps, the seeds still contained a significant amount of adsorbed compounds, especially phenolics and polysaccharides. An additional ethanol cleaning step was performed aiming to reduce their presence, which would contaminate the fractions to be extracted from the grape seed interior. The seeds were separated into small portions of 200 g each, placed into a large buchner funnel and soaked in ethanol for about 1 min. The wet material was layered into several metallic trays and dried in the oven at 303 K. The dried samples were then separated by sieving through sieves with a pore size of 4.0 and 2.8 mm. The middle size fraction was retained. Both the larger and smaller size particles, which were mainly composed of grape skin (**Figure 1.4**– sieve 1) and "dusty" particles of pulp (**Figure 1.4**– sieve 3) respectively, were discarded.

Figure 1.4 – Sieves and separated material (1 – skins, 2 – grape seeds, 3 – pulp).

The retained material (**Figure 1.4**– sieve 2) was introduced into 2.5 L glass jars that were covered with cotton soaked with toluene aiming to avoid microorganism contamination and stored in a refrigerator at 277 K until further use.

Batches of about 200 g were subjected to an addition cleaning before further use. During the first tests the cleaning procedure included the passage of the grape seeds over a balls mill. However, this procedure was abandoned as the mill had such a hard effect that parts of the grapes were damaged during the process. Instead, the seeds were submitted to several washes with water (200 g of seeds per 1 L of water) under gentle stirring with a magnetic bar at 277 K during a minimum of 3 days. Water was changed twice a day until turbidity was constant, ensuring that no remaining adherent tissues were present. Colour of the unwashed grape seeds was a strong purple (**Figure 1.5**) due to the high level of phenolic compounds, mainly anthocyanidins adsorbed at surface. After the washing, the colour almost disappeared. The cleaned seeds were once more washed with ethanol and dried, as described above.

Figure 1.5 – Grape seeds first screening.

Seed size reduction. The seeds were placed in a bath with liquid nitrogen, becoming very rigid. In this way the grinding process could be conducted without losing the oil into the machinery. Two different grinding appliances were employed during this study: a laboratory grinder (Model EM 1000, Retsch, Germany) (**Figure 1.6a**), and a domestic coffee mill (Model KSW 2669) (**Figure 1.7a**). The domestic coffee mill allowed a better control of the particle size produced, and therefore was preferred for the production of larger particles. However, the domestic coffee mill required a larger time span than the laboratory grinder and therefore it was preferred whenever the particle size was not fixed. During the phenolics extraction and analysis, where the particle size was not studied, a laboratory grinder was used. The seeds were loaded into the centrifuged chamber (10 000 rpm) and thrown against the perforated walls, which resulted into seed disintegration (**Figure 1.6b**). The filter used had a 0.5 mm orifice size (**Figure 1.6c**).

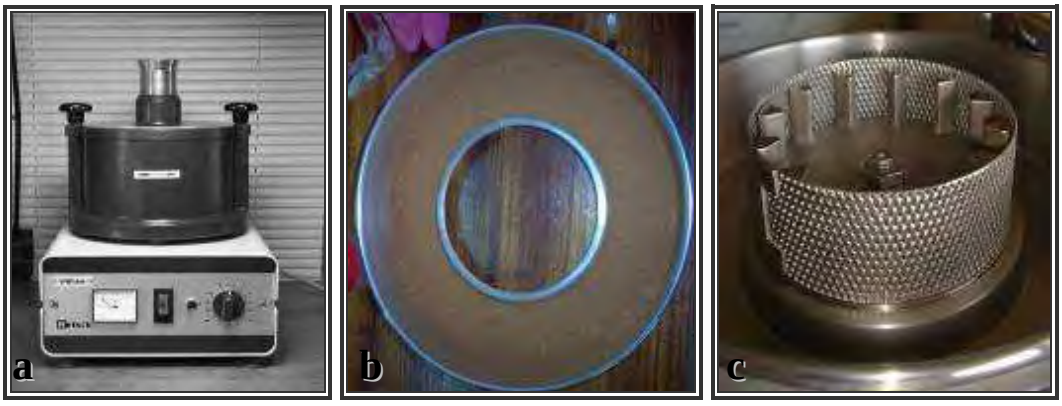

Figure 1.6 – (a) Laboratory mill; (b) milled seeds; (c) filter grid.

A domestic coffee mill (**Figure 1.7a**) was used for grinding the seeds before the enzymatic treatments (Chapter 2) and supercritical extractions (Chapter 3), where the particle size was rigorously controlled. Control of the particle size was ensured by using a sequence of short grinding stages (no more than 3 s per stage) followed by sieving. The process continued cyclically until the desired particle fractions were obtained. A siever shaker (Fritch Analysettle, Type 03.502, No.828) was used (**Figure 1.7b**). The grinded particles were pored into the first sieve with a pore size of 2.0 mm. The following sieves had 1.4, 1.0, 0.71, 0.6, 0.5, 0.4, 0.3 and 0.2 mm pore sizes. For the cataloguing of the particles intervals the pore sizes between sieve layers were assumed (**Figure 1.7c**). Specifically, an average particle diameter (d_{p}) for each fraction was calculated by Sauter's equation (Povh *et al.*, 2001):

$$d_{\mathrm{p}} = \frac{m_{\mathrm{t}}}{\sum_{i=1}^{k} \frac{m_i}{d_{\mathrm{p}i}}} \qquad \textbf{[1.2]}$$

where m_i is the mass of particles retained below mesh size $d_{\mathrm{p}i}$, m_{t} is the total mass of seeds, and k is the number of mesh sizes intervals. The seed fractions used in this work are shown in **Table 1.2**.

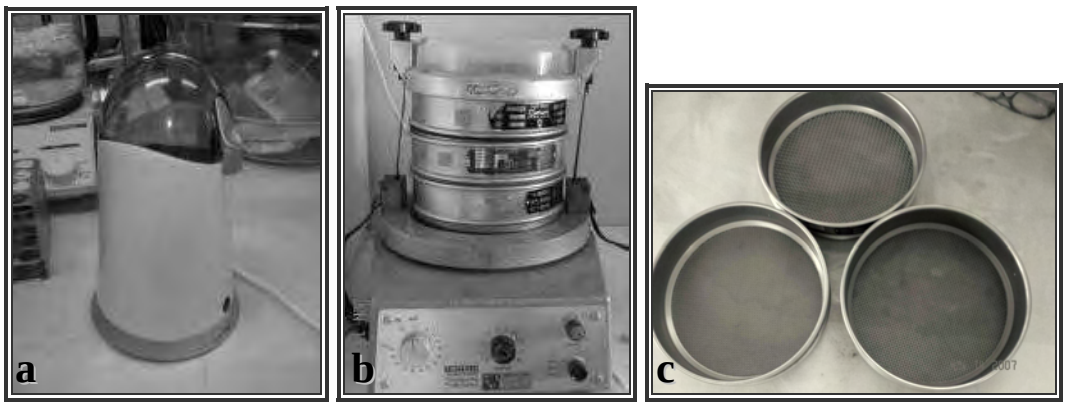

Figure 1.7 – (a) Coffee mill; (b) siever shaker; (c) different aperture sizes sievers.

Table 1.2 – Seed fractions used in this work.

Application	Grinding date	d_p (mm)	Mass distribution between sieve (mm) layers						Total	
			A	B	C	D	E	F	(g)	(%)
			<0.5	0.5-0.6	0.6-0.7	0.7-1.0	1.0-1.4	1.4-2.0		
Enzymatic pre-treatment (Chapter 2)	**09/01/2007**	**0.85**	64.7	52.6	75.0	418	723	-	**1332**	-
			5.00	4.00	6.00	31.0	54.0	-	-	**100**
SC-CO_2 (Chapter 3)	**04/02/2008**	**0.75**	120	70.7	109	1122	379	-	**1799**	
			7.00	4.00	6.00	62.0	21.0	-	-	**100**
High pressure pre-treatment (Chapter 3)	**20/03/2008**	**0.85**		93.5		175	358	43.8	**671**	-
				14.0		26.0	53.0	7.00	-	**100**

The particle size distribution inside each fraction was difficult to control, which could lead to differences in behaviour of fraction with supposedly the same d_p. Therefore, the corresponding batches of seeds needed for all experiments were prepared in each study, grinded at once, and then stored in the refrigerator at 253 K.

For measuring the water content of the seed, a standard procedure was used (IUPAC, 1987): 2.0 g of seeds were placed into a glass box, which was previously weighed in an analytical high precision electronic balance (± 0.01 mg) (Precisa, Precisa Gravimetrics AG, Switzerland) and dried overnight in an oven (WTB binder, Germany) at 378 K. Difference in sample weight before (m_i) and after (m_f) drying corresponded to the water content as described by:

$$H(\%) = \frac{m_i - m_f}{m_i} \times 100 \qquad \textbf{[1.3]}$$

1.2.2. Extraction and structural characterization

Procyanidin crude extract (PCE). The extraction methodology was adapted from Guyot *et al.* (2001) as described by Cardoso *et al.* (2005). Seed powder (about 40 g) was extracted three times with 0.4 L of *n*-hexane to remove the lipids at room temperature (**Figure 1.8a**). The bulk was decanted and the process was repeated two times more. After that, seeds were shaken during 15 min with methanol containing 5% acetic acid at room temperature maintaining the ratio solvent/seed equal to 10. This procedure was repeated three times with the aim to extract the lower weight phenolic compounds. The combined methanol extracts were filtered, first using a G1 (**Figure 1.8b**) and further with a G3 sintered glass filter (**Figure 1.8c**), concentrated under vacuum at 303 K with several additions of water to assure the complete removal of methanol and acetic acid, frozen and freeze-dried. The methanol procyanidin crude extract (PCE) resulted.

Figure 1.8 – (a) Solid-liquid extraction experiment; (b) filtration with a G3 sintered glass filter; (c) filtrates with a G3 and G1 sintered glass filters.

After the methanolic treatment, the seeds were subjected to the same solid-liquid extraction procedure (three times with acetone/water (4:6, v/v) solution containing 5% acetic acid). The acetone and acetic acid were then eliminated as described for methanol. The aqueous solution was frozen, and freeze-dried, obtaining the acetone/water PCE.

Procyanidin fractionation. Both methanol and acetone/water PCE from white and red grape seeds were fractionated according to the methanol/chloroform graded precipitations proposed by Saucier *et al.* (2001) as summarized in **Scheme 1.1**.

The PCE powder was dissolved in water (10 $g \cdot L^{-1}$) containing 5% acetic acid and the undissolved material (F_0) removed by centrifugation under 15 000 rpm at 283.15 K during 15 min (Centrifuge 3K30, Sigma, St. Louis, MO, USA). The supernatant was submitted three times to a liquid-liquid extraction with 40% (v/v) ethyl acetate aqueous solution. The solvent was added to the PCE solution and the first extraction performed. Afterwards, the organic phase was recovered from the bottom of the decantation flask. Another charge of acetate was then added, mixed and recovered again. The procedure was repeated a third time producing a total of three organic extracts that were combined (F_1). The remaining water solution became the aqueous phase (F_2). All solutions were concentrated, frozen and freeze dried. The F_2 solution was evaporated to dryness and redissolved in methanol (10 $g \cdot L^{-1}$). The undissolved material ($F_{2.0}$) was removed by centrifugation, with the supernatant submitted to successive additions of chloroform until a new precipitate was formed. In each addition, the solution remained stirring overnight at 277 K, and checked for the presence of precipitate in the following day. If no precipitated material was observed, another aliquot of chloroform would be added, and followed by agitation during more 2-3 hours in a freezing camera at 277 K. The precipitate was then collected by centrifugation (15 000 rpm, 283.15 K, 15 min), dissolved in water, rotary-evaporated with several additions of water, frozen and freeze-dried. These extracts were labelled as $F_{2.1}$, $F_{2.2}$, $F_{2.3}$, and further on.

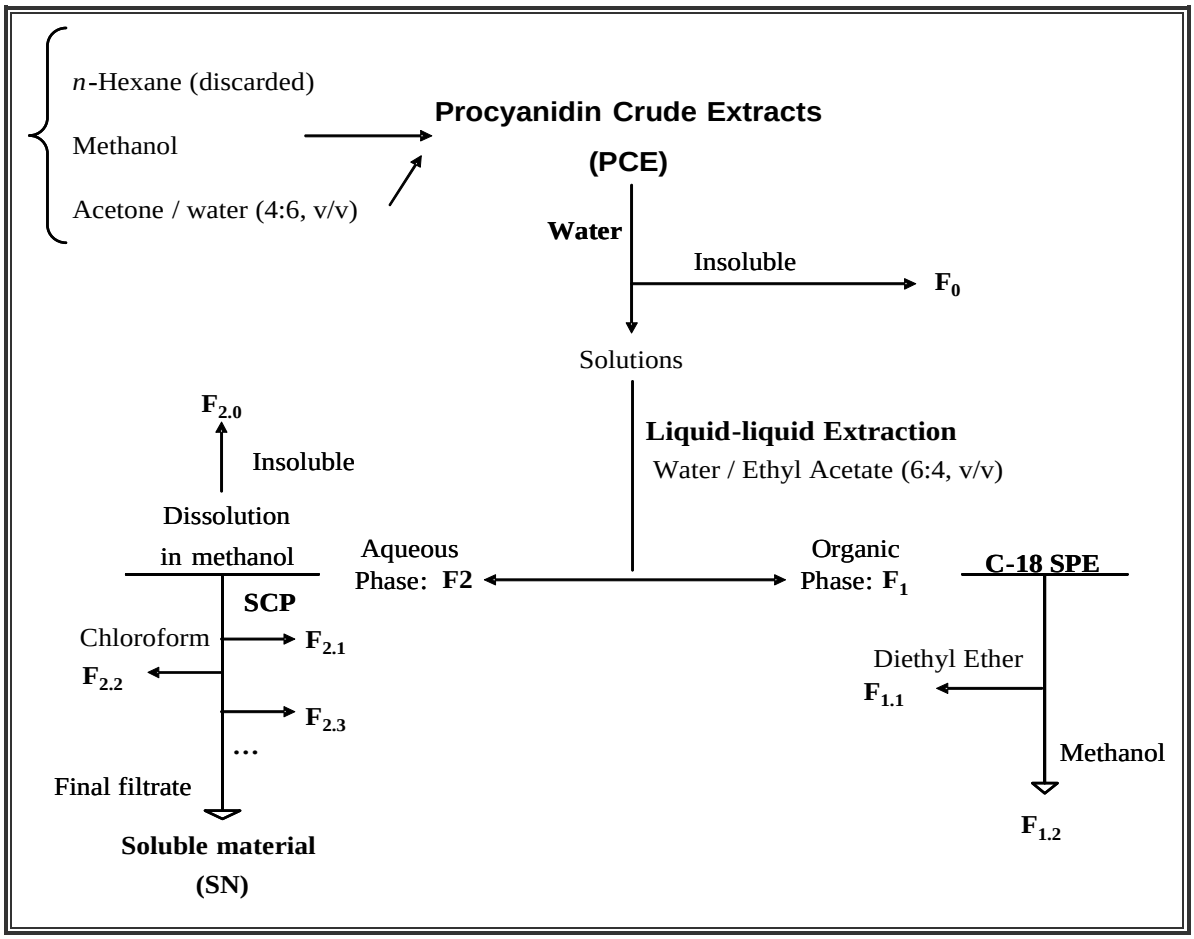

Scheme 1.1 – Extraction and fractionation of grape seed procyanidins. SPE: Solid Phase Extraction; SCP: Sequential Chloroform Precipitations.

The material still soluble in the methanol/chloroform solution, after the last precipitation, was tagged "SN" and recovered as previously described for the precipitated fractions.

The C_{18} solid-phase-extraction column (SPE, Supelco-Discovery – 5 g) was used to achieve a rough separation between monomers and oligomers from the F_1 solution. The SPE column was preconditioned with 2.0×10^{-2} L of methanol, followed by 2.0×10^{-2} L of water, and 2.0×10^{-2} L of 2% acetic acid. The column was then washed with 1.2×10^{-1} L diethyl ether. The procyanidins for ESI-MS analysis were eluted with 6.0×10^{-2} L methanol and dried by centrifugal evaporation (Univapo 100 ECH, UniEquip, Munich, Germany).

Each sample of about 2.0×10^{-2} g was dissolved in 2.0×10^{-2} L of acetic acid (2%, v/v) and loaded onto the preconditioned SPE column. The maximum quantity loaded in the column was determined by controlling the absorbance of the recovered material at 280 nm in a UV-Vis spectrophotometer. When the signal appeared, the column was overloaded, then the volume of the added sample was reduced. The column was then washed with 6.0×10^{-2} L of acetic acid (2%, v/v). The low

molecular weight phenolic compounds (mainly monomeric type – $F_{1.1}$) were eluted with 1.2×10^{-1} L of diethyl ether. As the polymerized molecules are expected mainly in the aqueous phase (F_2) the remaining phenolic compounds eluted through the SPE column are assumed to be mainly oligomers ($F_{1.2}$). These were eluted with 6.0×10^{-2} L of methanol also monitored at 280 nm. All corresponding aliquots of $F_{1.1}$ and $F_{1.2}$ were gathered and dried by centrifugal evaporation.

Thiolysis. Thiolysis was carried out according to the methodology described by Guyot *et al.* (2001). A 4.0 $g\cdot L^{-1}$ solution of each dry fraction was prepared by sonificating the residue in methanol. In an 1.5×10^{-3} L capacity eppendorf, 5.0×10^{-5} L of solution was mixed together with 5.0×10^{-5} L of methanol acidified with concentrated HCl (3.3%, v/v) and 1.0×10^{-4} L of benzyl mercaptan (toluene-R-thiol) in methanol (5%, v/v). After sealing, the reaction was carried out at 313.15 K for 30 min.

HPLC-UV analysis. The samples were analyzed previously to and after thiolysis. HPLC analyses followed the conditions described by Peng *et al.* (2001). In a HPLC apparatus (series 200, Perkin Elmer, USA) with UV-Vis Detector (785A UV-Vis Detector, Perkin Elmer, USA) the samples were loaded at 303.15 K into a C_{18} column (LichroCart 250-4 Superspher 100 RP-18, Merck, Germany). The column was equipped with a C_{18} guard cartridge (with the same packing material) equilibrated with 0.2% (v/v) formic acid (eluent A). Phenolic compounds were eluted by gradient with 82% (v/v) acetonitrile in water and 0.04% (v/v) formic acid in water (eluent B). It proceeded from 0% to 15% of eluent B in the first 15 min, 15% to 16% of eluent B from 15 to 40 min, 16% to 17% from 40 to 45 min, 17% to 43% from 45 to 48 min, 43% to 52% from 48 to 49 min, held isocratic at 52% of eluent B from 49 to 56 min, reduced from 52% to 43% of eluent B from 56 to 57 min, from 43% to 17% from 57 to 58 min, and reduced once more from 17% to 0% of eluent B from 58 to 60 min. Two replicates of each sample were run. Peaks were detected at 280 nm, where monomers and procyanidin B2 dimer were identified by comparison of their retention times with standards. The (-)-epicatechin thioderivative was identified by comparison with the retention time of the products of procyanidin B2 dimer after thiolysis, whereas the (+)-catechin and (-)-epicatechin-*O*-gallate thioderivatives were identified by their retention times and abundance, and confirmed by analysis of their mass spectra using a LC-MS (Waters Alliance 2690).

The average degree of polymerization was calculated as the ratio of all the areas of flavan-3-ols units (thioether adducts plus terminal units) to the sum of the areas of (+)-catechin, (-)-epicatechin, and (-)epicatechin-*O*-gallate corresponding to terminal units. The *DPn* estimated was in the range *DPn*±0.5.

The calibration curves for estimation of total procyanidin content were obtained using (+)-catechin, (-)-epicatechin, (-)-epicatechin-*O*-gallate, and procyanidin B2 dimer in the range of concentration of 0.005-0.5 $g \cdot L^{-1}$ (**Table 1.3**). The quantification of phenolics in the corresponding fractions was assessed by comparison of the chromatographic area after thiolytic degradation of the samples with the respective calibration curve. As thioderivative standards were not available, they were quantified by using the respective monomer calibration curves assuming a similar response factors to the correspondent monomeric units (Vivas *et al.*, 2004).

Table 1.3 – Calibration curves. Relationship between compound concentration ($g \cdot L^{-1}$) and the corresponding chromatographic area ($mV^{-1} \cdot s^{-1}$).

Compound	Slope $\left(g \cdot L^{-1} \cdot mV^{-1} \cdot s^{-1}\right) \times 10^{2}$	R^2
(+)-Catechin	1.5	0.988
(-)-Epicatechin	1.2	0.967
(-)-Epicatechin-*O*-gallate	0.5	0.968
Gallic acid	0.5	0.997
Procyanidin B2	1.2	0.994

ESI-MS analysis. The C_{18} solid-phase-extraction column (SPE, Supelco-Discovery – 5 g) was also used to exclude free sugars from procyanidin-rich extracts prior to the ESI-MS analysis (Cardoso *et al.*, 2005). Electrospray analyses were performed in samples (of $5.0 \times 10^{-1}\ g \cdot L^{-1}$) dissolved in MilliQ high purity water with 2.0% (v/v) formic acid further one hundred times diluted in methanol/water (1:1, v/v) solution with 1.0% (v/v) formic acid. Samples were introduced into the mass spectrometer using a flow rate of $1.0 \times 10^{-6}\ L \cdot min^{-1}$.

Positive ion mode ESI-MS and MS/MS spectra were acquired using a Q-TOF instrument (Q-TOF 2, Micromass, Manchester, UK) (**Figure 1.9**) setting the needle voltage at 3000 V with the ion source at 353.15 K and desolvation temperature at 423.15 K maintaining the cone voltage at 35 V.

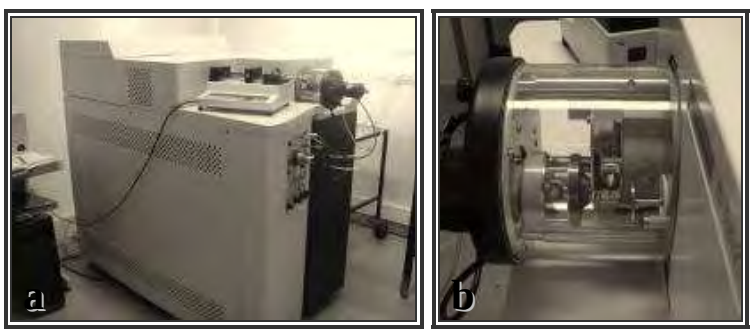

Figure 1.9 – (a) Q-TOF instrument (Q-TOF 2, Micromass); (b) Q-TOF instrument detail.

Tandem mass spectra (MS/MS) of molecular ions were obtained using collision induced dissociation (CID) using argon as the collision gas and varying collision energy between 20-35 eV. Each spectrum was produced by accumulating data during 1-2 min. In MS and MS/MS experiments TOF resolution was set to approximately 9.000 full weigh at half maximum (Reis *et al.*, 2003). The raw data were processed and transformed into values of molecular masses using a MassLynx software, version 3.5.

LC-MS analysis. A HPLC system (Waters Aliance 2690, Waters Aliance, USA) equipped with an UV detector (K-2500, Knauer, Germany) set at λ = 280 nm was used. Samples (1.0×10^{-5} L) were loaded at 293.15 K into a SPE (Supelco-Discovery® BIO Wide Pore C_{18}, Supelco, USA) HPLC column (1.0×10^{-1} m, 3.2×10^{-2} m i.d., 5.0×10^{-6} m bead diameter).

The mobile phase consisted of 10% (v/v) acetonitrile in water and 0.5% (v/v) formic acid in water (eluent A) and 100% (v/v) acetonitrile (eluent B). The eluent gradient was programmed as follows: 10 to 50% of eluent B in the first 40 min, held isocratic at 50% from 40 to 50 min, reduced from 50 to 10% from 50 to 65 min at $2.0\times10^{-2}\,\mathrm{L}\cdot\mathrm{min}$. After the UV detector the flow was redirected into the MS interface with a 1:20 home-made split. MS was performed as previously described for ESI-MS analyses.

1.2.3. Average degree of polymerization

FTIR spectroscopy and multivariate analyses. The FTIR spectra of each fraction were obtained using a Golden Gate single reflection diamond ATR system in a spectrometer (IFS-55, Bruker, USA) with a Deuterated Triglycine Sulfate (DTGS) detector.

The spectra were recorded at the absorbance mode from 4000 to 400 cm^{-1} (mid infrared region) with the resolution of 8 cm^{-1}. Five replicate spectra (128 co-added scans) were collected for each sample. The measured spectra were transferred via a JCAMP.DX format into the data analysis software developed in the Institut National Agronomique Paris-Grignon in collaboration with the University of Aveiro (Barros, 1999).

Calibration model. The multivariate calibration was applied in the 1800-700 cm^{-1} region and due to amplification spectrum effects they were pre-processed using SNV (Standard Normal Variate). **Figure 1.10** shows the used spectral region before (**Figure 1.10a**) and after (**Figure 1.10b**) the SNV correction.

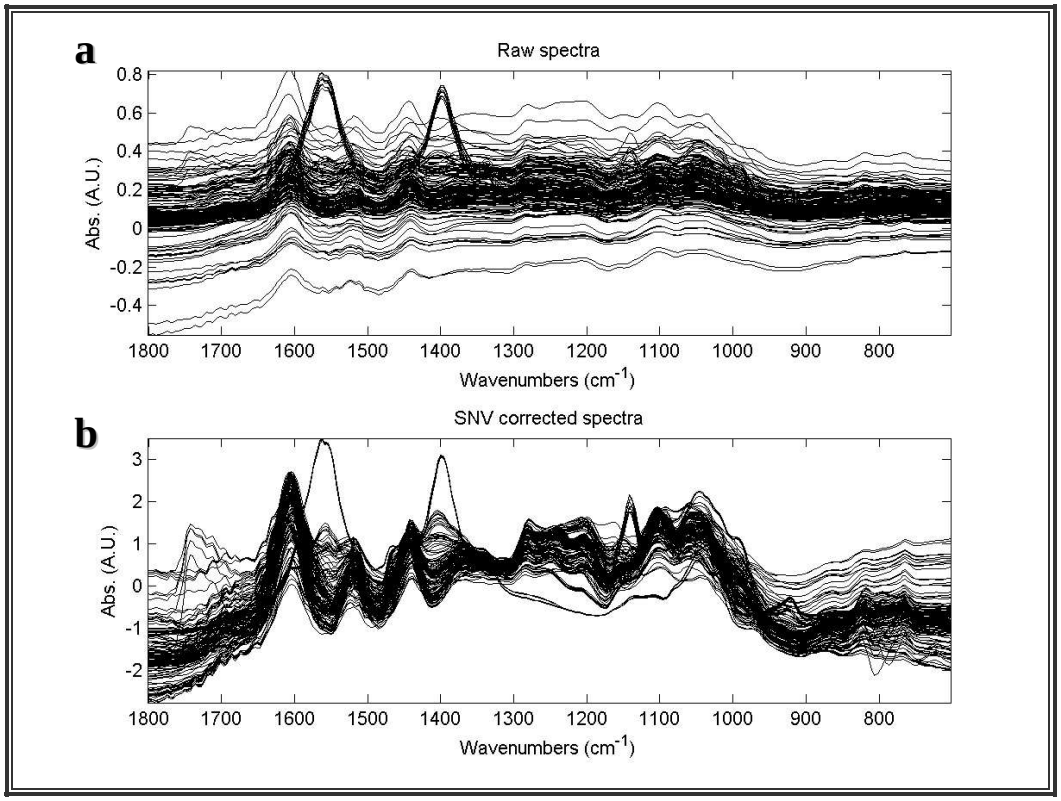

Figure 1.10 – FTIR spectra in the 1800-700 cm^{-1} region: (a) raw spectra; (b) SNV corrected spectra.

In order to build the calibration model for the quantification of the *DPn* a Monte Carlo cross-validation (Xu *et al.*, 2001) was used. The data set was split into a calibration (learning set) and validation (external) sets to assess the predictive power of the *DPn* model. **Table 1.4** includes the 26 samples used to calibrate and the four PCE samples (which are the crude extracts, containing a heterogeneous material) for prediction. The splitting process consisted in sorting the *DPn* values and then randomly select 40% of the samples (where replicates are considered a sample) that were used as validation set. The remaining 60% of the samples were used as calibration set.

Table 1.4 – PLS1 explained variance values for each LV for the estimation of procyanidin *DPn*.

LV	R^2X (%)	Accumulated R^2X (%)	R^2y (%)	Accumulated R^2y (%)
1	41.8	41.8	23.1	23.1
2	33.3	75.1	9.8	32.9
3	10.7	85.8	27.3	60.2
4	5.2	91.0	8.8	69.0
5	2.4	93.4	8.3	77.3
6	2.1	95.4	5.7	83.0
7	2.0	97.5	4.5	87.5
8	0.6	98.0	3.0	90.5

LV: Latent variables; R^2X: X variance; R^2y: y variance.

This procedure was repeated several times (iterations). 200 regression models were built and for each one the "optimal" model dimensionality based on the RMSECV (root mean square error of cross validation) value and LV (latent variable) number recovered. This allowed one to see how many times of a given LV/RMSECV "optimal" pair (distribution profile) was used to build a predictive model. The selection of model complexity was based on the most frequent pair of LV/RMSECV. Then, the selected model dimensionality was used to predict the parameters of interest from the external set, expressed as root mean square error of prediction (RMSEP).

Since this approach is very computational demanding when using only Partial Least Squares (PLS1) (Wold *et al.*, 1983), the Principal Component Transform PLS1 (PCT-PLS1) (Trygg and Wold, 2002; Barros and Rutledge, 2004) was used to build the calibration models, accelerating the Monte Carlo cross-validation process.

1.2.4. Antioxidant capacity

Free radical-scavenging activities of the previously described samples were evaluated by determining their abilities to chemically reduce the stable free radical α,α-diphenyl-β-picrylhydrazyl ($DPPH\cdot$). The extracts obtained in 2005 were analyzed at two different moments: in 2006 and 2007. Results obtained with difference of one year were compared with the aim to determine the storage effect upon these compounds. The antioxidant capacity was determined using the methodology described by Latté *et al.* (2004). The concentration of $DPPH\cdot$ was detected by measuring absorbance at 515 nm using a double beam UV-Vis spectrophotometer (Lambda 35, Perkin-Elmer, USA). The calibration curve was produced by measuring standard solutions of DPPH radical in methanol in the concentration range 0-100 g L^{-1}. The calibration curve is presented in **Figure 1.11**. The calibration was valid for at least one month.

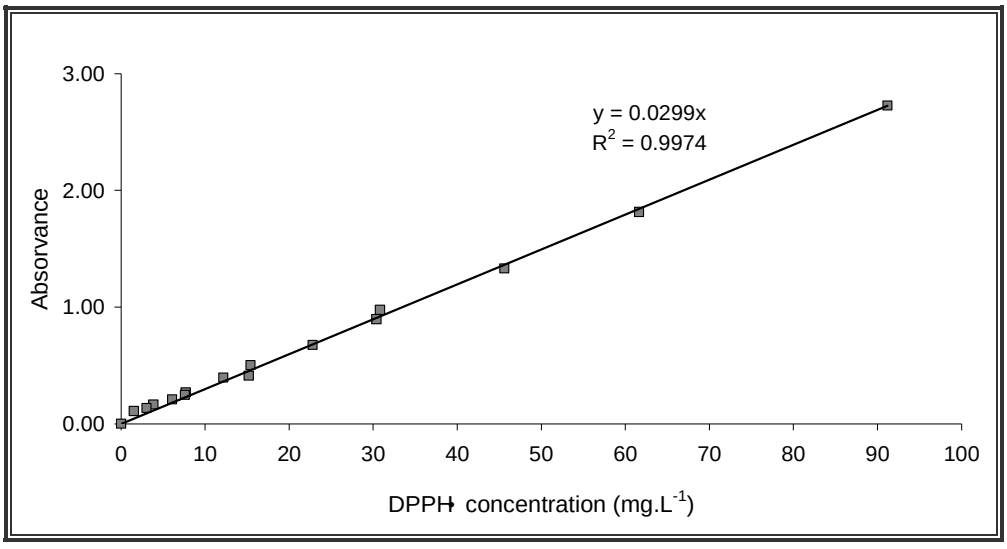

Figure 1.11 – Calibration curve to determine DPPH radical concentration.

In the standard assays, 3.2×10^{-3} L of phenolic samples of various concentrations ($0-100\ g\cdot L^{-1}$) were added to a methanolic solution of DPPH· (9.6×10^{-4} M) performing a final volume of 4.0×10^{-3} L. The mixture was shaken vigorously and allowed to react at room temperature during 30 min. Then, the remaining DPPH· in the sample was determined colorimetrically at 515 nm by blanking against an appropriate control (mixture without the radical).

The conversion of DPPH· (X_{DPPH}) was calculated by:

$$X_{DPPH} = \left(1 - \frac{A_{sample}}{A_0}\right) \times 100\% \qquad \textbf{[1.4]}$$

where A_0 is the initial absorbance, and A_{sample} is the absorbance measured after 30 min of reaction.

The radical scavenging activities of the standards and extracts were further expressed as IC_{50} values, which indicate the sample concentration required to reach 50% reduction of DPPH· concentration. The IC_{50} value was calculated from a linear-dose inhibition curve measured for (+)-catechin and ascorbic acid (positive controls), and all fractions presented in **Scheme 1.1** (TCE, F_0, F_1, $F_{2.0}$, $F_{2.1}$, …). **Figure 1.12** illustrates the case of (+)-catechin, where three replicates are shown. Similar curves were generated for ascorbic acid and all extracts. Although a log–dose inhibitory curve was adopted by Latté *et al.* (2004), the results showed that a linear fitting was sufficient in this work (**Figure 1.12**).

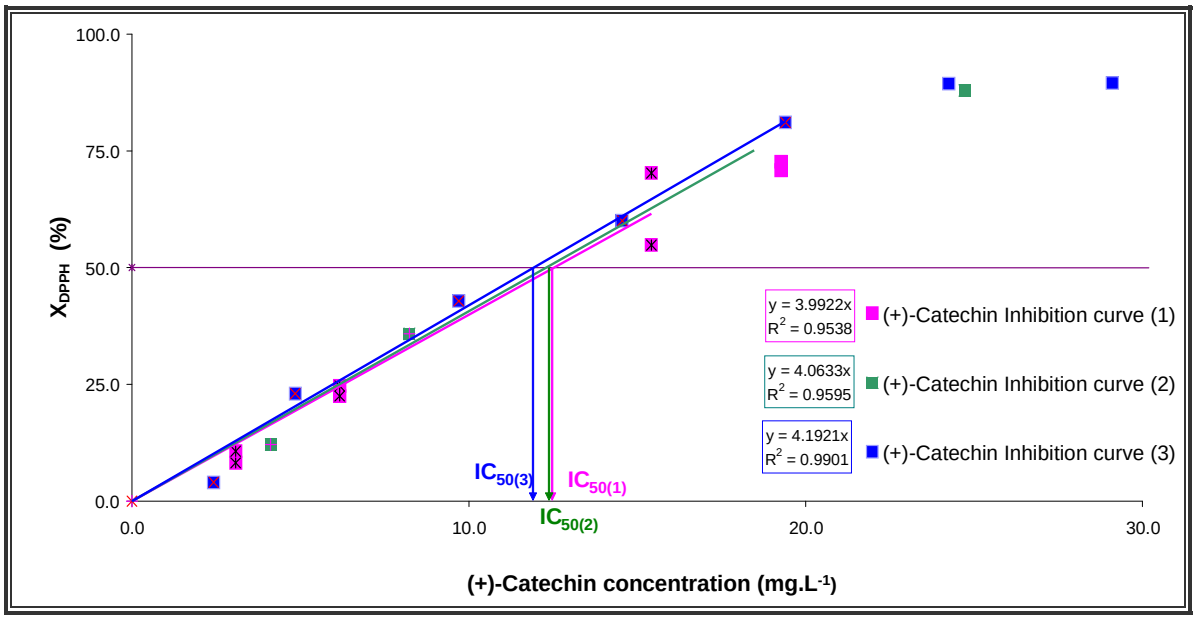

Figure 1.12 – (+)-Catechin linear-dose inhibitory curve.

1.3. Results and Discussion

1.3.1. Structural characterization

The detailed results obtained for the procyanidins compositions of the crude extracts (PCE) and individual fractions represented in Scheme 1 are compiled in **Table 1.5** along with the average degree of polymerization (*DPn*).

Procyanidins crude extracts. The PCE yields (%) presented in **Table 1.5** refer to the extracts initially recovered from the grape seed. For instance, for the white grape seed crude extract obtained with methanol (**Table 1.5**, WM-PCE) the yield is 21.4% (w/w). The total procyanidins content is 55.2% (w/w) of the mass of WM-PCE (see **Table 1.5**, *Total procyanidin* column). The subsequent extraction with acetone/water only increases the yield in 4.5%, maintaining a similar mass content in procyanidins (53.7%). For the red grape seeds, 7.6% of the initial material was obtained as PCE in the methanol extract (**Table 1.5**, RM-PCE), with an additional 3.0% recovered by extraction with aqueous acetone (see **Table 1.5**, RA-PCE). The mass content of procyanidins is reduced to 8.8% of its total mass with a slightly higher content of 20.2% in the acetone/water extract (**Table 1.5**, RA-PCE). Due to the low yield associated to the red grape seeds extracts, the antioxidant tests were only performed with white grape seed extracts (see Section 1.3.2).

HPLC-UV analysis. In order to estimate the amount of procyanidins in each extract the samples were submitted to a thiolytic degradation process, followed by HPLC separation and UV detection. **Figure 1.13** shows an example of the chromatograms obtained in this work before and after thiolysis.

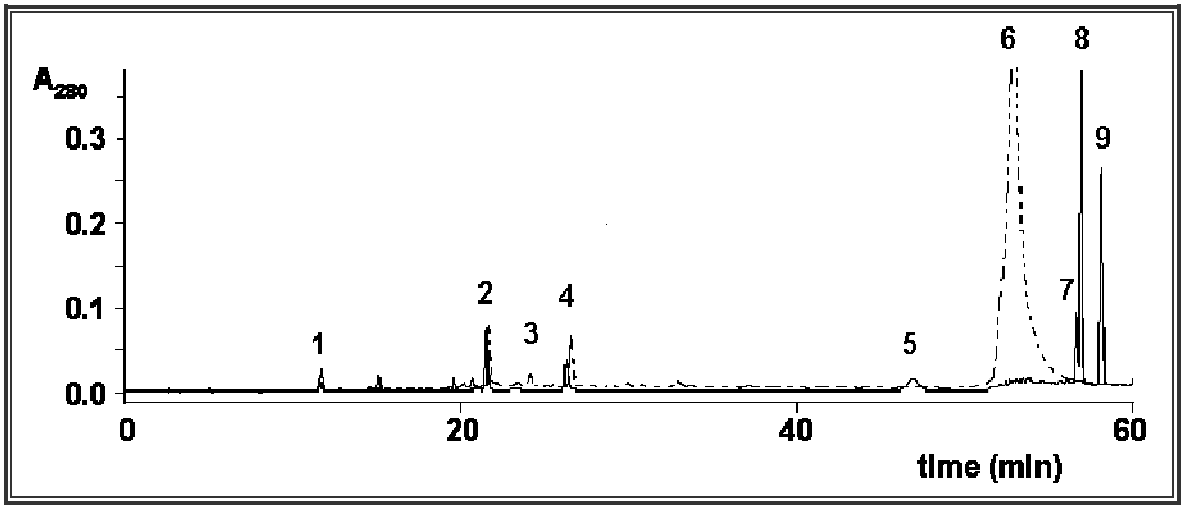

Figure 1.13 – Reversed-phase HPLC-UV chromatogram of methanol PCE obtained before (dashed line) and after (full line) thiolysis; peak detection at 280 nm. 1. Gallic acid; 2. (+)-catechin; 3. procyanidin B2; 4. (-)-epicatechin; 5. (-)-epicatechin-*O*-gallate; 6. polymeric procyanidins; 7. (+)-catechin thioderivative; 8. (-)-epicatechin thioderivative; 9. (-)-epicatechin-*O*-gallate thioderivative.

Table 1.5 – Procyanidins compositions and average degrees of polymerization of grape seed extracts obtained according to the fractionation methodology described in Scheme 1.1.

Fraction	$CHCl_3$ (%,w/w)	Yield (%,w/w)	Total procyanidin content in extract (%, w/w)	Flavan-3-ol composition (%)						*DPn*
				(+)-Catechin		(-)-Epicatechin		(-)-Epicatechin-*O*-Gallate		
				Terminal	Extension	Terminal	Extension	Terminal	Extension	
WM-PCE	-	**21.4**	**55.2**	**8.7**	**9.4**	**2.9**	**63.9**	**1.9**	**13.1**	**7.4 (7.5)$^+$**
WM-F_0	-	11.3	8.6	6.4	5.8	3.3	65.7	1.6	17.2	8.8
WM-F_1	-	8.7	84.1	34.5	17.5	17.4	22.5	3.7	4.4	1.8
WM-$F_{2.0}$	-	1.4	22.1	5.3	4.7	3.2	65.4	5.5	16.1	7.2
WM-$F_{2.1}$	29	5.6	35.2	5.9	4.1	3.6	68.8	1.2	16.4	9.4
WM-$F_{2.2}$	52	10.5	45.1	7.1	4.6	3.7	66.4	1.7	16.5	8.0
WM-$F_{2.3}$	66	8.5	43.6	8.3	5.1	4.9	65.6	2.4	13.8	6.4
WM-$F_{2.4}$	73	6.6	68.5	7.5	3.7	4.5	65.1	2.7	16.5	6.8
WM-$F_{2.5}$	79	4.2	49.2	9.8	6.5	5.5	65.8	2.2	10.1	5.7
WM-$F_{2.6}$	84	3.7	43.6	11.1	7.8	6.6	62.6	2.4	9.7	5.0
WM-SN*	-	18.5	13.4	13.4	33.9	11.7	34.4	4.3	2.4	3.4
WA-PCE	-	**4.5**	**53.7**	**11.4**	**5.6**	**9.9**	**58.4**	**2.5**	**12.2**	**4.2 (3.6)$^+$**
WA-F_0	-	21.4	33.2	7.7	4.7	4.6	64.1	1.8	17.1	7.1
WA-F_1*	-	5.4	70.6	34.3	5.9	29.9	21.9	3.4	4.6	1.5
WA-$F_{2.1}$	42	8.2	29.4	7.6	4.9	3.6	61.9	1.8	20.3	7.7
WA-$F_{2.2}$	58	7.2	31.7	8.6	3.2	3.6	64.2	2.5	17.9	6.8
WA-$F_{2.3}$	71	4.0	25.5	11.1	7.0	5.8	60.5	2.4	13.2	5.2
WA-$F_{2.4}$	84	2.8	13.6	13.6	6.1	10.0	60.5	2.0	7.7	3.9
WA-SN*	-	1.8	6.8	23.3	11.6	12.7	45.8	1.8	4.9	2.6
RM-PCE	-	**7.6**	**8.8**	**11.9**	**15.1**	**2.6**	**59.8**	**1.6**	**9.0**	**6.2 (7.0)$^+$**
RM-F_0	-	11.1	11.8	8.9	8.5	3.6	62.9	0.9	15.3	7.5
RM-$F_{1.1}$*	-	1.4	84.9	61.8	-	37.3	-	0.9	-	1.0
RM-$F_{1.2}$	-	0.7	28.2	25.5	18.1	7.8	35.6	2.4	10.6	2.8
RM-$F_{2.0}$	-	0.7	46.6	6.6	7.9	2.8	65.6	0.2	16.9	10.4
RM-$F_{2.1}$	43	3.1	27.3	6.9	7.4	2.5	67.0	0.9	15.2	9.7
RM-$F_{2.2}$	60	3.0	29.4	10.3	11.1	4.3	69.8	0.3	4.2	6.7
RM-$F_{2.3}$	82	2.2	27.0	15.7	11.7	6.9	59.0	1.1	5.5	4.2
RM-SN*	-	19.2	0.4	5.0	-	95.0	-	0.0	-	1.0
RA-PCE	-	**3.0**	**20.2**	**9.1**	**9.0**	**3.3**	**58.1**	**1.1**	**19.4**	**7.4 (7.5)$^+$**
RA-F_0	-	14.8	41.4	6.8	7.5	2.7	55.2	1.3	26.5	9.3
RA-$F_{1.1}$*	-	1.8	54.7	64.6	-	34.3	-	1.1	-	1.0
RA-$F_{1.2}$	-	2.3	44.7	10.7	10.2	3.9	42.8	4.7	27.8	5.2
RA-$F_{2.0}$	-	6.9	31.0	5.7	6.5	2.6	56.1	1.0	28.4	10.8
RA-$F_{2.1}$	43	8.6	55.2	8.4	7.1	3.5	57.8	1.2	21.8	7.6
RA-$F_{2.2}$	60	3.4	53.0	11.3	7.4	4.7	59.2	1.2	16.1	5.8
RA-$F_{2.3}$	79	5.2	15.5	21.4	9.3	9.4	40.8	2.5	16.5	3.0
RA-SN*	-	12.6	0.5	4.9	-	95.1	-	-	-	1.0

W: white grape seeds; R: red grape seeds. M: methanol extracts; A: acetone/water extracts. Yield: mass (g) of PCE extracted from 100 g of grape seed, and also mass (g) of individual fraction obtained from 100 g PCE. $^+$ In parenthesis are the values obtained by FTIR/O-PLS1 regression. * Samples were not used in the FTIR calibration set as they do represent mainly monomeric phenolic compounds.

The concentrations of monomeric (+)-catechin, (-)-epicatechin, and (-)-epicatechin-*O*-gallate were calculated using the calibration curves of **Table 1.3**. Finally, the concentration of procyanidins present in each extract was estimated as a sum of the contributions of each monomer plus their corresponding thioderivative.

The average degree of polymerization of procyanidins in the white grape seed was determined by thiolysis to be 7.4 and 4.2 for methanol and acetone/water PCE extracts respectively, and 6.2 and 7.4 for red grape seed (see **Table 1.5**). These results are in accordance with the ranges reported in literature (Peng *et al.*, 2001; Reed *et al.*, 2005; Le Bourvellec *et al.*, 2006).

The fraction insoluble in water, assigned as WM-F_0 in **Table 1.5**, represents 11.3% of the correspondent WM-PCE mass, which means $21.4 \times 0.113 = 2.42\%$ of the initial mass of white grape seed. It corresponds to a highly polymerized fraction with a *DPn* of 8.8, with flavan-3-ol composition similar to the preceding PCE. However it has low procyanidins content, namely only 8.6% of its total mass. Similar results were obtained for the remaining F_0 fractions.

In order to acquire a rough separation of the procyanidins to get fractions containing lower *DPn*, thus suitable for ESI-MS analysis, the PCEs were dissolved in water and submitted to a liquid-liquid extraction with ethyl acetate (see **Scheme 1.1**). The organic fractions (soluble in ethyl acetate), assigned as F_1 extracts in **Table 1.5**, represent high procyanidin content extracts, especially those obtained from white grape seed with a content of 84.1 and 70.6% for WM-F_1 and WA-F_1, respectively. However, the yields of such fractions are quite low, as they are 8.7 and 5.4%.

The F_1 fractions resulting from the red grape seed were further separated through a C_{18} solid-phase column to get $F_{1.1}$ and $F_{1.2}$ fractions. This process intended to further separate the monomeric fraction (**Table 1.5**, RM-$F_{1.1}$ and RA-$F_{1.1}$) recovered with diethyl ether from the remaining oligomeric procyanidins (**Table 1.5**, RM-$F_{1.2}$ and RA-$F_{1.2}$) further recovered with methanol. Such intention was clearly achieved as the $F_{1.2}$ fractions presented a higher *DPn* of 2.8 and 5.2, respectively for RM-$F_{1.2}$ and RA-$F_{1.2}$, whereas the corresponding $F_{1.1}$ only contained monomeric procyanidins with a representative *DPn* of 1.0.

The aqueous fractions obtained were redissolved in methanol and precipitated with chloroform (the proportion methanol/chloroform used is shown in **Table 1.5** in the column assigned as $CHCl_3$). According to the data in **Table 1.5** an increase in the percentage of chloroform allows to obtain precipitated procyanidin fractions with lower *DPn* (**Table 1.5**, F_2 extracts).

In the whole, the procyanidins content varied from 0.4% in RM-SN to 84.9% in RM-$F_{1.1}$ having an average of 36.0% and standard deviation of 20.9%, thus covering a large range of procyanidin concentrations in the samples (**Table 1.5**). These extracts are composed by the flavan-3-ol

(+)-catechin, (-)-epicatechin, and (-)-epicatechin-*O*-gallate, and by procyanidins (oligomers and polymers) with the same three constituting units. In particular, the procyanidin crude extracts which initially had *DPn* in the range from 4.2 to 7.4 (**Table 1.5**, PCE), after the fractionation process ranged from *DPn* 1.0 to 10.8 (**Table 1.5**, Fractions F_0 to SN). For the majority of the samples, (+)-catechin is the main terminal unit whereas (-)-epicatechin occurs as the main extension unit. The (-)-epicatechin-*O*-gallate unit accounts for 2.4-20.3% of the total procyanidin residues. The $F_{1.1}$ extracts only present terminal units since they correspond to monomers ($DPn = 1$).

The fractions that precipitated in the solutions containing between 73 and 79% (WM-$F_{2.5}$) and between 79 and 84% (WM-$F_{2.6}$) of chloroform from the white grape seed extract, and the fraction that precipitated in the solutions containing between 43 and 60% of chloroform from the red grape seed extract (RM-$F_{2.2}$) were analyzed by ESI-MS. Fraction WM-$F_{2.5}$ accounted for 4.2% of WM-PCE, and had a procyanidin content estimated as 49.2%, and a *DPn* of 5.7; fraction WM-$F_{2.6}$ accounted also for 3.7% of WM-PCE, a procyanidin content was estimated as 43.6% and had a *DPn* of 5.0. Fraction RM-$F_{2.2}$ accounted for 3.0% of RM-PCE, had a procyanidin content estimated as 29.4% and a *DPn* 6.7. These fractions were chosen for analysis by ESI-MS because within polymerized fractions they contained the phenolics with lower *DPn*. These samples were further purified by passage through a C_{18} solid-phase column prior to ESI-MS analyses with the aim to eliminate the presence of sugars.

ESI-MS analysis. The positive electrospray mass spectrum of fraction WM-F2.5 shows the presence of ions between *m/z* 440 and 2000 (**Figure 1.14**). These ions were identified as the protonated molecules, $[M+H]^+$ of different procyanidins. The major ions observed at *m/z* 579, 867, 1155, 1443 and 1731, showing a series with a mass difference of 288 Da, can be attributed to the $[M+H]^+$ type-B procyanidin nongalloylated species, with *DP* between 2 and 6 (P_{2-6}). The ion at *m/z* 577, with 2 mass units less than the corresponding P_2, can be attributed to a $[M+H]^+$ type-A nongalloylated procyanidin (P_2*). The ions at *m/z* 443, 731, 1019, 1307, 1595 and 1883 also belong to a series with a mass difference of 288 Da. These ions correspond to the $[M+H]^+$ ion of type-B procyanidin monogalloylated species, $P_{1-6}G_1$. Sodium and potassium adducts of type-B galloylated and nongalloylated procyanidins, as well as adducts with type-A nongalloylated procyanidins were also observed, although in very low abundance. Other ions in the spectrum correspond to the different combinations of double charged of the procyanidin ions with H^+, Na^+ and K^+ over their *DP* ranges.

The chloroform precipitated samples contained a large percentage of compounds other than procyanidins, especially sugars. After purification by passage through the C_{18} solid-phase column they were constituted mostly by procyanidins, which allows their structural analysis by ESI-MS.

Table 1.6 summarizes the protonated charged ions detected in the ESI-MS spectrum of **Figure 1.14**, their identification, and their abundances in relation to the type-B dimer. The ions observed at *m/z* 883, 1171, 1459, and 1747, showing a mass difference of 288 Da, and having 152 mass units higher than the correspondent $[M+H]^+$ of type-B procyanidin monogalloylated species, can be attributed to the $[M+H]^+$ ions of type-B digalloylated procyanidin series, $P_{2\text{-}5}G_2$.

The ions observed at *m/z* 577, 865, 1153 and 1441 having 2 mass units less than the corresponding $[M+H]^+$ ion of type-B procyanidin nongalloylated series, can be attributed to the $[M+H]^+$ ions of type-A nongalloylated procyanidins, $P_{2\text{-}5}$*. Furthermore, the of ions at *m/z* 729, 1017, 1305 and 1593, can be attributed to the $[M+H]^+$ ions of type-A galloylated procyanidins ($P_{2\text{-}5}G_1$*) whereas the ions at *m/z* 881 and 1169, can be attributed to the $[M+H]^+$ ions of type-A digalloylated procyanidins ($P_{2\text{-}3}G_2$*). All the ions observed in the ESI-MS spectrum of fraction WM-F2.5 of white seed extract were also observed in fraction WM-F2.6 and in fraction RM-F2.2 from the red grape seed extract (**Table 1.6**).

Similar relative abundances are observed for the samples from white and red grape varieties, showing that the structural features reported are not characteristic for a single sample or grape variety but can be attributed to the grape seeds in general.

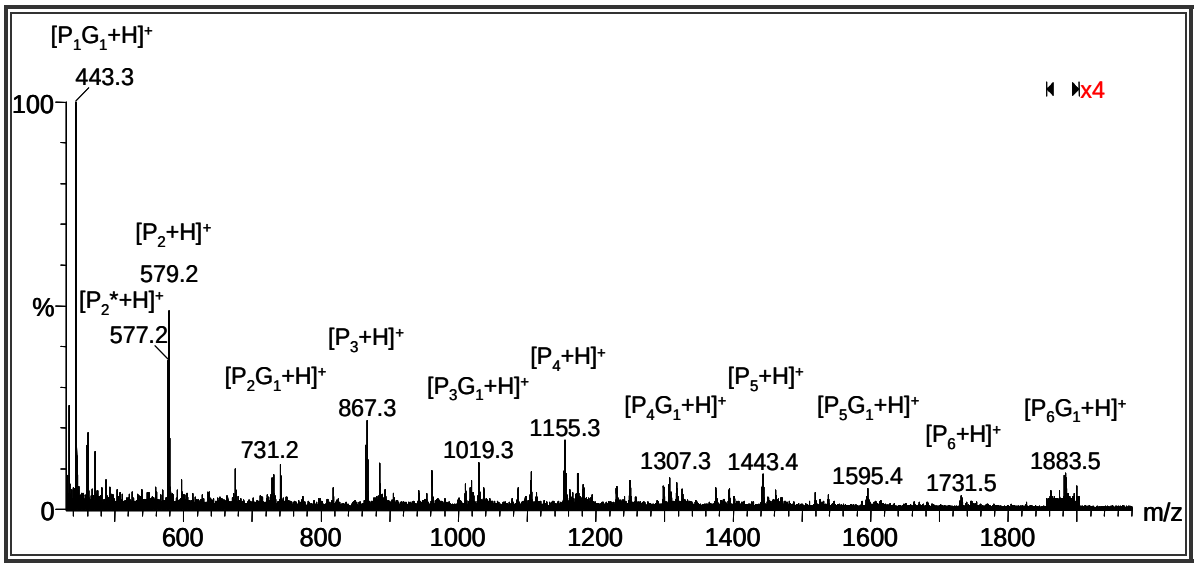

Figure 1.14 – ESI-MS spectrum of fraction WM-$F_{2.5}$ from white grape seeds.
Type-B nongaloyllated procyanidin series: $[P_n+H]^+$, m/z = 290+288*(n-1)+1, (n=2-6); Type-B monogaloyllated procyanidin series: $[P_nG_1+H]^+$, m/z = 290+288*(n-1)+152+1, (n=1-6); Type-A nongaloyllated procyanidin: $[P_2*+H]^+$, m/z 577).

Table 1.6 – Identification of protonated grape seed procyanidins and their abundance in relation to the type-B dimer (m/z=579).

Protonated compound	Type	Molecular weight	Relative abundance in ESI-MS spectra		
			WM-$F_{2.5}$	WM-$F_{2.6}$	RM-$F_{2.2}$
P_1	B	290.1	24	39	59
P_1G_1	B	442.1	229	126	346
P_2	B	578.2	100	100	100
P_2*	A	576.1	73	71	90
P_2G_1	B	730.2	16	16	22
P_2G_1*	A	728.2	15	16	16
P_2G_2	B	882.2	4	4	9
P_2G_2*	A	880.2	6	5	7
P_3	B	866.2	51	70	26
P_3*	A	864.2	30	35	19
P_3G_1	B	1018.2	15	19	10
P_3G_1*	A	1016.2	12	13	9
P_3G_2	B	1170.2	4	6	4
P_3G_2*	A	1168.2	tr	tr	tr
P_4	B	1154.3	33	49	10
P_4*	A	1152.3	23	20	8
P_4G_1	B	1306.3	13	17	8
P_4G_1*	A	1304.3	10	7	6
P_4G_2	B	1458.3	4	6	tr
P_5	B	1442.3	17	23	5
P_5*	A	1440.3	10	8	5
P_5G_1	B	1594.3	10	9	tr
P_5G_1*	A	1592.3	5	5	tr
P_5G_2	B	1746.4	tr	tr	tr
P_6	B	1730.4	6	8	tr
P_6G_1	B	1882.4	4	4	tr

P_nG_m – Molecule with *n* monomeric units and *m* galloylated units; tr – traces (lower than 4%); * Type-A procyanidins.

Type-A procyanidins are present as nongalloyated as well as mono- and digalloyated (P_nG_m, where $n = 2 – 5$ and $m = 0 – 2$; consult **Table 1.6**). Nongalloylated and monogalloylated account for 50-90% of the corresponding type-B ions (**Figure 1.15a**).

This abundance seems to be independent of the occurrence of galloylation. Also the abundance of type-A in relation to type-B tends to decrease as the degree of polymerization of the oligomers increases. Monogalloylated dimers accounted for 20% of the corresponding nongalloylated dimers independently of the interflavanic linkage (**Figure 1.15b**).

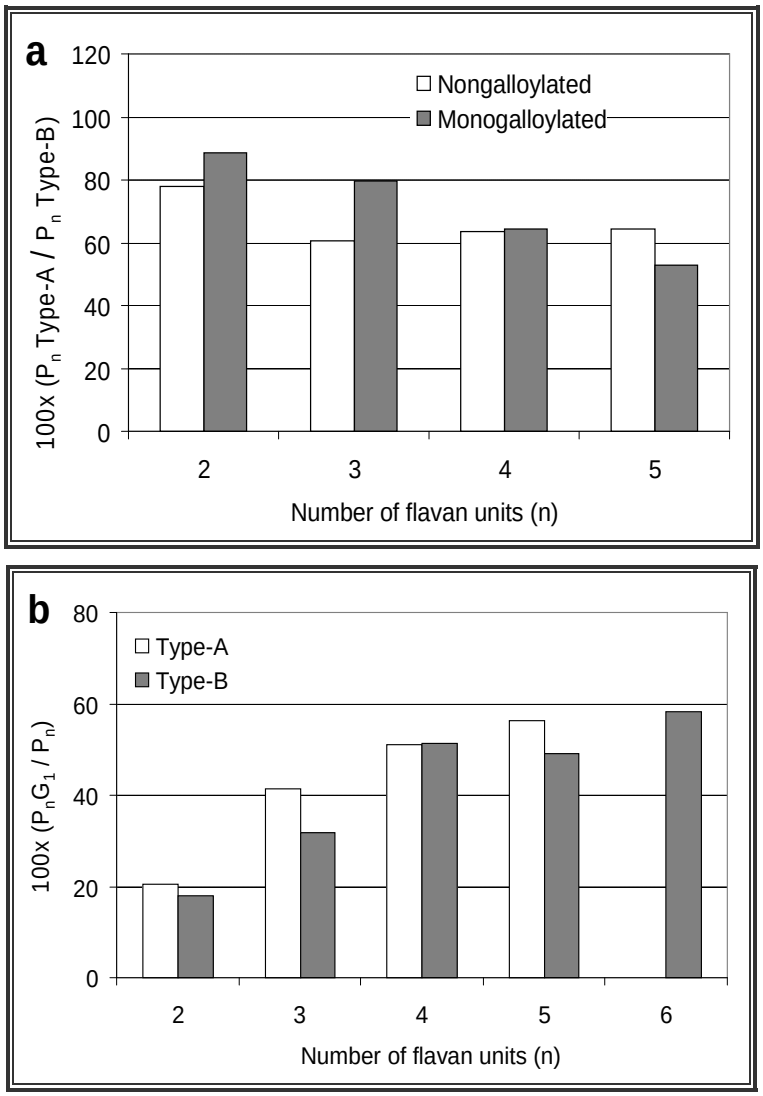

Figure 1.15 – Relative abundance of procyanidin oligomers present in fractions WM-F2.5, WM-F2.6, and RM-F2.2. (a) Type-A/Type-B; (b) monogalloylated/nongalloylated.

The abundance of monogalloylated oligomers observed in the ESI-MS spectra showed a tendency to increase with increasing *DPn* reaching almost 60% of the abundance of the corresponding nongalloylated oligomers (**Figure 1.15b**).

According to the literature type-A procyanidins were not found in the grape seeds extracts analyzed by ESI-MS in positive (Gabetta *et al.*, 2000) or negative modes (Flamini, 2003, Hayasaka *et al.*, 2003). This might be due to the sample complexity and instrumental conditions used by other authors. In our work, the fractionation steps used could have been determinant for a higher homogeneity of the highly soluble chloroform fractions obtained from PCE, resulting in more informative spectra, and allowing reporting for the first time the occurrence of type-A procyanidins as components of grape seeds. This is also in accordance with the results presented by Krueger *et al.* (2000) that showed an unattributed $[M+Na]^+$ ion at *m/z* 1175 in a MALDI-TOF mass spectrum

resulting from a purified grape seed extract that could correspond to a nongalloylated type-A procyanidin tetramer (P_4*). Further analyses (e.g., MS/MS) able to confirm its presence at that time were however lacking. Tandem mass spectrometry of the identified ions was performed in this work in order to confirm the occurrence of type-A in grape seed procyanidins, as well as the occurrence of type-A galloylated procyanidins, which have also never been reported.

Tandem mass spectrometry (ESI-MS/MS) analysis. The MS/MS spectrum of a trimer with a type-A interflavanic linkage, $[P_3^*+H]^+$ ion, at *m/z* 865 is shown in **Figure 1.16**.

The major fragment at *m/z* 577 is presumably formed by cleavage of the Type-B interflavan bond through a Quinone-Methide (QM) cleavage (Gu *et al.*, 2003a) with loss of a neutral fragment with 288 Da corresponding to the elimination of an extension unit (Flamini, 2003). The elimination of an extension unit gives rise to a fragment ion with larger π–π hyperconjugated system than any of the other units being more energetically favourable (Gu *et al.*, 2003a). The complementary fragment ion at *m/z* 289 formed by the same QM fragmentation with the charge retained in the extension unit (**Scheme 1.2**) is also observed.

Fragment ions at *m/z* 847, 695, 559, 407 and 271 have resulted from the loss of water from ions at *m/z* 865, 713, 577, 425 and 289 (**Scheme 1.2**). These results are in accordance with the fragment paths from $[M-H]^-$ proposed by Gu *et al*. (2002) for proanthocyanidins.

Type-A fragmentation paths except for the fragments containing double linkage were the same as for the well characterized type-B molecules (Karchesy *et al.*, 1986).

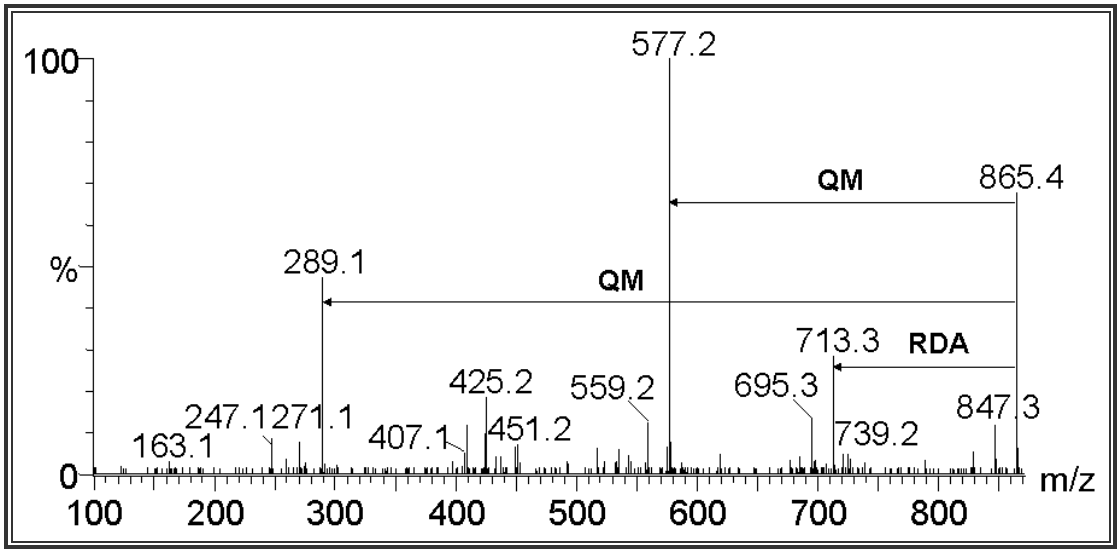

Figure 1.16 – ESI-MS/MS spectrum of type-A procyanidin $[M+H]^+$ ions of a trimer (P_3*). Fragmentations: Quinone-Methide (QM); Retro-Diels-Alder (RDA).

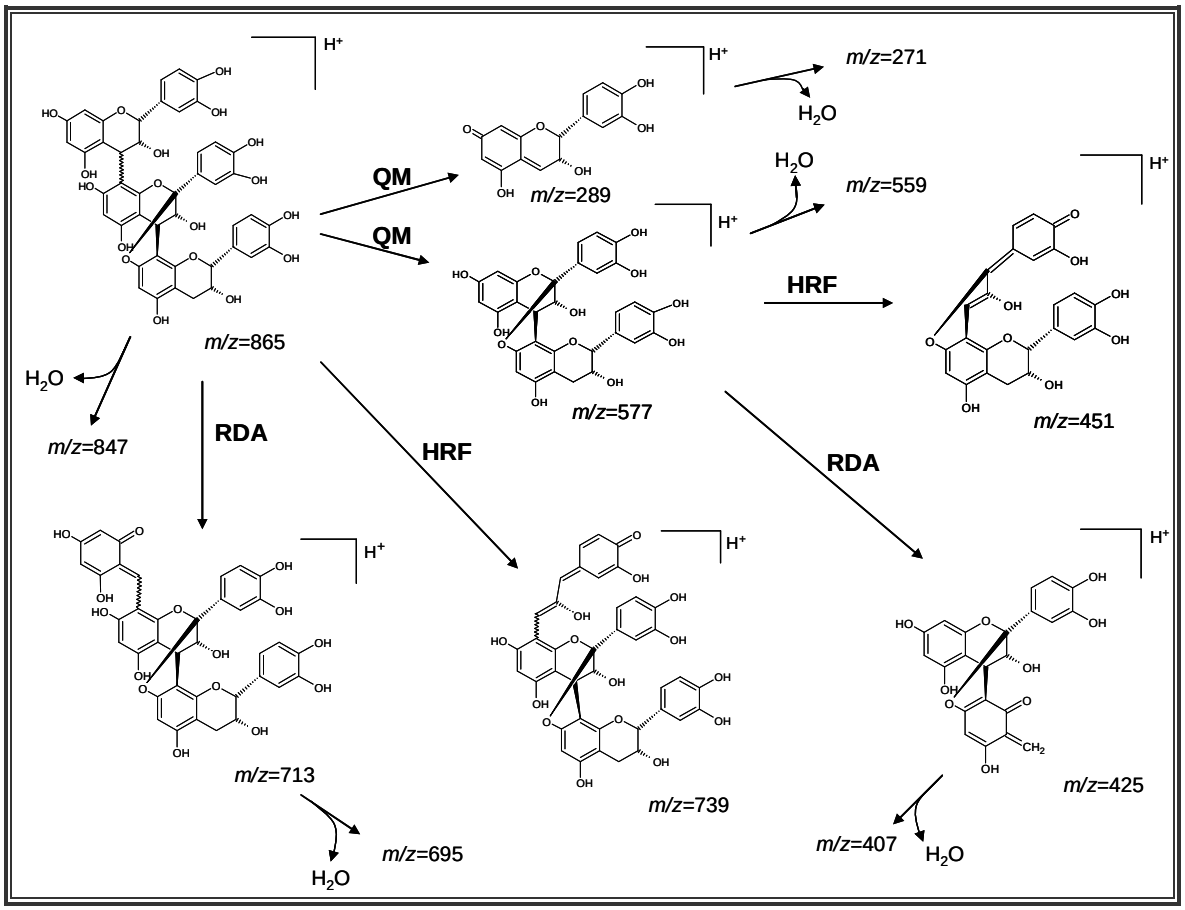

Scheme 1.2 – ESI-MS/MS fragmentation pathways of a type-A procyanidin trimer $[P_3{*}+H]^+$. Fragmentations: Quinone-Methide (QM); Retro-Diels-Alder (RDA); Heterocyclic-Ring-Fission (HRF).

Figure 1.17 shows the MS/MS spectrum of a trimer with a monogalloylated type-A procyanidin, $[P_3G_1{}^*+H]^+$ ion, at *m/z* 1017.

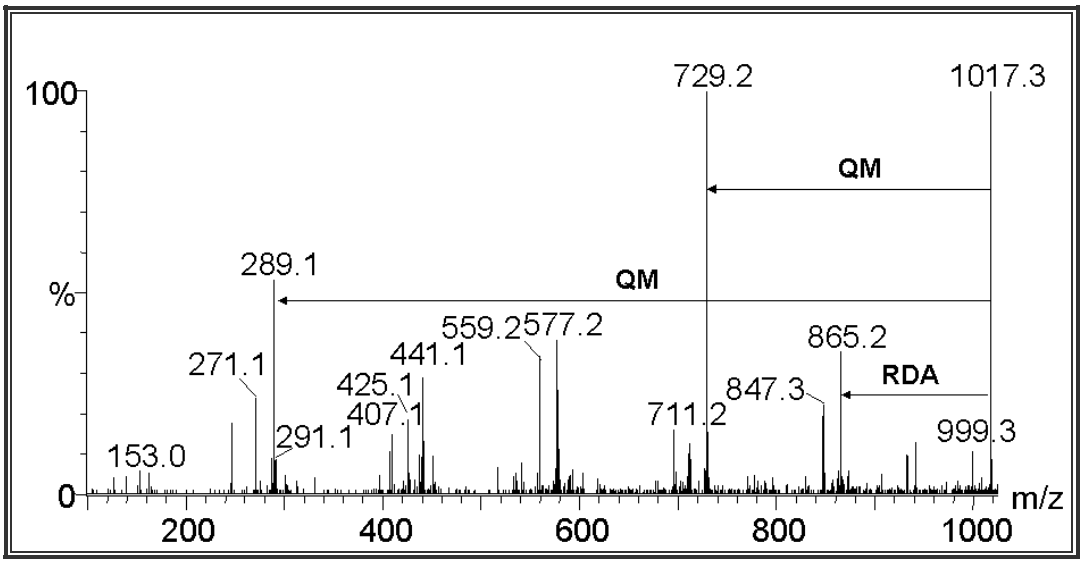

Figure 1.17 – ESI-MS/MS spectra of type-A procyanidin $[M+H]^+$ ions of a monogalloylated trimer ($P_3G_1{*}$). Fragmentations: Quinone-Methide (QM); Retro-Diels-Alder (RDA).

The fragment ions at *m/z* 729 and 289 resulting from losses of 288 (extension flavan unit) and 728 Da (terminal galloylated type-A dimer) can be attributed to the QM cleavage of the type B interflavan bond showing that the gallic acid residue occurs in the type-A moiety of the trimer. The loss of a gallic acid residue (-152 Da) and a gallic acid unit (-170 Da) from this type-A moiety (*m/z* 729) can originate the ions at *m/z* 577 and *m/z* 559, respectively.

The fragment ions at *m/z* 577 and 441 can also be attributed to the QM cleavage of the type-B interflavan bond resulting from the loss of a procyanidin residue esterified with gallic acid showing that the gallic acid residues can also occur in the type-B moiety of the molecule (**Scheme 1.3a**). These fragment ions allowed to infer that different galloylated isomers are present. Furthermore, the presence of fragment ions at *m/z* 291 and 727 allow inferring also the existence of the type-A bound residues as extension units.

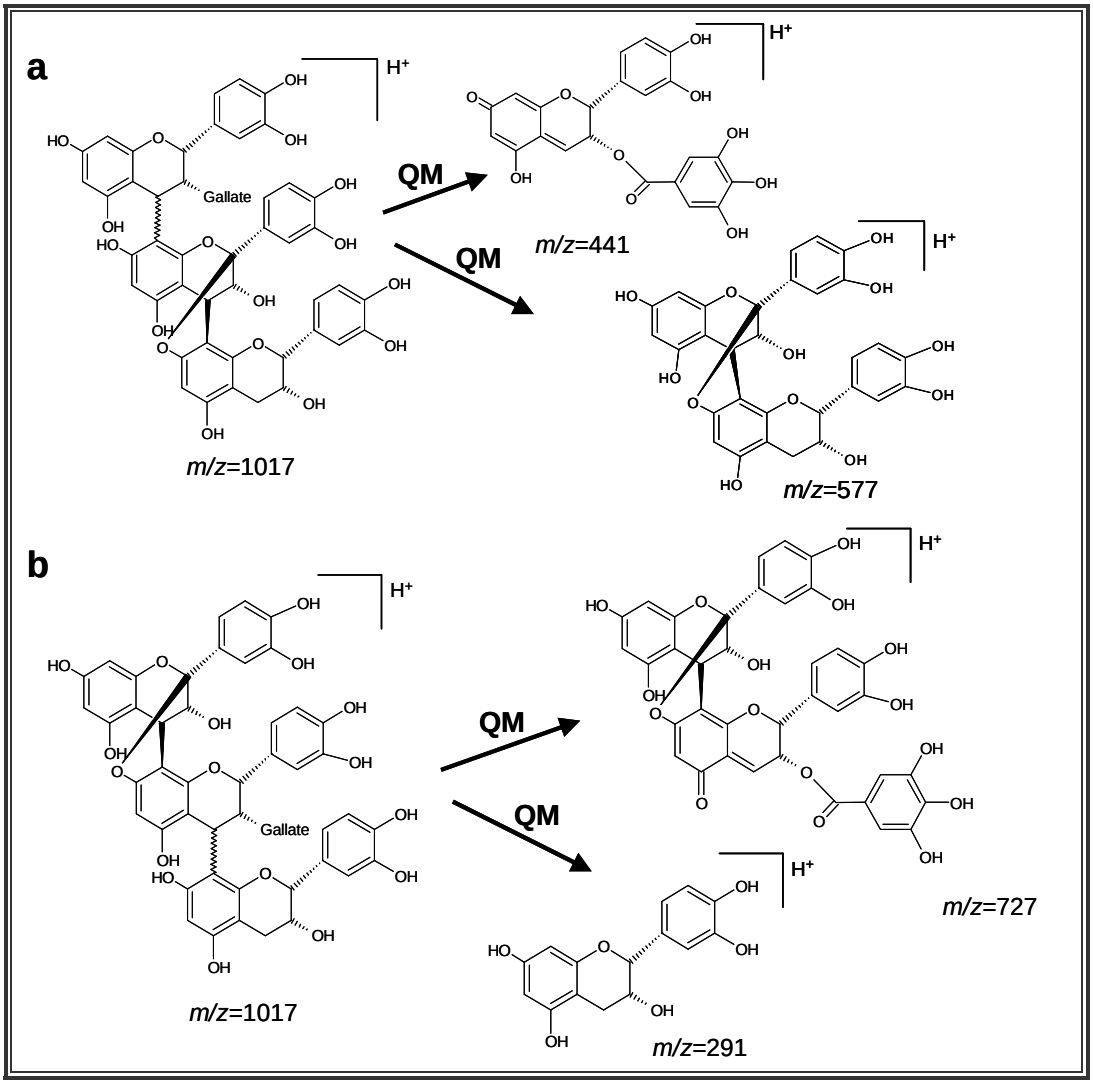

Scheme 1.3 – ESI-MS/MS Quinone-Methide fragmentation pathway of a monogalloylated type-A procyanidin trimer $[P_3G_1*+H]^+$ containing a type-B unit. (a) Terminal type-A unit; (b) Extension type-A unit.

Scheme 1.3b shows one of the two isomers that can be attributed to these type-A extension units. The other possible isomer contains galloylated residue in the other monomeric type-A unit. According to Gu *et al.* (2003b) the cleavage between the middle and the terminal unit is unique for type-A as it converts the hydroxyl group on C5 of the middle unit into a quinone (**Scheme 1.3b**) in contrast to C7 as the preferred conversion site in all other cases (**Scheme 1.3a**). This generates an unique complete monomeric nongalloylated unit at *m/z* 291 (**Scheme 1.3b**) or a galloylated unit at *m/z* 443 for the $[M+H]^+$ ions under study. However, the absence of the fragment ion at *m/z* 443 in the MS/MS spectrum of the $[P_3G_1^*+H]^+$ ion (**Figure 1.17**) allows to conclude that this molecule is not composed by a type-B galloylated procyanidin residue as a terminal unit. Instead the presence of the ions 577 and 441 **(Figure 1.17)** implies the existence of a type-A procyanidin terminal unit similar to **Scheme 1.3a**.

The fragment ion at *m/z* 865 resulting from a loss of 152 Da can be attributed to RDA fragmentation or to the loss of a gallic acid residue from the $[M+H]^+$ ion at *m/z* 1017. The fragment ion at *m/z* 425 can be attributed to a RDA fragmentation with a loss of 152 Da from the ion at *m/z* 577. Fragment ions at *m/z* 999, 847, 711, 559, 407 and 271 are resulting from the loss of water from ions at *m/z* 1017, 865, 729, 577, 425 and 289.

The MS/MS spectrum of a dimer with a digalloylated type-A procyanidin, $[P_2G_2^*+H]^+$ ion at *m/z* 881 is shown in . The major fragment ion is observed at *m/z* 711 resulting from a loss of a gallic acid unit (-170 Da). The presence of the ion at m/z 729 can be attributed to a loss of a gallic acid residue (-152 Da). Loss of a second gallic acid residue/unit is also observed with formation of the ions at *m/z* 559/541. RDA fragmentation leads to the ion at *m/z* 577 through the loss of 304 Da (-152+gallic acid residue). The opening of the (C4-C8)-(C2-C7) ring of the P_2G_2* dimer enables the occurrence of the fragment ions at *m/z* 441 due to the loss of 440 Da corresponding to the galloylated monomer from $[M+H]^+$ and the fragment ion at *m/z* 289 resulting from a loss of a gallic acid residue (152 Da) from the galloylated monomer fragment at *m/z* 441.

Type-A interflavan bonds do not undergo observable QM cleavage in the presence of a type-B interflavan bond as reported by Gu *et al.* (2003b) and observed in this work for the trimer procyanidin structures (**Figures 1.16** and **1.17**). However, QM cleavage can be observed in type-A dimers () as was also described by Karchesy *et al.* (1986). Fragment ions at *m/z* 863, 693, 541, 423 and 271 are resulting from loss of water from ions at *m/z* 881, 711, 559, 441 and 289 respectively.

Sample WM-F2.6 was subjected to thiolysis, after which the galloylated derivatives were separated and analyzed by HPLC-MS, in order to study the position of the galloylated type-A in the backbone of grape seed procyanidins.

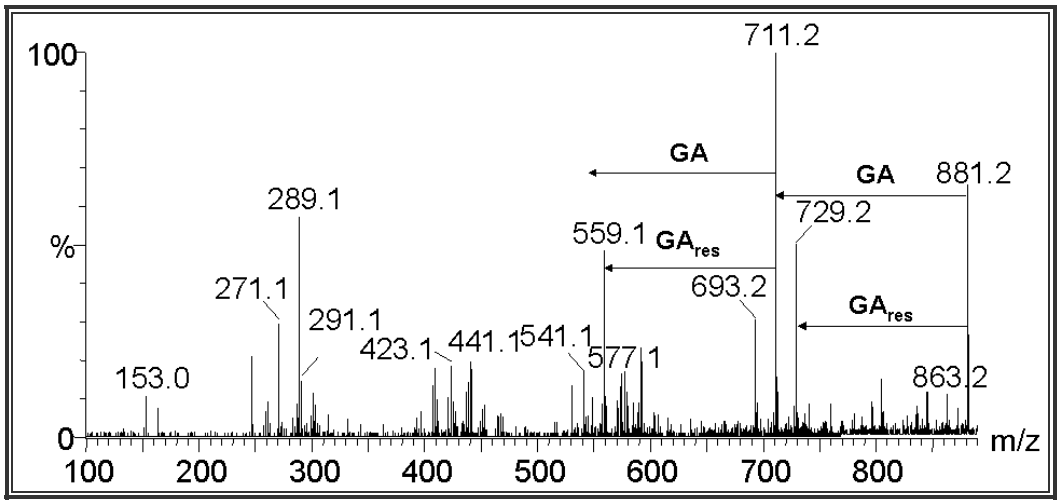

Figure 1.18 – ESI-MS/MS spectra of type-A procyanidin $[M+H]^+$ ions of a digalloylated dimer (P_2G_2*). Fragmentations: Loss of gallic acid unit (GA); Loss of gallic acid residue (GA_{res}).

Analysis of galloylated procyanidin derivatives after thiolysis. The corresponding LC-MS mass spectrum of peak 9 in **Figure 1.13** for HPLC-UV, where the polymeric galloylated procyanidins and their thioderivatives eluted, is shown in **Figure 1.19**. The mass spectrum shows the presence of ions between *m/z* 100 and 1500. The main ion observed in the spectrum with *m/z* 565 can be attributed to the thioderivative of (-)-epicatechin-*O*-gallate monomer (P_1G_1). The higher abundance of this ion compared to the $[P_2G_1+thiol+H]^+$ dimer with *m/z* 853 allows inferring that the thiolysis reaction had a high level of efficiency. Also, the occurrence of a small peak attributed to type-A procyanidin dimers and the absence of type-B procyanidin dimers observed after thiolysis in the LC-MS chromatogram confirm the resistance of type-A linkages to thiolytic degradation when compared to type-B.

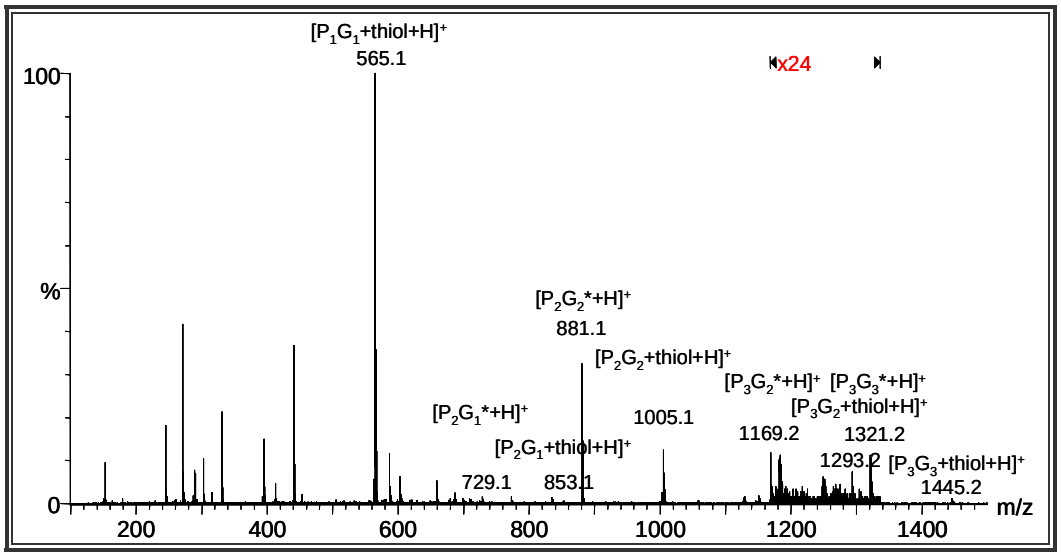

Figure 1.19 – LC-MS mass spectrum of galloylated procyanidin derivatives obtained after thiolytic degradation. * Type-A procyanidins.

The presence of type-A interflavan linkages prevents the interflavanic cleavage due to the existence of the C2-C7 ether bond bridge. The type-A terminal units are released as dimers whereas the type-A extension units are released as benzylthioether type-A dimers (Gu *et al.*, 2003a). The ions at *m/z* 881 and 1005 can be attributed to type-A digalloylated procyanidin dimer (P_2G_2*) and type-B digalloylated procyanidin dimer associated with a thiol group (P_2G_2+thiol), respectively.

Although in very low abundance, a type-A monogalloylated procyanidin dimer (P_2G_1*) at *m/z* 729, a type-A digalloylated procyanidin trimer (P_3G_2*) at *m/z* 1169 and a type-B digalloylated procyanidin trimer associated with a thiol group (P_3G_2+thiol) at *m/z* 1293 were also observed. The ions at *m/z* 1321 and *m/z* 1445 can be attributed to the trigalloylated type-A trimer (P_3G_3*) and trigalloylated type-B trimer thioderivative (P_3G_3+thiol), respectively. The presence of dimers and trimers with high levels of galloylation allows inferring that although the thiolysis reaction had high efficiency it did not cleave all the interflavanic linkages. This fact is possibly due to a higher resistance of these structures to thiolysis conferred by the presence of the high amount of gallic acid residues. This observation shows that the DP values of highly galloylated procyanidins by thiolysis could be underestimated.

In this spectrum all type-B procyanidin ions occurred as thioderivatives whereas all type-A procyanidin ions occurred without the thiol group. These results were also observed in the nongalloylated procyanidins spectra separated by LC-MS (data not shown), which allows to conclude that the type-A interflavanic linkages were present in the terminal flavan units whereas the type-B interflavanic linkages were present as extension units. This is in accordance with the observations based on the MS/MS spectrum shown in **Figure 1.16**. The extension type-A interflavan linked units detected in the spectrum of **Figure 1.17** seems to occur as small features that were not detected by thiolysis. The occurrence of type-A units only as terminal interflavan linkages has already been detected in plums, whereas the occurrence of type-A units only as extension interflavan linkages has been detected in avocado, curry and cinnamon. Both structures were identified in cranberry and peanuts (Gu *et al.*, 2003a).

FTIR characterization. The characteristic wavelengths related to the phenolic compounds are associated to the presence of an OH band between 3600-3200 cm^{-1}. Also, they show aromatic, ester, alcohol, and ether bands in the region between 1800-700 cm^{-1}. All spectra have a similar profile (**Figure 1.10**) and, according to the literature (Ramos-Tejada *et al.*, 2002; Contreras-Domínguez *et al.*, 2006), changes in the procyanidins aromatic ring bands are expected to occur in this spectral region.

Calibration model for *DPn* procyanidin calculations in grape seed extracts using PCT-PLS1 (principal component transform and partial least squares regression). Using the 1800-

700 cm^{-1} region of the FTIR spectra of the procyanidin extracts compiled in **Table 1.5**, a PLS1 regression procedure was applied to the estimation of their *DPn*. A calibration model with 8 Latent Variables (LVs) using an internal-cross validation (leave-5-out) procedure was calculated by PCT-PLS1. The relative Root Mean Square Error of Cross Validation (RMSECV) obtained was 11.7%, with a coefficient of determination (R^2) of 0.91 and a Root Mean Square Error of Prediction (RMSEP) of 2.58. However, the relative high number of LVs and the relatively high RMSECVs in the previous model introduce difficulties in the interpretation of the **b** vector profiles. In fact, the scores scatter plot between the first PLS1 component of scores X (**t**) and scores Y (**u**) shows that there is not much correlation between **t** and **u** for the first PLS1 component (**Figure 1.20a**); while the **y** variance explained by this PLS1 regression model shows some irregularity concerning LV2 (**Table 1.4**) indicating that there are variations in the FTIR spectra that are not related to *DPn* and will hindered the regression vectors interpretation. In these cases, one approach is to remove from the model all spectra variations orthogonal to the factor of interest (*DPn*). One such method is the O-PLS (Trygg and Wold, 2002). Therefore, this procedure was applied with the aim of improving the interpretation of the PLS1 regression model by removing orthogonal artefacts not related to the *DPn* profile. Nonetheless, it should be noted that O-PLS method does not improve the robustness of a calibration model.

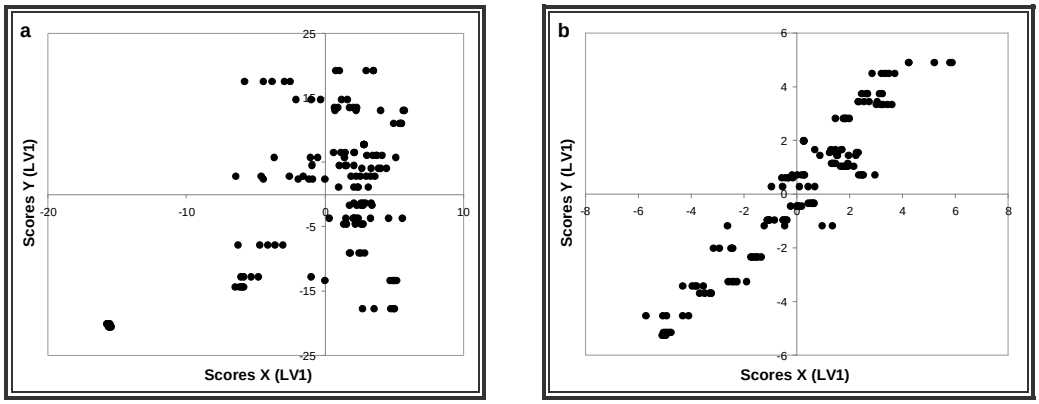

Figure 1.20 – First PLS1 component t-u scores plot for (a) the original PCT-PLS1 model and (b) the O-PLS pre-treated PCT-PLS1 model using the 1800-700 cm^{-1} region.

Calibration model for *DPn* procyanidin calculations using O-PLS. The O-PLS was applied to remove orthogonal systematic variations from the spectra with respect to the *DPn* values. In order to assess if the chosen model can be considered robust, it was compared to the dimensionality given by Monte Carlo cross-validation (data not shown). The Monte Carlo cross-validation indicated seven O-PLS components to be removed from the regression model resulting into a one LV predictive PCT-PLS1 model for calibration/interpretation purposes. This procedure has removed 88% of non correlated variations present in FTIR spectra. For this model, the scores scatter plot between the first PLS1 component of scores X (**t**) and scores Y (**u**) presents a clear

correlation between **t** and **u** for the first PLS1 component (**Figure 1.20b**), indicating that the variations in the FTIR spectra can now be related to the *DPn* in a much simpler way. The regression model obtained presented a relative RMSECV of 8.6%, with a R^2 of 0.95 and a RMSEP of 2.58 (**Figure 1.21a**), which shows that it is not significantly different from the PLS1 model with eight LVs.

Validation of O-PLS1 model for estimation of procyanidin *DPn*. In order to validate the regression model obtained for the estimation of the procyanidins *DPn* using the O-PLS model (**Figure 1.21a**), the procyanidin crude extracts (PCE) were used. The results show that similar values were obtained using the FTIR/O-PLS1 calibration curve and measured by the thiolysis/HPLC procedures (see **Table 1.5**, *DPn* column). Such evidence is even more important considering that the PCE extracts represent a more complex matrix than the fractionated extracts, allowing inferring that this approach can be an useful tool for the estimation of *DPn* in non purified extracts.

Molecular features relating the infrared absorbance characteristics and procyanidins *DPn*. **Figure 1.21b** shows the **pp** vector profile of the O-PLS/PCT-PLS1 regression model where it is possible to identify the most important bands related to the *DPn* value. Since this model was built using one LV, its interpretation is easier than the previous eight LV PCT-PLS1 model.

The observation of the positive peaks at 1203 and 1099 cm^{-1} suggests a possibility to assess the *DPn* of procyanidins by monitoring the aromatic substitutions. The 1,2-disubstitutions on the aromatic rings have been related with the existence of three peaks (two medium and one strong) in the range of 1200-900 cm^{-1}, whereas the 1,3-disubstitutions on the aromatic rings have been related with the existence of four peaks (two medium and two strong) in 1100-700 cm^{-1} range (Ramos-Tejada *et al.*, 2002).

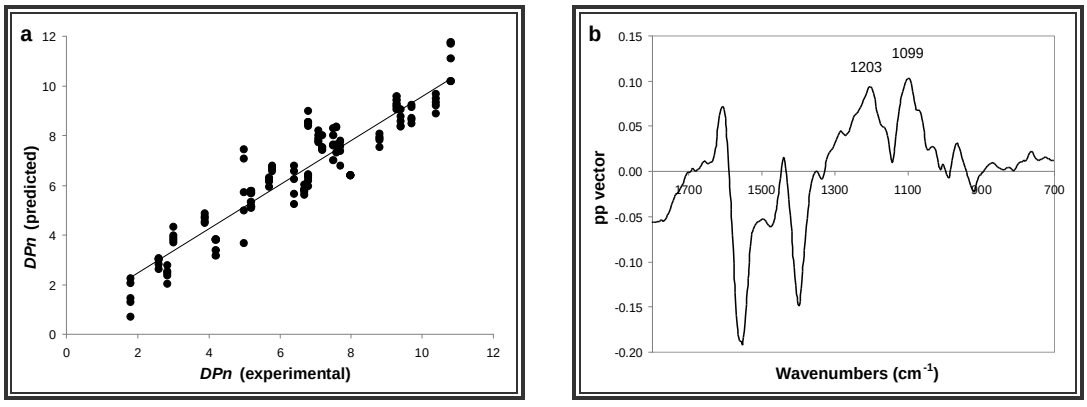

Figure 1.21 – Regression model for estimation of procyanidin *DPn*. (a) Relationship between *DPn* values estimated by FTIR/O-PLS1 and experimentally determined by thiolysis/HPLC; (b) O-PLS pp vector profile with one LV.

As previously discussed, the *DPn* is obtained by the balance between one terminal and several extension units. If considering the molecular structure of a dimer, such as the one generically represented in **Figure 1.22**, which comprises two flavan-3-ol residues (one terminal and one extension unit) bonded by an interflavanic linkage, each flavan-3-ol residue is composed by two aromatic rings (A and B) and a non-aromatic ring (C). The hydroxyl groups on ring A occur in C5 and C7, resulting in a 1,3-disubstitution (meta-substitution), whereas on B ring, the hydroxyl groups occur in C3' and C4', forming a 1,2-disubstitution of the aromatic ring (ortho-substitution). The interflavanic linkage between the two composing units of the dimer originates an extra C7-C8 ortho-substitution of the aromatic ring A of the terminal unit of the procyanidin. In total, a dimeric procyanidin with a *DP* = 2, formed by two flavan-3-ol units, has one meta-substitution and one ortho-substitution per unit plus one ortho-substitution due to the bond formed between the two composing units. In general, a procyanidin formed by *n* flavan-3-ol units (*DP* = *n*), has [*n*+(*n*-1)] 1,2-disubstitutions and *n* 1,3-disubstitutions. As a consequence, the ratio 1,2-disubstitutions/1,3-disubstitutions can be expressed by the following formula: [(2*n*-1)/*n*].

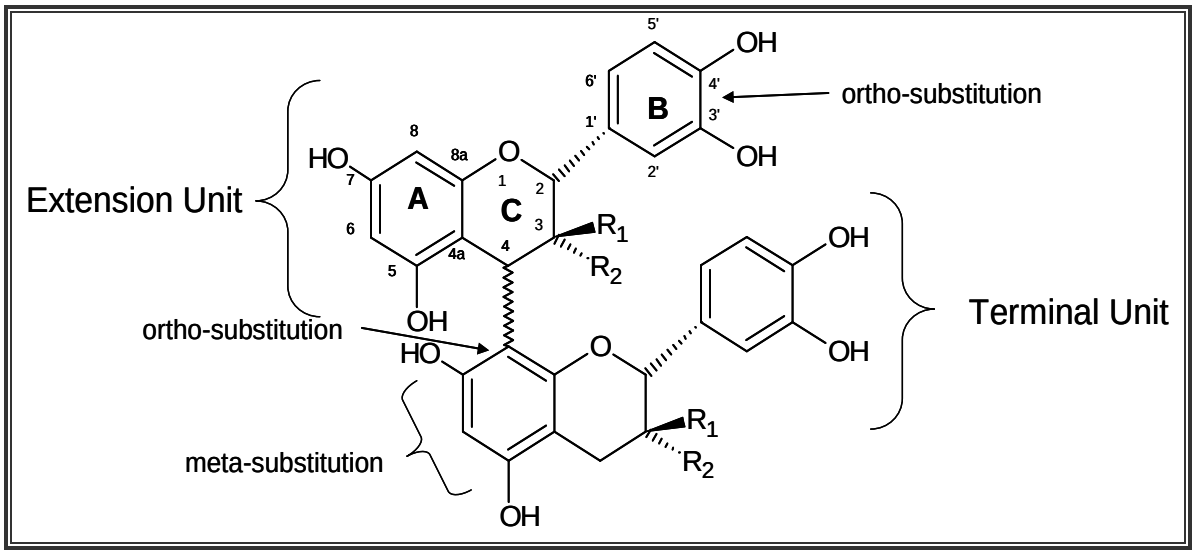

Figure 1.22 – Type of substitutions in a procyanidin dimer containing a C4-C8 interflavanic linkage.

Relation of procyanidins *DPn* and solubility in methanol/chloroform solutions. **Figure 1.23** shows the relationship between the solubility of procyanidins in methanol/chloroform solutions and their average degree of polymerization. The material that precipitate in solutions of approximately 43% chloroform tend to have a *DPn* of 8-10, the material that precipitate in solutions near 60% chloroform tend to have a *DPn* of 6-7, and the samples that precipitate in solutions in the order of 80% chloroform tend to have a *DPn* of 4-6. The samples that do not precipitate in these solutions contain mainly flavan-3-ol or, at least, procyanidin dimers (**Table 1.5**, SN extracts).

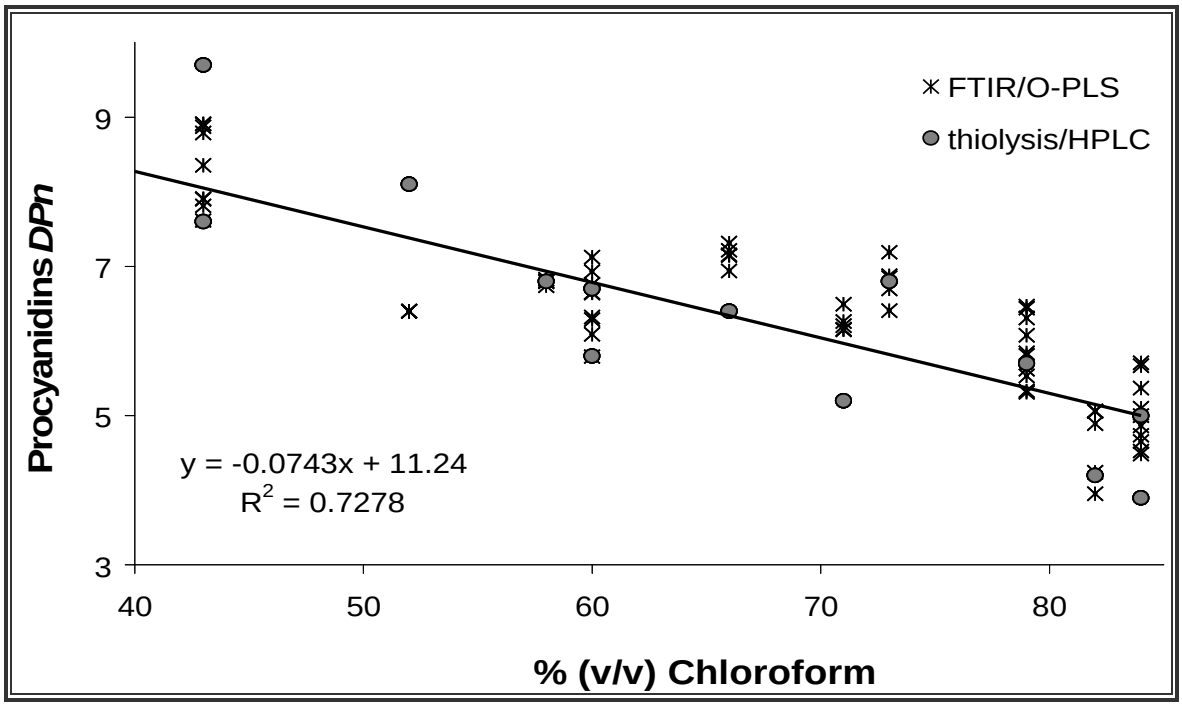

Figure 1.23 – Procyanidin *DPn* of fractions $F_{2.1}$ to $F_{2.6}$ estimated by FTIR/O-PLS (correlation) and measured by thiolysis/HPLC (experimental data) *versus* the concentration of the methanol/chloroform solution which precipitates each fraction.

The graded precipitation in methanol/chloroform solutions is a simple and quick method to evaluate the *DPn* of procyanidins in a fraction, as well as a rough but suitable methodology to recover enriched fractions of procyanidins with a defined degree of polymerization that can be used, for example, in industry. In this work, the precipitation methodology was an undoubtedly important step in order to obtain samples for performing a suitable calibration/validation data set.

1.3.2. Antioxidant capacity (AOC)

The most commonly used standard compounds in the AOC study of phenolics are (+)-catechin and ascorbic acid. Our results showed that (+)-catechin is slightly more efficient than ascorbic acid, and it will be used for comparison during the following discussion.

AOC of the fractionated extracts. All the extracts previously characterized (**Table 1.5**) were tested for the AOC as presented in **Figure 1.24**. All extracts, except the supernatant (SN in **Table 1.5**), presented a high activity profile compared to the pure (+)-catechin. The low activity associated to the supernatant extracts can be explained by their low content of phenolic compounds (less than 14%) (**Table 1.5**). No influence of the extracting solvent on the AOC was observed as both methanol and acetone/water extracts showed similar antioxidant activity. Such similarity is in agreement with the similar *DPn* and composition given by the HPLC analyses (**Table 1.5**) obtained using either methanol or acetone/water solvents.

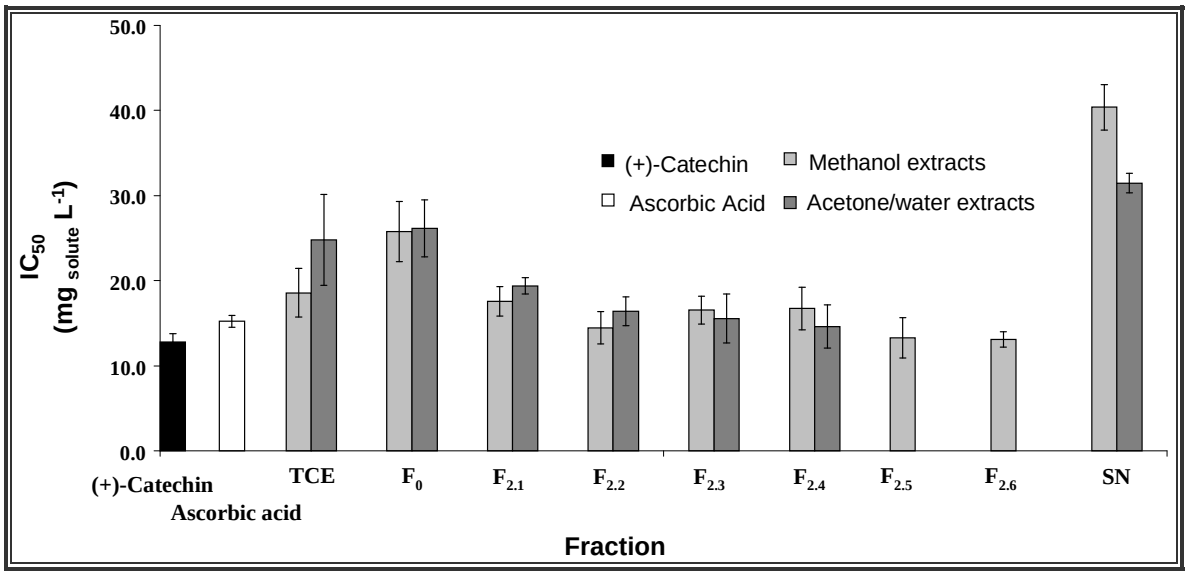

Figure 1.24 – Scavenging activity of (+)-catechin and ascorbic acid (standards), and both methanol and acetone/water extracts of phenolic compounds obtained in the year of 2006.

Effect of storage. It is believed that phenolic antioxidant activity also depends on the storage conditions decreasing under effect of temperature, oxygen and/or light. The lack of data concerning the influence of long-term storage on the antioxidant capacity of these compounds leads to the following investigation.

The extracts stored in the dark at room temperature for approximately 1 year did not show significant changes in their AOC. Furthermore, even a slight increase in the AOC of most methanol and acetone/water extracts was observed after one year of storage (**Figure 1.25**). Both decrease and increase of the phenolic compounds activity during storage were reported. But, while most literature assumes that the decrease in the AOC is due to the compounds oxidation with consequent loss of activity, the work by Talcott *et al.* (2000), later referred by Kaur and Kapoor (2001), shows that the antioxidant properties of polyphenols may change depending on their oxidation state. Polyphenols with an intermediate oxidation state may exhibit higher radical scavenging activity than non-oxidized polyphenols. The higher antioxidant activity of the partially oxidized polyphenols could be attributed to their increase ability to donate a hydrogen atom from the aromatic hydroxyl group to a free radical and/or to the capacity of their aromatic structure to support unpaired electrons through delocalization around π-electron system. Therefore, partial oxidation of the polyphenols during their storage can thus lead to the formation of the compounds with higher AOC.

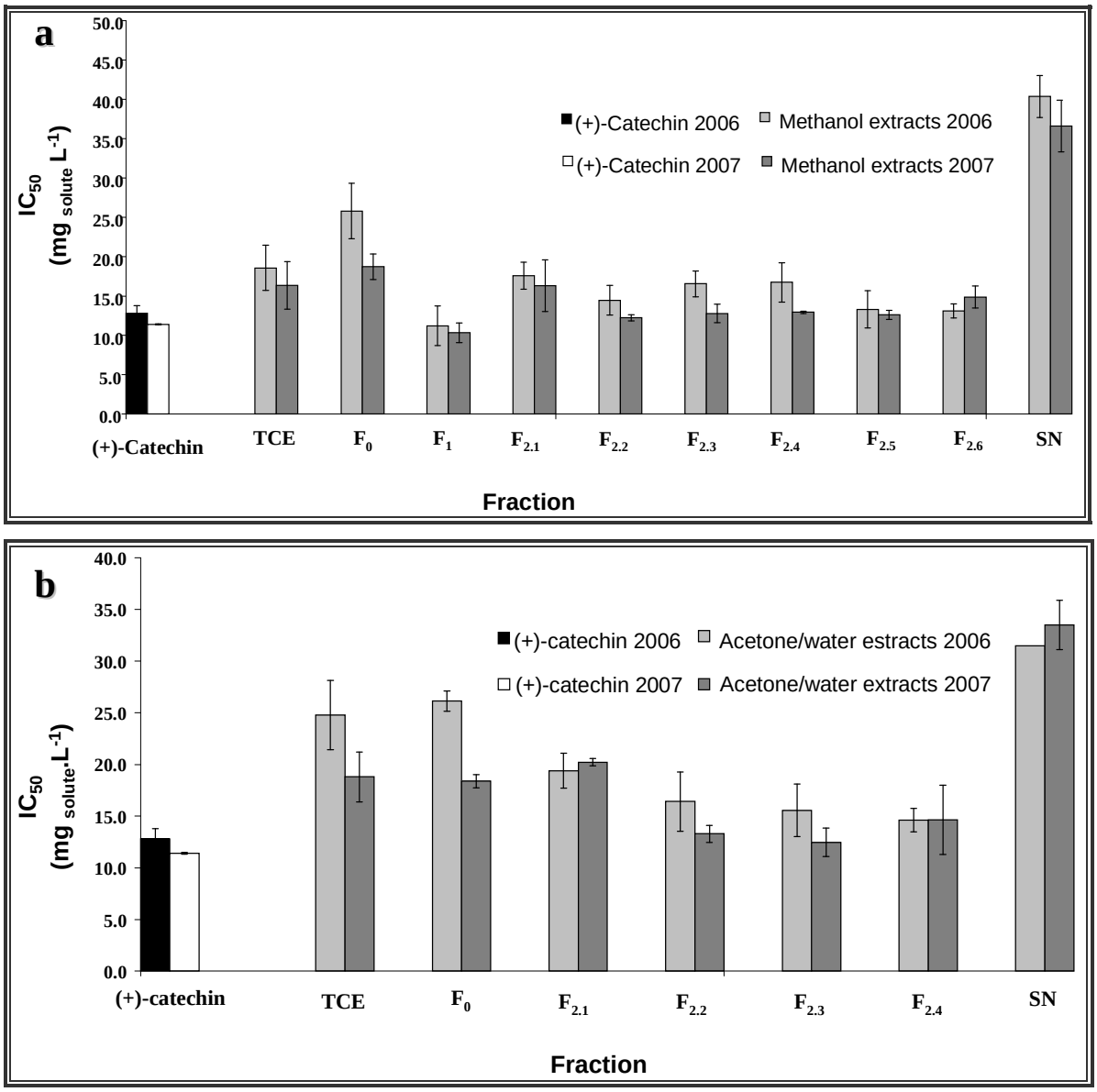

Figure 1.25 – Effect of storage on the antioxidant activity of: (a) methanol and (b) acetone/water extracts from grape seeds.

2. Enzymatic Pre-treatment

The dictionary is the only place that success comes before work.
[Vince Lombardi]

2. Enzymatic Pre-treatment

This chapter focuses on the enzymatic pre-treatment of grape seed. The grape seed is subjected to an enzymatic pre-treatment prior to the oil extraction with the aim of improving the extraction yield. This pre-treatment partly destroys seed internal structure facilitating solvent penetration to otherwise inaccessible oil containing areas.

The most common conventional unitary process for improving extractability is milling since it breaks down the vegetable cells and therefore augments available oil, and interfacial area for mass transfer. However, applying only mechanical treatment can be inefficient not allowing an extensive oil removal. Additionally, extended milling of the seeds produces fine powders, which is not desirable in the industrial process. Partial hydrolysis of the cell walls by means of appropriate enzymes has been indicated as an alternative approach for enhancing oil recovery (Fullbrook, 1983).

A range of conditions for the enzymatic treatments was employed in different studies including different levels of pH, enzyme concentration, temperature, reaction time, particles size, etc. However none of the previous studies considered the effects of all these parameters on the extraction outcome (several examples were given in the review by Rosenthal *et al.* (1996)). This chapter is dedicated to the analysis of the influence of all the parameters mentioned on the extraction yield. The results obtained will be further use in combination with more environmentally friendly extraction methodologies such as the supercritical extraction.

2.1. Introduction

2.1.1. Cell wall composition

The success of the enzyme application inherently depends on the knowledge of seeds' composition. Plant cell walls are composed of carbohydrate polymeric molecules. The primary cell wall is an amorphous matrix of pectic polysaccharides: - hemicelluloses which are mixed with proteins and cellulose microfibrils; - while in the secondary wall cellulose and hemicellulose together with lignin prevails (Dominguez *et al.,* 1994; Copeland and McDonald, 1995; Sineiro *et al.*, 1998a; Roberts, 2001). The oil is situated inside the plant cells, confined to discrete spherical organelles called oil bodies (0.6-2 μm). As schematically shown in **Figure 2.1a**, they consists of a triacylglycerides (TAG) matrix surrounded by a monolayer of phospholipids linked together by proteins (mostly structural proteins called oleosin and caleosin) (Tzen *et al.*,1993; Dominguez *et al.*, 1995; Capuano *et al.*, 2007).

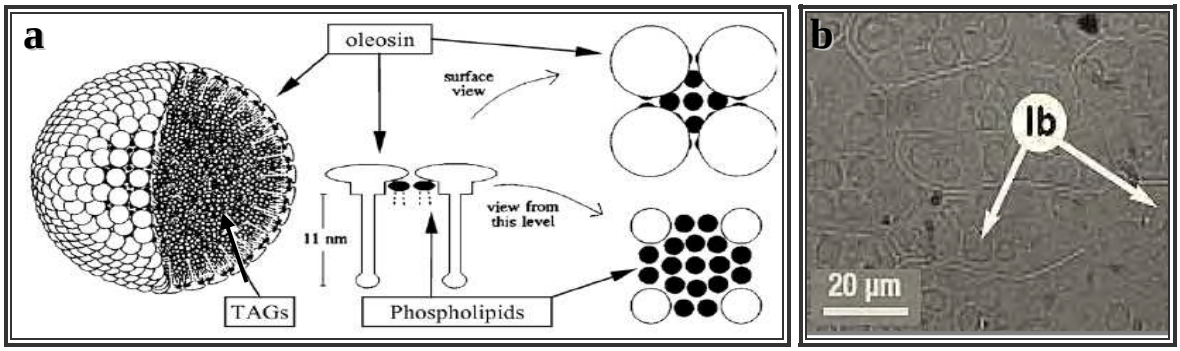

Figure 2.1 – (a) Proposed model of an oil body (Huang *et al.*, 1992); TAG – Triacylglycerides; (b) light micrographs of transverse sections from the mature embryo of R. Mosqueta seeds (Dourado *et al.*, 2000); lb – lipid bodies (or oil bodies).

Dourado *et al.* has shown that oil bodies or lipid bodies are stored in the cotyledon cells in Rosa Mosqueta seeds (2000) (**Figure 2.1b**), hazelnut (2003) and almond (2004).

2.1.2. Enzymes

Enzymatic formulations. Cellulase, xylanase and pectinase are adequate for breaking primary cell walls due to its composition on these carbohydrates as exemplified in **Figure 2.2** for the grape seeds wall composition (Vasco *et al.*, 2003). An example of the effect of the enzymatic treatment on the degradation of the cell walls has been given by Sineiro *et al.* (1998a) who showed the partial degradation of the cell walls of soybean seed after enzymatic hydrolysis. Easier access of proteases to the proteins surrounding the lipid bodies inside the cell is provided after the hydrolysis of the cell walls, which consequently causes the collapse of the global structure and release the enclosed oil.

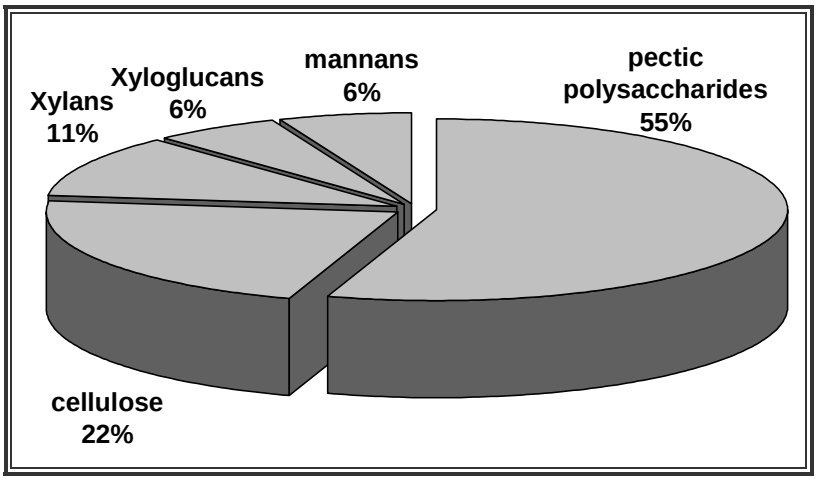

Figure 2.2 – Composition of the cell walls polysaccharides of grape seed (Vasco *et al.*, 2003).

2.1.3. Parameters affecting the treatments

The enzymatic treatment is highly influenced by parameters such as time, enzyme and substrate concentrations, pH, temperature, water-to-seed ratio, stirring rate, and presence of inhibitors, activators and co-factors.

According to the literature data some of these parameters have a more significant impact on the enzymatic pre-treatment than others (Tucker, 1995). In this work, the influence of inhibitors, activators and co-factors has not been studied and therefore will not be discussed further.

Enzymatic pre-treatments have firstly known an effusive interest and became a popular topic of investigation, presenting however quite modest results. Several investigators have been using enzymatic hydrolysis processes to achieve enhanced release of extractable oil from fruits and seeds such as avocado, coconut, olive, sunflower kernel, rice bran, borage, and soybeans, *Jatropha curcas* L., lupin, sesame, rapeseed, soybean, sunflower, palm, and peanut (Sineiro *et al.*, 1998a, 1998b; Hanmoungjai *et al.*, 2000, 2002; Shah *et al.*, 2005; Kashyap *et al.*, 2007; Soto *et al.*, 2007). Enhancement of the extraction yield however, was only about 2-12% higher.

Time. Presumably, the main cause for such small yields on previous works was the small reaction time between enzyme and sample (generally from 15 to 120 min), which was not enough for significant degradation of the cell walls to occur. The example in **Figure 2.3** demonstrates the importance of the reaction time in the dismantling process of the cell walls of an onion tissue, for which the effect of hydrolysis was detectable only after 24 h of reaction (Mattusch *et al.*, 2006).

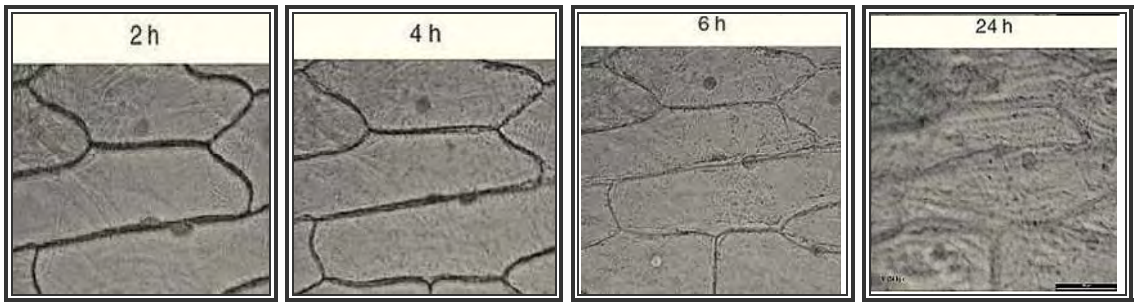

Figure 2.3 – Time dependence in dismantling the cell walls of an onion tissue (Mattusch *et al.*, 2006).

Enzyme concentration. While it is often assumed that enzymatic reaction rates are directly proportional to enzyme concentration, this is only true as long as the substrate is in great excess and therefore the reaction rate is not substract-dependent. In practice, the concentration levels of enzyme are usually kept on a low level due to economical reasons, and a linear dependence is observed between enzyme concentration and extraction yield (Fullbrook, 1983; Dominguez *et al.*, 1994; Tucker, 1995).

Temperature. There is no agreement in the literature with respect to the temperature effect and its impact on the effectiveness of the enzymatic pre-treatment. Though some authors have considered temperature as an essential parameter (several examples have been considered in the review by Dominguez *et al.* (1994)), others did not detect any considerable effect (Hanmoungjai *et al.*, 2000; Sarkar *et al.*, 2004).

The rate of an enzyme-catalysed reaction is related to temperature: where for low temperatures, increasing it leads to the increase on the reaction rate; at the same time, instability of the enzymes results in their rapid inactivation at higher temperatures. It has been demonstrated that below 303 K the enzymatic activity is not maximized, therefore the oil extraction yield increases with increasing temperature, while just above 333 K most of the enzymes suffer from inactivation and no further improvements were observed (Dominguez *et al.*, 1994). Therefore, the optimum will always represent a compromise between increased reaction rate and minimum enzyme inactivation (Tucker, 1995; Soto *et al.*, 2007).

pH. Enzyme activity is also markedly affected by pH. While some enzymes may exhibit activity over a broad pH range, in most cases each enzyme has a maximum activity only within a narrow range suffering from instability problems at pH far from the optimum (Rosenthal *et al.*, 1996; Whitaker *et al.*, 2003). Such instability affects not only the exogenous enzymes, that are added during the pre-treatment, but also seed proteins already present in the sample such as oleosin (referred in **Figure 2.1a**) and caleosin, which also facilitates the structure collapse and the oil removal into the solvent phase (Rosenthal *et al.*, 1996).

Water-seed ratio. The water-seed ratio should be established on the minimum water content to promote the formation of an aqueous solution enough concentrated to promote the interaction of the substract with the enzymes.

Stirring effect. Most of the times, no substantial effect of the stirring rate on the oil extraction is observed. However, this parameter must also be controlled, as a low stirring of the reaction media will let the solids to settle down and reduce the contact with the enzymes. Thus, a relatively high stirring is necessary to ensure the uniformity of the suspension but apart from that, high agitation speed is not needed (Hanmoungjai *et al.*, 2000).

Synergism. The synergetic effect may be observed when several enzymes are acting together. The synergistic effect becomes evident when the rate of hydrolysis of the cell walls with several enzymes is higher than the sum of the rates of hydrolysis by individual enzymes (Rosenthal *et al.*, 1996; Mattusch *et al.*, 2006; Soto *et al.*, 2007). The synergetic effect becomes even more important when one of the enzyme is a precursor of the other (Sineiro *et al.*, 1998b).

2.2. Experimental Section

2.2.1. Materials and Reagents

Plant material. The seeds (**Figure 2.4**) used in the enzymatic pre-treatment experiments were collected from the red grapes (*Vitis vinifera* L.) of the variety 'Touriga Nacional' provided by an experimental vineyard at the Bairrada Appellation region (Estação Vitivinícola da Bairrada, Anadia, Portugal). Seeds were obtained during transfer of the musts for wine fermentation at the year of 2006. The raw material was conditioned and prepared according to the screening procedure already presented and discussed in section 1.2.1.

Materials and reagents. Four types of enzymes were selected (cellulase, xylanase, pectinase, and protease) based on the polysaccharides composition of grape seed cell walls and purchased from Fluka Sigma-Aldrich Co. (St. Louis, MO).

Cellulase (commercial code nº 22178) with declared activity at pH 5 and 310.15 K of 1.44 U per mg of solids (1 U corresponds to the amount of enzyme which produces 1 $\mu mol \cdot min^{-1}$ of glucose from carboxymethylcellulose) was produced from *Aspergillus niger*.

Xylanase (commercial code nº X2753) with declared activity of 2750 FXUW per g of solids (FXUW stands for fungal xylanase units wheat) was produced from *Thermomyces lanuginosus*. The pH range recommended is $4-6$ at temperatures up to 348.15 K.

Pectinase (commercial code nº P2611) with declared activity at pH 3.5 (optimum) and 293.15 K of 28472 PG per mL of suspension (the standard activity is determined by measuring the viscosity reduction of a pectic acid solution where PG stands for polygalacturonase), was produced from *Aspergillus aculeatus*.

Protease (commercial code nº 93614) with a declared activity at pH 7.6 and 298.15 K of 11909 U per mg of solids (where 1 U corresponds to the amount of enzyme which increases the absorbance at 253 nm by 0.001 per minute having N-benzoyl-L-arginine ethyl ester as the substrate) was produced from porcine pancreas.

2.2.2. Enzymatic treatments

Samples of 10 g of milled seed were treated with enzymatic cocktails of cellulase, protease, xylanase and pectinase. Initial tests that were performed with individual enzymes did not produce visible results. Therefore a mixture of enzymes was used for further experiments. The enzymatic suspension-to-seed ratio was kept equal to 4×10^{-3} $L \cdot g^{-1}$ (dry basis) throughout all experiments, a

value based on earlier studies presented in the review by Rosenthal *et al.* (1996). The pH was fixed with a buffer solution of citric acid and sodium hydrogenphosphate. Experiments were run at several pH levels. pH values were controlled by a pH meter (micropH 2000, Crison, Spain) (**Figure 2.4a**). The reaction proceeded isothermal under continuous stirring at 200 rpm by standing in a controlled temperature water bath (**Figure 2.4b**). When the desired reaction time was reached, the reaction was stopped by freezing the suspension with liquid nitrogen (**Figure 2.4c**). After which, the samples were introduced into the freeze drier (Virtis Sentry 5L).

Experimental design. In this work the influence of several variables upon extraction yield has been analyzed, namely: time (*t*), temperature (*T*), pH, particle diameter (d_P), and enzymes concentration (*C*). The experimental conditions adopted are listed in the **Table 2.1**.

The following parameters' values were used: reaction time, 8, 16, 24, 48 and 120 h; temperature, 303.15, 313.15 and 323.15 K; pH from 3 to 7; two particle diameters, between 1.0-1.4 mm and less than 0.5 mm, and two enzyme concentrations: C_1 (cellulase = 29, protease = 1191, xylanase = 21, and pectinase = 569 $\mathrm{U \cdot g_{seed}^{-1}}$) and C_2 (cellulase = 72, protease = 2977, and xylanase = 55, and pectinase = 1708 $\mathrm{U \cdot g_{seed}^{-1}}$). Control experiments have been carried out to quantify the yield increment (Δ) due to enzymatic action. They consisted in Soxhlet extractions of untreated samples with $d_P \in [1.0:1.4]$ mm and $d_P <$ 0.5 mm. They are denoted as Control 1 and Control 2, respectively (see **Table 2.1**).

Exp. 1 in **Table 2.1** corresponds to the most adopted pre-treatment conditions according to literature data: t = 24 h, T = 313.15 K, $d_P \in [1.0:1.4]$ mm, and $C = C_1$. These values were further used to generate the remaining parameter settings. Experimental conditions have been defined by changing one variable while fixing the others, except for the enzymes concentration and pH, which were varied simultaneously.

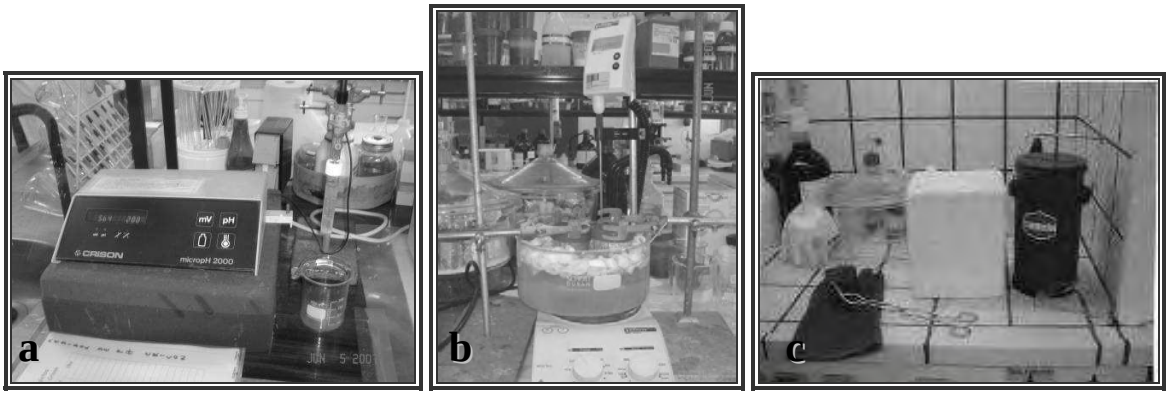

Figure 2.4 – (a) pH meter; (b) enzymatic treatment apparatus; (c) freezing process apparatus.

Table 2.1 – Operating conditions and results obtained for the Soxhlet extractions of grape seed oil.

		Operating Conditions					Results		
Exp. nº	**Variable under study**	***t* (h)**	***T* (K)**	**pH**	**d_p (mm)**	***C***	**η (%)**	**σ (%)**	**Δ (%)**
Control 1	-	No enzymatic treatment			1.0-1.4	-	6.7	0.2	-
Control 2	-				< 0.5	-	15.3	0.2	-
1	Reference♦	24	313.15	6	1.0-1.4	C_1	9.8	0.2	46.5
2	*t*	8					7.3	0.3	8.9
3		16					8.0	0.8	19.5
4		48					10.7	0.7	60.2
5		120					15.7	0.1	136.0
6	pH	24		3			13.8	1.0	107.1
7		24		4			13.7	0.7	106.3
8		24		5			10.5	0.4	57.7
9		24		7			8.7	1.1	29.9
10	*t*, pH	120		4			17.5	0.8	163.2
11	*T*	24	303.15	6			9.7	0.8	45.1
12		24	323.15				6.7	0.9	0.7
13	d_p, pH	24	313.15	4	< 0.5		19.5	0.2	191.0/27.5♣
14	*C*	24	313.15	6	1.0-1.4	C_2	12.0	2.0	80.2
15	*C*, pH	24		3			14.0	2.0	109.5
16		24		4			15.8	0.8	136.5
17		24		5			14.1	1.4	111.5
18		24		7			9.6	1.4	43.7

d_p – average particles diameter; *C* – concentration of the enzymatic cocktail: C_1 (cellulase = 29, protease = 1191, xylanase = 21, and pectinase = 569 $U \cdot g_{seed}^{-1}$ sample), C_2 (cellulase = 72, protease = 2977, and xylanase = 55, and pectinase = 1708 $U \cdot g_{seed}^{-1}$ sample); η - extraction yield; σ - standard deviation; Δ - increment over control case.

♦ Reference: set of experimental conditions from which the remaining ones were specified; ♣ Δ=191.0% in relation to Control 1, and Δ=27.5% in relation to Control 2.

Statistical analysis. Statistical analysis has been carried out using Student's *t*-test and outliers' analysis (Miller and Miller, 2000). **Equation 2.1** was used for the outliers analysis where the suspect value is rejected if $Q > Q_t$ (**Table 2.2**).

$$Q = \frac{|\text{suspect value - nearest value}|}{|\text{largest value - smallest value}|} \quad \textbf{[2.1]}$$

For the Student's *t*-test, significance was defined at $p < 0.025$. All final results embodied at least three valid replicates.

Table 2.2 – Reject values for outlier analysis.

Q_t	Number of samples
0.831	4
0.717	5
0.621	6
0.570	7

2.2.3. Soxhlet extraction and solvent evaporation.

Gomez *et al.* (1996) referred that a conventional Soxhlet extraction should be performed during 16 h or more. In our study, several tests were performed during 4, 16, and 72 h for different particle sizes. The results showed that just 4 h are sufficient to ensure maximum extraction, with no measurable increment been assessed even for 72 h long. Therefore, the Soxhlet was continued throughout this work by using 1.5×10^{-1} L of *n*-hexane in a Soxhlet apparatus (5.0×10^{-2} L capacity; 23×100 mm cartridge) during 4 h (**Figure 2.5**).

The initial volume of solvent in the recovery vessel is always 3-4 times the volume of the Soxhlet chamber. The amount of grinded seeds introduced in each experiment was 10 g, which represented the maximum charge allowed in the cellulose cartridge for the highest particles size studied ($d_p \in [1.0:1.4]$ mm). The recovering flask was submersed in a water bath (Model: Grant, Keison International Ltd, United Kingdom) at the controlled temperature of 353.15 K.

The mass of extracted oil was determined gravimetrically after solvent evaporation, and after ensuring that it contained no water by passing the extracted samples through sodium sulphate anhydrous. The glass material was cleaned several times with *n*-hexane to reduce possible oil loss.

Figure 2.5 – Soxhlet conventional extraction. (a) Soxhlet chamber, first cycles; (b) laboratory scale extraction equipment.

The *n*-hexane was then recovered, and evaporated in a rotary evaporator (Rotavapor R-114, Büchi Water Bath B-480) at 303.15 K. The oil was further transferred to speed-vacuum tubes and dried by centrifugal evaporation (Univapo 100H Unicryo MC2L). During the centrifugation process the samples are maintained under vacuum with a speed rotation of about 1250 rpm; the solvent is captured in a recovery vessel kept at very low temperatures (approximately 213.15 K). The tubes were weighed several times during centrifugal evaporation to ensure that there were no solvent left in the sample. Evaporation was stopped when no weight changes were detected. It was found that 1 h is sufficient for correct procedure. The yield of the process (η), was then expressed as the mass of oil extracted from 100 g of dried grape seed.

2.3. Results and Discussion

Obtained results (η, σ, and Δ) are listed along with experimental conditions in **Table 2.1**. Furthermore, the effects of t, pH, T, C, and d_p upon extraction yield are discussed.

2.3.1. Time effect

Most of the previous studies concerning pre-enzymatic treatments only consider short reaction times (generally 0.25 to 2 h) (Dominguez *et al.*, 1994; Rosenthal *et al.*, 1996; Sineiro *et al.*, 1998b). However, enhancement in the extraction yield was not observed for such short times. Therefore, in this work experiments with longer duration of the treatments were tested. An enhancing extraction yield with increasing reaction time was observed (experiments 1 to 5, **Table 2.1**). The rise of the extraction yields of 8.9, 19.5, 46.5, 60.2 and 136.0% compared to control 1 have been measured after 8, 16, 24, 48 and 120 h of the reaction, respectively. Results are shown in **Figure 2.6**. These results show a continuous increase in the oil extraction yield with pre-treatment duration. Most of the earlier studies that used relatively short reaction times produced quite disappointing results with achieved yield enhancing inferior to 15% (Dominguez *et al.*, 1995; Sineiro *et al.*, 1998b; Sarkar *et al.*, 2004; Soto *et al.*, 2007).

In our case, only a small increase of the yield (8.9%) compared to the Control 1 conditions was observed after 8 h of reaction. This value is comparable to the best results achieved by Soto *et al.* (2007) in the extraction of borage oil, where Δ = 10.0% increment was obtained using a similar conditioning time (9 h of treatment). A yield increase of 46.5% that was achieved after 24 h of treatment clearly exceeds the results from the majority of earlier studies.

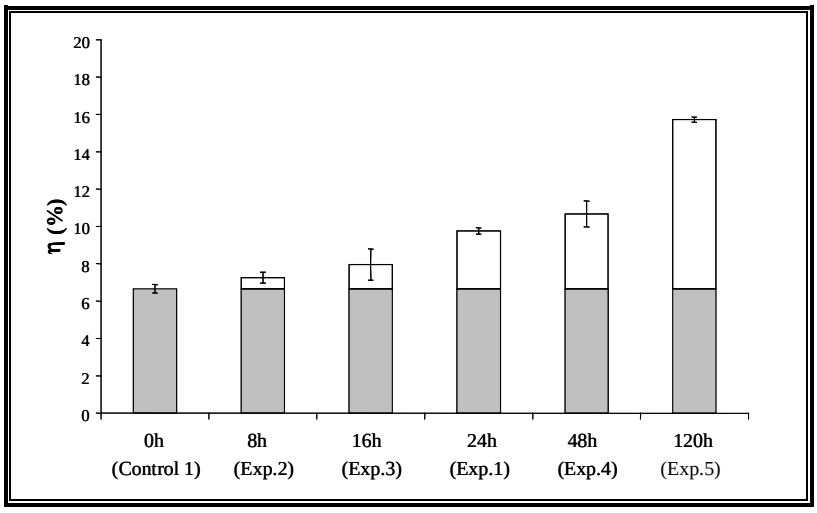

Figure 2.6 – Extraction yield (%) against enzymatic pre-treatment time. Control 1 refers to untreated samples; remaining parameters (see Table 2.1): T = 313.15 K, pH 6, $C = C_1$, and $d_p \in$ [1.0:1.4].

The yield improvement reached 163.0% when reaction was run for 120 h (Exp. 5) in an attempt to exhaust oil content of the grape seed. Despite an astonishing increase of the process effectiveness such long reaction times are not viable in practice. Nonetheless, it emphasizes the important role that enzymes play in the degradation of the cell walls of the grape seed thus making oil available for extraction. The effect of time on the enzyme action was discussed in the introductory section. According to the literature data the oil yield increases linearly with time until it reaches a maximum, after which no further improvements are seen. In this work the tendency to inflect the linear behaviour towards the maximum under the studied conditions was only observed after longer reaction times as shown in the **Figure 2.7**. Increments of the extraction yield rise quadratically with time up to the 24 h of the reaction, after which this dependence inflects (see **Figure 2.7**). Therefore, 24 h has been assumed as a good compromise between reaction time and yield improvement (46.5%), albeit other parameters affecting the process have not yet been considered or optimised.

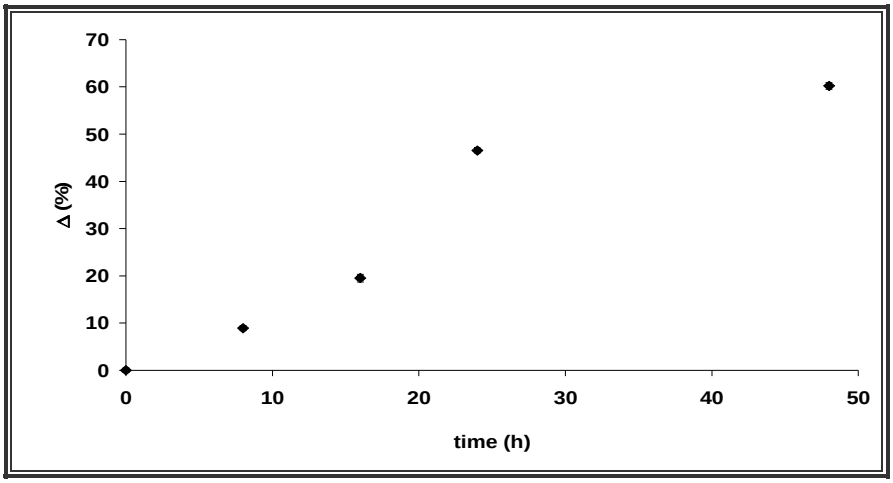

Figure 2.7 – Oil yield increments achieved after extraction vs. enzymatic pre-treatment period.

2.3.2. pH effect

Under some conditions the extraction yields obtained with and without enzymatic pre-treatments of seeds, are very close. This occurs when endogenous enzymes (not added enzymes) play an essential role in the cell destruction. It was found that the effect of such endogenous enzymes could not be measured under the experimental conditions used in this work. Therefore, these phenomena were excluded from further discussion.

Each enzyme has an optimum pH where its activity is the highest. When a mixture of several enzymes with different optimum pHs is used, a range of experimental conditions may give a similar result. Such results take place as different pH levels favour performance of different enzymes of the mixture. In practice, it complicates an optimization of the experimental conditions and also has resulted in the discrepancies between published data. An example reported in the

review by Rosenthal *et al.* (1996) refers four different studies which presented the same maximum extractability from peanuts at pH of 4.0, 7.0 or 10.0. This clearly shows that study of the pH effect is indeed imperative. The recommended pH working ranges for the individual enzymes were: for pectinase pH 3 to 5, for cellulase pH 5 to 8, for xylanase pH 4 to 6 and for protease pH 7 to 9. It means that a broad spectrum of optimal enzymatic activity/pH combination may indeed exist.

Experiments 1, and 6 to 9 (**Table 2.1**) were carried out with the aim to clarify pH influence on the extraction yield. pH were varied from 3 to 7 while the remaining parameters were fixed at t = 24 h, T = 313.15 K, d_p = 1.0-1.4 mm, and $C = C_1$. Values of the η, σ and Δ are shown in **Table 2.1** and in **Figure 2.8**. It was found that the yield increment was increasing with decrease of pH. In fact, the smallest yield increment was achieved at the highest pH tested (pH 7, Exp. 9, **Table 2.1**) for which η = 8.7% and Δ = 29.9%, followed by pH 6 and 5 (Exp. 1 and 8) with increments respectively of 46.5% and 57.7%. Significantly better performance was observed at pH 4 and 3 (Exp. 7 and 6) where similar Δ = 106.3% and Δ = 107.1% were obtained, respectively. At pH 4, pectinase, cellulase, and xylanase have been clearly favoured, whilst protease has been out of the optimum pH. Nonetheless, it is important to note that seed proteins themselves are influenced by the pH, as values far from the isoelectric point destabilize the proteomic matrix and facilitate seed oil removal (Rosenthal *et al.*, 1996). The isoelectric points of seed proteins inclosuring the oil bodies purified from diverse seeds are pH 6.0 to 6.5 (Tzen *et al.*, 1993). Therefore, the combined effect by distortion of the cell wall proteins in combination with the enzymes applied should be responsible for the significant yield increment at pH 4, as described above.

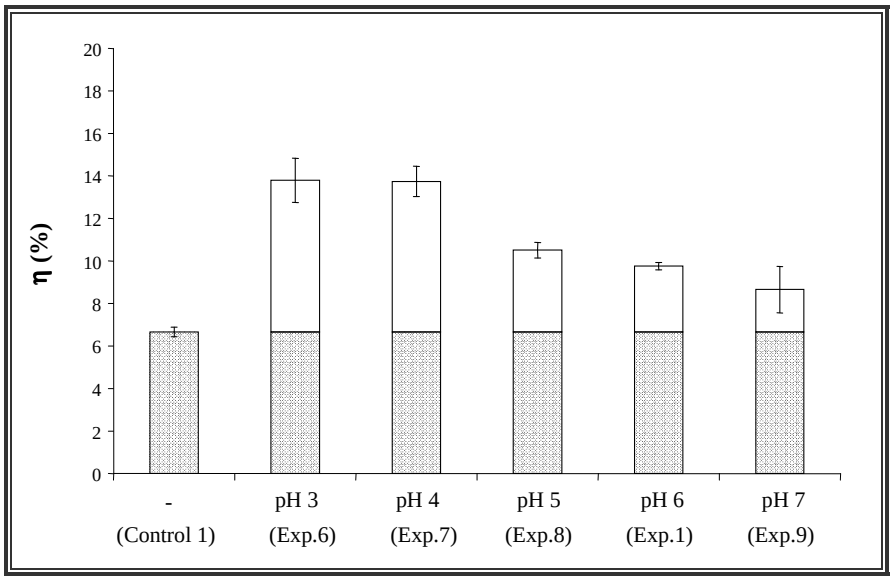

Figure 2.8 – Extraction yield (%) as function of the pH of the enzymatic pre-treatment. Control 1 refers to untreated samples; remaining parameters (see Table 2.1): t = 24 h, T = 313.15 K, $C = C_1$, and $d_p \in$ [1.0:1.4].

An additional experiment (Exp. 10, **Table 2.1**) confirmed a similar trend for higher treatment times by comparing the outcome of the experiments run at pH 4 and 6 for 24 and 120 h, while other parameters being kept the same (T = 313.15 K, d_p = 1.0-1.4 mm, and $C = C_1$). The higher yield increment was obtained at pH 4 compared to 6: 106.3% (Exp.7) and 46.5% (Exp.1), 163.2% (Exp.10) and 136.0% (Exp.5) for the reaction duration of 24 and 120 h, respectively. These results corroborate the expectation, as surmounts the values of both Exp. 6 and 7.

2.3.3. Temperature effect

There is no agreement in the literature data about the temperature impact on the enzymatic treatment. Several experiments were carried out to evaluate the temperature effect on the extraction (Exp. 1, 11 and 12 in **Table 2.1**). Reactions were run at three temperatures: 303.15, 313.15 and 323.15 K. The lowest temperature used in most literature studies is 303.15 K. Therefore, this temperature was chosen as the lowest temperature used in this study. It is also known that enzyme activity increases with temperature until inactivation of the enzymes. Therefore, temperatures higher than 323.15 K were not tested to avoid enzyme inactivation. The other parameters were the same of Exp. 1. Results of these experiments are presented in **Figure 2.9**. Nonlinear dependence between yield increment and temperature was observed, the increment reaching a maximum of 46.5% at 313.15 K (Exp. 11) and decreasing drastically to 0.751% at 323.15 K (Exp. 12). The fact that no visible profit has been observed at 323.15 K compared to Control 1 (Δ = 0.7%) means that at this temperature most of the enzymatic activity has been lost.

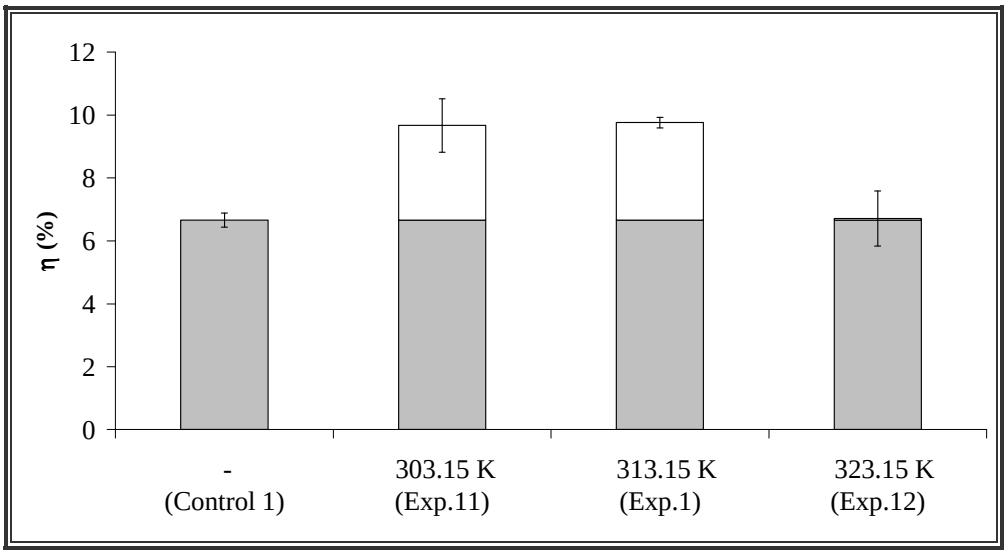

Figure 2.9 – Extraction yield (%) *versus* temperature of the enzymatic pre-treatment. Control 1 refers to untreated samples; remaining parameters (seeTable 2.1): t = 24 h, pH = 6, $C = C_1$, and $d_p \in$ [1.0:1.4].

2.3.4. Concentration effect

The effect of the enzymes concentration has been studied in Exp. 14 for pH 6 (**Table 2.1**). The remaining parameters were the same as in Exp. 1: t = 24 h, T = 313.15 K, and $d_p \in [1.0:1.4]$. Increasing enzymes concentration 2.5-3 times resulted in a significant yield improvement: $\eta = 9.8\%$ and $\Delta = 46.5\%$ for C_1, and $\eta = 12.0\%$ and $\Delta = 80.2\%$ for C_2, respectively.

Additional experiments have been conducted to analyse the effect of pH upon extraction yield for $C = C_2$, namely Exps. 14-18 (**Table 2.1**). All other parameters have been settled equal to Exp. 1. Results are plotted in the **Figure 2.10**. The trend of $\eta = f$ (pH) is the same between pH 4 and 7, with C_2 giving higher yield compared to C_1, and C_1 compared to Control 1 in all cases. At pH 3 no difference between enzymes concentration has been detected, as $\Delta(C_1)$ = 107.1% ≅ $\Delta(C_2)$ = 109.5%. This result marks pH 4 as the optimum pH with maximum extractability gain of 136.5% over untreated material (Exp. 16).

It is important to emphasize that enzyme concentration may disguise other parameters. Actually, high concentrations may counterbalance the small effect of other non-optimised variables. For instance, the same yields may be obtained using lower enzymatic concentrations and longer reaction times and vice-versa. Hence, compromise settings should be chosen on the basis of the economical considerations taking into account the cost of enzymes *versus* running reaction for the longer times.

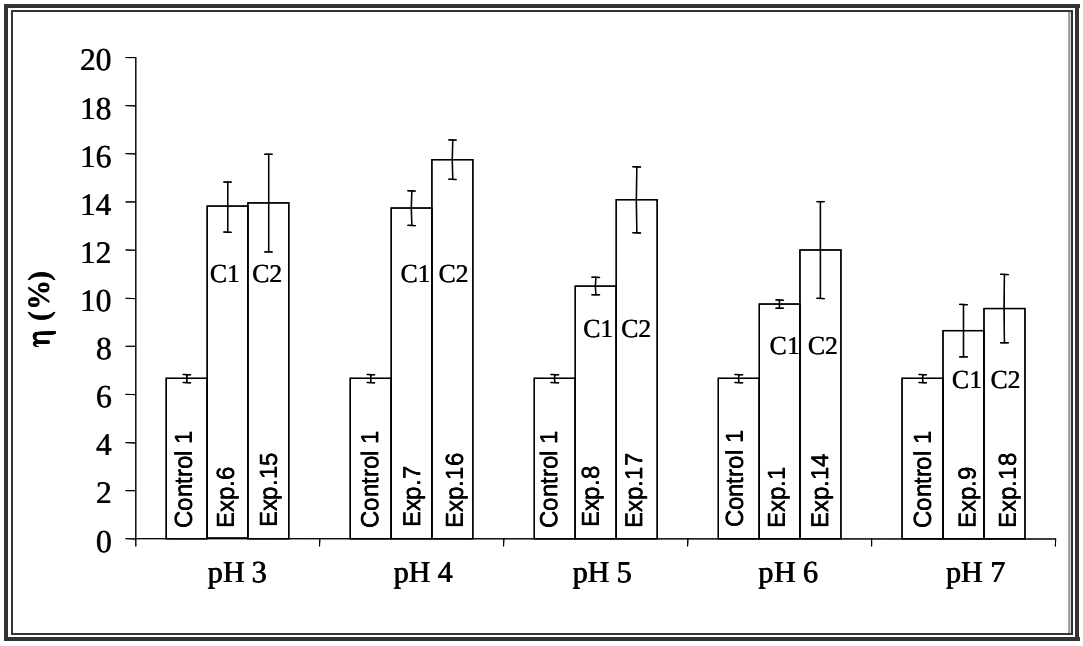

Figure 2.10 – Extraction yield (%) as function of pH and concentration level (C_1 and C_2) of the enzymatic pre-treatment. Control 1 refers to untreated samples; remaining parameters (see Table 2.1): t = 24 h, T = 313.15 K, and $d_p \in$ [1.0:1.4].

2.3.5. Particle size effect

Most of earlier studies on enzymatic pre-treatments did not take particle diameter into account. Frequently whole seeds were immersed into the aqueous medium during the treatment and grinded in *situ*, with no further classification. However, the present research underlines that this parameter is absolutely unavoidable. Furthermore, misleading conclusions can be drawn when comparisons between results are obtained without considering the particle size.

It is well known that mechanical treatment of grape seed has large impact on the oil removal since it breaks down plant cell walls augmenting oil accessibility. Hence, the lower the particle size is the higher the extraction yield will be. However, very small particles are not recommendable as sometimes it is almost impossible to process such fine powders industrially. Materials with high oil content and week structuring collapse when exposed to the flow of solvents and loose their macroporosity which prevents a uniform and convenient percolation severely. Furthermore, there also appear wetability problems.

The effect of d_p upon the extraction yield has been firstly measured using untreated milled samples and two particle sizes: 1.0-1.4 mm and less than 0.5 mm (Controls 1 and 2, **Table 2.1**). According to the expectations, significantly higher yield was achieved with the smaller particle size, i.e. $\eta = 6.7\%$ for $d_p \in [1.0:1.4]$ mm and $\eta = 15.3\%$ for $d_p < 0.5$ mm (**Table 2.1**, **Figure 2.11**).

Experiments were also run with enzymatically pre-treated seeds with a particle size less than 0.5 mm. The other experimental conditions were chosen based on the previous results: t = 24 h, T = 313.15 K, pH 4 and C_1 (Exp. 13).

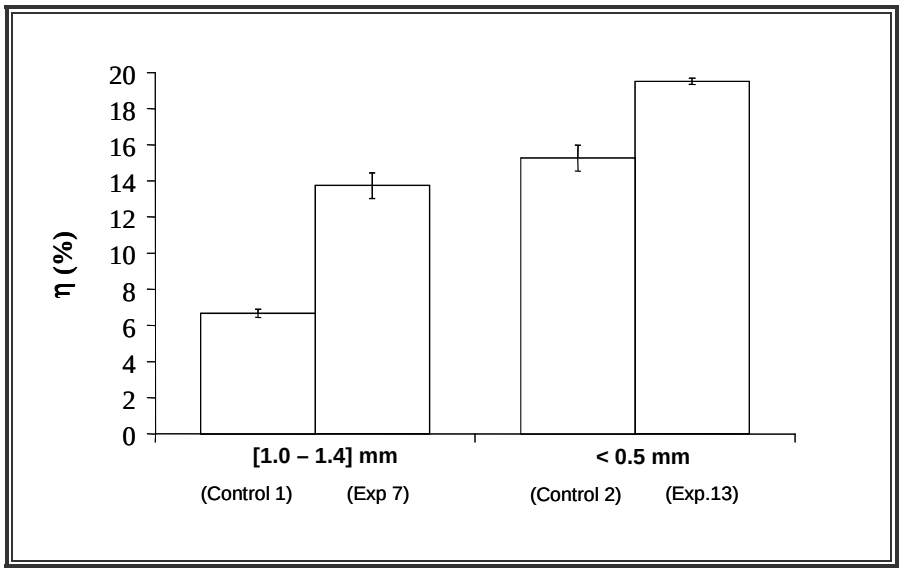

Figure 2.11 – Extraction yield (%) against granulometry of seed particles. Control 1 and 2 refer to untreated samples; remaining parameters (see Table 2.1): t = 24 h, pH = 6, $C = C_1$, T = 313.15 K.

An yield of 19.5% with a corresponding yield increment of 191.0% over Control 1 was achieved. Enhancement due to the enzymatic action was more modest surmounting to only 27.5% of yield increment compared to the Control 2 (**Figure 2.11**). This result is due to the fact that many oil bodies of the smaller particles have already been exposed after milling. Nonetheless, the enzymatic pre-treatment was still significant for seeds with $d_p < 0.5$ mm .

3. Supercritical Fluid Extraction of Grape Seed Oil

Hard work is the price we must pay for success.
[Vince Lombardi]

3. Supercritical Fluid Extraction of Grape Seed Oil

The extraction of grape seed oil has been carried out with supercritical carbon dioxide (SC-CO_2). Supercritical extraction (SFE) curves were measured and the influence of the operating pressure and temperature discussed. The effect of the enzymatic pre-treatment of the seed on the SFE was analyzed also under different pressure conditions. The analyses of the extraction curves included also the effect of a high pressure pre-treatment of the seed.

Being a home made set up unit, some detailed description is devoted to the SFE unit. The experimental conditions for applying the enzymatic pre-treatment have already been described in the previous chapter while this chapter addresses the necessary conditions to perform the high pressure pre-treatment to the seed. In opposition to the enzymatic pre-treatment the high pressure pre-treatment is still an exploratory study and reveals only the potential application of such technology. All results obtained are presented and discussed. Modelling is performed in Chapter 5.

3.1. Introduction

Supercritical fluid (SCF) technology is a rapidly growing alternative to some of the conventional methods of extraction, reaction, fractionation, and analysis. Ultimately, being capable to improve product quality while being a more environmentally friendly technology (Rezaei *et al.*, 2007).

3.1.1. Supercritical fluids

As shown in **Table 3.1**, the supercritical solvents have densities comparable to liquids, viscosities equivalent to gases, and diffusion coefficients in between, which lends to better extracting capability. The SCFs are particularly useful in the extraction of solutes from solid matrices as, besides the aforementioned properties, they possess a null superficial tension (Brunner, 1994; Arai *et al.*, 2002; Silva and Barbosa, 2003). As a consequence, better penetration into pores and matrices and hence faster mass transfer and more efficient extraction is achieved with SCFs compared to normal solvents (King and Bott, 1993; Lang and Wai, 2001; Beckman, 2004). The aforementioned advantages are probably the main focus in its potential industrial application.

Table 3.1 – Orders of magnitude of SCF's, gases and liquids (Silva and Barbosa, 2003).

Properties	Liquid	SCF	Gas
Density ($kg \cdot m^3$)	600-1600	200-900	0.6-2.0
Viscosity ($Pa \cdot s$) $\times 10^5$	20-300	1.0-9.0	1.0-3.0
Diffusion coefficient ($m^2 \cdot s^{-1}$) $\times 10^9$	0.2-2.0	20-70	10000-40000

The state condition of a pure fluid is described as a function of two intensive properties (e.g. **Figure 3.1** represents the $P\rho T$ diagram of CO_2). Compressibility in the supercritical region is high with large density variations caused by small changes in pressure or temperature. Up to a reduced temperature of 1.3, compressibility rapidly decreases with pressure as **Figure 3.1** shows. In this range, the density of a supercritical compound is strongly dependent on pressure and temperature, and solvent power, also determined by density, will present the same behaviour (Brunner, 1994). Above a reduced temperature of 1.3, considerable high pressure must be applied to the solvent in order to achieve densities sufficiently high for the extraction effect to become appreciable, which is not industrially profitable (King and Bott, 1993). Examples of some well-known industrial applications are indicated in **Figure 3.1** denoted as A (extraction of hops), B (decaffeination of coffee and tea), and C (extraction of flavours and fragrances).

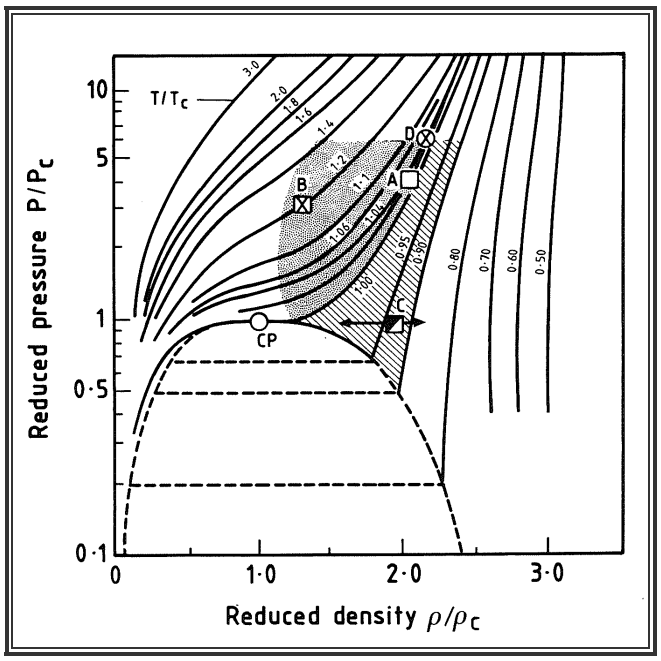

Figure 3.1 – $P\rho T$ diagram of CO_2 in reduced coordinates. Range of application of some industrial processes: [A] - extraction of hops; [B] - decaffeination of coffee and tea; [C] - extraction of flavours and fragrances (King and Bott, 1993).

Solubility of solutes. The solubility is controlled by two factors – the volatility of the substance, which is an important function of temperature, and the solvation effect of the SCF, which is a function of fluid density (Modey *et al.*, 1996). At pressures just above the critical point, the increase in solute vapour pressure due to temperature increase is insufficient to fully compensate the loss of solvent power caused by reduction in solvent density. When the temperature is increased at higher pressure, the corresponding increase in solute vapour pressure may compensate the reduction in solvent density, resulting in an overall higher solubility (Mansoori *et al.*, 1988; Palmer and Ting, 1995).

This is called *retrograde phenomenon* or *temperature inversion effect* and is a manifestation of the complex relationship between solubility and temperature.

This effect can be observed in **Figure 3.2a** for the solubility of soybean oil in SC-CO_2 where this inversion occurs at about 300 bar (King and Bott, 1993). At the cross-over point (equal solubility in CO_2 at different temperatures) the dependence on temperature becomes negligible. Therefore, compromise conditions have to be found for maximizing solubility of extractives (Sanders, 1993).

Grape seed oil, at the extraction conditions experimented in this essay, presents a solubility behaviour as below the cross-over point. Therefore, both higher pressures and lower temperatures will induce an increasing effect on oil solubility as it is represented in **Figure 3.3**. The correlation by del Valle and Aguilera (1988) (**Equation [A1.1]** in **Appendix A1**) has been extensively used to calculate the solubility of vegetable oils in SC-CO_2 for pressures between 152-892 bar, temperatures between 293.15-353.15 K, and oil solubility below 100 $kg \cdot m^{-3}$. It was adopted also in this work to generate **Figure 3.3**.

The number of polar groups and molecular weight of solutes affects obviously volatility. The concentration of apolar hydrocarbons in the gaseous phase increases with decreasing molecular weight until complete miscibility (c. 500 Da) is reached within a homologous series (e.g. **Figure 3.2b** for fatty acids) and decreases with the addition of polar groups such as hydroxyl, carboxyl, amino, etc. At higher molecular weight the influence of the nonpolar part of the molecules dominates solubility; while at lower molecular weight the influence of the polar functional groups dominates (Brunner, 1994; Palmer and Ting, 1995; Rezaei *et al.*, 2007).

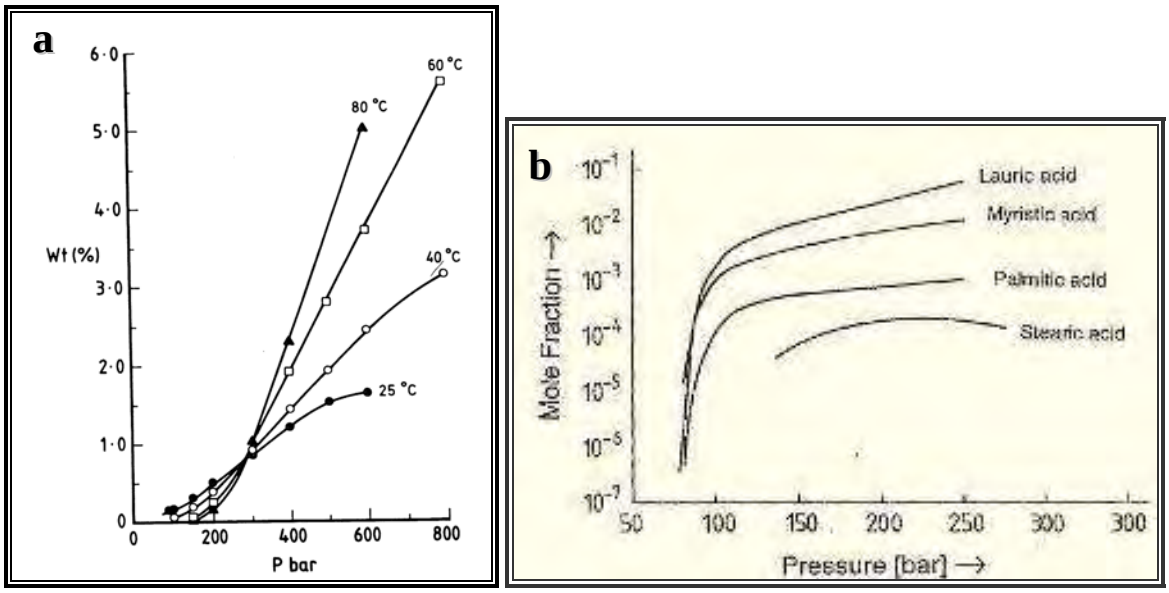

Figure 3.2 – (a) Solubility of soybean oil in near-critical CO_2 as function of pressure and temperature (Quirin, 1982); (b) Solubility of homologous fatty acids in SC-CO_2 (Brunner, 1994; Arai *et al.*, 2002).

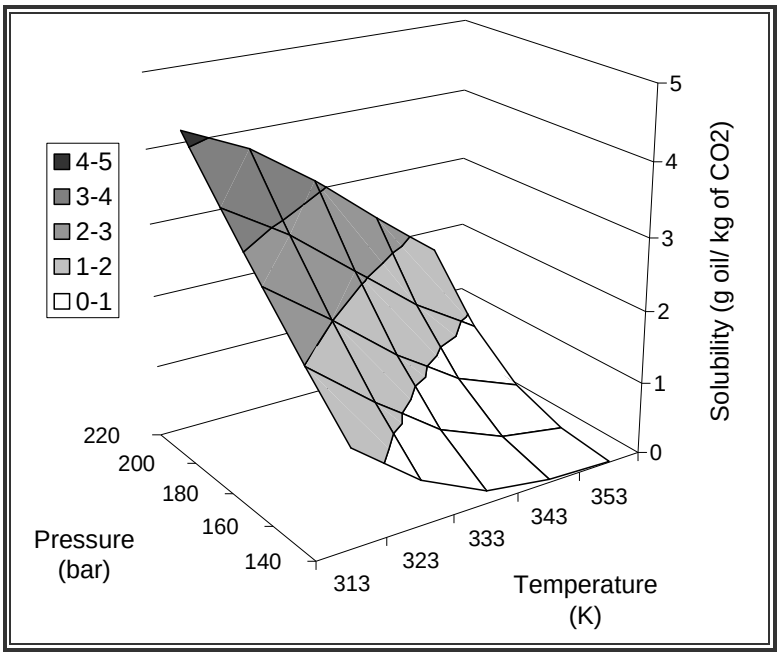

Figure 3.3 – Dependence of the solubility of vegetable oils in SC-CO_2 on pressure and temperature according to the correlation of del Valle and Aguilera (1988).

3.1.2. Supercritical fluid extraction

Supercritical fluids are touted as a replacement for organic solvents, which is beneficial from environmental and health points of view. Thermal degradation and decomposition of labile compounds as well as many undesirable reactions such as hydrolysis and oxidation are avoided under supercritical conditions due to the operation at reduced temperature and absence of light and oxygen (Sanders, 1993; Bartley and Foley, 1994; Basile *et al.*, 1998; Palma *et al.*, 1999; Diaz-Reinoso *et al.*, 2006; Rezaei *et al.*, 2007).

The extraction rate of solutes from vegetable matrices will depend on several parameters: the convective mass transfer coefficient, effective diffusivity in the solid, and solubility in the supercritical solvent (del Valle *et al.*, 2005).

As schematically represented in **Figure 3.4** the CO_2 is fed directly from a storage tank (point 0; about 60 bar, atmospheric temperature) and further cooled to point 2. In a continuous process, it comes from the separation unit in gas state (point 1), and it is refed to the unit (point 2) by cooling and compressing above the corresponding critical pressure (point 3, above 73 bar for SC-CO_2), and heated to the operating temperature above critical temperature (point 4). The SC-CO_2 is then fed to the extractor where it flows through the extractable material and dissolves the soluble components (solutes). The extract stream is then expanded below critical pressure, which leads to the precipitation of the solute in the separation vessel (point 1). The CO_2 is then purified, liquefied, and returned to the extraction unit where another cycle proceeds (Silva and Barbosa, 2003).

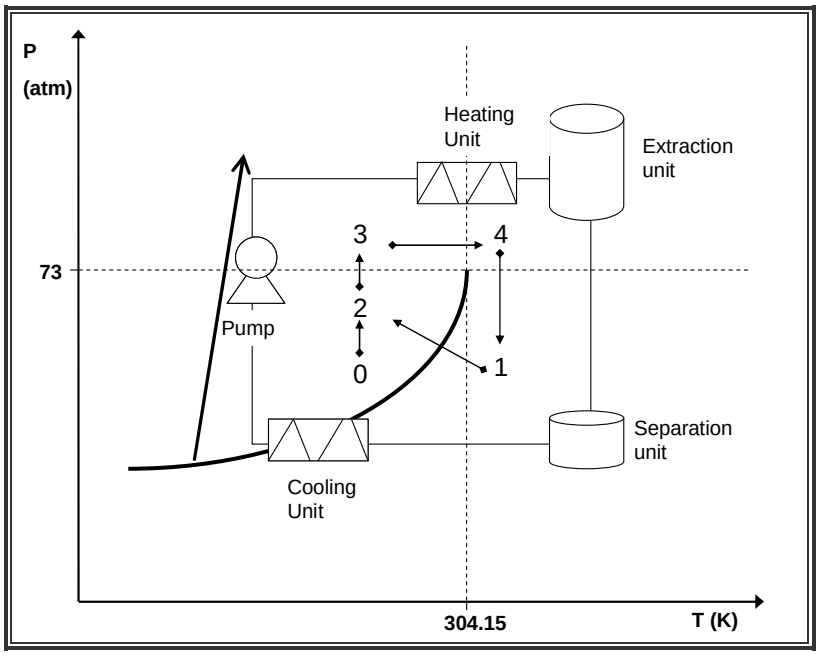

Figure 3.4 – Scheme for a SCF extraction process (Silva and Barbosa, 2003).

The main disadvantages associated to the use of SCFs comparatively to the conventional solvents, which eventually induce higher capital cost, is the requirement for high security and technological capabilities associated, such as proper thick and well isolated extractors equipped with relief systems (King and Bott, 1993; Sanders, 1993; Lucas *et al.*, 2003; Silva and Barbosa, 2003; Beckman, 2004).

Carbon dioxide has been especially adopted since it is essentially non-toxic, inert, non-flammable, inexpensive, readily available, can be recycled, is totally dissipated from extracts at atmospheric pressure and has easily accessible critical conditions of pressure and temperature (Sanders, 1993; Brunner, 1994; Hancu and Beckman, 2001; Silva and Barbosa, 2003; Beckman, 2004; Rezaei *et al.*, 2007). The dissolved solutes can be easily separated by depressurization as the solubility is significantly reduced at low pressure and almost vanishes in the gas state. For a similar mass of seed to be extracted, a SFE may need or not a few amount of an organic solvent (cosolvent) while a typical solid-liquid extraction method would require tens to hundreds times more that amount (Otterbach and Wenclawiak, 1999; Lang and Wai, 2001). Therefore, SFE can eliminate the sample concentration step which usually is time and energy-consuming and often results in loss of volatile components (Henning *et al.*, 1994).

In terms of food products, SC-CO_2 gives the extracts the most natural smell and taste (Moyler, 1993; Bernardo-Gil *et al.*, 2001, 2002; Carvalho *et al.*, 2005; Lopes and Bernardo-Gil, 2005). At the same time SCF can reach extraction yields equivalent to those achieved by conventional Soxhlet with *n*-hexane (Gomez *et al.*, 1996).

Experimental SFE equipment. Different experimental setups have been used to assess kinetics of SC-CO_2 extraction of seeds. Analytical experimental systems use standard HPLC, air driven diaphragm or syringe pumps for solvent compression, small cells (≤ 25 cm^3) for extraction, conventional ovens for heating, and glass flasks for the recovery of dissolved solutes (Sovová *et al.*, 1994; Subra *et al.*, 1998; Reverchon *et al.*, 2000; del Valle *et al.*, 2004b). Most one-pass screening systems comprise the solvent compressing with mechanically driven diaphragm or piston pumps or compressors, large extraction vessels (50-1000 cm^3) immersed in a water bath or equipped with heating jackets or electrical heating tapes, and high-pressure devices such as cyclone separators for the precipitation of dissolved solutes from extract stream (Perrut *et al.*, 1997; Reverchon *et al.*, 1999; Berna *et al.*, 2000, del Valle *et al.*, 2000, 2004b; Papamichail *et al.*, 2000; Reis-Vasco *et al.*, 2000; Bernardo-Gil *et al.*, 2001; Fiori, 2007). Process development units are characterized by large extraction vessels (>1 dm^3), multiple high-pressure separators and solvent recycle capability (Catchpole *et al.*, 1996b; Perrut *et al.*, 1997; Berna *et al.*, 2000; Eggers *et al.*, 2000; del Valle *et al.*, 2004b).

Cumulative SFE curves. The SFE data is normally represented as a plot of the cumulative yield *versus* consumed solvent or extraction time. A curve with an inverted exponential decay is produced as in **Figure 3.5** which is characterized by a steep initial slope decreasing afterwards asymptotically towards the maximum yield (Catchpole *et al.*, 1996b). In cases where the initial concentration of solutes in the solid substrate is high, the SFE behaves as curves (a) or (b) respectively without or with significant solid mass resistance. A second period common to both curves follows, where the rate of extraction drops rapidly. In cases of low initial concentration of solutes the extraction rate is not so high at the beginning of the SFE. Therefore, only one distinct period is observed, continuously declining over whole time course – curve (c) (Maxwell, 1996; del Valle *et al.*, 2004b).

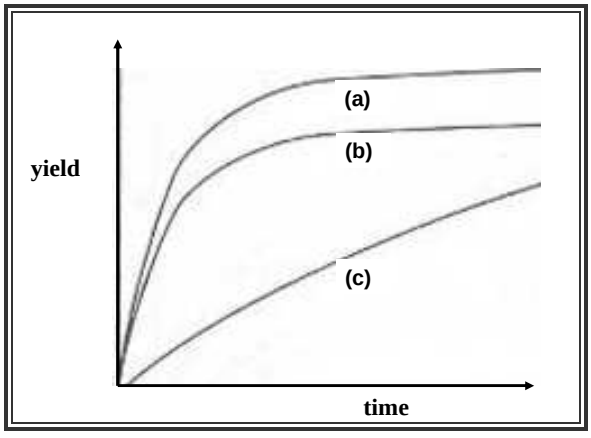

Figure 3.5 – Typical oil extraction curves with SC-CO_2: (a) diffusion-controlled; (b) significant matrix effect and (c) very low solubility of solute or low oil content of the solid (Maxwell, 1996).

Operating conditions – Pressure. The solubility is one outmost important factor for extraction efficiency (Wheeler and McNally, 1989), which increases with rising pressure. In most cases, it is more advantageous to extract the samples under pressure conditions right above the point where the desired compounds just become soluble in the fluid, so that the extraction of other compounds can be minimized. However, the co-extracted compounds can be sometimes of great importance because of their properties (e.g. antioxidant properties (Papamichail *et al.*, 2000)).

Operating conditions – Temperature. The effect of temperature is as important as pressure but more difficult to describe and relate to solubility due to the known *temperature inversion effect* already discussed. The following studies present three examples showing the three possibilities. In the work presented by Akgun *et al.* (2000), on extraction of lavender flower essential oil, the extraction rate increases as the effect of the vapour pressure increase overcomes the effect of the solvent density reduction, and as a result the yield increases with increasing temperature. In the work of Eggers *et al.* (2000), on extraction of rose hip seed oil, it is assumed that the negligible effect of temperature is probably due to the proximity of the cross-over point. The results on extraction of celery seed oil presented by Papamichail *et al.* (2000) show a decrease in the extraction rate with temperature increase, with a clear supremacy of solvent density decrease over the increase of solute vapour pressure.

Operating conditions – Mass flow rate. The effect of mass flow rate on the cumulative SFE yield curves has also been studied (e.g. in the extraction of cherry seed oil by Bernardo-Gil *et al.* (2001) and pennyroyal essential oil by Reis-Vasco *et al.* (2000)). For high-oil-content seeds, all curves showing the cumulative extraction yields *versus* the normalized mass of consumed solvent ($kg_{CO_2} \cdot kg_{seed}^{-1}$) converge to a single line (del Valle *et al.*, 2004b). Therefore, it is assumed that the extraction yield does not depend on the solvent flow rate. Essential oils with low oil content behave differently, there the solvent flow rate has a strong effect on extractability. It was shown in the work by Papamichail *et al.* (2000) on extraction of celery seed oil that the lowest flow rate led to a highest amount of extracted oil per kg of CO_2.

In most cases the SFE process varies dramatically after the majority of the compounds are removed from the easily accessible portion of the solid matrix near the end of the extraction. Therefore, using a prolonged extraction time to gain a slightly higher recovery may not be economically worthwhile (Lang and Wai, 2001). Most commercial extraction processes are considered to be finished when just 90% of the solute has been removed. Beyond that limit, increased operational costs are not compensated by increments in product quantity (del Valle and Galan, 2005). At this stage other options such as the association of pre-treatments became an advisable alternative.

3.1.3. Pre-treatments application to SC-CO_2 extractions

The most commonly used pre-treatment is the mechanical one, although most studies do not mention its effect. Catchpole *et al.* (1996b) reported the effect of particle diameters on the extraction for both essential (**Figure 3.6a**) and edible oils (higher oil content) (**Figure 3.6b**).

The first example in **Figure 3.6a** shows that the rate of extraction of the essential oil is limited by intraparticle diffusion, therefore only one distinct period is observed, continuously declining along experiment and behaving like curve (c) in **Figure 3.5**. The resulting curves all behave differently with different seed particle sizes, although the mass flow rate is similar ($\dot{m} = 0.15\ \mathrm{kg \cdot min^{-1}}$). In such cases, the particle size is a factor that dominates the rate of extraction. Other authors have observed similar behaviour for other essential oils (e.g. celery seed oil (Papamichail *et al.*, 2000) and lavender flower essential oil (Akgun *et al.*, 2000)).

The second example given in **Figure 3.6b** shows that during the 1st period of extraction all SFE curves, independently of particle size and/or solvent flow, are governed by equilibrium and fit onto a straight line, as long as the initial concentration in the solid substrate is high enough to saturate the solvent at beginning. In such cases, seed particle size differentiations do not inflect changes in the initial slope of the cumulative curves. Although the particle size will present itself an important effect on the oil yield maximization. The same figure shows coincident SFE curves under different flow rates ($\dot{m}$ = 0.086 and 0.213 $\mathrm{kg \cdot min^{-1}}$) but similar particle sizes (0.56 mm), therefore showing the fluid saturation stage; while at higher solvent flow rate ($\dot{m}$ = 0.271 $\mathrm{kg \cdot min^{-1}}$) the resulting curve underfits the previous ones as the outlet stream is no longer saturated. The same flow of 0.086 kg.min^{-1} is used for a higher particle size of 0.92 mm set. The resulting SFE curve reproduces the one for 0.56 mm at the 1st extraction period but achieves a different maximum stage (approximately 28% for 0.92 mm and 58% for 0.56 mm).

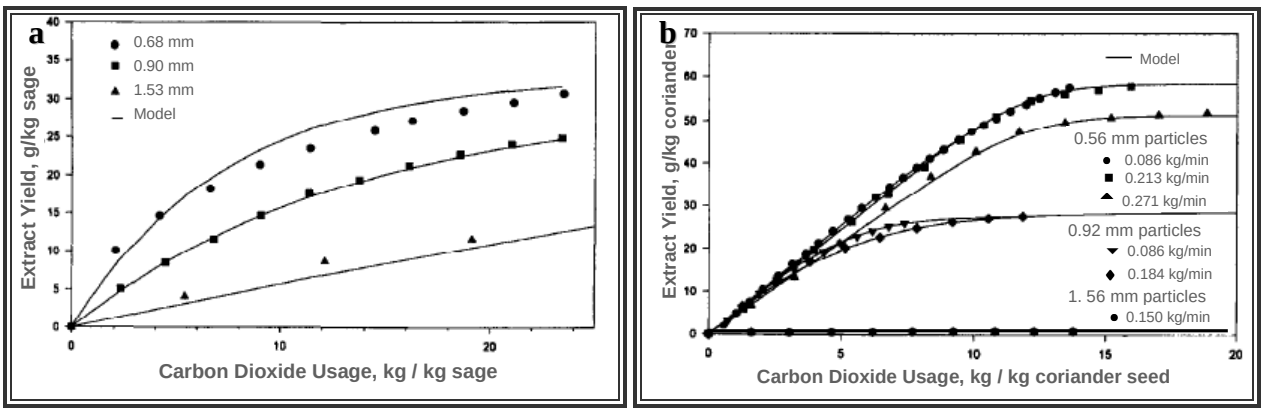

Figure 3.6 – Cumulative curves for the extraction of (a) oleoresin, and (b) coriander seed, for different particle sizes (Catchpole *et al.*, 1996b).

The same behaviour has been confirmed by other authors and for other seed species (e.g. rosehip (del Valle *et al.*, 2004b), hiprose (Reverchon *et al.*, 2000), almonds (Marrone *et al.*, 1998), and grape seed (Sovová *et al.*, 1994; Fiori, 2007)).

Reducing the particle size has a beneficial effect on the bed density. It is then possible to put more of the smallest particle size material into the fixed volume of the extractor, and thus increase the yield per batch of loaded solids. On a production scale, this means that more solids could be processed and more extracts obtained per day. However, a minimum particle size limit must not be passed over to avoid solvent channelling, high pressure drop, and lost of volatile compounds during the intensive grinding (Catchpole *et al.*, 1996b; Rozzi *et al.*, 2002, Rozzi and Singh 2002; Kaiser *et al.*, 2004; Reverchon and De Marco, 2006; Gomes *et al.*, 2007).

High pressure pre-treatment (HPP). Current research activities using non-thermal pre-treatment methods such as high pressure processing are used not only as an alternative to the food pasteurization (Rastogi *et al.*, 2007) but also for alteration of other properties of plant foods. As a result of such treatments food products may acquire novel structure and texture due to the rearrangement in the tissue architecture. This can improve retention and availability of extractives while increasing their mass transfer (Saraiva *et al.*, 2002; Knorr, 2003; Castro *et al.*, 2006).

In a typical HPP, the product is packed in a flexible container and loaded into a high pressure chamber filled with a pressure transmitting (hydraulic) fluid. The hydraulic fluid (normally water) in the chamber is pressurized with a pump, compresses the packed material, into the food for a specific period of time. The processed product is then removed and stored/distributed in the conventional manner. Because the pressure is transmitted uniformly (in all directions simultaneously) food retains its shape even at extreme pressures. Because no heat is needed, the sensory characteristics of the food are retained without compromising microbial safety. Knorr (2003) has presented the potential of using HPP in the extraction of grape juice and anthocyanidins from grape skins. In both cases, higher yields were achieved when HPP was applied prior to the extraction. Although the mechanism of action of high pressure on the cellular structures are yet to be disclosed, it is already evident that HPP is a useful technique for aiding the extraction process.

3.2. Experimental set up

The SFE unit used in this work is presented in detail in **Figure 3.7**. The construction of this unit has been developed in conjunction with a Master thesis, thus a more exhaustive description of the associated equipment can be found elsewhere (Silva, 2008).

Carbon dioxide of food quality (96%) is fed from a storage tank (CO_2 container), whose pressure is indicated on the first manometer (M1). During the experimental runs the pressure inside the CO_2 container varied between 50-65 bar. The CO_2 is cooled in a water/ethylenoglycol bath inside a cooling refrigerator (**Figure 3.8a**). The negative temperatures maintain the CO_2 in the liquid state, which is an essential condition for the functioning of the high pressure liquid pump assembled. The air driven pump (Model: MCPV-71, Haskel, USA) is used to compress the carbon dioxide inside to the high pressure accumulator up to approximately 320 bar.

The pump, that has a maximum allowed hydrostatic pressure of about 600 bar, is switched on/off by an electro-valve (V3) (Model: PL-VS-1/8, Paralab, Portugal), actuated by a controller connected to the pressostate (Model: PL-Pswt-1, Paralab, Portugal), which is connected to the high pressure accumulator. The pump switches on when the pressure falls below 200 bar, and switches off when pressure rises above 320 bar. The same electric signal activates the purge a few seconds before the pump starts, to avoid cavitation.

In order to further prevent the liquid CO_2 to follow backwards in the line, two check valves (V2 and V4) were included in the unit. As a security measure, and to allow its isolation, two cut valves (V5 and V6) were included just before and after the accumulator, due to the highest pressure conditions involved. A filter was included in the line with the aim to prevent residual dusty particles in the CO_2 to flow into the line. This will be also particularly important for the future functioning of CO_2 recycling. The pressure control inside the extractor is assured by FPR1. Two manometers (M2 and M3) located before and after the forward pressure regulator (FPR1) (Model: FPR-PL-400-80, ABJ Engineering PVT. Ltd., India) show respectively the pressure in backward and forward tube. Following the line, a mass flow meter (MFM) (Model: RHM007, Rheonic, USA) measures the mass flow rate. The MFM has a maximum allowed pressure of 450 bar and temperature of 393.15 K.

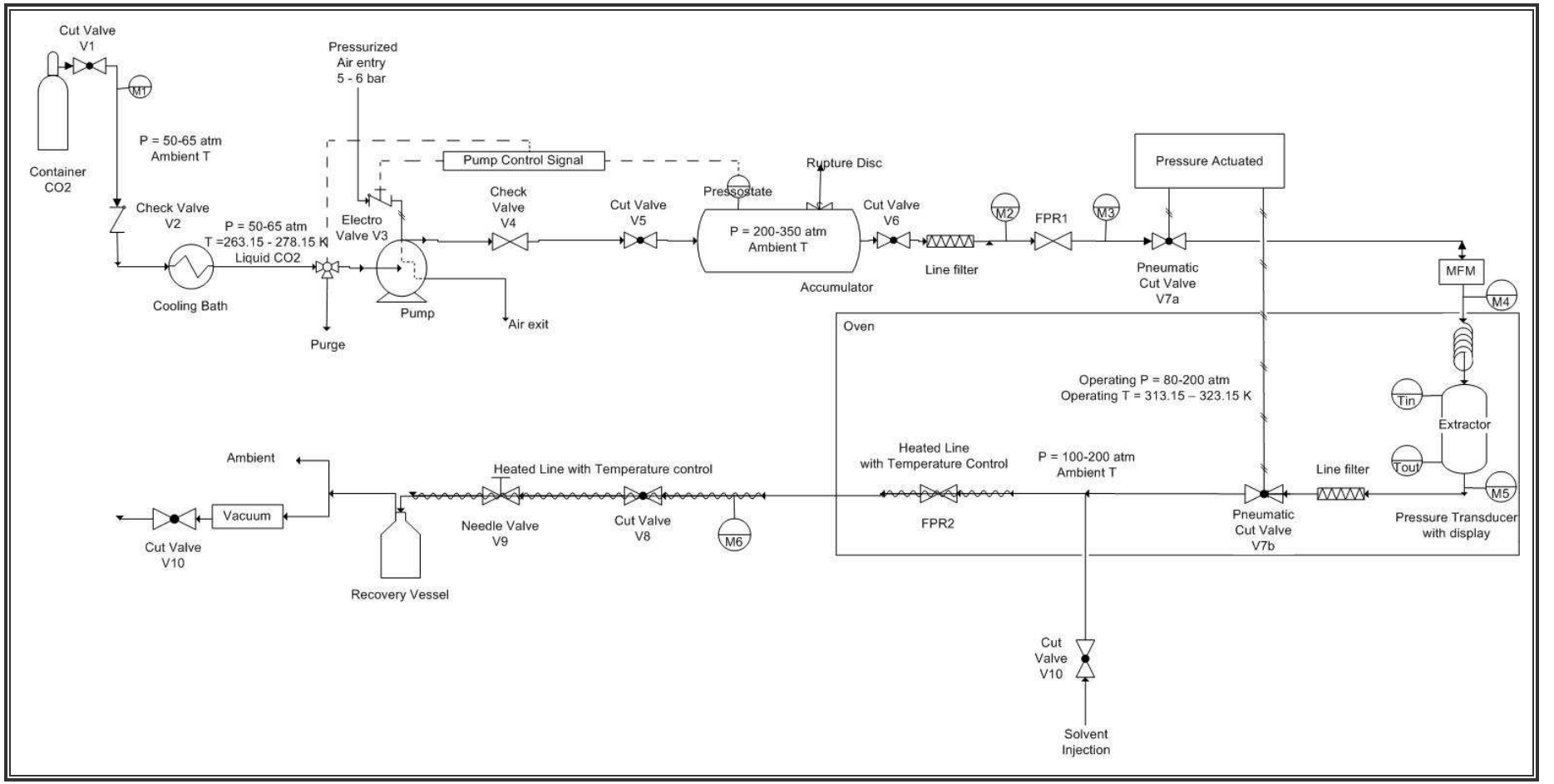

Figure 3.7 – Supercritical fluid extraction unit assembled in this work.

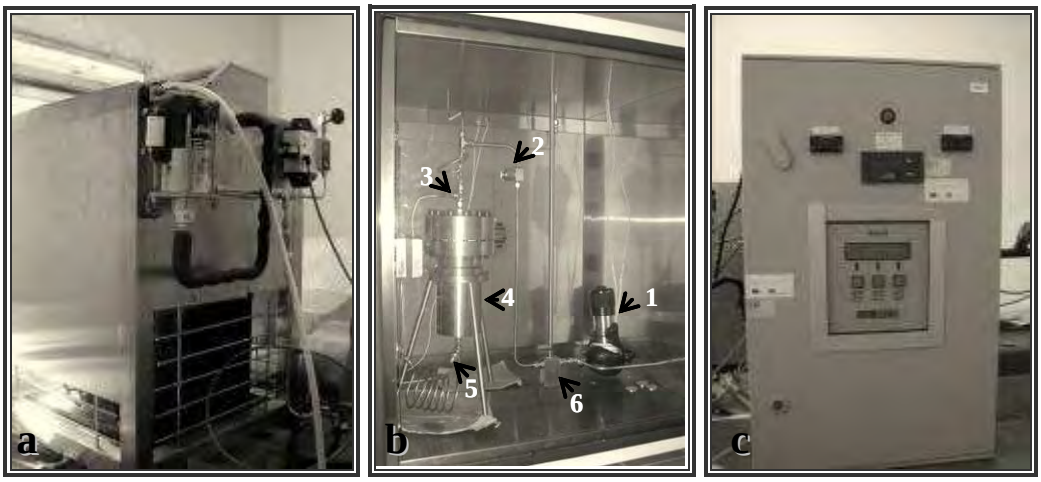

Figure 3.8 – Elements of the supercritical fluid extractor: (a) Cooling refrigerator; (b) Extraction unit (details); (c) Control Panel (Reading unit).

The flow rate is displayed in a secondary control panel (Reading unit, Model: RH07, Rheonic, USA) (**Figure 3.8c**) along with temperatures displays (Ero electronic), T_{in} and T_{out}, measured before and after the extractor by two coupled thermopars. A pneumatic pressure actuator valve (Model: AT05 SR6, Air Torque, Italy) connected to the inlet and exit of the extractor allows us to close the system using valves V7a and V7b. The pressure inside the extractor is measured by a manometer display M4 and pressure transducer M5.

The CO_2 flows inside a twisted line inside the oven (thermostatic casing) (Model: 992, Scientific Engineering, South Africa) (**Figure 3.8b**) before entering the extractor. Therefore, the solvent is maintained inside the pipeline enough time for reaching required temperature. The thermostatization of the system is confirmed by the temperature readings of T_{in} and T_{out}. The CO_2 percolates the extractor (**Figure 3.8b** – point 4) from top to bottom. The extractor volume is 1.6×10^{-4} m^3. Before reaching the second forward pressure regulator (FPR2) (Model: FPR-PL-250-50, ABJ Engineering PVT. Ltd., India) (**Figure 3.8b** – point 1) the tube includes a second filter (**Figure 3.8b** – point 2) in order to avoid the drag of solid particles from the extractor vessel. Point 6 in **Figure 3.8b** is the second acting position of the pressure actuator valve (V7b). Also the line splits at this point, which is used for cleaning the outbound pipeline.

The FPR2 controls the downstream pressure by reducing the working pressure down to 60-80 bar checked by manometer M6. At this point the extract expands, thus dropping the temperature. A heater jacket (Model: M2174/0295, Omega Engineering, Canada) is added around the pipeline to avoid blocking. The temperature of the heated line is controlled by a thermopar connected to the outside of the metal line with a set point of 335 K, and the temperature is shown in an associated display. Because the pressure reduction is high and difficult to control, FPR2 is assisted by valve

V8. The existence of V8 improves the control of the flow rate that is then finely adjusted by a needle valve (V9) at the end. The last equipment piece is the recovery vessel. The CO_2 flows to the recovery vessel and bubbles throughout a solvent to capture the extracted compounds.

Most of the extracted oil precipitates just after FPR2 and along the pipeline. It is then removed by injecting an organic solvent through valve V10, when valves V7a and V7b are closed and the line connected to vacuum. The washing stream containing the precipitated oil is also collected in the recovery vessel. Afterwards the system returns to the normal functioning mode by closing V10 and reopening the pipeline by activating the pneumatic actuator (opening valves V7a and V7b).

3.3. Experimental Section

3.3.1. Plant Material and Reagents

Seeds were collected from grapes (*Vitis vinifera* L.) of the red variety 'Touriga Nacional' provided by "Caves Messias" (Anadia, Portugal). Grape seeds were obtained during transfer of the musts for wine fermentation in the year of 2007. The grinded seeds to be extracted (0.07 kg) were placed in the extractor vessel and stamped down carefully. More detail about the grape seeds assemble used in each experimental set is shown in **Table 3.2**. Other solid characteristics such as the true and bulk density, and the porosity (experimentally determined by gravimetry) are also shown in **Table 3.2**.

Free stable DPPH radical, stearic acid, palmitic acid, methyl heptadecanoate, and dl-α-tocopherol were purchase from Sigma-Aldrich Co. (St. Louis, MO, USA). FAME Misture of C8-C24 was purchase from Supelco (Bellefonte, PA, USA). Grape seed commercial oil was purchase from New Directions (Portugal).

Table 3.2 – Grape seed characteristics, pre-treatment conditioning, and SFE operating conditions.

Exp.		Pre-treatment	Operating Conditions			Seed Characterization				
			P (bar)	T (K)	$^{*}\rho_{CO_2}$ ($kg \cdot m^{-3}$)	ρ_{bulk} ($kg \cdot m^{-3}$)	ρ_s ($kg \cdot m^{-3}$)	ε	d_p (10^{-3} m)	m_{seed} (kg)
Soxhlet	1	-	-	-	-	688	1100	0.37	0.75	0.01
	2	-	-	-	-	496		0.55	0.85	
	3	Enzymatic♠	-	-	-	688		0.37	0.75	
	4	HPP (1000 bar)♦	-	-	-	496		0.55	0.85	
	5	HPP (3000 bar) ♦	-	-	-					
SFE	1	-	160	313.15	794.9	688		0.37	0.75	0.07
	2	Enzymatic♠								
	3	-	180		819.7					
	4	Enzymatic♠								
	5	HPP (1000 bar) ♦				496		0.55	0.85	
	6	HPP (3000 bar) ♦								
	7	-		323.15	756.7	688		0.37	0.75	
	8	-	200	313.15	840.2					
	9	Enzymatic♠								
	10	-		323.15	784.2					
	11	-	220	313.15	857.7					

♠ Enzymatic pre-treatment conditions: 24 h, pH 4, 313.15 K, and an enzymatic cocktail with cellulase, xylanase, pectinase, and protease, whose concentrations are respectively 29, 1191, 21, and 569 U per gram of seed sample. ♦High pressure pre-treatment conditions: 15 min at 295.15 K. *Carbon dioxide density estimated using Bender's equation of state with parameters for pure CO_2 listed by Brunner (1994).

3.3.2. SFE experimental conditions and extraction procedures

Approximately 0.07 kg of grinded grape seeds (m_{seed} , **Table 3.2**) were charged into the extractor and a small amount of steel shreds was packed at the top to prevent seed powder to escape. All the

preparation procedures applied to the seeds (such as cleaning, grinding and sieving) have been described in Chapter 1, and all information necessary to perform the enzymatic pre-treatments may be found in Chapter 2.

To analyse both the effect of *P* and enzymatic pre-treatment on the SFE yield, experiments were accomplished at 160, 180, and 200 bar, at constant temperature ($T = 313.15$ K) and carbon dioxide flow rate ($\dot{m} = 1.7 \times 10^{-4}$ kg·s^{-1}), for both untreated and pre-treated samples. The experimental conditions of the enzymatic pre-treatment selected from the previous chapter were: 24 h, pH 4, 313.15 K, and an enzymatic cocktail with cellulase, xylanase, pectinase, and protease, whose concentrations are respectively 29, 1191, 21, and 569 U per gram of seed sample. The effect of *T* was also considered by measuring SFE curves at 180 and 200 bar at the new temperature of 323.15 K. Additional conditions include extraction at 220 bar and 180 bar with high pressure (HPP) pre-treated seed. The CO_2 mass flow was maintained constant through experiments. The extraction curves were obtained by representing yield (η) against consumed CO_2. The yield is defined as the mass of extracted oil divided by the mass of dried seed loaded. Whenever an experiment was interrupted to assess a new data point of its extraction curve, the oil precipitated along the pressure drop section (between FPR2 and V8, **Figure 3.7**) was recovered by washing with *n*-hexane, dried and weighed.

Conventional Soxhlet extractions. Conventional extraction was carried out for comparison using 0.15 L of *n*-hexane in a Soxhlet apparatus (0.25 L round bottom flask; Soxhlet chamber of 0.05 L capacity; 23x100 mm cartridge) during 4 h. All particle sizes were studied and the most favourable conditions of the enzymatic pre-treatment selected in Chapter 2.

3.3.3. HPP experimental conditions

This section focus a first exploratory attempt to a new pre-treatment approach through HPP. More information about the selection of pre-treatment operating conditions may be found elsewhere (Magalhães, 2008). The HPP experimental work has been accomplished in a Hydrostatic press (Unipress Equipment, Model U33, Poland). The equipment has a maximum capacity of 0.1 L, a maximum operating pressure of 7000 bar and a temperature range of 293.15 K up to 373.15 K. The milled seeds were previously water floated overnight (2 $mL_{water} \cdot g_{seed}^{-1}$) and only then submitted to the HPP. Two different pressures were used, 1000 and 3000 bar, during 15 min at 295.15 K. The seed samples were frozen, freeze dried and storage. Afterwards the pre-treated samples were extracted with SC-CO_2 at 180 bar and 313.15 K.

3.4. Results and Discussion

The results obtained in this work by Soxhlet and SFE of both treated and untreated grape seed are compiled in **Table 3.3**. The operating conditions are repeated from **Table 3.2** for clarity. The pre-treatments refer to HPP and enzymatic.

3.4.1. SFE – Pressure effect

The cumulative SFE curves obtained with untreated seeds at $T = 313.15\,\text{K}$, $\dot{m} = 1.7\times10^{-4}\ \text{kg}\cdot\text{s}^{-1}$, and $P = 160$, 180, 200 and 220 bar (**Table 3.3**, Exp. **SFE 1**, **3**, **8**, **11**) are shown in **Figure 3.9**, where yield (η,% w/w) is plotted against solvent consumption (m_{CO_2}). Additionally, **Table 3.3** presents results from Soxhlet experiments, namely yield and the standard deviation (σ) associated to a minimum of three experiments.

The cumulative curves of **Figure 3.9** exhibit the two characteristic extraction periods. During the 1st extraction period, the yield increase is approximately linear. The 2nd part has a smooth asymptotic shape and represents only 3-8% of the total oil extracted. Such trends corroborate the hypothesis of the broken+intact cells model proposed by Sovová (1994, 2005) which assumes that the extraction kinetics is governed by two mechanisms: first, a rapid extraction from surface occurs, which is followed by a diffusion-controlled extraction from inner intact cells.

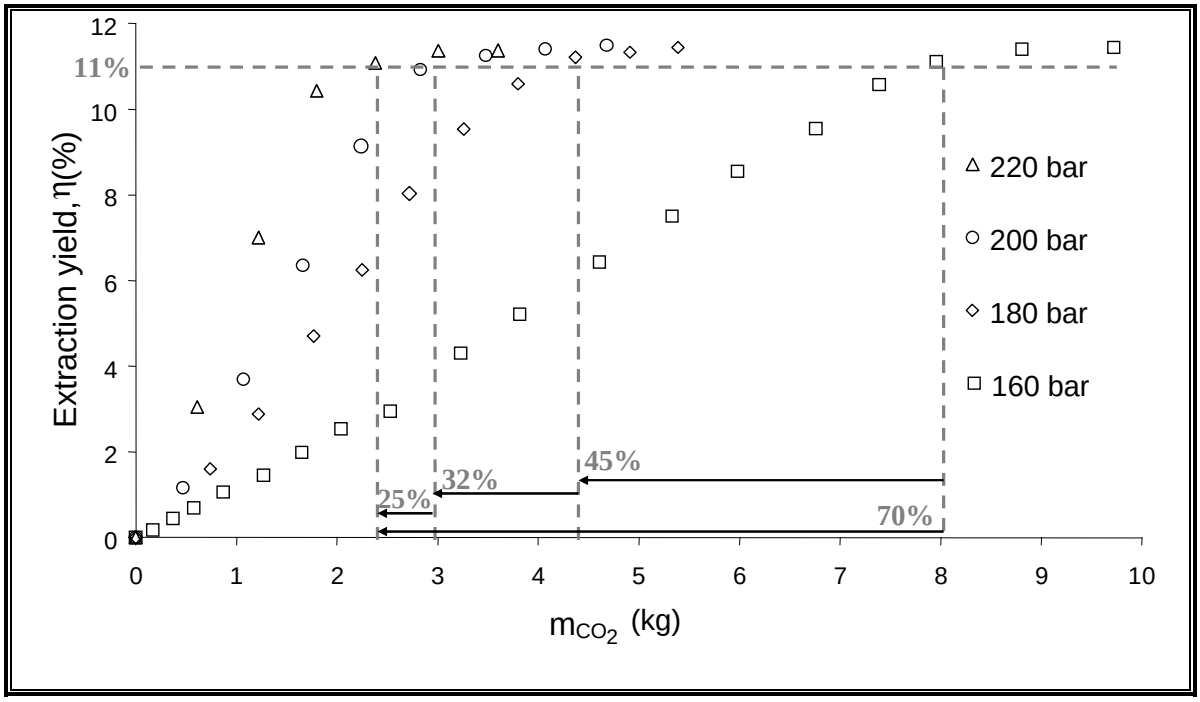

Figure 3.9 – Extraction curves for the SFE of untreated grape seed oil at 313.15 K (Exp. SFE 1, 3, 8, 11 of Table 3.2). The vertical lines limit the end of the 1st period of extraction.

Table 3.3 – Grape seed characteristics, pre-treatment and SFE operating conditions, and extraction yields.

Exp.		Pre-treatment applied	Operating conditions					Experimental results			Correlations				
			P (bar)	T (K)	ρ_{CO_2} ($kg \cdot m^{-3}$)	d_p (10^{-3} m)	m_{seed} (kg)	η (%)	σ (%)	y_0 ($g_{oil} \cdot kg_{CO_2}^{-1}$)	y_s ($g_{oil} \cdot kg_{CO_2}^{-1}$)	N_{Re}	N_{Sc}	k_f (10^{-6} $m \cdot s^{-1}$)	D_{12} (10^{-9} $m^2 \cdot s^{-1}$)
Soxhlet	1	-	-	-	-	0.75	0.01	11.6	0.62	-	-	-	-	-	-
	2	-	-	-	-	0.85		6.72	0.03	-	-	-	-	-	-
	3	Enzymatic	-	-	-	0.75		17.2	0.27	-	-	-	-	-	-
	4	HPP (1000 bar)	-	-	-	0.85		6.54	0.02	-	-	-	-	-	-
	5	HPP (3000 bar)	-	-	-			6.43	0.03	-	-	-	-	-	-
SFE	1	-	160	313.15	794.9	0.75	0.07	11.4	-	1.54	1.99	1.56	22	7.87	3.85
	2	Enzymatic						16.4	-	1.76					
	3	-	180		819.7			11.4	-	1.76	2.68	1.54	24	7.50	3.63
	4	Enzymatic						15.8	-	2.46					
	5	HPP (1000 bar)				0.85		6.93	-	2.27				6.34	
	6	HPP (3000 bar)						6.75	-						
	7	-		323.15	756.7	0.75		12.0	-	1.51	2.01	1.59	19	7.73	4.35
	8	-	200	313.15	840.2			11.5	-	2.72	3.41	1.51	26	7.39	3.46
	9	Enzymatic						16.2	-	2.94					
	10	-		323.15	784.2			12.0	-	1.94	2.85	1.56	21	7.62	4.08
	11	-	220	313.15	857.7			11.4	-	3.90	4.17	1.49	27	7.30	3.32

ρ_{CO_2} – carbon dioxide density estimated using Bender's equation of state with parameters for pure CO_2 listed by Brunner (1994); y_0 – oil concentration at the extractor outlet; y_s – grape seed oil solubility estimated with the correlation of del Valle and Aguilera (1988); N_{Re} – Reynolds number; N_{Sc} – Schmidt number; k_f – convective mass transfer coefficient calculated by the correlation of Tan *et al.* (1988); D_{12} – binary diffusivity calculated with the correlation of Catchpole and King (1994).

Discussion of the assumptions of this model and the results achieved in our work will be presented in Chapter 5. The maximum yield reaches $\eta = 11.5\%$ being common to all four curves, and is similar to $\eta = 11.6\%$ obtained by Soxhlet extraction (**Table 3.3**, **S1**). Such fact means SFE is able to perform the complete extraction of the available oil.

The increments of η in **Figure 3.9** prevail when passing from 160 to 180 bar, with a horizontal spacing $m_{CO_2} \approx$ 4.4-8.0 kg in the top. The spacing between adjunct curves for 160, 180, 200 and 220 bar results in a decreasing CO_2 consumption to reach η_{max}, still significant for the highest pressures: 200 $\rightarrow$ 220 bar, 3.0 $\rightarrow$ 2.4 kg. An operational consequence of this relation is that the time or, equivalently, the mass of CO_2 needed to reach a definite extraction yield decreases at higher pressures at constant flow rate.

According to **Figure 3.9** one spends approximately 2.4, 3.0, 4.4, and 8.0 kg to reach the end of the 1st period of extraction ($\eta \cong 11\%$) at 220, 200, 180 and 160 bar respectively. The highest yield to CO_2 consumption ratio for untreated seeds was obtained using the highest pressure of 220 bar. Only 2.4 kg of CO_2 per seeds batch was spent using such conditions considering getting 11% of oil. As a result, more than 70% of CO_2 is saved when considering the highest CO_2 consumption at 160 bar, and only 4% of oil is lost (necessary to reach η_{max} =11.4%, Exp. **SFE 1** of **Table 3.3**). When considering small increments of 20 bar (i.e., passing from 160 to 180, 180 to 200, and 200 to 220 bar) the CO_2 consumption is reduced by 45, 32 and 25%, respectively. These results show that the impact in the CO_2 consumption is highest for the lowest pressure ranges and decreases when pressure increases. These data corroborates results reported by Fiori (2007) who studied the extraction of grape seed oil in the range of 280 to 550 bar, which showed a decrease of 60% on solvent consumption from 280 to 350 bar, and only of 8% from 350 to 550 bar.

3.4.2. SFE – Temperature effect

Experiments with untreated seed at 180 and 200 bar were run also at 323.15 K (**Table 3.3**, Exp. **SFE 7** and **10**), being compared to those obtained at 313.15 K (Exp. **SFE 3** and **8**) in **Figure 3.10**. The η is once more plotted against solvent consumption. All extraction curves present the initial linear extraction period followed by a smooth asymptotic plateau described before. The maximum yield reached $\eta \cong 12\%$ (Exp. **SFE 7**, **10**). This result slightly overcomes that from conventional Soxhlet extraction (**Table 3.3**, Exp. **S1**), though it is within the error interval. However, the lowest CO_2 consumption at the end of the 1st period ($\cong$ 11%) was obtained using the highest pressure and the lowest temperature (200 bar/313.15 K), spending only 3.0 kg of CO_2 per seed batch in such case. As a result, more than 40% of CO_2 is saved in relation to 180 bar/323.15 K.

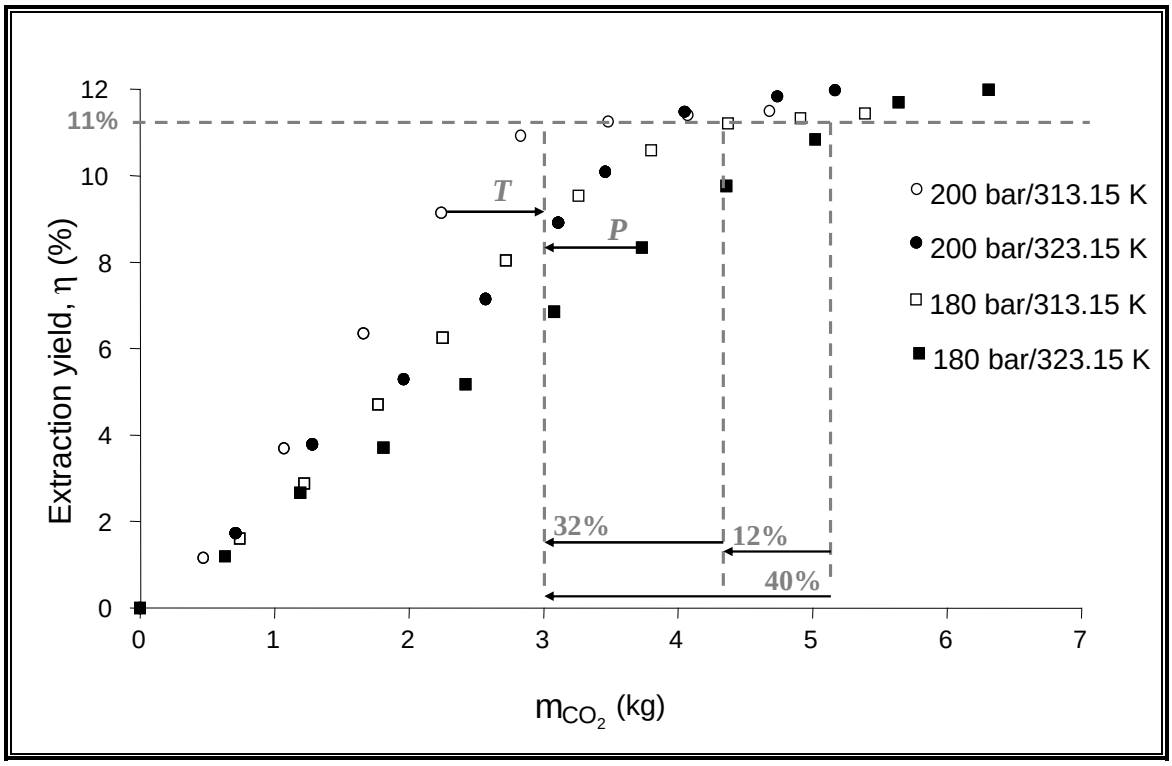

Figure 3.10 – Extraction curves for the SFE of untreated grape seed oil at 313.15 K (Exp. SFE 3 and 8 of Table 3.2) and 323.15 K (Exp. SFE 7 and 10 of Table 3.3). The vertical lines limit the end of the 1st periods of extraction.

Figure 3.10 also presented the overlap between the cumulative curves for 180 bar/313.15 K and 200 bar/323.15 K, emerging a similar behaviour between a positive pressure variation (ΔP) of 20 bar and the decrease of operating temperature (ΔT) by 10 K.

By using literature correlations to estimate both the values of oil solubility in SC-CO_2 and convective mass transfer coefficient (k_f), one may interpret and explain previous results. Solubility listed in **Table 3.3** as y_s has been calculated using the correlation of del Valle and Aguilera (1988) (see **Appendix A1**). Under the same temperature conditions, higher pressures give rise to higher densities (ρ), which increase oil solubility, while under the same pressure conditions, lower temperatures leads to higher densities which, once again, increase oil solubility. Consequently, oil solubility rises with both increasing pressure and decreasing temperature enhancing the extraction rate in both cases. **Table 3.3** also presents k_f predicted by the correlation of Tan *et al.* (1988) (see **Appendix A2**). Other expressions, such as those by Wakao and Kaguei (1982) and King and Bott (1993), were included also in **Appendix A2**. None of these models however is able to completely agree with the validity range of both Reynolds (N_{Re}) and Schmidt (N_{Sc}) numbers. Nonetheless, whichever the correlation used, the predicted values of k_f are almost independent of both pressure and temperature conditions of this work. Therefore, one concludes that the effect of solubility is the

utmost important driving the extraction curves behaviour found, furthermore experimentally justified by the overlap of the 180 bar/313.15 K and 200 bar/323.15 K curves, as both conditions present y_S =2.68 and 2.85 $g_{oil} \cdot kg_{CO_2}^{-1}$, respectively.

Another important conclusion driven from the SFE curves has to deal with the fluid phase concentration at extractor outlet (y_0). A simple material balance during the 1st period of extraction may be used to determine it:

$$\dot{m}_{CO_2} \times t \times y_0 = \eta(t) \times m_{seed} \quad \textbf{[3.1]}$$

The results for y_0 were included in **Table 3.3** for untreated seed, and deviate 20.2-34.3% to the estimated y_s, which point out that the outlet stream is not saturated.

3.4.3. SFE of pre-treated seed

Enzymatically pre-treated seed. The cumulative curves obtained for the enzymatically pre-treated seed are shown in **Figure 3.11**. Extractions were carried out at the same experimental conditions of untreated seeds to allow comparisons with previous results: $T = 313.15$ K, $\dot{m} = 1.7 \times 10^{-4}$ kg $\cdot s^{-1}$ and $P = 160$, 180 and 200 bar (see **Table 3.3**: untreated Exp. **SFE 1**, **3**, and **8**; enzymatically pre-treated Exp. **SFE 2**, **4**, and **9**). Soxhlet extraction has also been performed (**Table 3.3**, Exp. **S3**).

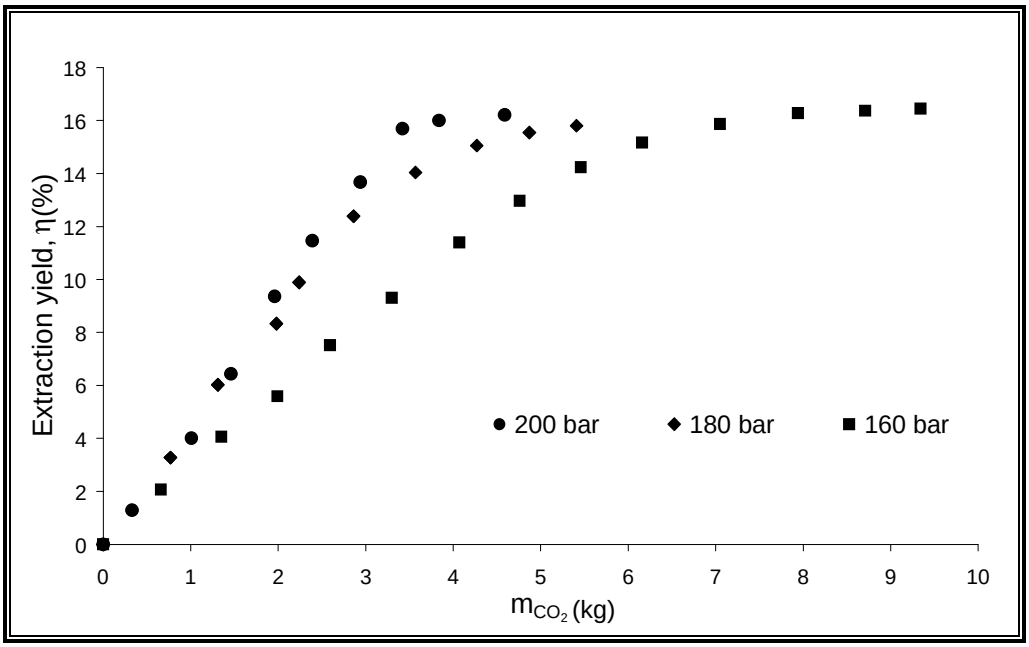

Figure 3.11 –Extraction curves for the SFE of enzymatically pre-treated grape seed oil at 313.15 K (Exp. SFE 2, 4 and 9 of Table 3.2).

All curves exhibit once more both characteristic extraction periods (i.e. linear plus asymptotic). However, the maximum extraction yield was now η =16.4%, which represents an increment of 43% over η for untreated seeds (η =11.5%). Such enhancement is due to the enzymatic action that increases seed oil availability.

Yield for the SFE of pre-treated seed is close to the one obtained by Soxhlet (η =17.2%; see **Table 3.3**, Exp. **S3**) under the best enzymatic conditions fixed in Chapter 2. Comparison of results obtained with treated and untreated grape seeds at 160, 180 and 200 bar is presented in **Figure 3.12**. It is possible to verify that each pair of correspondent curves reached the maximum extraction yields for untreated and pre-treated seeds at nearly the same CO_2 consumption levels (8.0, 4.4-5.0, and 3-3.8 kg per seeds batch at 160, 180 and 200 bar).

We have determined the fluid phase concentration at extractor outlet (y_0) from the slope of the curves by **Equation [3.1]**. It has been assumed in the literature that, as long as the extract is saturated, y_0 would correspond to the oil solubility in the supercritical solvent. However, if the extract is not saturated, the value calculated by **Equation [3.1]** is considered only an apparent solubility. From the results of **Table 3.3** for untreated seed it has been concluded that the solvent has not achieved saturation. The comparison presented in **Figure 3.12** reinforces this fact.

It is worth noting that the slopes of the cumulative curves for untreated and pre-treated seed are clearly different from each other (**Figure 3.12**). The vertical spacing at 160 bar/313.15 K is about 53% when m_{CO_2} = 3.3 kg (**Figure 3.12a**), which means the output extract is indeed not saturated along time. If it was the case, the first linear parts of the extraction curves should overlap. Therefore, the extraction is not exclusively controlled by equilibrium under the experimental conditions used. The difference between both curves arises because the enzymatic pre-treatment enlarges the broken/intact cells ratio increasing the oil availability in contact with the solvent. This effect decreased with increasing pressure. It was less pronounced at 180 bar/313.15 K (**Figure 3.12b**) where the vertical spacing is about 37% at m_{CO_2} = 2.20 kg, and was almost not observed at 200 bar/313.15 K (**Figure 3.12c**) where it only increased 9% at m_{CO_2} = 1.2 kg, which indicates that at this pressure the extract stream is getting closer the saturation. The calculations of y_s agree with these observations as the deviation from the experimental value is the minimum (13.8%).

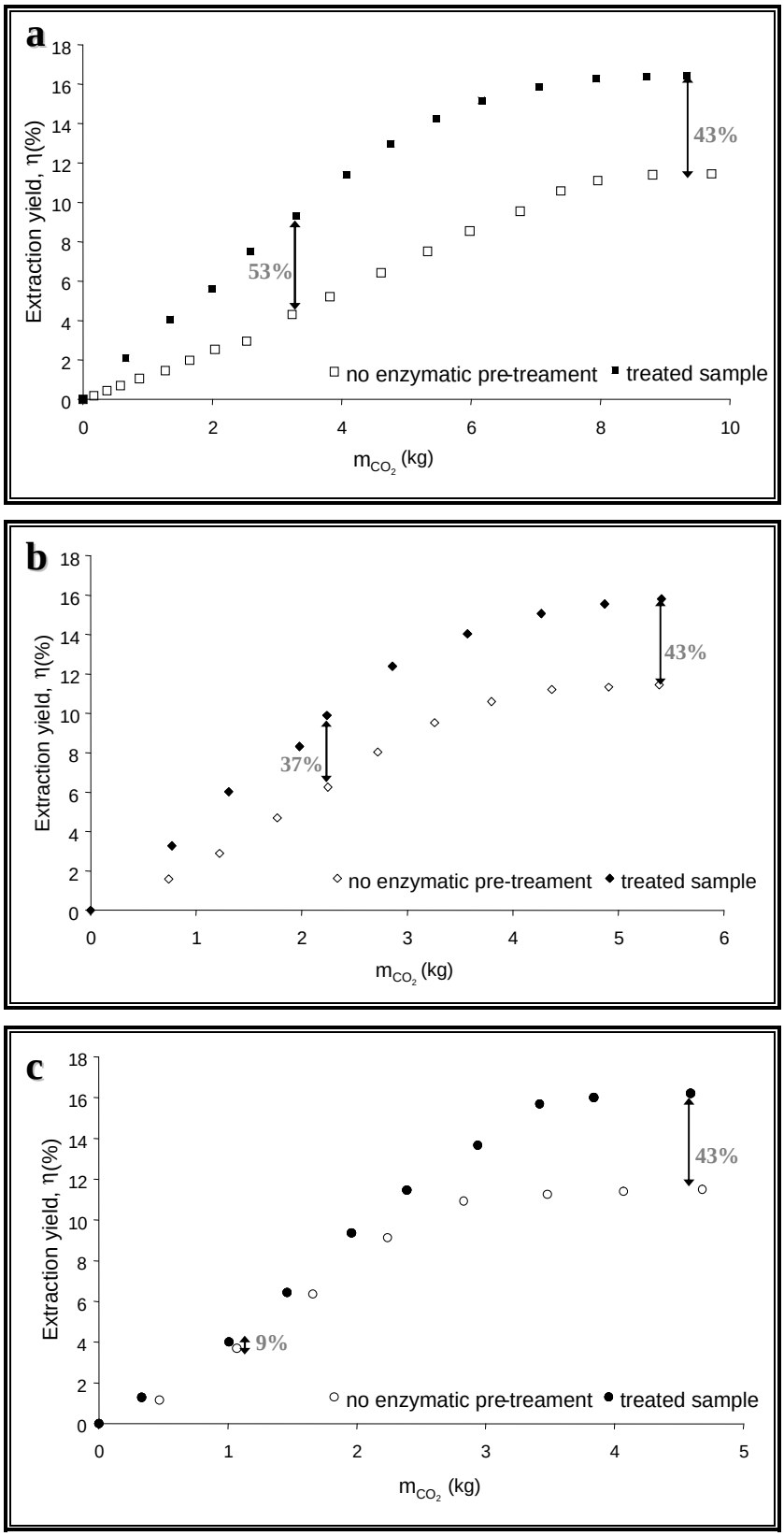

Figure 3.12 – Extraction curves for the SFE of untreated and enzymatically pre-treated grape seed at 313.15 K and: (a) 160 bar (Exp. SFE 1 and 2); (b) 180 bar (Exp. SFE 3 and 4); (c) 200 bar (Exp. SFE 8 and 9).

High pressure pre-treated seeds. The SFE curves of high pressure processed (HPP) seed are shown in **Figure 3.13** together with one for untreated grape seed (results in **Table 3.3**, Exp. **SFE 5**, **6** and **3**, respectively). All curves were obtained at $P = 180$ bar, $T = 313.15$ K and $\dot{m} = 1.7 \times 10^{-4}$ kg·s^{-1}. The average particle diameter used in the HPP study was 0.85 mm, whereas for untreated seed was 0.75 mm. It has been impossible to carry out HPP runs for 0.75 mm due to an equipment failure, which unfortunately was not fixed until the end of our experimental program.

The curves for HPP treated and untreated seed exhibit the same general trend with both extraction periods presented. The maximum yields were however distinct because of the dissimilar sizes used: from **Table 3.3**, $\eta = 6.93$ and 6.75% (d_p = 0.85 mm, HPP+SFE, Exp. **SFE 5** and **6**) against 11.4% (d_p = 0.75 mm, Exp. **SFE 1**). Soxhlet extractions for d_p = 0.85 mm followed by HPP were also performed for comparison giving rise to $\eta = 6.54$ and 6.43% (see **Table 3.3**, Exp. **S4** and **S5**). It is worth noting the large yield increment gained just by size reduction, as the extraction by Soxhlet for d_p = 0.75 mm originated η =11.6% (Exp. **S1**, untreated seed). Contrarily to the enzymatic pre-treatments analyzed above, the HPP did not improve the oil yield of both Soxhlet and SFE.

The two pressure conditions used during HPP (1000 and 3000 bar) did not inflect any change in Soxhlet and SFE yields.

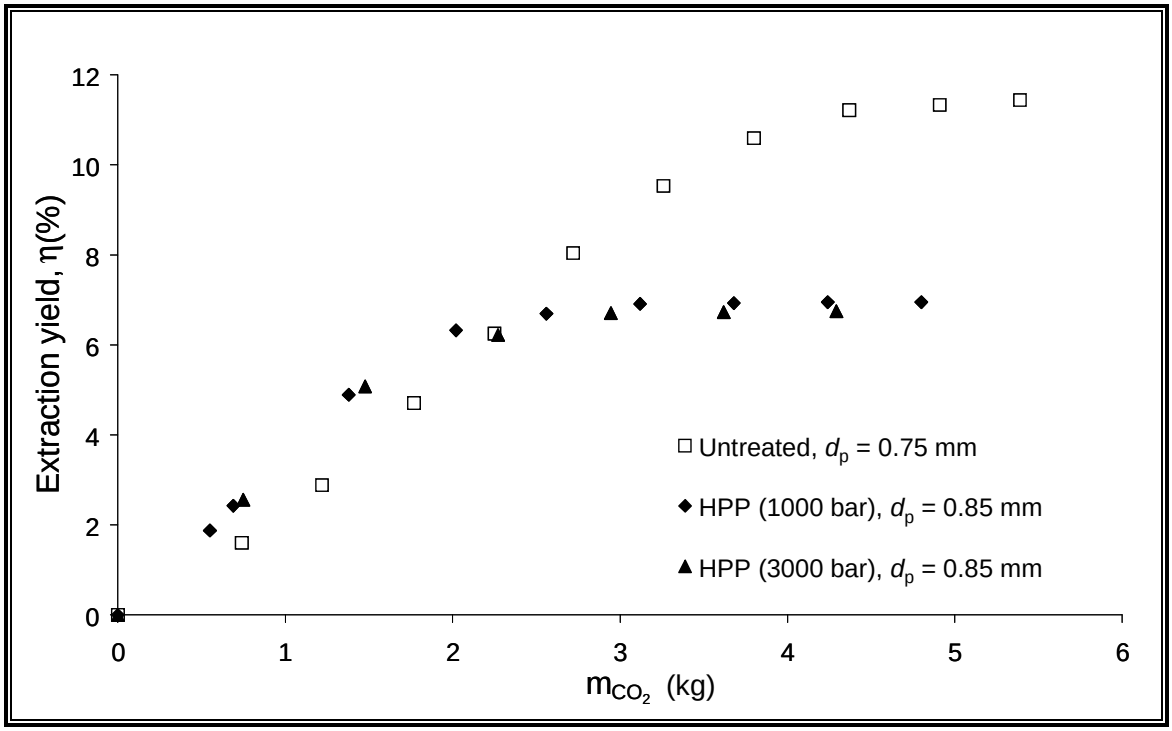

Figure 3.13 – Comparison between the measured extraction curves for untreated and high pressure pre-treated grape seed at 313.15 K and 180 bar. (Exp. SFE 3, 5 and 6 of Table 3.2).

Final remarks. The operating pressure is unquestionably one of the most relevant process parameters that can be used to tune the selectivity of a SCF. The general rule is: the higher is the pressure, the larger is the solvent power though the smaller is the extraction selectivity. Several studies reported the use of extremely high pressures (Reverchon and Marrone, 2001; Reverchon and De Marco, 2006; del Valle *et al.*, 2005; Fiori, 2007) in order to achieve good solvent capacity of SC-CO_2. It was demonstrated in this work that oil production can be improved under relatively mild operating conditions if the SFE is combined with an enzymatic pre-treatment.

Use of pre-treatments become especially important if considering the capital cost of the SFE units, which rises significantly with the increase of the operating pressure. Moreover, the pressure ratings of certain vital equipment are available in discrete steps (e.g., 60 and 100 bar). In addition, the number of companies with experience in supercritical process design drops as the operation pressure rises above 200 bar (Beckman, 2004). Clearly, these caveats strongly recommend operating at pressures as low as possible. The enzymatic pre-treatment seems a viable option since it becomes possible to achieve good results operating the SFE unit at lower pressure, furthermore achieving similar or even better oil extractability results in relation to non-treated raw material.

The enzymes used in the pre-treatment need also to be recycled to assure the industrial viability of the process. As enzymes are soluble in water, a simple decantation of the seeds, a filtration, or a centrifugation will allow obtaining an aqueous solution, which can be reused. Knowledge about the loss of enzyme activity is also required. Finally, use of any pre-treatment requires an additional drying stage that will have to be accounted for in the operating costs.

4. Grape Seed Oil Quality

I think you can accomplish anything if you are willing to pay the price.
[Vince Lombardi]

4. Grape Seed Oil Quality

In this chapter the quality of the grape seed oil, obtained by SFE, is evaluated in order to analyse the influence of the operating pressure and temperature upon it.

The oil triacylglycerides (TAG) content and the fatty acids profile have been determined both in the individual fractions obtained along the SFE, and in the global extract at the end.

The antioxidant capacity (AOC) of these samples has also been evaluated by measuring its total free radical scavenger capacity (by spectrophotometric methodology), therefore studying how the operating conditions and the seed pre-treatments affect this property.

4.1. Introduction

The industrial processes commonly adopted to produce edible oils from vegetable seeds comprehend several stages, where the extraction with *n*-hexane is an important one. However, this organic solvent is usually non-selective and accomplishes the simultaneous removal of non-volatile pigments and waxes, giving rise to dark coloured and viscous extracts contaminated with solvent residues. This renders them difficult to handle without further refining, and may inclusively dictate the future commercial viability of the oil (Hanmoungjai *et al.*, 2000; Gomes *et al.*, 2007). For instance, the introduction of organic solvents may even threat the biological status of oils obtained from seeds of biological agriculture (Fiori, 2007).

The use of supercritical fluids as alternative solvents has been attracting widespread interest owing to their particular properties, as has been already discussed in previous chapters. Particularly interesting in the SFE of seed oils with CO_2 is the preservation of their natural phytochemicals, such as antioxidant tocopherols (Diaz-Reinoso *et al.*, 2006; Kornsteiner *et al.*, 2006), ensuring the conservation of their high quality. The colour of the extracts produced has been reported to be clearer compared to those of the products obtained with conventional solvents (Carvalho *et al.*, 2005). Several literature reports confirm that SC-CO_2 extracted oils have lighter final colour as reported for instance for cherry seed (Bernardo-Gil *et al.*, 2001), hazelnut (Bernardo-Gil *et al.*, 2002) and acorn oil (Lopes and Bernardo-Gil, 2005).

4.1.1. Grape seed oil triacylglycerides composition

The quality of grape seed oil is due to its high level of unsaturated fatty acids (ca. 90%), particularly linoleic (C18:2) and oleic (C18:1); traces of linolenic (C18:3) and palmitoleic (C16:1)

may be found also (Crews *et al.*, 2006; Bail *et al.*, 2008). On the characterization of cherry seed (Bernardo-Gil *et al.*, 2001), hazelnut (Bernardo-Gil *et al.*, 2002), and acorn oils (Lopes and Bernardo-Gil, 2005), no significant differences with respect to TAG composition were found between oils obtained by distinct extraction methodologies. The only detected differences were the decrease of the ratio LOO[*]/OOO[†] with lower percentage of unsaturation by solvent extraction (LOO/OOO = 4) compared to supercritical extraction (LOO/OOO = 6) of hazelnut oil. Similarly, a decrease of the POO[‡]/OOO ratio was observed from conventional to supercritical extraction of cherry seed oil, though the difference in the TAG saturation level is small.

Significant influence of the grape variety on the oil TAG composition was reported for oils extracted using organic solvents, whereas with SC-CO_2 it is less important. The work presented by Crews *et al.* (2006) embodied thirty grape varieties from three wine-producing countries (France, Italy and Spain) and shown that the composition of the oil obtained by Soxhlet extraction depends upon grape variety, growing location and maturity, and soil composition. However, results by Beveridge *et al.* (2005) for grape seed oil extracted with SC-CO_2 revealed no significant differences between varieties (linoleic/oleic ratio between 4-6).

Fatty acids methyl esters (FAME) analysis. Several chromatographic methods have been reported for the separation of lipids. The most widespread ones involve normal-phase systems in which the solutes are retained according to their relative polarity. Although fatty acids can occur in nature in the free (unesterified) state, they are most often found as esters, linked to glycerol, cholesterol or long-chain aliphatic alcohols. Prior to separation and analysis by GC, it is generally recommended to hydrolyze the triacylglycerides to the free form or convert them to suitable derivatives of low molecular weight and polarity, and high volatility. Often, they are prepared as methyl ester derivatives obtained by direct transesterification, where both acidic and basic procedures are available. The methyl esters derivatives are the simplest in structural terms, with well documented and understood properties, therefore been the most commonly used standards as a guide to identification. Another approach is to use a standard consisting of a mixture of known composition. The retention times of the methyl esters derivatives prepared from that mixture are measured under identical operating conditions (Christie, 1987, 1993; Eder, 1995; Gutnikov, 1995).

[*] LOO – Linoleic/Oleic/Oleic acid triacylglyceride composition;
[†] OOO – Oleic/Oleic/Oleic acid triacylglyceride composition;
[‡] POO – Palmitic/Oleic/Oleic acid triacylglyceride composition.

4.1.2. Grape seed oil lipophylic antioxidants

The primary characteristic required for most high value consumption oils is liquidity at ambient temperature while maintaining high-stability, i.e. high resistance to oxidation. Most vegetable oils that are liquid at room temperature generally contain high level of polyunsaturated fatty acids, which results in low melting points, but also extremely high susceptibility to oxidation (O'Brien, 1998). Therefore, it is imperative in the food industry to find ways of preventing oil oxidation. The following guidelines can be laid down to avoid/reduce rancidity (Berger and Hamilton, 1995):

i. maximal retention of natural antioxidants;
ii. low temperatures during processing and storage;
iii. reduce access of air;
iv. minimise the interaction of the oil with catalytic metals.

SFE methods are indeed a good practice as they comply the last three requirements, whereas the first one can be also addressed.

Tocopherol, commonly known as vitamin E, is widespread in vegetable oils. Unrefined oils may contain tocopherol and other bioactive compounds at concentrations of about 0.02-1.2 g/kg, which in most applications is a sufficient level to provide the necessary food antioxidant properties (Ong and Goh, 2002; Lopes and Bernardo-Gil, 2005; Bail *et al*., 2008). Nonetheless, such compounds are frequently lost during food processing, which demands not only mild operating conditions, but also its higher extractability and selectivity (Nicoli *et al*, 1999; Bravi *et al.*, 2007).

During the extraction of cherry seed oil, Bernardo-Gil *et al.* (2001) obtained a similar tocopherol content using both SC-CO_2 and organic solvent, which resulted in similar stability. However, Lopes and Bernardo-Gil (2005) showed that, while the extraction methodology did not inferred significant differences in tocopherols content in the acorn seed oil, the same did not occur with hazelnut oil where higher tocopherol quantities were obtained by Soxhlet in relation to SFE at 220 bar and 308.15 K. Hence, the evaluation of the AOC of the extracted oil should be performed to tailor the extraction methods and operating conditions in order to preserve their bioavailability in the final product (Nicoli *et al*, 1999; Diaz-Reinoso *et al.*, 2006).

As far as tocopherol extraction is concerned, the concentration in the oil extracted with SC-CO_2 increases with temperature, which is coherent with its higher solubility at higher temperatures found by Chrastil (1982) and later by Bravi *et al.* (2007), who showed such increase from 313.15 to 353.15 K.

Some oils may contain other natural antioxidants in addition to tocopherols as, for example, sesamol in sesame seed oil (Berger and Hamilton, 1995). A common characteristic of many natural

antioxidant mixtures is synergism. Synergistic systems take advantage of the greater potency produced by the mixture, without increasing total antioxidants content (O'Brien, 1998). In the work presented by Lopes and Bernardo-Gil (2005), higher stability of the conventional extracted oil compared to the supercritical one was observed despite the fact that both samples contained similar amounts of tocopherols, which was explained by the synergetic effect of phospholipids (not extracted with SC-CO_2 conditions) with tocopherols. However, the opposite effects of mixtures possessing lower antioxidant activity compared to the individual components has also been proved to exist (Peschel *et al.*, 2006). Sovová *et al.* (2004) observed a negative effect of chlorophylls on the inhibitory antioxidant action of grape seed extracts. Interestingly, their effect in extracts from SC-CO_2 is minimized due to their polarity, which implies they are weakly soluble in SC-CO_2 and explains in part why such extracts exhibit normally lighter colour than Soxhlet extracts (Sovová *et al.*, 2004).

In this chapter the effect of seed pre-treatments and SFE operating conditions on the quality of the individual extracts (collected along an experiment) and on the final oil is presented. The TAG content, the fatty acids profile, and the AOC of the oil samples were determined in order to provide information about suitable processing conditions. The AOC was evaluated by measuring the total free radical scavenger capacity of the samples, following the well known DPPH· methodology (Espín *et al*., 2000).

4.2. Experimental Section

4.2.1. Triacylglycerides profile

The FAMEs were obtained by transesterification of triacylglycerides with sodium methoxide since it is a very simple and fast methodology, and especially because it proceeds at ambient temperature, therefore reducing the risk of decomposition of polyunsaturated fatty acids (Aued-Pimentel *et al.*, 2004). In general lines, the procedure includes the preparation of an internal standard solution of heptadecanoate methyl ester with concentration 7.5×10^{-2} kg·L^{-1}. The oil sample (4.0×10^{-4} kg) was dissolved in 1.0×10^{-3} L of *n*-hexane with further addition of 4.0×10^{-3} L of the internal standard solution. 2.0×10^{-4} L of a methanolic KOH solution (2 M) were added, the sample was sealed and mixed vigorously for 30 s in a vortex shaker. After that, 2.0×10^{-3} L of saturated sodium chloride solution were introduced, and the sample submitted to centrifugation (Kubota 2000, Kubota, Germany) at 2000 rpm during 5 min. Finally, 1.0×10^{-3} L of the organic phase was taken to another tube. Aliquots (0.1-0.5 μL) of this organic phase were used in GC analysis.

GC-FID. Following the transesterification, the FAMEs were analyzed and separated in a Gas Chromatograph (Perkin Elmer Clarus 400, USA) (**Figure 4.1a**) equipped with a 30 m×0.32 mm (i.d.), 0.25 μm film thickness DB-FFAP fused silica capillary column (DB-FFAP, J&W Scientific Inc., USA) and a flame ionization detector. The characteristics of this high polarity column, which is specifically indicated for the analysis of volatile fatty acids and phenols, include a stationary phase of nitroterephthalic acid modified by polyethylene glycol and a temperature limit of 313-523 K. Split injection mode was used with a ratio of 20:1 (5 min).

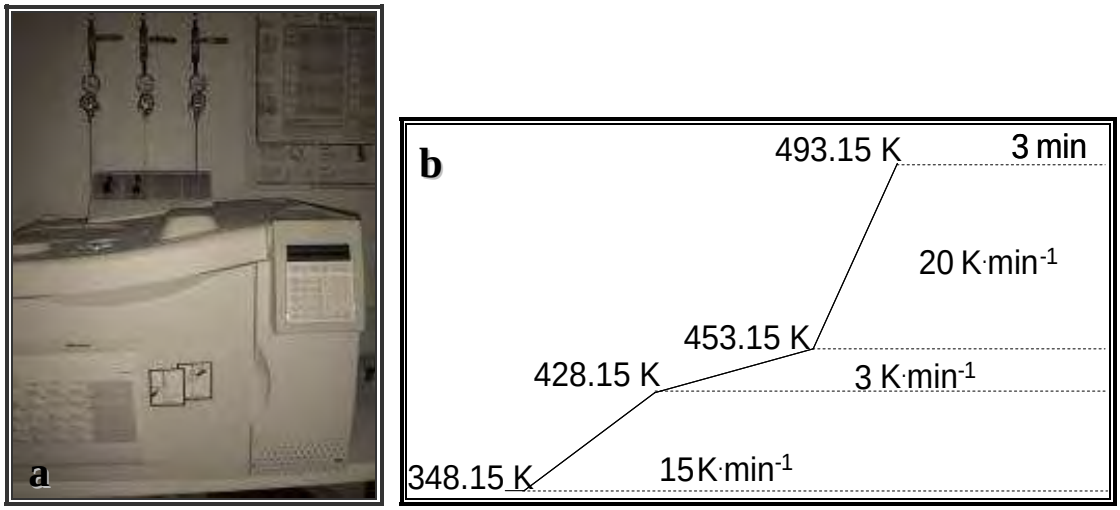

Figure 4.1 – (a) Gas Chromatograph (Clarus 400, Perkin Elmer); (b) GC Program.

The GC injection port was programmed at 518.15 K and the detector at 523.15 K. Oven temperature was programmed in three ramps, from 348.15 to 428.15 K at 15 $K \cdot min^{-1}$, from 428.15 to 453.15 K at 3 $K \cdot min^{-1}$, and from 453.15 to 493.15 K at 20 $K \cdot min^{-1}$, and held isothermal for 3 min, performing 17.67 min totally. The temperature program is shown graphically in **Figure 4.1b**. The carrier gas was hydrogen flowing at 5.0×10^{-2} $L \cdot min^{-1}$. The compounds were identified by comparing their retention times (**Figure 4.2**, **Table 4.1**) with those of a commercial FAME mixture (C8-C24).

GC-qMS. Besides previous GC-FID analyses, several tests were also performed in a GC-qMS Agilent Technologies 6890N gas chromatograph (Agilent 6890N, Agilent Technologies, USA) equipped with a 30 m × 0.32 mm (i.d.), 0.25 μm film thickness DB-FFAP fused silica capillary column (DB-FFAP, J&W Scientific Inc., USA), connected to an Agilent 5973 quadrupole mass selective detector. Splitless injection mode was used for 5 min. The oven temperature was programmed similarly to the GC-FID analyses above. The carrier gas was helium flowing at 1.7×10^{-3} $L \cdot min^{-1}$. The mass spectrometer was operated in the electron impact mode (EI) at 70 eV, scanning the range of 33–300 m/z in a 3 s cycle, in a full scan acquisition mode. Compounds identification was accomplished by comparing GC retention times (**Figure 4.2**, **Table 4.1**) and mass spectra with those of standard substances. All mass spectra were also compared with data system library (Wiley 275). All measurements involved at least three replicates, each one representing the analysis of one different aliquot (10^{-4} kg) of grape seed oil. The reproducibility is represented with error bars in the corresponding figures.

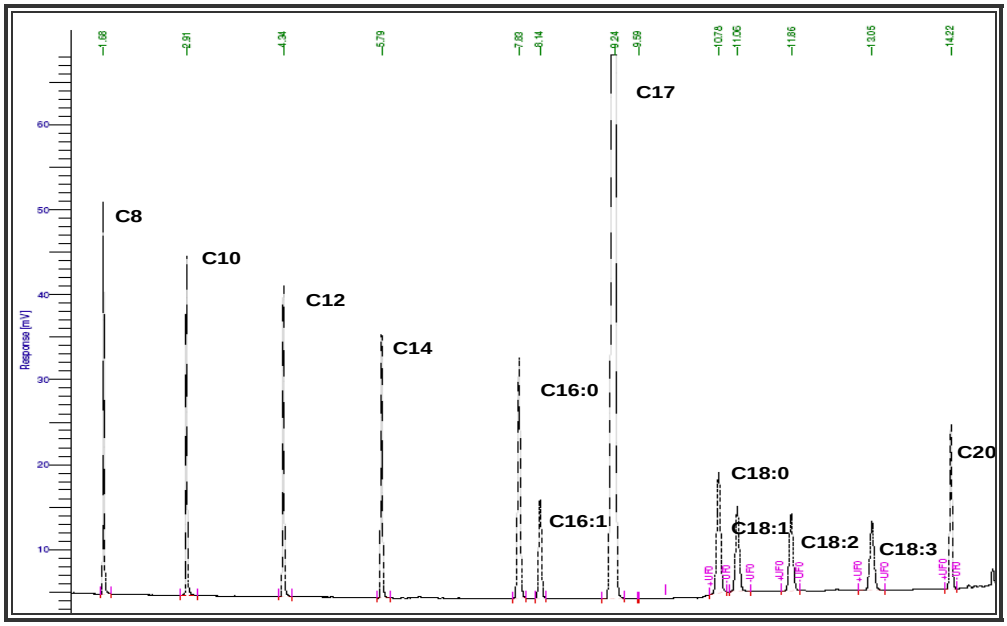

Figure 4.2 – Fatty acids methyl esters standard oil chromatographic profile. Compounds identification in Table 4.1.

Table 4.1 – Fatty acids methyl esters retention times.

Compound	Designation	Retention time (min.)
Methyl Octanoate	C8:0	1.69
Methyl Decanoate	C10:0	2.92
Methyl Laurate	C12:0	4.35
Mehtyl Myristate	C14:0	5.80
Mehtyl Palmitate	C16:0	7.84
Mehtyl Palmitoleate	C16:1 (w-9)	8.15
Methyl Margaric	C17:0	9.27
Mehtyl Stearate	C18:0	10.80
Mehtyl Oleic	C18:1 (w-9)	11.08
Mehtyl Linoleate	C18:2 (w-6)	11.87
Methyl Linolenate	C18:3 (w-3)	13.08
Methyl Arachidate	C20:0	14.24

4.2.2. Spectrophotometric assays

The antioxidant capacity of the oil samples was evaluated by the total free radical scavenger capacity (RSC) following the methodology described by Espín *et al.* (2000). Accordingly, the RSC is the variation of the concentration of $\mathrm{DPPH}\cdot$ free radical, previously dissolved in ethyl acetate, after 60 min of reaction with the samples:

$$\mathrm{RSC} = C_{\mathrm{DPPH,i}} - C_{\mathrm{DPPH,f}} \qquad \textbf{[4.1]}$$

where the initial and final concentrations (indexes i and f, respectively) are spectrophotometrically measured at 515 nm. The AOC of the grape seed oil extracted is then expressed in terms of tocopherol equivalents, i.e. the concentration of a tocopherol solution which gives rise to the same RSC.

Calibration curve. The first step was the RSC determination of several tocopherol solutions to build a calibration curve. Accordingly, a series of tocopherol standard solutions in ethyl acetate in the range of $[0-6]\times10^{-3}\,\mathrm{M}$ were prepared. Afterwards, aliquots of $5.0\times10^{-5}\,\mathrm{L}$ of the previous solutions were added to $3.95\times10^{-3}\,\mathrm{L}$ of a $\mathrm{DPPH}\cdot$ solution in ethyl acetate with concentration $1.5\times10^{-4}\,\mathrm{M}$. The reactional mixture was shaken vigorously and allowed to react at room temperature in the dark. After 60 min, the concentration of the remaining $\mathrm{DPPH}\cdot$ was determined colorimetrically using a glass cuvette at 515 nm, by blanking against an appropriate control (mixture without the radical). A double beam UV-Vis spectrophotometer (Lambda 35, Perkin-Elmer, USA) was used to read samples absorbance. In **Figure 4.3** the calibration curve obtained is plotted, corresponding to the following relation expressed in molar concentrations:

$$C_{\mathrm{tocopherol}}\left[\mathrm{mol\ (tocopherol)\cdot L^{-1}}\right] = 43.4\times\mathrm{RSC}\left[\mathrm{mol\ (DPPH\cdot)\cdot L^{-1}}\right] \qquad \textbf{[4.2]}$$

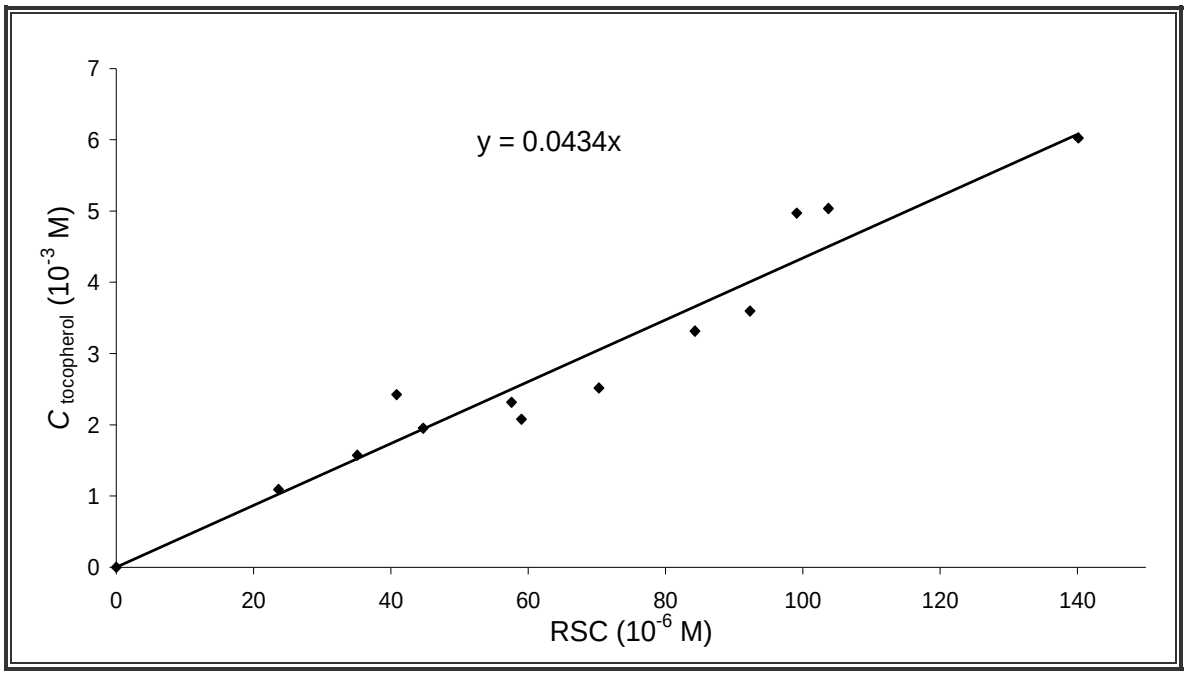

Figure 4.3 – Calibration curve for the antioxidant capacity: tocopherol concentration against radical scavenger capacity.

Antioxidant capacity of oil samples. The RSC of grape seed oil was determined using the same procedure described above. Oil samples of 5.0×10^{-5} kg were taken and added directly to 3.95×10^{-3} L of a $DPPH\cdot$ solution in ethyl acetate with concentration 1.5×10^{-4} M. The oil was utilized without any pre-treatment. The AOC of the oil is expressed as the concentration of an equivalent tocopherol solution which produces the same RSC. Thus, taking into account **Equation 4.2**:

$$\mathrm{AOC} = C_{\mathrm{tocopherol}}(\mathrm{M}) = 43.4\times\mathrm{RSC}(\mathrm{M}) \qquad \textbf{[4.3]}$$

Each result presents the mean and the standard deviation for a minimum of three experiments. Statistical analysis has been carried out using Student's t-test and outliers analyses (Miller and Miller, 2000). Significance was defined at $p < 0.025$.

4.3. Results and Discussion

4.3.1. First impression by visual assessment

The quality of the oil is often judged by consumer by its appearance. If the product is dark or has a strong smell, it can make a difference in consumer's choice. Therefore, a rough qualitative description is presented here considering the appearance of the resulting oils along distinct SFE curves. Four levels have qualitatively been considered: level 1 – light yellow; level 2 – yellow; level 3 – dark yellow; level 4 – greenish/dark green.

It is clear from **Figures 4.4a-b**, where both pressure and temperature are different, that by only changing the operating conditions the colour trend of the extracts does not change, rendering the more coloured oil for the final extracted fractions of the SFE curve. However, the inclusion of both enzymatic and high pressure pre-treatments has introduced changes in the oil visual perception (**Figures 4.4c-d**), which foresees changes in composition. While the enzymatically pre-treated seeds appear to have the darkest colour extracts at the beginning of the SFE curve (**Figure 4.4c**) such darker coloured extracts seem not to be existent at all after HPP application (**Figure 4.4d**).

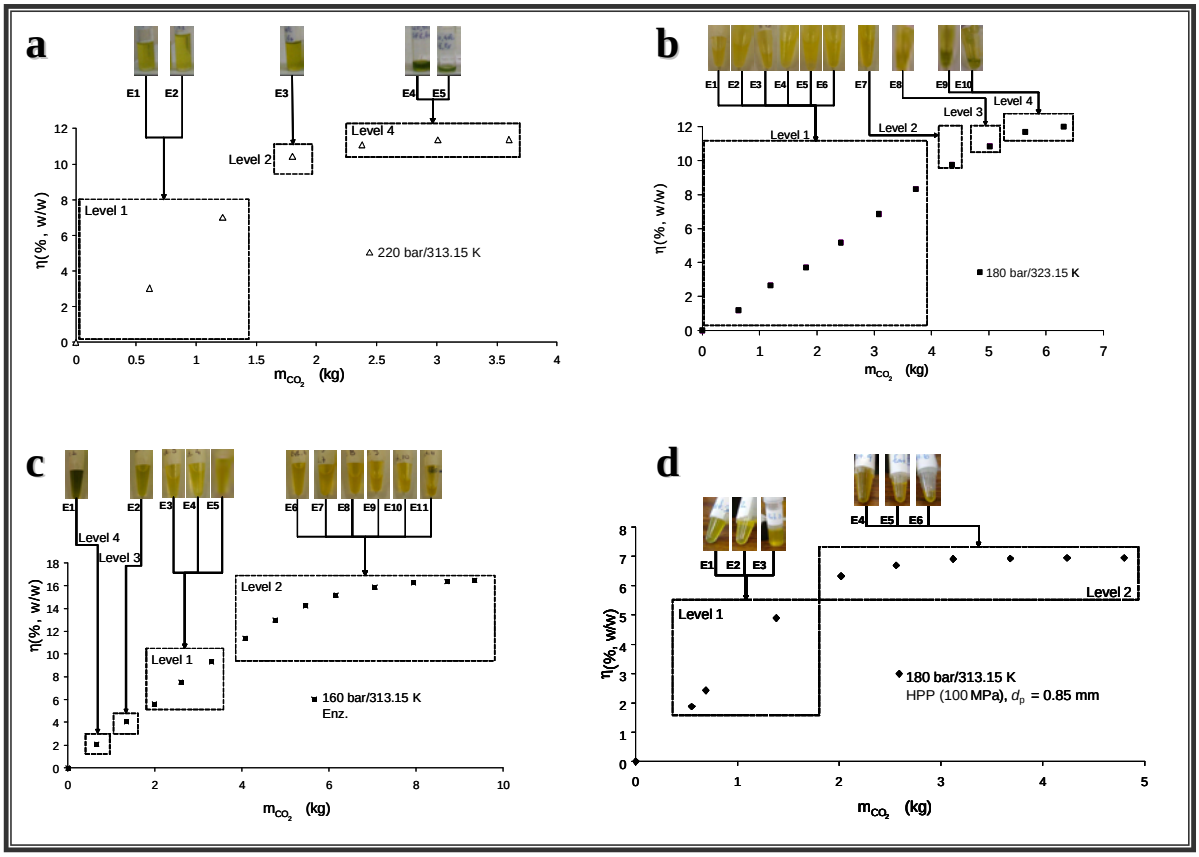

Figure 4.4 – SFE curve with corresponding extracts (colour detail). (a) Untread seeds, 220 bar/313.15 K; (b) untread seeds, 180 bar/323.15 K; (c) enzymatically pre-treated seeds, 160 bar/313.15 K; (d) high pressure pre-treated seeds (HPP), 180 bar/313.15 K. Levels: 1 – light yellow; 2 – yellow; 3 – dark yellow; 4 – greenish/dark green.

4.3.2. Triacylglycerides composition

In this section the triacylglycerides (TAG) content and fatty acids profile of the grape seed oil obtained by SFE of treated and untreated seed are presented and discussed. Global oil and individual fractions of cumulative curves are analyzed.

Figure 4.5 compares the SFEs run at 200 bar/313.15 K and 200 bar/323.15 K; in **Figure 4.6** the total triacylglycerides content of extracts E1, E4 and E7 (of **Figure 4.5**) shows that it is almost invariant along time, although higher percentages were found in the middle of the curve. Furthermore, the increment of temperature from 313.15 to 323.15 K has a slight increasing effect in all extracts included, though within the error bars.

The slightly lower content of TAG at the beginning of the extraction is explained by the higher selectivity of SC-CO_2 towards free fatty acids compared to the esterified ones (Sovová *et al.*, 2001). On the other hand, the fractions collected at the end of the process had a darker colour, which suggests the extraction of, for example, chlorophylls (Ferreira de França *et al.*, 1999) and other coloured compounds gains relevance.

Figure 4.6 also includes the trend for enzymatically pre-treated samples, which seems to be slightly increasing its TAG content along SFE.

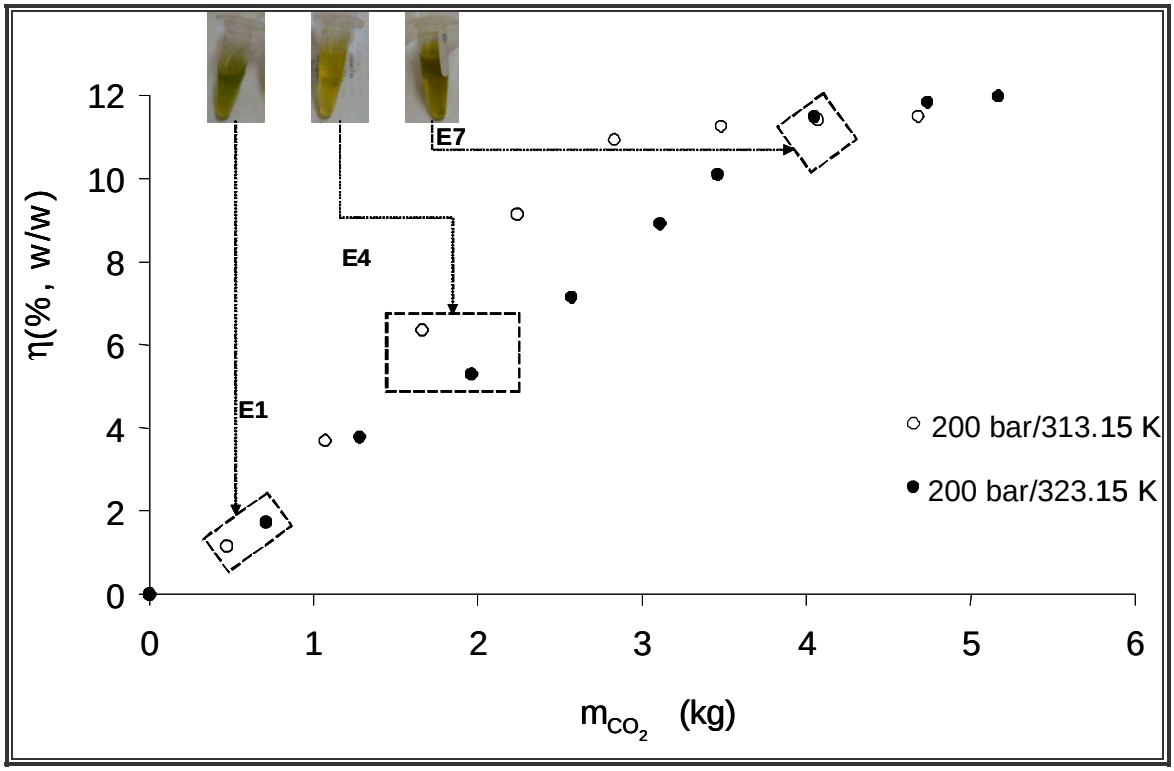

Figure 4.5 – SFE curves at 200 bar/313.15 K and 200 bar/323.15 K of untreated grape seed, and colour detail of these extracts.

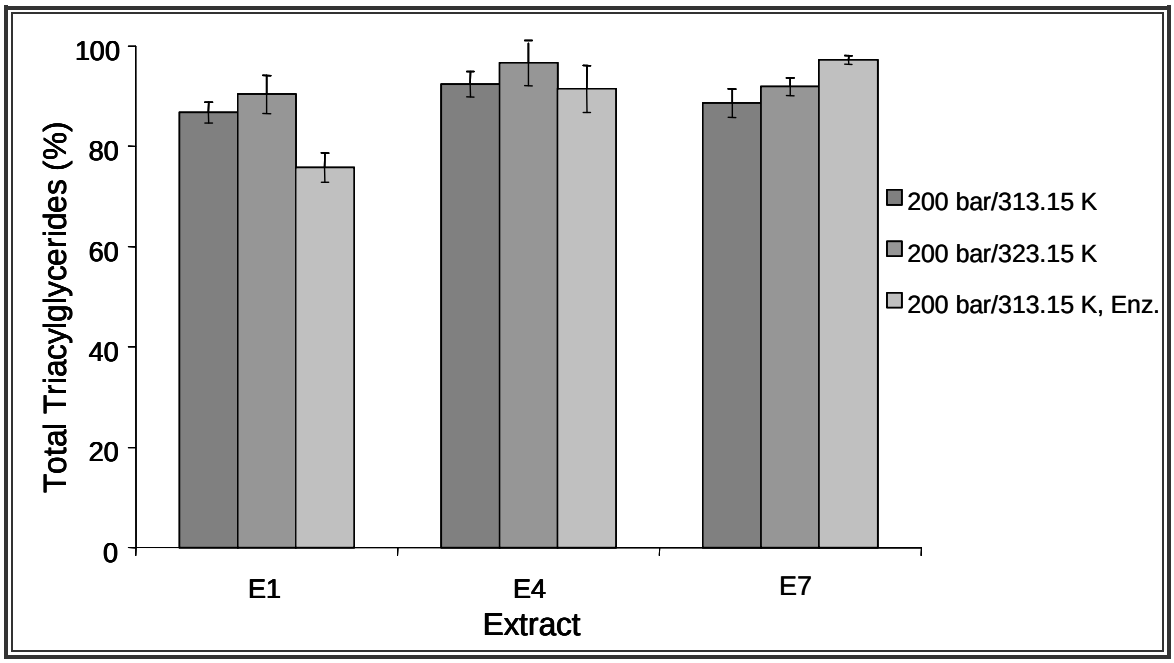

Figure 4.6 – Triacylglycerides content of different extracts obtained at 200 bar/313.15 K and 200 bar/323.15 K, with and without enzymatic pre-treatment (Consult Figure 4.5 as well).

Detailed results have been compiled in **Table 4.2**, where the individual values for each sample (selected extracts representative of the 200 bar SFE curves) are given. In the whole, the triacylglycerides content of the global oil obtained (by joining all extracts together) lies between 88.8 and 95.3%. It is worth noting that the grape seed oil extracted by Soxhlet produces similar results, namely an average concentration of 94.1%, whereas a commercially purchase oil sample (obtained by cold pressing) had the highest average concentration of 97.3%.

In **Figure 4.7** the fatty acids profiles of the three extracts previously presented (E1, E4, E7) are depicted. It seems that the ratio of the main fatty acids is practically independent of the pre-treatments and operating conditions used. The major acids detected are palmitic (16:0), stearic (18:0), oleic (18:1), linoleic (18:2), and small amounts of linolenic (18:3). Other components include free fatty acids, fat-soluble antioxidants and other fat-soluble compounds. No significant discrepancies were observed between experimental conditions (including the effect of the enzymatic pre-treatment): palmitic acid, 5-8%; stearic acid, 4-6%; oleic acid, 14-17%; linoleic acid, 60-65%; linolenic acid, 0.3-0.4%. Additionally, only traces of palmitoleic acid were identified (less than 0.1%). It should be emphasized the considerable content of unsaturated fatty acids found, which totalizes 75-80%.

Table 4.2 – Triacylglycerides content of oil samples as function of operating conditions.

Extract	Pre-treatment	Operating conditions		Triacylglycerides content (%)	
		P (bar)	*T* (K)	Average	σ
E1	–	200	313.15	86.7	2.1
E4				92.4	2.6
E7				89.9	1.8
E1			323.15	88.2	1.0
E4				96.6	4.5
E7				91.9	1.8
E1	Enzymatic		313.15	75.8	2.9
E4				91.4	4.7
E7				96.6	0.9
Global Oil*	–	160	313.15	94.3	3.4
		180		92.7	2.5
			323.15	92.5	4.1
		200	313.15	90.8	1.2
			323.15	89.0	1.9
		220	313.15	95.3	1.9
	Enzymatic	160	313.15	91.4	1.9
		180		93.3	4.3
		200		88.8	0.9
	HPP	180		92.5	0.9
Soxhlet	-			94.1	2.0
Commercial	-			97.3	0.3

*Oil obtained by joining all extracts together.

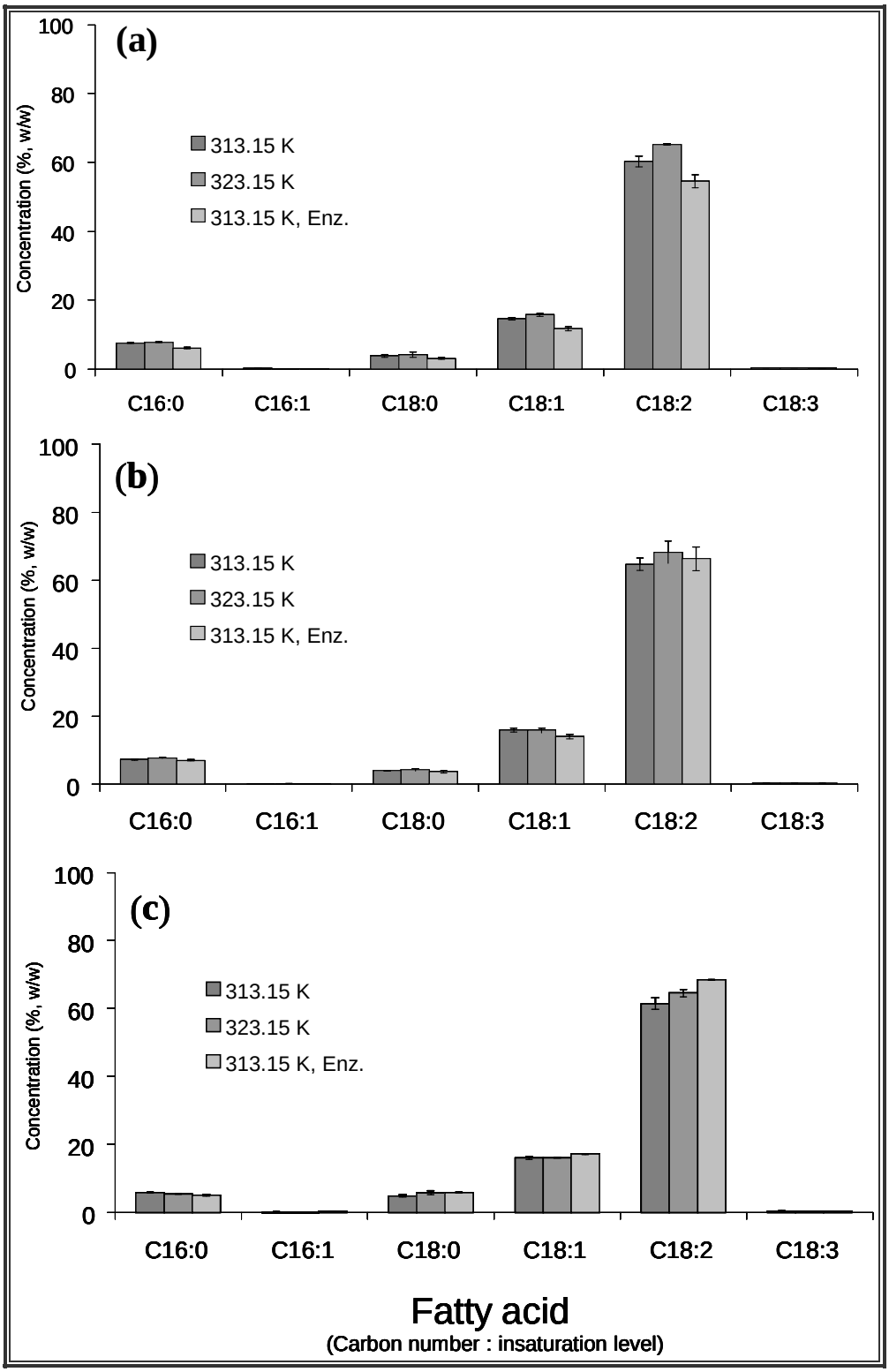

Figure 4.7 – Fatty acids profiles of extracts E1, E4 and E7 of the SFE curves obtained at 200 bar/313.15 K and 200 bar/323.15 K, with and without enzymatic pre-treatment.

4.3.3. Antioxidant capacity (AOC)

Global Oil. The AOC of the oil of the previous SFE curves and Soxhlet extractions have been measured and expressed in terms of tocopherol equivalents. In **Figure 4.8** the antioxidant capacity of the global oil obtained by joining all extracts together is presented as function of the SFE operating conditions. Results show that the AOC increases with increasing pressure and/or temperature, although temperature imparts the strongest effect. For instance, at 313.15 K the equivalent tocopherol concentrations are 3.7, 5.8, 6.2 and 7.4×10^{-4} M for 160, 180, 200 and 220 bar, respectively. Nonetheless, at 180 bar the AOC jumps from 5.8 to 8.7×10^{-4} M, when temperature increases from 313.15 to 323.15 K, and from 6.2 to 9.1×10^{-4} M at 200 bar. Such results may be interpreted by the influence that pressure and temperature exert on solubility, more precisely upon SC-CO_2 density, and vapour pressure of the antioxidant molecules of interest. The increasing pressure increases solvent density, which enhances solubility. On the contrary, when temperature raises the density decreases inherently, while solute vapour pressure increases instead. Nevertheless the last effect is more pronounced in this case, which implies larger solubilities and so higher antioxidant capacity.

None of the SFEs generated results as high as those obtained by Soxhlet, i.e. 10.2×10^{-4} M or 0.045% (w/w) of tocopherol equivalents (see **Figure 4.8**). It may be referred that this value is close to the addictive limits in most formulations, which correspond to levels up to 0.02-0.06% of the total fat weight (Berger and Hamilton, 1995; O'Brien, 1998).

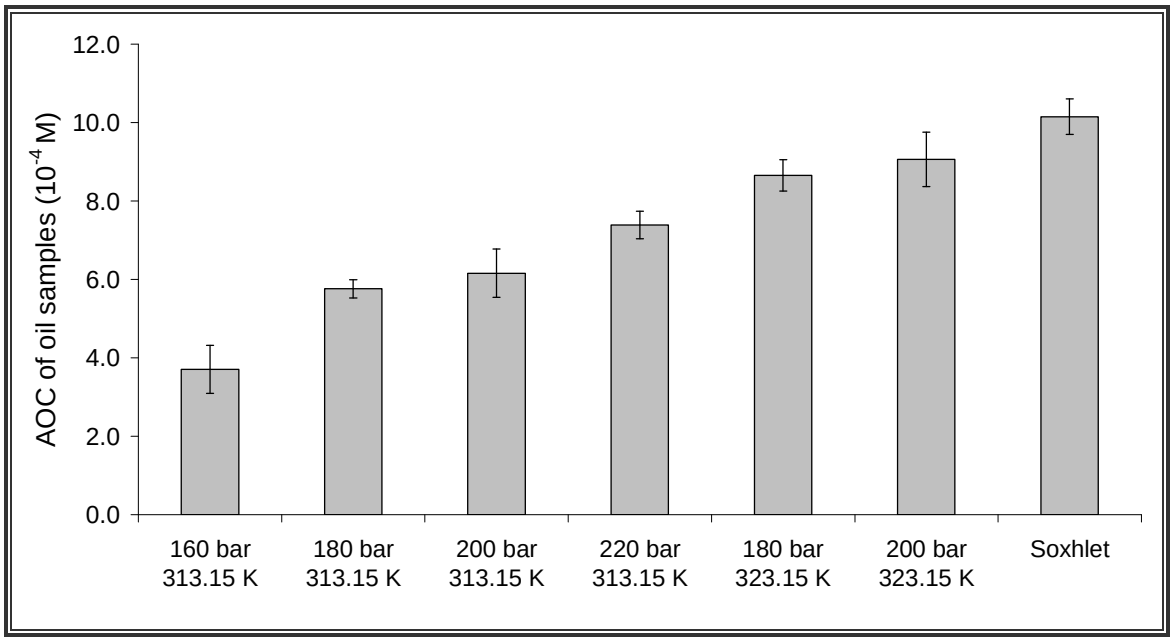

Figure 4.8 – Antioxidant capacity of the global extracted oil, expressed as concentration of an equivalent tocopherol solution.

Effect of seed pre-treatment. In **Figure 4.9** the AOC of the global oil obtained by SFE of untreated seed is compared with that obtained from pre-treated seeds, (enzymatic and high pressure), illustrated at 313.15 K for different pressures (160, 180, and 200 bar). The value obtained for oil produced by Soxhlet is also given for comparison. Besides the already mentioned improvements in the AOC of the oil extracted from untreated seeds, when higher pressure conditions are used, it is even more notorious the effect of the pre-treatments.

The pre-treated samples at 180 bar/313.15 K present the highest AOC, with values of 9.6 and 9.0×10^{-4} M, respectively for the enzymatically and HPP pre-treated seed, compared to the corresponding 5.8×10^{-4} M for the untreated seed. Such results present an increase of about 66 and 56%, respectively when the enzymatic and the HPP pre-treatments were applied, which opens a new perspective on using seed pre-treatments. During previous discussions, it has been concluded that the enzymatic pre-treatment gave the highest oil yield achievements, whereas the HPP inflected no visible changes. At this point, an HPP pre-treatment would be as advantageous as an enzymatic one in terms of co-extraction of antioxidants.

According to the literature, chlorophylls, for example, are commonly responsible for most darkening of oil extracts while reducing its antioxidant properties. The absence of dark green colour from HPP extracts may be associated to their higher AOC. Further experimental tests would however be required to further fundament this hypothesis.

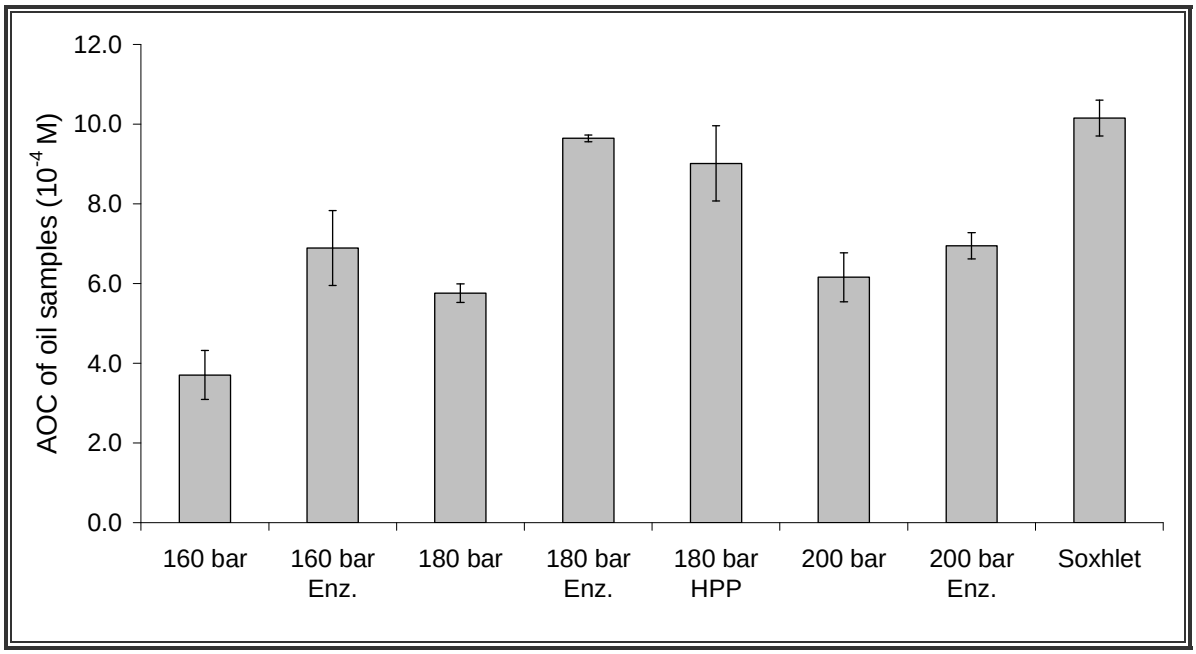

Figure 4.9 – Antioxidant capacity of the global oil extracted, expressed as concentration of an equivalent tocopherol solution, against pressure at constant temperature (313.15 K). Enz. – enzymatic pre-treatment; HPP – high pressure pre- treatment.

Individual extracts. The previous characterization has been also performed along three complete extraction curves in order to evaluate the effects of temperature and enzymatic pre-treatment on the AOC trend, namely at 200 bar/313.15 K and 200 bar/323.15 K for untreated seeds, and 200 bar/313.15 K for enzymatically pre-treated seeds.

The evolution of the AOC along the SFE of untreated grape seed at 200 bar/313.15 K and 200 bar/323.15 K are illustrated in **Figure 4.10**. The AOC is represented against the extract label and the corresponding oil removal percentage. The bar for the oil obtained by Soxhlet is also graphed for comparison. It may be observed that the antioxidant activity is more pronounced in the first stages of the extraction, than at the end of the experiment. Nonetheless, it is worth noting the sharp variation found at 200 bar/323.15 K at 32% of the extraction (i.e., from E2 to E3), a behaviour not followed at 200 bar/313.15 K. Actually, the AOC of the first two collected fractions at 323.15 K are approximately the double of those at 313.15 K (7.8 and 11.2×10^{-4} M *versus* 13.7 and 20.1×10^{-4} M) whereas the remaining samples are not so markedly different. Taking these facts into account, and confronting the individual AOCs (**Figure 4.10**) with those of the global oils obtained (**Figure 4.9**), it is possible to conclude that the first stages of the extraction period are responsible for the large difference found between the activities of the final oils at 200 bar: 6.2×10^{-4} M at 313.15 K and 9.1×10^{-4} M at 323.15 K.

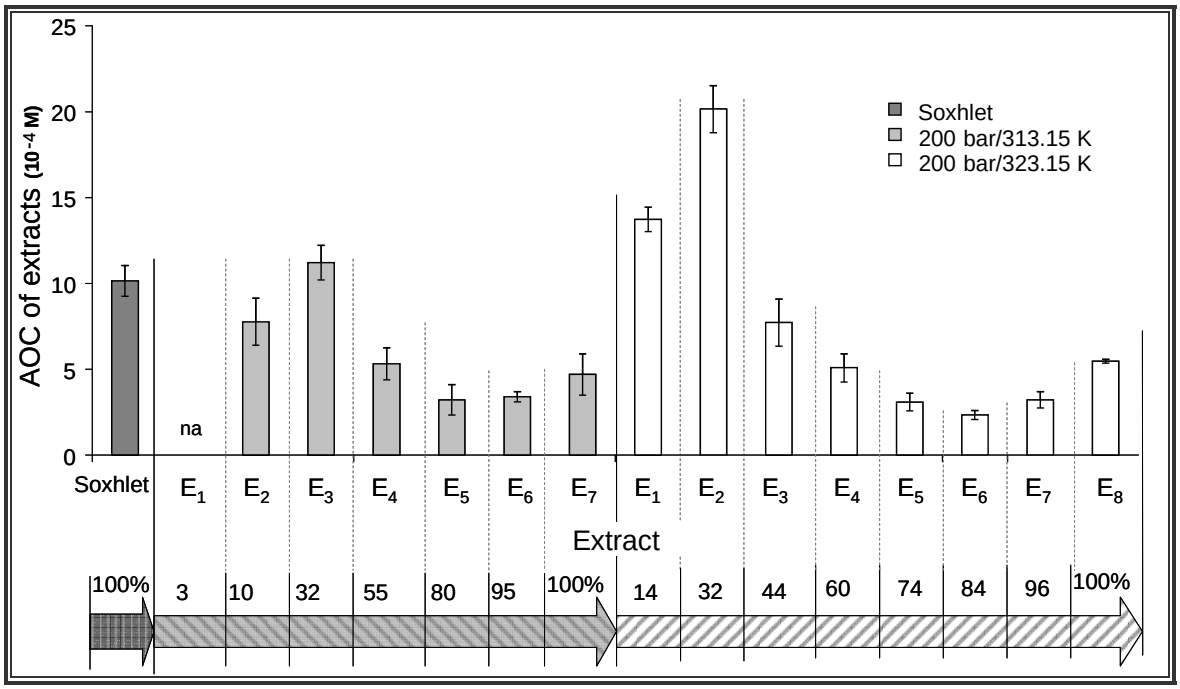

Figure 4.10 – Antioxidant capacity of extracts along the cumulative curves for 200 bar/313.15 K and 200 bar/323.15 K, expressed as concentration of an equivalent tocopherol solution. Soxhlet value is given for comparison. The labels over horizontal arrows are the percentages of extracted oil relative to maximum yield. na: not available.

Comparing now the AOCs of E1 and E2 with that from Soxhlet (**Figure 4.10**) one recognizes they are roughly similar at 200 bar/313.15 K (7.8 and 11.2×10^{-4} M *versus* 10.2×10^{-4} M), but visibly different at 200 bar/323.15 K (13.7 and 20.1×10^{-4} *versus* 10.2×10^{-4} M). In this case, the first and second extracts alone overcome Soxhlet reference value by 35 and 98%, respectively.

The results for the enzymatically pre-treated samples presented in **Figure 4.11** showed a behaviour similar to that of **Figure 4.10** for untreated seed at 200 bar/313.15 K.

A final remark on optimal operation policy for the SFE of grape seed oil may be suggested by these results. It may be adopted with advantage an optimal temperature progression through the course of the extraction, to maximize the antioxidant activity of the natural oil and minimize the mass flow rate of SC-CO_2. Accordingly, the temperature may be higher during the initial stages of extraction, to enhance antioxidant compounds removal, and reduced afterwards in order to decrease CO_2 consumption.

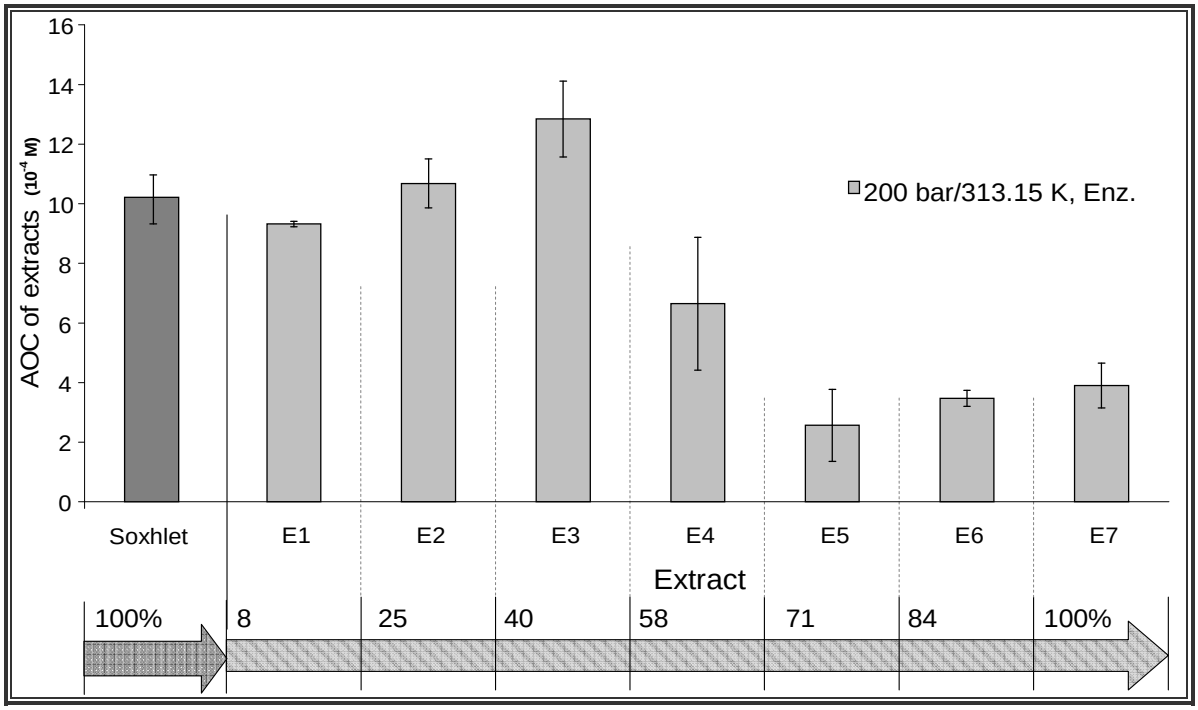

Figure 4.11 – Antioxidant capacity of extracts along the cumulative curve for 200 bar/313.15 K of enzymatically pre-treated seed (Enz.), expressed as concentration of an equivalent tocopherol solution. Soxhlet value is given for comparison. The labels over horizontal arrows are the percentages of extracted oil relative to maximum yield.

5. Modelling

People might not get all they work for in this world, but they must certainly work for all they get.
[Frederick Douglass]

5. Modelling

Modelling and simulation of the supercritical fluid extraction of grape seed oil has been carried out. The key parameters are determined from the numerical solution of the corresponding differential equations. The model comprehends a set of coupled material balances distributed into three control volumes: one mass balance to the fluid phase (extractor bed), another to the freely available oil in the seed, and a third mass balance to the tied oil existent inside the core of the seed. In order to describe the mechanisms of transport within the solid particle a series mass transfer hypothesis is considered. The results obtained for several distinct operating conditions such as pressure, temperature, and seed pre-treatments are compared with experimental data provided as extraction curves and traduced into concentration wave fronts inside the extractor.

5.1. Models Description

Several approaches have been proposed in literature in order to describe SFE curves. Some examples include: empirical, diffusion-based, and two-stage models. (*i*) The *empirical models* consider the extractor as a "black box". (*ii*) The *diffusion models* assume the internal diffusion as the only mass transfer mechanism during the SFE. (*iii*) The *stage models* are based on differential mass balances along the extractor bed accounting not only on the particle characteristics but also on the bed properties. Extraction is described regarding a local dissolving rate, convective mass transfer and intraparticle diffusion. These last models imply many assumptions and/or require determination of several coefficients involved in the equations to reflect the various mechanisms that contribute to the overall behaviour of the extraction process (Subra *et al.*, 1998; del Valle and de la Fuente, 2006; Diaz-Reinoso *et al.*, 2006).

Broken and intact cells concept. In the literature while the mass balance in the moving phase is well understood the hardest task has been the representation of the biomass matrix (Sineiro *et al.*, 1998a). The existence of broken and intact cell fractions has been considered for accounting to the sudden extraction rate reduction from the 1st to the 2nd stage of the SFE curve (see **Figure 3.5**). During the 1st period of extraction, and while the easily accessible solute is extracted in one section of the fixed bed, the extraction from the inside of the particles takes place in another section. After the "free oil" depletion from the particles, the extraction rate is determined by internal mass transfer from the tied oil and thus it continues with slower rate. Such stage is considered the 2nd extraction period and the aforementioned plot approaches the oil yield maximum asymptotically

(see **Figure 3.5**) (Sovová, 1994, 2005; Sovová *et al.*, 1994; Reverchon *et al.*, 1999, 2000; Reverchon and Marrone, 2001; del Valle *et al.*, 2004a).

Series and Parallel models. The model used in this work is based on the work by Sovová (2005) which assumes the concept of broken/intact cells. The work proposed by Marrone *et al.* (1998) used the same approach while using a distinct oil trajectory. The *series* model proposed by Sovová (1994, 2005) assumes that the oil is placed inside seed cavities or tied to the internal structure and transits to the free oil region of the seed and from there to the solvent, while in *parallel* model (Marrone *et al.*, 1998) it is assumed that both regions are exposed directly to the solvent. Comparison between the two approaches has been proposed elsewhere (Silva *et al.*, 2009). In this work, only the series approach model will be employed.

Equilibrium representations. When the solute concentration in the solid phase is high enough, the fluid-phase concentration in equilibrium is independent of matrix and equals the oil solubility (y_s , $\mathrm{kg_{solute}} \cdot \mathrm{kg_{CO_2}^{-1}}$). When the equilibrium is solute-matrix controlled it is represented by a linear relationship between the solid and the fluid concentrations, whose constant of proportionality is the partition coefficient (K , -). The main difficulty is to represent the transition in between. The simplest cases given in literature assumed only one preponderant effect: solute-matrix controlled (essential oils) or matrix independence (highly-oil content seeds) regimes. To account for both regimes, Goto *et al.* (1998) applied BET isotherm considerations, while Perrut *et al.* (1997) assumed a sigmoid curve representation that within limits has been traduced into distinct segments. Such approach assumed the existence of a discontinuity between the two extreme cases as schematically represented in **Figure 5.1**.

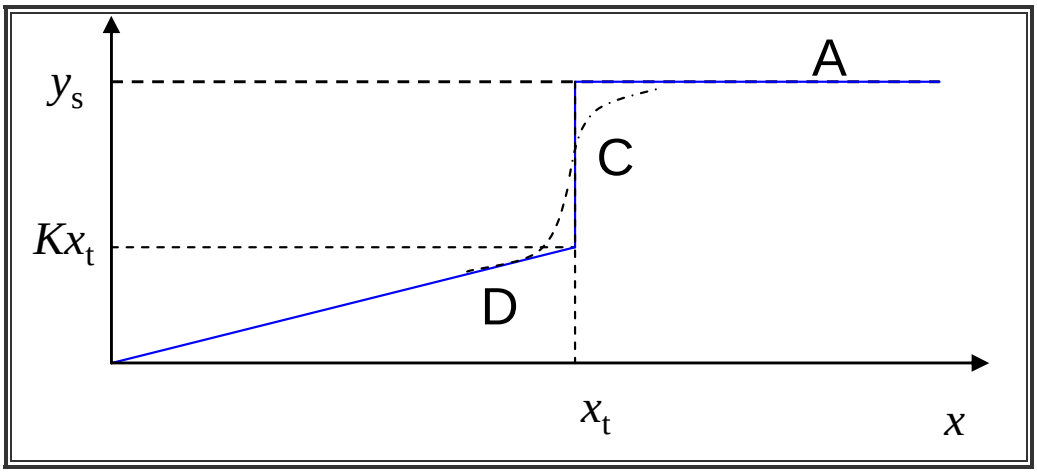

Figure 5.1 – Schematic view of the solute equilibrium curve:--- realistic shape; – discontinuous equilibrium.

Three distinct segments have been identified:

(i) The discontinuity, which occurs at the transition concentration x_t ($\mathrm{kg_{solute} \cdot kg^{-1}_{insoluble\ solid}}$) is linked to the matrix capacity for interaction with the solute (C in **Figure 5.1**);

(ii) At solid-phase concentrations lower than x_t, all solute interacts with matrix and the phase equilibrium is determined by the partition coefficient K (D in **Figure 5.1**);

(iii) At concentrations higher than x_t, the solid phase contains also free solute, so the equilibrium fluid-phase concentration is equal to the solubility, y_s (A in **Figure 5.1**).

5.2. Numerical Solution

5.2.1. General assumptions

(i) Several oil components are involved in the extraction as has been shown in Chapters 3 and 4. It is however assumed that their behaviour with respect to mass transfer is similar enough to be described by a single pseudo component called the solute.

(ii) The commonly accepted continuous description of the extraction bed has been assumed with implicit hypothesis that the relevant concentration gradients in the fluid phase develop along the axial coordinate. Both solute concentrations in the solid (x, $\mathrm{kg_{solute} \cdot kg^{-1}_{insoluble\ solid}}$) and in the fluid phase (y, $\mathrm{kg_{solute} \cdot kg^{-1}_{CO_2}}$) depend only on time t (s) and on the axial coordinate l (m).

(iii) The solvent flow rate $\dot{m}$ ($\mathrm{kg_{CO_2} \cdot s^{-1}}$), with interstitial velocity u ($\mathrm{m \cdot s^{-1}}$), is uniformly fed to the extractor. The pressure drop as well as axial dispersion and temperature gradients can be neglected within the column.

(iv) The void fraction of the bed ε is not affected by the extraction as the particles are essentially determined by the insoluble solids whose concentration is given by $1-co$, where co ($\mathrm{kg_{solute} \cdot kg^{-1}_{seed}}$) is the solute content in the solid. The surface of a particle contains a structure of broken cavities which enclose both the free oil available at the surface of broken cells whose concentration is x_1 ($\mathrm{kg_{solute} \cdot kg^{-1}_{insoluble\ solid}}$) as well as the remaining tied oil contained inside closed cells whose concentration is x_2 ($\mathrm{kg_{solute} \cdot kg^{-1}_{insoluble\ solid}}$). Such cells should not be confused with the biological cells, which are much smaller. **Figure 5.2** schematically represents all contributions to the normalized volume of the extractor bed.

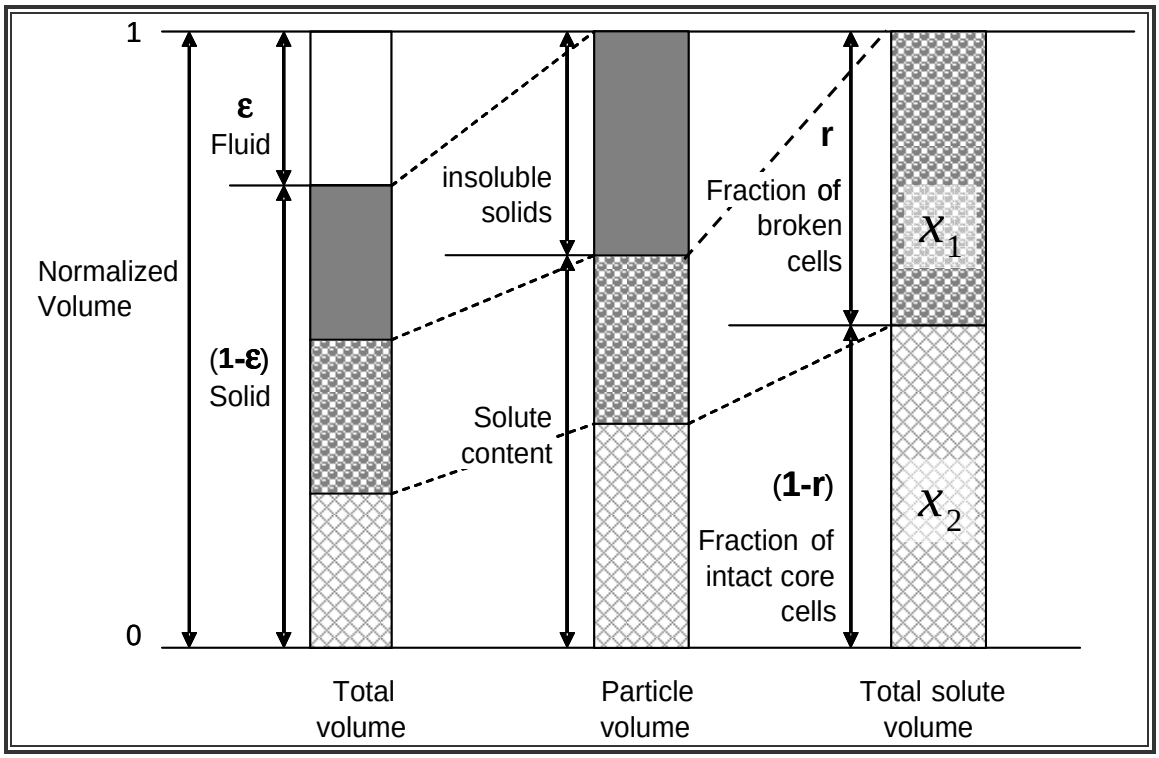

Figure 5.2 – Partition scheme of the bed volume, representing all different phases and correspondent contributions to the solute balance in the model.

(v) The equilibrium between the fluid phase and the solid with broken cells is established during pressure and temperature stabilization before the extraction start.

(vi) Grinding efficiency r relates the volumetric fraction of broken cells to the total volume of particles as:

$$r = \frac{V_{\text{broken}}}{V_{\text{broken}} + V_{\text{intact}}} \qquad \textbf{[5.1]}$$

(vii) The surface area per unit of volume of extraction bed $a_0\,(\text{m}^{-1})$ is directly proportional to the solid-phase volumetric fraction in the extraction bed $(1-\varepsilon)$ and inversely proportional to particle size d_p. The surface area between the regions of broken and intact cells $a_s\,(\text{m}^{-1})$ is equal or lower than a_0. For spherical particles **Equations [5.2]** may be developed to estimate them:

$$a_0 = 6\frac{(1-\varepsilon)}{d_p} \qquad \text{and} \qquad a_s = a_0\,(1-r)^{2/3} \qquad \textbf{[5.2]}$$

5.2.2. Material Balances

The model assumes a biomass multi-scale representation as shown in **Figure 5.3**. The mass transport phenomena occurring on the extraction column are represented in **Figure 5.3a**, whereas **Figure 5.3b** represents the mass transport fluxes in detail according to the series model hypothesis.

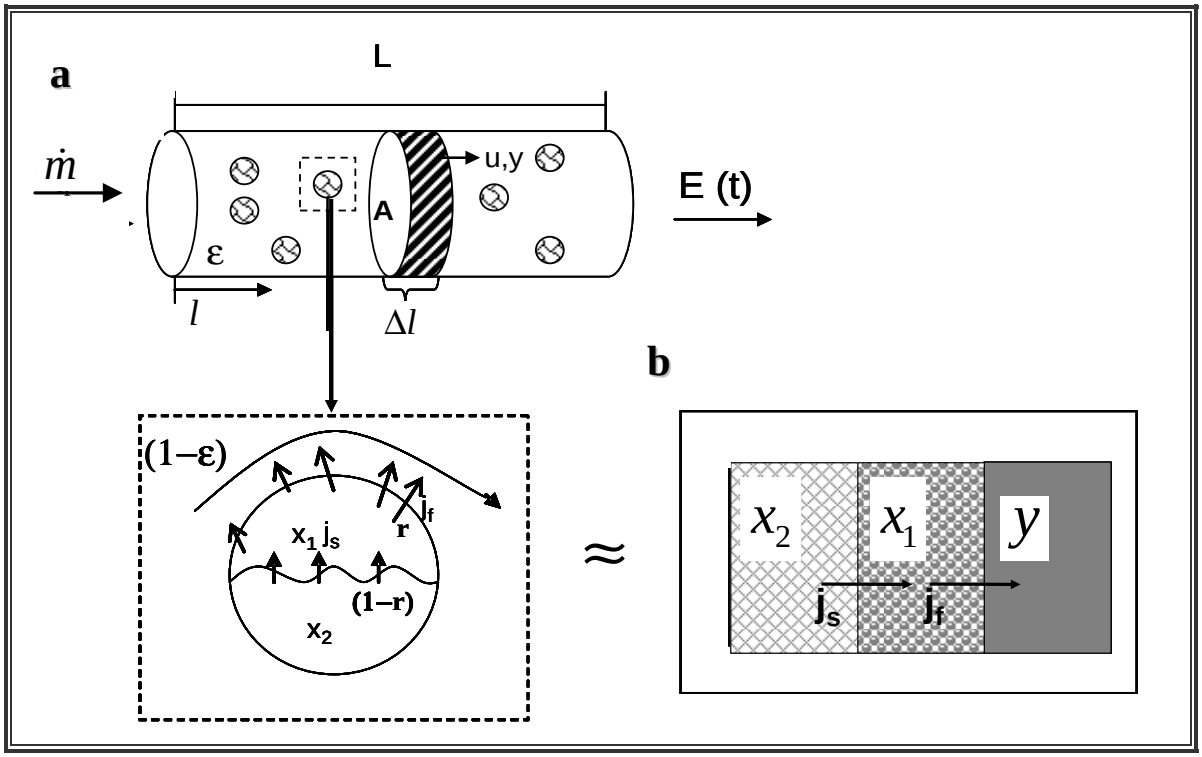

Figure 5.3 – Model assumptions for the: (a) extraction column; (b) mass transfer fluxes from intact core cells to broken cells and then to fluid.

Mass balances to the oil. A global mass balance to the differential element of volume shown in **Figure 5.3** is described by:

$$\left[\varepsilon\rho_{\mathrm{f}}\frac{\partial y}{\partial t}\right]+\left[\varepsilon\rho_{\mathrm{f}}u\frac{\partial y}{\partial l}\right]+\left[(1-\varepsilon)\cdot(1-r)\rho_{\mathrm{s}}\frac{\partial x_2}{\partial t}\right]+\left[(1-\varepsilon)r\rho_{\mathrm{s}}\frac{\partial x_1}{\partial t}\right]=0 \qquad \textbf{[5.3]}$$

where ρ_{f} is the solvent density, and ρ_{s} ($\mathrm{kg}_{\text{insoluble solid}}\cdot\mathrm{m}^{-3}_{\text{seed}}$) is the solid density. The first term is the accumulation in the fluid, the second is the convective term in the bed, the third one is the accumulation in the intact cells, and the fourth is the accumulation in the broken cells. The easily accessible oil from broken cells is transferred directly to the fluid-phase (flux j_{f}), while the solute from intact cells diffuses firstly to broken cells (flux j_{s}) and then to the solvent – see **Figure 5.3b**.

The individual mass balances to the fluid, broken cells and intact core are given by, respectively:

$$\varepsilon\rho_{\mathrm{f}}\frac{\partial y}{\partial t}+\varepsilon\rho_{\mathrm{f}}u\frac{\partial y}{\partial l}=j_{\mathrm{f}} \qquad \textbf{[5.4]}$$

$$(1-\varepsilon)r\rho_{\mathrm{s}}\frac{\partial x_1}{\partial t}=j_{\mathrm{s}}-j_{\mathrm{f}} \qquad \textbf{[5.5]}$$

$$(1-\varepsilon)\cdot(1-r)\rho_{\mathrm{s}}\frac{\partial x_2}{\partial t}=-j_{\mathrm{s}} \qquad \textbf{[5.6]}$$

The mass transport from broken cells to the solvent is characterised by a convective fluid-phase mass transfer coefficient $k_{\mathrm{f}}\,(\mathrm{m}\cdot\mathrm{s}^{-1})$ which is by several orders of magnitude larger than the diffusion solid-phase mass transfer coefficient $k_{\mathrm{s}}\,(\mathrm{m}\cdot\mathrm{s}^{-1})$ which relates the diffusion from intact cells to broken cells. The fluid phase concentration in equilibrium with the free oil is represented by $y^{*}(x_1)\,(\mathrm{kg}_{\mathrm{solute}}\cdot\mathrm{kg}_{\mathrm{CO_2}}^{-1})$. The corresponding mass transfer fluxes $j_{\mathrm{f}}\,(\mathrm{kg}_{\mathrm{solute}}\cdot\mathrm{m}_{\mathrm{bed}}^{-3}\cdot\mathrm{s}^{-1})$ and $j_{\mathrm{s}}\,(\mathrm{kg}_{\mathrm{solute}}\cdot\mathrm{m}_{\mathrm{bed}}^{-3}\cdot\mathrm{s}^{-1})$ are given by:

$$j_{\mathrm{f}}=k_{\mathrm{f}}a_0\rho_{\mathrm{f}}\left[y^{*}(x_1)-y\right] \qquad \textbf{[5.7]}$$

$$j_{\mathrm{s}}=k_{\mathrm{s}}a_{\mathrm{s}}\rho_{\mathrm{s}}(x_2-x_1) \qquad \textbf{[5.8]}$$

Boundary conditions. At the inlet boundary of the extraction column the solute concentration in the fluid phase ($y|_{l=0}$) is the feed concentration:

$$y|_{l=0}=y_{\mathrm{feed}}=0 \qquad \textbf{[5.9]}$$

Initial conditions. The initial conditions (just before opening the feed valve) are:

$$y|_{t=0}=y_0;\qquad x_1|_{t=0}=x_{1,0};\qquad x_2|_{t=0}=x_{2,0} \qquad \textbf{[5.10]}$$

Oil mass balance to the extractor initially in equilibrium. During the model presentation it has been assumed that the equilibrium between the fluid phase and the solid with broken cells is established during the extractor pressurization (assumption iv). Therefore, the total oil content

(solid matrix initial content) in the extractor will be divided into tied oil plus free oil in equilibrium with the fluid phase:

$$\underbrace{(1-\varepsilon)\rho_s \cdot x_u}_{\textit{initial oil content}} = \underbrace{(1-\varepsilon) r \rho_s \cdot x_{1,0}}_{\textit{free oil}} + \underbrace{(1-\varepsilon)(1-r)\rho_s \cdot x_{2,0}}_{\textit{tied oil}} + \underbrace{\varepsilon \rho_f \cdot y_0}_{\textit{solved oil}} \quad \textbf{[5.11]}$$

It is assumed that the concentration of intact cells remains unchanged and equal to the concentration of the original seed, x_u ($kg_{solute} \cdot kg^{-1}_{insoluble\ solid}$), up to the start of the extraction, while assuming that the free oil alone participates in the initial equilibrium of the bed:

$$x_{2,0} = x_u; \qquad y_0 = y^*(x_{1,0}) \quad \textbf{[5.12]}$$

To calculate $x_{1,0}$ one have to substitute both relations of **Equation 5.12** in **Equation 5.11**. However, attending to **Figure 5.1** there are three possibilities for the final equilibrium situation, namely: $x_{1,0} > x_t$, $x_{1,0} = x_t$ and $x_{1,0} < x_t$. Such fact originates the three sets of relations for $x_{1,0}$ and y_0 shown in **Table 5.1**.

Table 5.1 – Initial concentrations in the fluid and broken cells (consult Figure 5.1).

A	$x_{1,0} > x_t$	$x_{1,0} = x_u - \left[\frac{\gamma}{r} \cdot y_s\right]$, with $\gamma = \frac{\varepsilon \rho_f}{(1-\varepsilon)\rho_s}$	$y_0 = y^* = y_s$
C	$x_{1,0} = x_t$	$x_u - \left[\frac{\gamma}{r} \cdot y_s\right] < x_{1,0} < x_u - \left[\frac{\gamma}{r} \cdot K x_t\right]$	$K x_{1,0} < y_0 = y^* < y_s$
D	$x_{1,0} < x_t$	$x_{1,0} = x_u \frac{r}{r + \gamma K}$	$y_0 = y^* = K x_{1,0} < y_s$

Extraction curve. The extraction curve is obtained by integration of the solute mass flow rate at column exit ($l = L$):

$$E(kg_{solid}) = \dot{m} \int_0^t y\big|_{l=L}\, dt \quad \textbf{[5.13]}$$

5.3. Model Solution

5.3.1. Numerical methods

The partial differential equations of the hyperbolic type resulting from the mass balances were rewritten in dimensionless form in **Table 5.2**, along with both fluxes, and the initial and boundary conditions. The main dimensionless variables introduced were: $\tau = t/t_r = t/(L/u)$, $z = l/L$, $Y = y/y_0$, $X_1 = x_1/x_{1,0}$, $X_2 = x_2/x_{1,0}$. Both dimensionless fluxes J_f and J_s were inversely related to an external Θ_e and internal Θ_i mass transfer resistances, respectively.

The spatial derivatives were discretized using backward finite differences of the 1st and 2nd orders, and the model integrated applying the method of lines (Schiesser, 1991), as exemplified in **Figure 5.4**. The numerical integration was accomplished in Matlab using the function ode45 whose algorithm is based on an explicit 4th order Runge-Kutta with a 5th order error.

The grid included 20 and 50 points. Several other tests performed with more than 50 points revealed no further improvement while implying further CPU time. The SFE curves resemble a stiff problem due to the transition between the two extraction periods. However, the concentration profiles are smooth enough to be well calculated by ode45 function, avoiding the necessity of using the ode15s function, which is recommended for stiff systems. In our case it does not show any advantage in the simulations. The "false boundary condition" was used to the first node (Hangos and Cameron, 2001), where finite difference of the 1st order was applied. The resulting system of ordinary differential equations are given in **Table 5.3**.

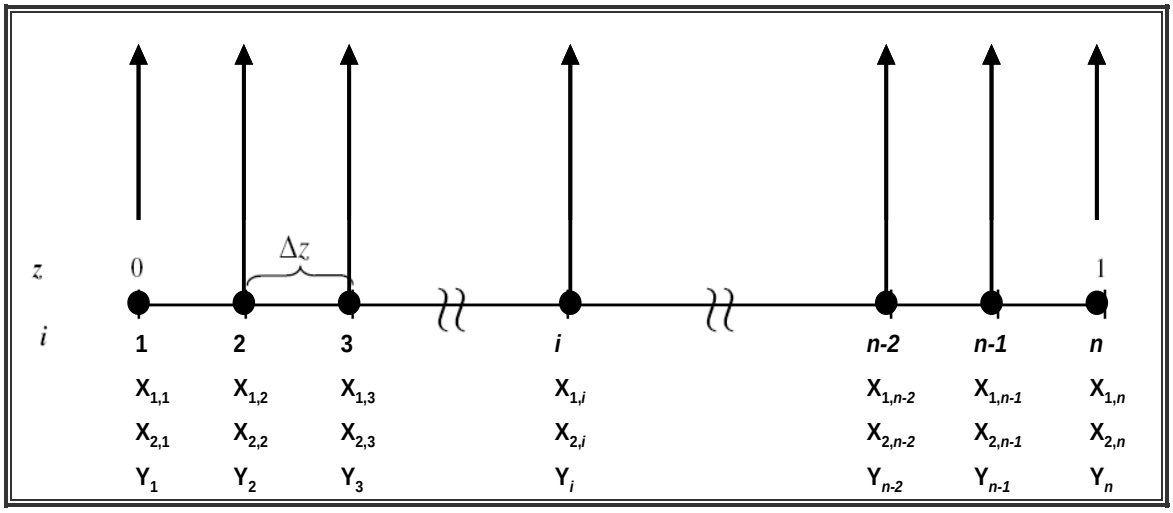

Figure 5.4 – Method of lines. Representation of the mathematical discretization.

Table 5.2 – Dimensionless set of equations for the SFE mathematical model.

Dimensionless variables	
$z=\frac{l}{L};\ \tau=\frac{t}{t_r}=\frac{t}{L/u};Y=\frac{y}{y_0};X_1=\frac{x_1}{x_{1,0}};\ X_2=\frac{x_2}{x_{1,0}};$ $\phi=\eta/co=E/m_{seed}\cdot co$	**[5.14]**
Mass Fluxes	
$J_f=\frac{t_r\cdot j_f}{\rho_f\cdot\varepsilon\cdot y_0}=\frac{\left(Y^*-Y\right)}{\Theta_e}$ **, with** $\Theta_e=\frac{\varepsilon}{k_f\cdot a_0\cdot t_r}$ $J_s=\frac{t_r\cdot j_s}{\rho_s\left(1-\varepsilon\right)x_{1,0}}=\frac{\left(X_2-X_1\right)}{\Theta_i}$ **, with** $\Theta_i=\frac{\left(1-\varepsilon\right)}{k_s\cdot a_s\cdot t_r}$	**[5.15]**
Material Balances	
(Fluid Phase): $\frac{\partial Y}{\partial z}+\frac{\partial Y}{\partial\tau}=J_f$	**[5.16]**
(Free Oil Region): $\frac{\partial X_1}{\partial\tau}=\frac{1}{r}J_s-\Gamma J_f$ **, with** $\Gamma=\frac{\rho_f\cdot\varepsilon\cdot y_0}{\rho_s\left(1-\varepsilon\right)r\cdot x_{1,0}}$	**[5.17]**
(Tied Oil Region): $\frac{\partial X_2}{\partial\tau}=-\frac{1}{\left(1-r\right)}J_s$	**[5.18]**
Initial and boundary conditions	
$Y\big\vert_{\tau=0}=1;\ X_1\big\vert_{\tau=0}=1;\ X_2\big\vert_{\tau=0}=1+\Gamma;$ $Y\big\vert_{z=0}=0$	**[5.19]**
Extraction Curve	
$\phi=\frac{\Gamma\cdot r}{1+\Gamma}\int_0^\tau Y\big\vert_{z=1}\,d\tau$	**[5.20]**

Table 5.3 – Discretized equations for the SFE dimensionless model.

Assumptions	
$\Delta z = 1/(n-1);\ z = (i-1)\Delta z;\ n =$ number of grid points	**[5.21]**
Material Balances and fluxes	
(Fluid Phase): $\frac{dY_1}{d\tau} = -\frac{Y_1 - Y_0}{\Delta z} + J_{f,1}$ **with** $J_{f,1} = \frac{(Y_1^* - Y_1)}{\Theta_e}$ **(**$i = 1$**)** $\frac{dY_2}{d\tau} = -\frac{3Y_2 - 4Y_1 + Y_0}{2\Delta z} + J_{f,2}$ **with** $J_{f,2} = \frac{(Y_2^* - Y_2)}{\Theta_e}$ **(**$i = 2$**)** $\frac{dY_i}{d\tau} = -\frac{3Y_i - 4Y_{i-1} + Y_{i-2}}{2\Delta z} + J_{f,i}$ **with** $J_{f,i} = \frac{(Y_i^* - Y_i)}{\Theta_e}$ **(**$i = 3,...,n$**)**	
(Free Oil Region): $\frac{dX_{1,i}}{d\tau} = \frac{1}{r} J_{s,i} - \Gamma J_{f,i}$ **with** $J_{s,i} = \frac{(Y_i^* - Y_i)}{\Theta_i}$ **(**$i = 1,...,n$**)**	**[5.23]**
(Tied Oil Region): $\frac{dX_{2,i}}{d\tau} = \frac{1}{1-r} J_{s,i}$ **(**$i = 1,...,n$**)**	**[5.24]**
Initial and boundary conditions	
$Y_i\big\vert_{\tau=0} = 1;\ X_{1,i}\big\vert_{\tau=0} = 1;\ X_{2,i}\big\vert_{\tau=0} = 1+\Gamma;\ Y\big\vert_{z=0} = Y_0 = 0$	**[5.25]**
Extraction Curve	
$\frac{d\phi}{d\tau} = \left(\frac{\Gamma r}{1+\Gamma}\right) Y_n$ **, with** $\phi\big\vert_{\tau=0} = 0$	**[5.26]**

5.3.2. Program code and optimization procedure

The optimization of parameters of a large set of nonlinear ordinary differential equations requires a good set of initial guesses. Sovová (2005) tried to eliminate such limitation by making a previous estimation of the model parameters, which will also be applied in this work as subsequently shown.

The SFE curve has been represented as a plot of cumulative yield η *versus* extraction time t, or in dimensionless form ϕ *versus* τ. Another possibility uses the consumed mass of solvent m_{CO_2} (kg), representation chosen in previous chapters, from which the apparent solubility y_0 can easily be fitted to the experimental data.

The two extraction periods of **Figure 5.5** may be represented by the following equations:

$$\phi = \frac{y_0 \gamma}{x_u} \tau \qquad \text{, when } 0 \le \tau \le \tau_c \qquad \textbf{[5.27]}$$

$$\phi = 1 - C_1 \exp\left(-C_2 \tau\right) \qquad \text{, when } \tau > \tau_c \qquad \textbf{[5.28]}$$

where $\gamma = \varepsilon \rho_f / \left[(1-\varepsilon) \rho_s \right]$ is the solvent-to-matrix masses ratio. Hence the parameters C_1, C_2, and y_0 may be fitted to experimental extraction curves. Additionally the interception (ϕ_c, τ_c) in **Figure 5.5** is determined by equating **Equations [5.27]** and **[5.28]**.

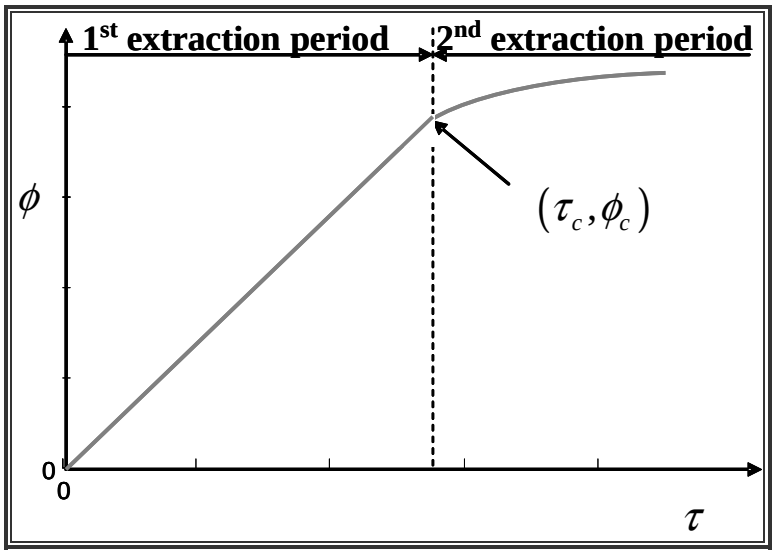

Figure 5.5 – Supercritical fluid extraction (SFE) curve representation in the dimensionless form.

The convective k_f ($m \cdot s^{-1}$) and diffusional k_s ($m \cdot s^{-1}$) mass transfer coefficients are associated to the specific surface areas a_0 and a_s, being fitted together as $k_f a_0$ (s^{-1}) and $k_s a_s$ (s^{-1}).

A first guess for parameters *r* and $k_s a_s$ may be obtained from C_1, C_2 and τ_c through the following relations:

$$r = 1 - C_1 \exp\left(-C_2 \tau_c / 2\right) \qquad \textbf{[5.29]}$$

$$k_s a_s = (1-r)(1-\varepsilon) \dot{m} C_2 / \left[m_{seed} (1-co) \gamma \right] \qquad \textbf{[5.30]}$$

Figure 5.6 presents a schematic view of the program. The introduction of all necessary experimental data is considered during the initial steps (**Figure 5.6a**). Afterwards, the initial

guesses for r and $k_s a_s$ are obtained from experimental data, and **Equations 5.29** and **5.30** (**Figure 5.6b**). Then, r and $k_s a_s$ may be fixed and the $k_f a_0$ is optimized **Figure 5.6c**). Alternatively, $k_f a_0$ may be estimated using correlations, and the values of r and $k_s a_s$ may be refined by optimization (**Figure 5.6d**). Sections **c** and **d** of **Figure 5.6** use the full model presented in **Table 5.2** and discretized in **Table 5.3**.

Data insertion (Figure 5.6a). This section may include one or several individual experiments run at different flow rates, each one with its own SFE individual curve (t, η). The *Global Data* compilation includes: *Bed*, *Extractor* and *Process Data*. The *Process Data* compilation includes temperature T (K), pressure P (bar) and the amount of solid loaded in the extractor m_{seed} (kg) which are considered the extraction operating conditions (**Table 3.2**). The *Bed Data* compilation includes the initial oil content of seed, co ($kg_{solute} \cdot kg_{seed}^{-1}$), bed void fraction ε, and the solid density ρ_s. The first parameter, co, was obtained as the maximum oil extracted by conventional Soxhlet (Exp. 13, **Table 2.1**). The remaining parameters, ε and ρ_s, were obtained by gravimetric measurements, being given in **Table 3.2**. The remaining secondary parameters and variables necessary in the calculations are: x_u, the interstitial velocity u, and the extractor cross sectional area A:

$$x_u = \frac{co}{1-co}; \quad u = \frac{\dot{m}}{\rho_f \cdot \varepsilon \cdot A}; \quad A = \pi \frac{d_E^2}{4} \qquad \textbf{[5.31]}$$

The *Extractor Data* compilation are the internal diameter (d_E = 0.040 m), length (L = 0.130 m), and A (m^2).

Approximated model (Figure 5.6b). At this stage the parameters C_1, C_2 and τ_c are fitted to the experimental data to obtain a first guess of r and $k_s a_s$, but are not necessarily required during the following optimization stages. The fit of the experimental data also permits gathering several important parameters such as the apparent solubility (y_0) from the slope of the experimental curve, and the partition coefficient (K), when the case for solute-matrix controlled regime applies. The value of y_s is also estimated using the correlation of del Valle and Aguilera (1988). The fittings of C_1, C_2 and y_0 were accomplished using the fminsearch function of Matlab with a tolerance of 10^{-5}. The objective function was defined as the summation of the square deviations between experimental and calculated values:

$$\text{O.F.} = \sum_{i=1}^{\text{Number of Exp. Data}} \left[\phi_i^{\exp}(\tau) - \phi_i^{\text{calc}}(\tau) \right]^2 \qquad \textbf{[5.32]}$$

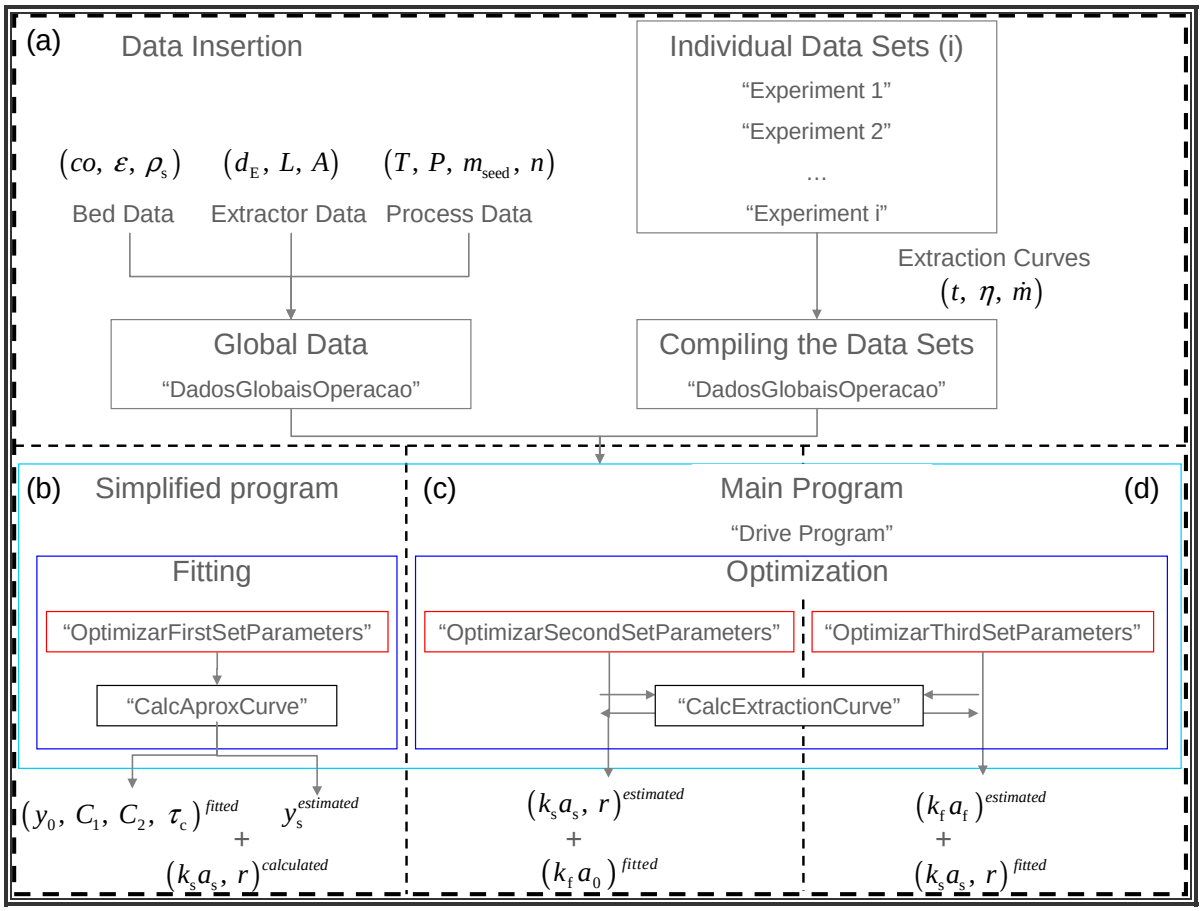

Figure 5.6 – Schematic representation of the model. (a) – Data entrance; (b) – simplified model; (c-d) – full model optimization stages.

Full model – $k_f a_0$ optimization (Figure 5.6c). The convective mass transfer group $k_f a_0$ is the optimized parameter. In opposition to r and $k_s a_s$, an initial guess for $k_f a_0$ is not available from the approximated model. However, there are several correlations given in the literature for k_f, involving the Sherwood (N_{Sh}), Reynolds (N_{Re}), and Schmidt (N_{Sc}) numbers. More information about the applicability range of such correlations can be found in the **Appendix A2**. In our case, the operating conditions assumed the correlation of Tan *et al.* (1988) to be the most appropriated. The surface area per unit of bed volume parameter (a_0) is estimated by **Equation 5.2**. Hence a first guess for $k_f a_0$ may be thus obtained.

In spite of optimizing distinct values of $k_f a_0$, a common parameter p may be correlated using data for different $\dot{m}$ but equal *P* and *T*, according to Sovová (2005):

$$k_f a_0 = p \times \dot{m}^{0.54} \qquad \textbf{[5.33]}$$

The determination of p was accomplied using the fminsearch function of Matlab with a tolerance of 10^{-3}.

Full model – r and $k_s a_s$ optimization (Figure 5.6d). The final section of the optimization stage comprehends both r and $k_s a_s$ simultaneous optimization (it also permits the optimization of $k_f a_0$ if necessary), using the fminsearch function of Matlab with a tolerance of 10^{-3}.

Figure 5.7 represents a simplified view of the models' functionalities and how they are interrelated.

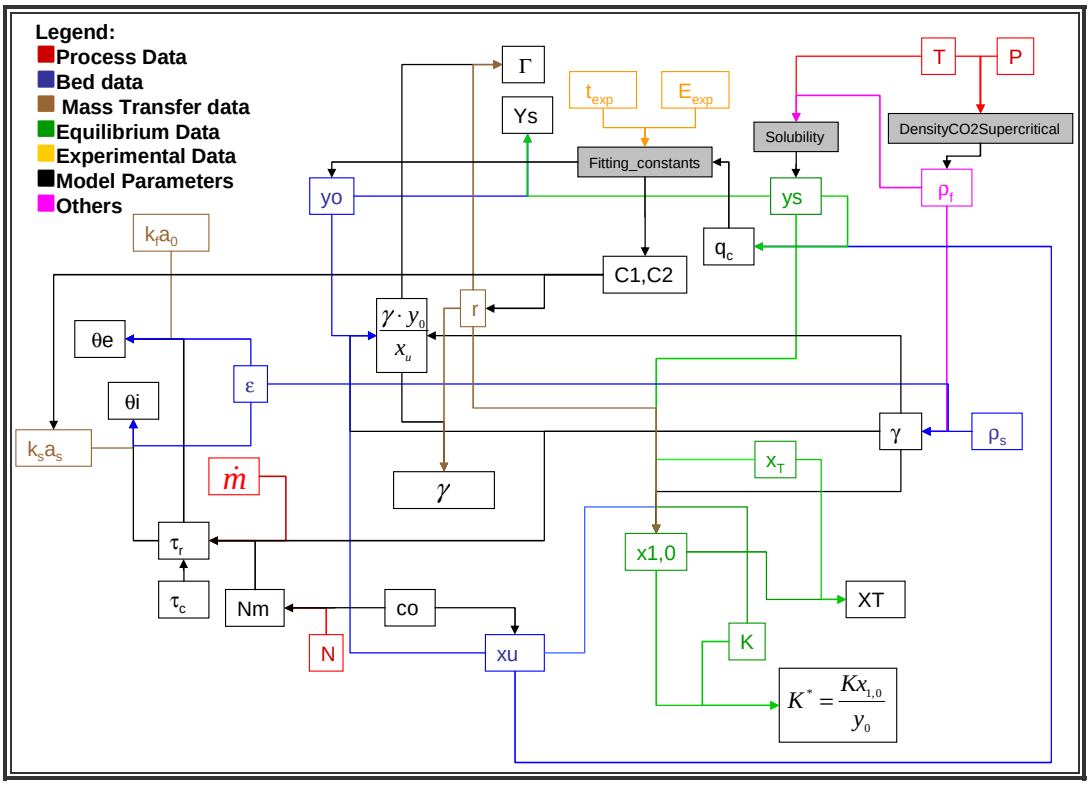

Figure 5.7 – Structure graph of calculated parameters from experimental data and optimization procedure.

5.3.3. Validation of the Model

In order to test the model and its numerical solution, the results for two examples given by Sovová (2005) are presented. Such examples consider the extraction of crushed almonds seed oil (Marrone *et al.*, 1998) and pennyroyal essential oil from leaves and flowers (Reis-Vasco *et al.*, 2000).

Fluid-phase controlled regime (Figure 5.1, Case A). The first example, extraction of almonds oil from crushed seeds (Marrone *et al.*, 1998), exhibits an equilibrium relationship common to rich oil-containing seeds. The results optimized in this work are very close to those given by Sovová, therefore validating the model and the numerical solution.

Table 5.4 – Parameters optimized using both a 1st and a 2nd order spatial discretization options with backwards finite differences. Comparison with values by Sovová (2005).

d_p (mm)	(Sovová, 2005)		(1st order discretization)			(2nd order discretization)		
	$k_s a_s$ (s^{-1})	r	$k_s a_s$ (s^{-1})	r	AAD (%)	$k_s a_s$ (s^{-1})	r	AAD (%)
0.3	1.0E-05	0.71	1.0E-05	0.72	6.2	1.0E-05	0.72	6.2
0.7	1.0E-05	0.53	9.0E-06	0.53	4.2	8.8E-06	0.52	4.5
1.9	7.8E-06	0.35	7.9E-06	0.32	5.0	7.0E-06	0.31	5.1

Solute-matrix controlled regime (Figure 5.1, Case D). The extraction of pennyroyal essential oil at 100 bar/323.15 K (Reis-Vasco *et al.*, 2000) traduces a relationship common to essential-oil-type seeds (oil content lower than 3%). The results optimized within this work, both with a 1st and 2nd order spatial discretization, and those by Sovová (2005) are listed and compared in **Table 5.5**.

Table 5.5 – Parameters optimized using both a 1st and a 2nd order spatial discretization options. Comparison to the work by Sovová (2005).

	(Sovová, 2005)			(1st order)						(2nd order)				
$\dot{m}$ ($g \cdot s^{-1}$)	n	$k_f a_0$ (s^{-1})	$k_s a_s$ (s^{-1})	n	p ($kg^{-1} \cdot s^{-0.49}$)	$k_f a_0$ (s^{-1})	$k_s a_s$ (s^{-1})	r	AAD (%)	p ($kg^{-1} \cdot s^{-0.49}$)	$k_f a_0$ (s^{-1})	$k_s a_s$ (s^{-1})	r	AAD (%)
0.31	-	-	-	50	-	0.06	1.7E-05	0.78	8.1	-	0.03	1.1E-05	0.80	8.4
	2	0.19				0.12					0.06			
0.43	4	0.23	1.2E-05	50	0.22	0.14	1.3E-05	0.80	14.7	0.12	0.08	1.0E-05	0.80	14.9
0.62	50	0.28				0.17					0.09			

Two options have been further considered: the possibility to model the results in each mass flow condition individually, or by optimizing the results for several mass flows simultaneously. Two sets of optimized parameters results, one (r, $k_s a_s$ and $k_f a_0$) for the individual mass flow ($\dot{m} = 0.31\ g \cdot s^{-1}$), and another set ($r$, $k_s a_s$ and p) for the simultaneous optimization of all given mass flows represented in **Table 5.5**. In this last case, the values of $\dot{m}$ are related to $k_f a_0$ through the parameter p given by **Equation [5.33]**. The resulting optimized parameters, are compared in **Table 5.5**, and were used to generate the curves in **Figure 5.8**. The main difference between the individual (represented by the green curve) and the combined set of parameters (represented by the blue curve) was restrained to the values of $k_f a_0$, which deviated by half from the coupled to the individual set. Such results demonstrated that the use of a combined set will be a good estimation (with an AAD <15%) to predict the behaviour of other experimental runs (under similar experimental operating conditions) within variable mass flow rates.

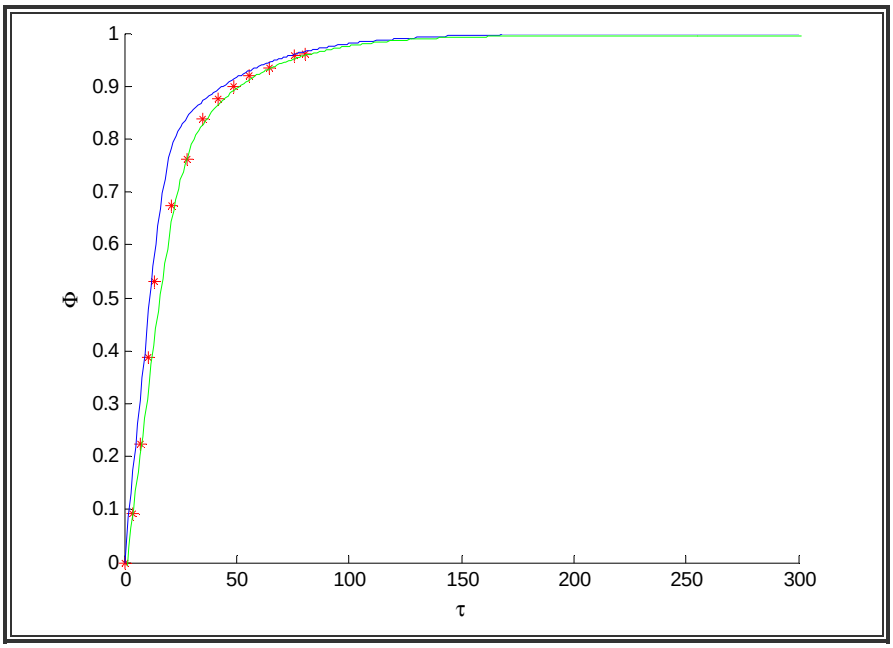

Figure 5.8 – Calculated results (this work) and experimental data (Reis-Vasco *et al.*, 2000) for the extraction of pennyroyal essential oil from leaves and flowers for $\dot{m} = 0.31$ g.s^{-1}. Blue line: curve generated using *p* optimized from data for three solvent mass flows (0.31, 0.43 and 0.62 g.s^{-1}); green line: Correlation obtained by fitting $k_f a_0$ for 0.31 g.s^{-1}.

The results obtained under a 1st and a 2nd order model approached each other and represented similar behaviour, being only distinguishable by $k_f a_0$, which for a 2nd order is about half the value given by the 1st order option (**Table 5.5**). Such deviation however, was not able to inflect any distinction in the final results, and therefore the corresponding extraction curves overlapped, while represented either by the 1st or the 2nd order model approaches (**Figure 5.8**).

The reduction in about 23% for the 2nd order value of $k_s a_s$ does not seem to be providing visible alterations in the SFE curve. To further verify such assumptions, we analyse the behaviour of the corresponding axial profiles using both 1st and 2nd order approaches. The axial profiles were given in a 3D view in **Figure 5.9** for the 1st order option only, and in a 2D view such as in **Figure 5.10** for both the 1st order and 2nd order options, respectively.

The 3D view shows the concentration waves, as function of time and position, while the 2D view shows concentration profiles for specific dimensionless times ($\tau = 10$, 30 and 50). From the 2D view plot, it is possible to identify and associate more dispersed waves to the 2nd order option (**Figure 5.10**). Such results show that the 2nd order discretization introduces some additional numerical dispersion into the model as can be detected in the decrease of the mass transfer fluxes in **Figure 5.10b** compared to **Figure 5.10a**, which may explain the lower value obtained for $k_f a_0$, but which is not significative to change the final SFE curve, as previously discussed and represented by **Figure 5.8** (blue curve).

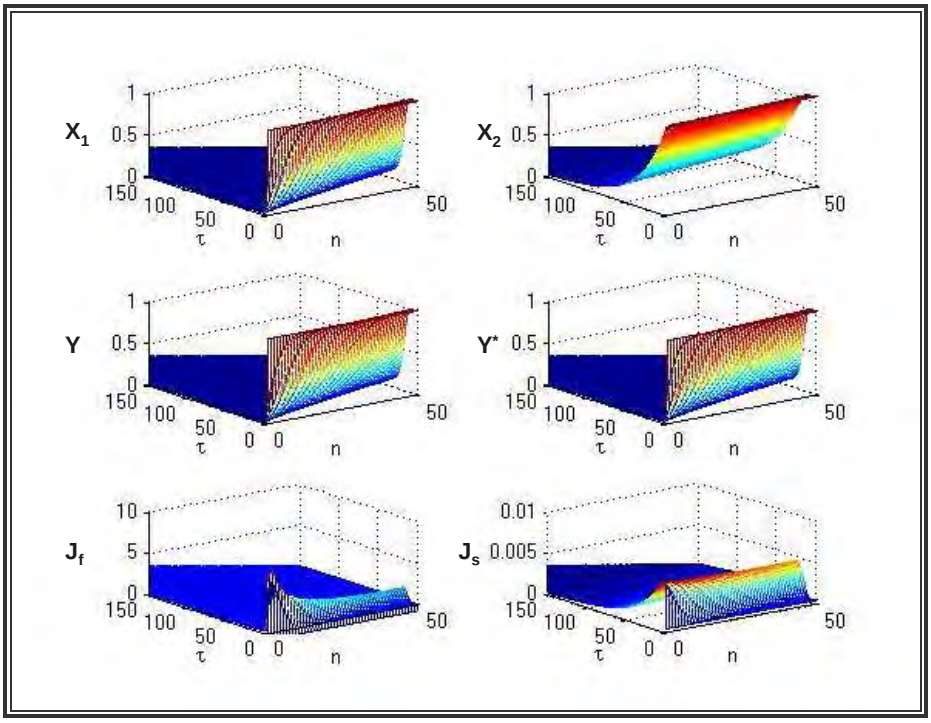

Figure 5.9 – 3D visualization of axial profiles for the extraction of pennyroyal essential oil from leaves and flowers with a flow rate of 0.31g.s^{-1}(data from Reis-Vasco *et al.* (2000)). Modelled according to a 1st order spatial discrimination option as function of dimensionless time and column segments (*n*=50).

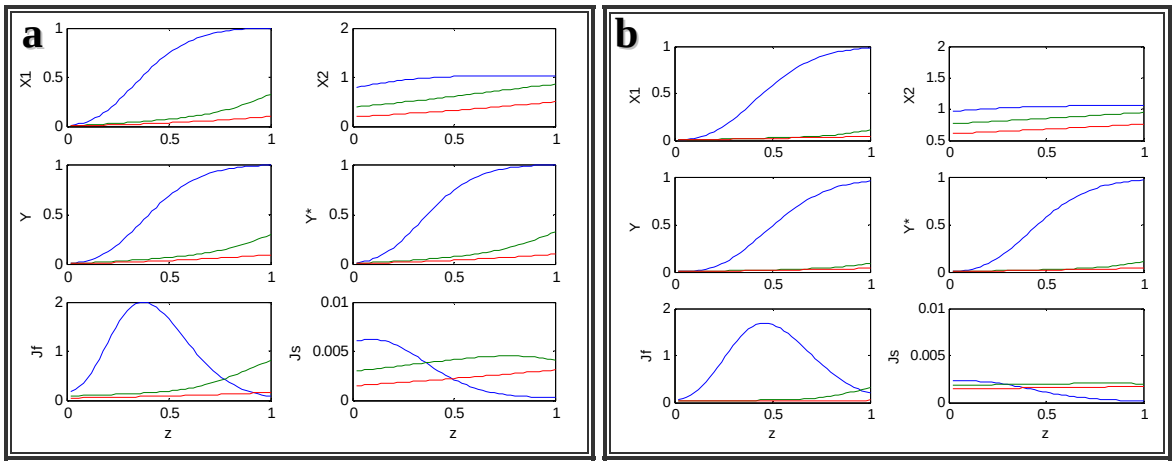

Figure 5.10 – 2D visualization of concentration profiles and fluxes for the extraction of pennyroyal essential oil from leaves and flowers with a flow rate of 0.31 g·s^{-1} (data from Reis-Vasco *et al.* (2000)). Model using spatial discretization option of (a) 1st order; (b) 2nd order. Dimensionless times of $\tau = 10$ (blue), 30 (green) and 50 (red).

The width of the mass transfer zone (δ_{MTZ}) was comparatively determined for $\tau = 10$ based on the reference limits of 0.05 and 0.95 of solute concentration in the fluid (Y) using both 1st and 2nd order approaches. The results presented a δ_{MTZ} = 62% and 66% of bed length for 1st and 2nd orders respectively, which show that the 2nd order has only increased δ_{MTZ} in 4% (**Figure 5.11**). Within such low differences, while presenting similar results for the optimized parameters in **Table 5.5**,

and similar SFE curves such as in **Figure 5.8**, it is possible to assume that both approaches are valid also in solid-matrix control regimes. Furthermore, and in accordance with the literature, the use a 2nd order option should increase both accuracy and computation times (Constantinides, 1988). However, the results presented above show that the use of 2nd order differences approach by increasing the δ_{MTZ}, smoothed the axial internal profiles associated, which in turn become easier to integrate and therefore resulted in a consequent reduction in the computation times of about 10-30%.

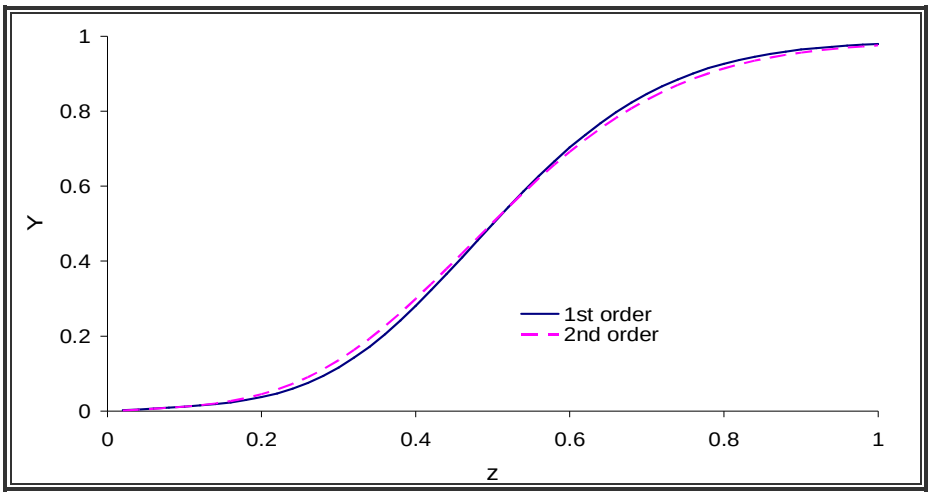

Figure 5.11 – Predicted concentration profiles for $\tau = 10$. Blue line: spatial discretization of 1st order; pink line: spatial discretization of 2nd order.

Axial dispersion. Sovová (2005) analyzed the effect of parameter n, which defines the grid, which for sufficient large values traduces a plug flow regime. The relation with the bed length is $n = 1 + \Delta z^{-1}$. By optimizing n, Sovová (2005) embodied an intrinsic numerical dispersion into the model as in a series model approach, whereas Reis-Vasco *et al.* (2000) introduced it explicitly with an axial dispersion term. In **Figure 5.12a** the data from Reis-Vasco *et al.* (2000) were used to fit *p* fixing $n = 50$, whereas in **Figure 5.12b** three individual *n* have been optimized in conjunction with parameter *p*. The results are obviously better in the second situation since three additional parameters have been optimized.

Under the experimental conditions used in this work, the axial dispersion has been neglected. In order to confirm such assumption the Peclet numbers have been estimated, based on the correlations for the axial dispersion coefficient in the bed, D_{ax}, presented in the **Appendix A2** (**Equation [A2.1]** due to Catchpole *et al.* (1996a)). The results, for both cases are given in **Table 5.6**.

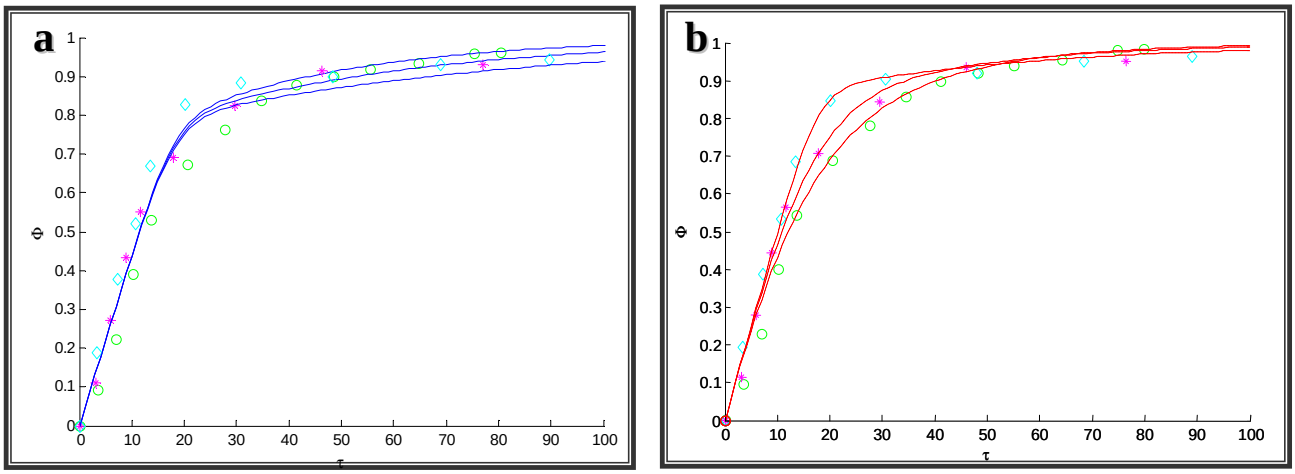

Figure 5.12 – Calculated results (this work) and experimental data (Reis-Vasco *et al.*, 2000) for the extraction of pennyroyal essential oil from leaves and flowers for three mass flow rates (see Table 5.5). (a) *p* optimized with *n* = 50; (b) *p* and three values of *n* optimized (*n* = 2, 4 and 50).

Acccording to Froment and Bischoff (1979), as long as $L/d_p > 50$ (which is true in both cases) the assumption of negligible axial dispersion is valid. An alternative analysis considers $N_{Pe,L}$, where axial dispersion is negligible for $N_{Pe,L} > 100$. Goto *et al.* (1996) showed that for $10 < N_{Pe,L} < 100$ and under supercritical conditions, axial dispersion is still considered small as to be negletected. Accordingly, the results from ($N_{Pe,L} > 35$) show that plug flow assumption is valid.

Table 5.6 – Calculated results for the evaluation of axial dispersion in the bed.

T (K)	P (bar)	d_p (mm)	L/d_P	$\dot{m}$ ($kg \cdot s^{-1}$)	u ($m \cdot s^{-1}$)	N_{Re}	N_{Sc}	$N_{Pe,d}$	D_{ax}^* ($m^2 \cdot s^{-1}$)	$N_{Pe,L}$	Data
313.25	350	0.3	383	2.38E-02	2.42E-04	83.5	24.0	0.09	7.21E-05	35.25	Marrone *et al.* (1998)
		0.7	164			195		0.21	1.69E-04	35.08	
		1.9	60.5			529		0.58	4.60E-04	35.00	
323.15	100	0.5	230	6.20E-04	1.15E-04	0.65	23.4	0.38	2.78E-07	87.69	Reis-Vasco *et al.* (2000)
				4.30E-04	7.95E-04	0.45		0.47	1.58E-07	107.25	
				3.10E-04	5.73E-04	0.33		0.57	9.28E-08	131.51	

* (Catchpole *et al.*, 1996a).

5.4. Supercritical Fluid Extraction Curves

All experimental SFE curves have been modelled and solved numerically using backward finite differences of 1st and 2nd order. The evolution of the concentration profiles obtained under both discretization approaches, as well as the corresponding extraction curves, overlap. More information on the subject can be found elsewhere (Silva *et al.*, 2009). Estimated values were given in Chapter 3 for the convective mass transfer coefficient k_f and solubility y_s, therefore reducing the number of parameters to be optimized here to only $k_s a_s$ and r. Details about the experimental conditioning have been given in Chapter 3.

5.4.1. SFE of untreated seed

Figure 5.13 represents the SFE curves at 160, 180, 200, and 220 bar at constant temperature (313.15 K) and solvent mass flow rate ($\dot{m} = 1.7 \times 10^{-4}$ kg·s^{-1}) (see **Table 3.3**), whereas **Figure 5.14** considers both pressure and temperature variations (180 and 200 bar; 313.15 and 323.15 K). As long as pressure is increased and/or temperature is decreased the mass transfer rate is also increased, although all curves approach approximately 60% of the maximum oil content ($\eta = 19.5\%$) achieved by conventional Soxhlet extraction under the best enzymatic pre-treatment conditions (**Table 2.1**: $t = 24$ h, pH = 4, $T = 313.15$ K, and concentration C_1).

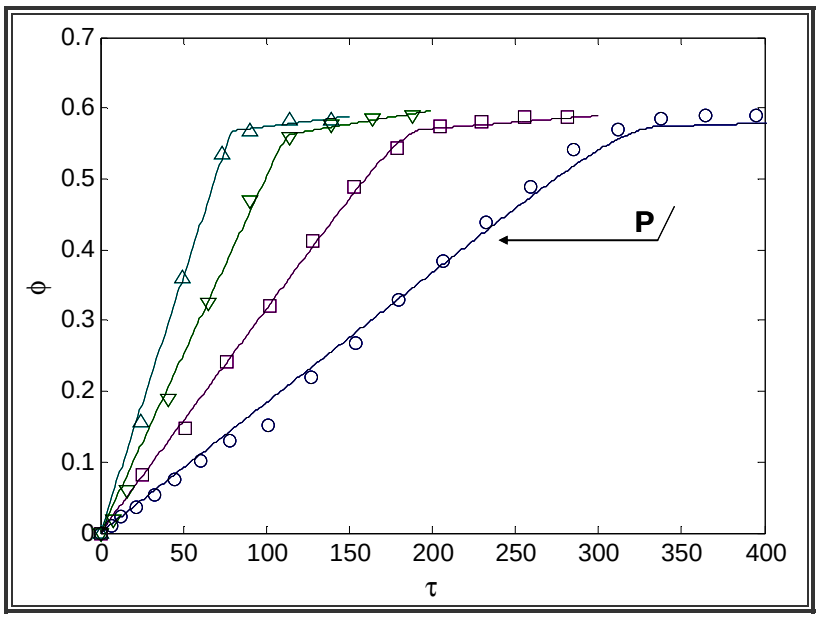

Figure 5.13 – Experimental and calculated dimensionless extraction curves at 313.15 K. Data: O - 160 bar; □ - 180 bar; ∇ - 200 bar; Δ - 220 bar.

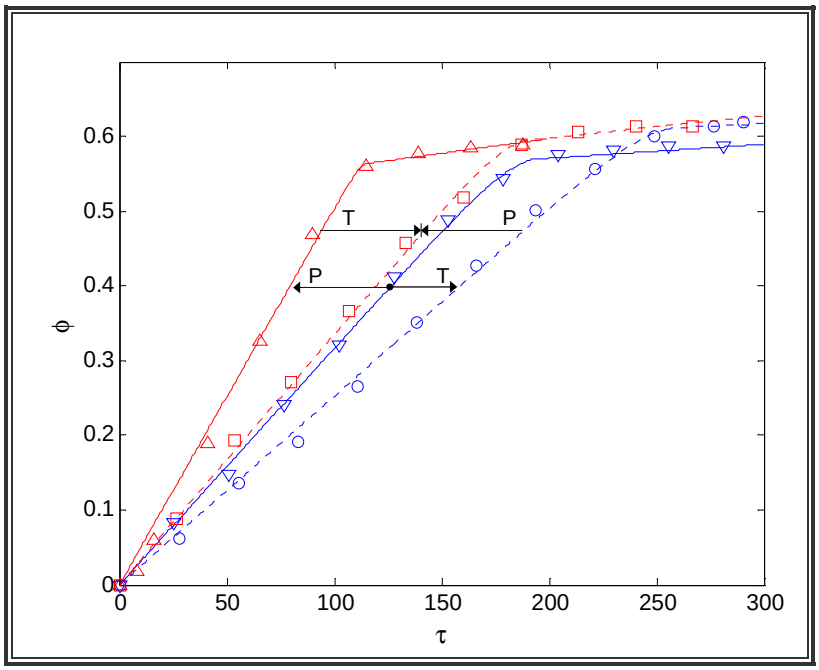

Figure 5.14 – Experimental and calculated dimensionless extraction curves. Data: ∇ - 180 bar/313.15 K; Δ - 200 bar/313.15 K; O - 180 bar/323.15 K; □ - 200 bar/323.15 K.

The parameters fitted to the experimental data are presented in **Table 5.7**, along with the deviations found. The calculated AADs are inferior to 5.14%. From **Figures 5.13** and **5.14** it is clear that the two characteristic periods are well represented.

Table 5.7 – Optimized parameters ($k_s a_s$, and r) for grape seed oil extraction modelled for various operating conditions.

Operating conditions		Optimized Parameters			Derived parameters		
P (bar)	T (K)	$k_s a_s$ (s^{-1})	r	AAD (%)	k_s ($m \cdot s^{-1}$)	k_f ($m \cdot s^{-1}$)	$k_f a_0$ (s^{-1})
160	313.15	0.65E-06	0.56	5.14	2.25E-10	7.74E-06	3.87E-02
180		0.89E-06	0.55	1.96	3.04E-10	7.19E-06	3.60E-02
200		1.84E-06	0.54	4.05	6.17E-10	6.40E-06	3.20E-02
220		1.32E-06	0.56	2.27	4.35E-10	6.16E-06	3.08E-02
180	323.15	1.40E-06	0.59	3.10	5.07E-10	9.47E-06	4.74E-02
200		0.92E-06	0.58	2.62	3.27E-10	8.50E-06	4.25E-02

Grinding efficiency, r. One main advantage from the broken+intact approach was the introduction of a grinding efficiency parameter (r) which differentiates two distinct zones in the particle. The results obtained present similar values of r for all runs, namely 0.54-0.59 (see **Table 5.7**). This independency of r on the operating conditions corroborates the initial assumption of an external volume of the particle essentially determined by the structure of the insoluble solids, which in turn should not be affected by the extraction.

Mass transfer coefficients. As has been mentioned before, a SFE curve comprehends an external convective controlled step where $k_f a_0$ has most impact, followed by a diffusional controlled step where $k_s a_s$ prevails. In the first period approximately 90-95% of oil is removed which is in accordance with the magnitude of the individual mass transfer coefficients. In fact from **Table 5.7** it is possible to see that the values of $k_f a_0$ range from 3.08×10^{-2} to 4.74×10^{-2} s^{-1}, in opposition to the much smaller $k_s a_s$ for which one founds values between 0.65×10^{-6} and 1.84×10^{-6} s^{-1}.

Concentration profiles. Figure 5.15 shows the dimensionless concentration profiles of X_1 (free oil), X_2 (tied oil), and Y (solute concentration in solution) for different times ($\tau = 51, 101...$ with $\Delta\tau = 50$) and for all pressures studied. The figure shows an intimate relation between X_1 and Y, because the free oil is almost the unique responsible to feed the fluid phase. Additionally it is possible to observe that X_2 deviates from unit only when X_1 vanishes.

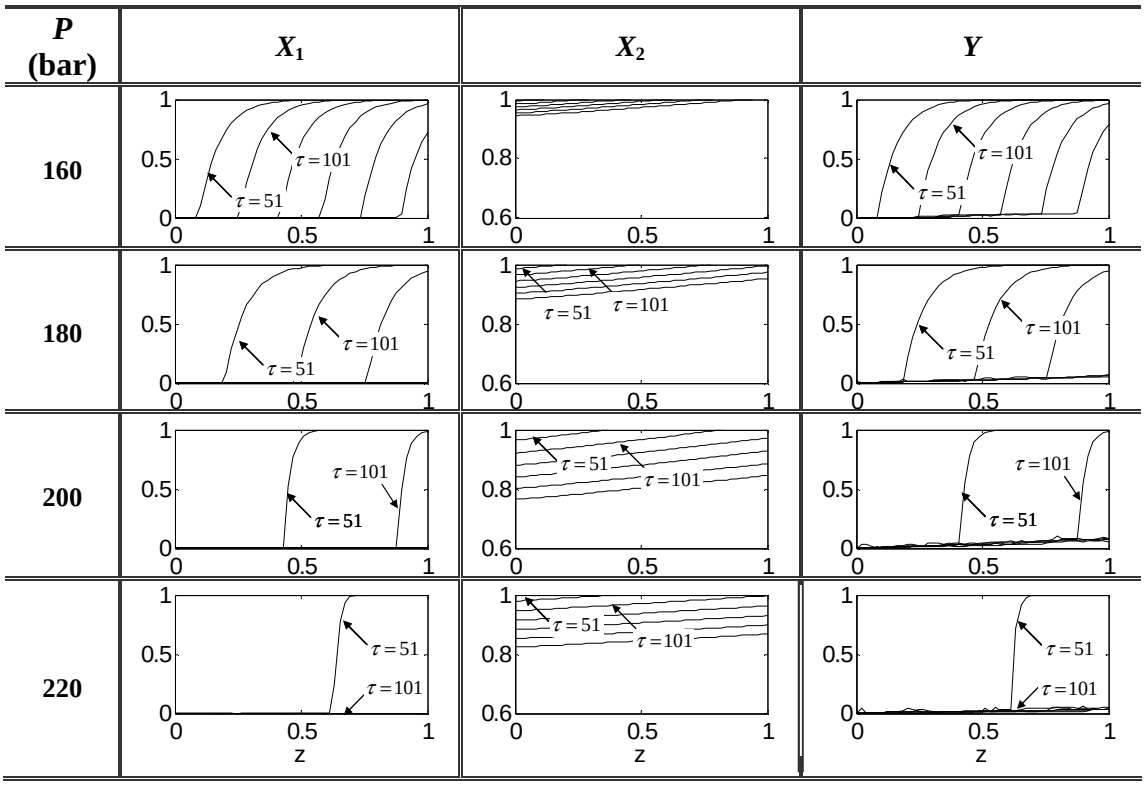

Figure 5.15 – Dimensionless concentration profiles of X_1, X_2, and Y predicted in the extractor bed for dimensionless time intervals of $\Delta\tau = 50$.

The width of mass transfer zones (δ_{MTZ}) for all experimental conditions previously presented have now been calculated for τ = 30, 50, 80 using the reference limits of 0.05 and 0.95 for *Y*. The results

obtained for the constant temperature of 313.15 K were: δ_{MTZ}(160 bar) = 23.4%, δ_{MTZ}(180 bar) = 24.3%, δ_{MTZ}(200 bar) = 8.1%, and δ_{MTZ}(220 bar) = 7.6%. For the constant temperature of 323.15 K: δ_{MTZ}(180 bar) = 20.0%; δ_{MTZ}(200 bar) = 20.7%. The MTZ exhibited a decrease with increasing pressure, and an increase with decreasing temperature tendency.

Figure 5.16 elucidates the effect of temperature with sharper waves running at the lowest temperature used (313.15 K comparatively with 323.15 K), specially for the highest pressure of 200 bar in comparison with 180 bar.

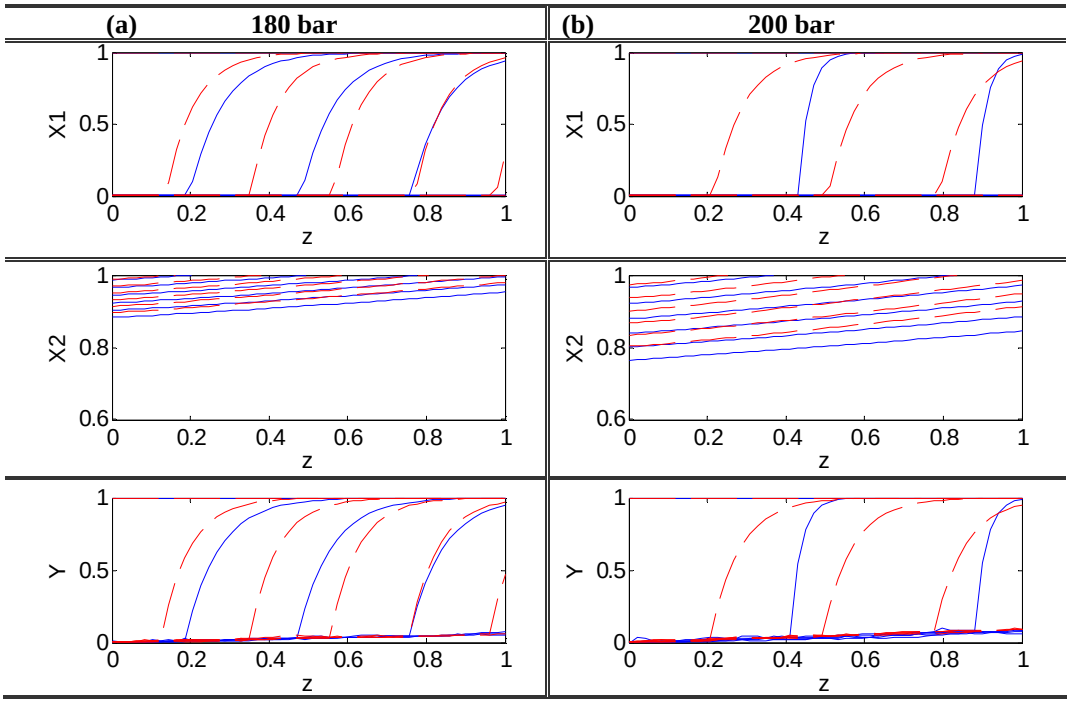

Figure 5.16 – Dimensionless concentration profiles of X_1, X_2, and Y for $\Delta\tau$ =50 at: (a) 180 bar; (b) 200 bar. Full blue line, 313.15 K; dashed red line, 323.15 K.

Figure 5.17 shows the elution curves for the SFE of grape seed oil at different pressure/temperature conditions similarly to the breakthrough curves of a percolation process from which the stoichiometric time can be determined. A clear overview finds that the stoichiometric time increases by decreasing pressure and temperature. For the constant temperature of 313.15 K the stoichiometric times are 1076, 420, 279 and 197 minutes, for 160, 180, 200 and 220 bar, respectively. Such results imply a variation of 2.6, 1.5, and 1.4 times in each ΔP = 20 bar leap, from the lowest to the highest pressures studied. For a constant temperature of 323.15 K, stoichiometric times of 558 and 450 min were obtained for 180 and 200 bar, respectively. At this temperature, the jump from 180 to 200 bar implies a variation of 1.2 in the stoichiometric time, which is similar to what happened with the lowest temperature of 313.15 K, already described above. When considering the temperature effect, one finds that at 180 bar the stoichiometric times

vary 1.3 times by increasing 10 K; at 200 bar the variation is 1.6. All these results due to the major effect of solubility over the weak role played by interstitial velocity. In fact, at higher pressure the density is higher and thus velocity is inferior, which would imply a lower concentration wave velocity in the bed and higher stoichiometric time. Nonetheless, at higher pressure solubility is higher, and so less time is required to exhaust the oil in the bed. This second effect overlaps the first.

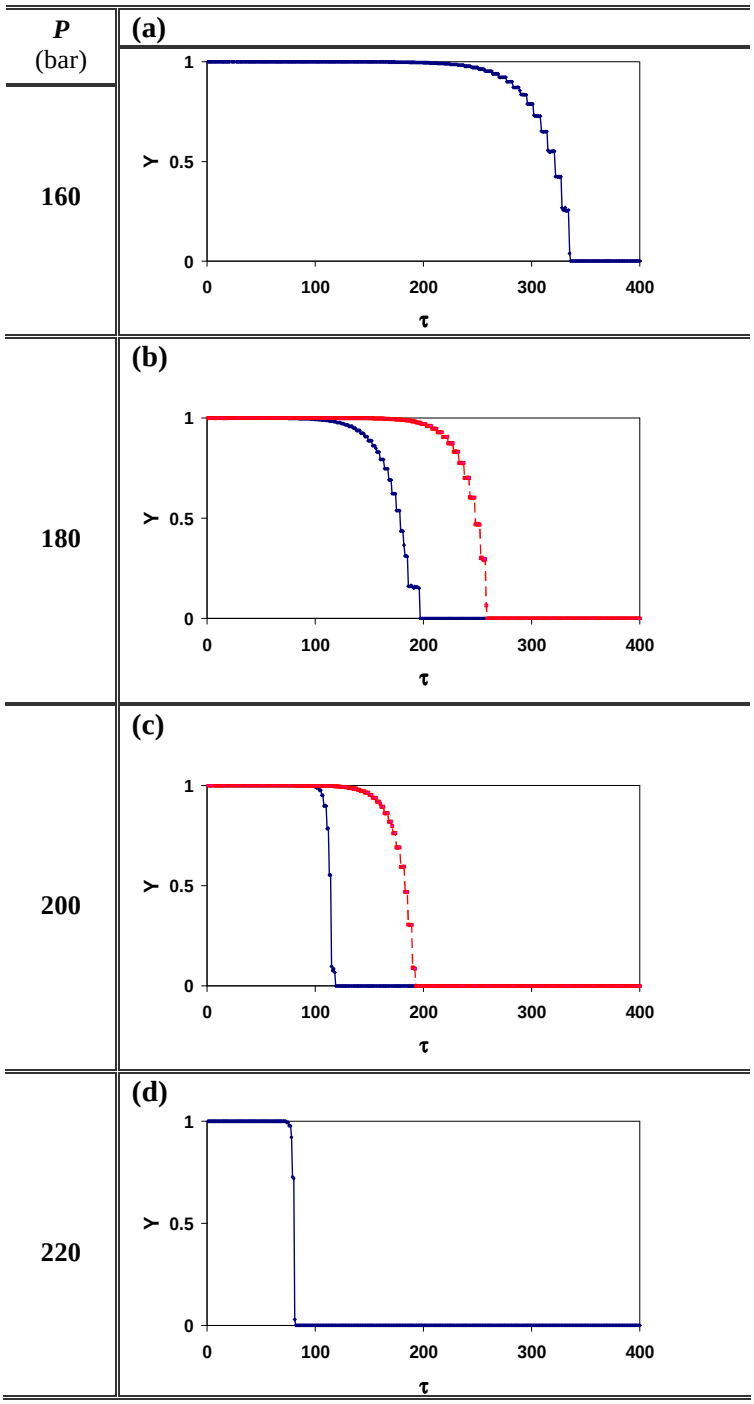

Figure 5.17 – Dimensionless elution curve calculated for: (a) 160 bar; (b) 180 bar; (c) 200 bar; (d) 220 bar. Full blue line: 313.15 K; dashed red line: 323.15 K.

5.4.2. SFE of enzymatically pre-treated seed

The influence of the enzymatic pre-treatment of seed in the SFE will be discussed now. **Table 5.8** shows the optimized parameters obtained in this case along with those for untreated seed (taken from **Table 5.7**) for correspondent experimental conditions. **Figure 5.18** represents the SFE curves for the enzymatically pre-treated seed. The results shows that the model represents well the experimental data, AAD = 4.15-6.19%, being the highest deviation obtained for 180 bar/313.15 K.

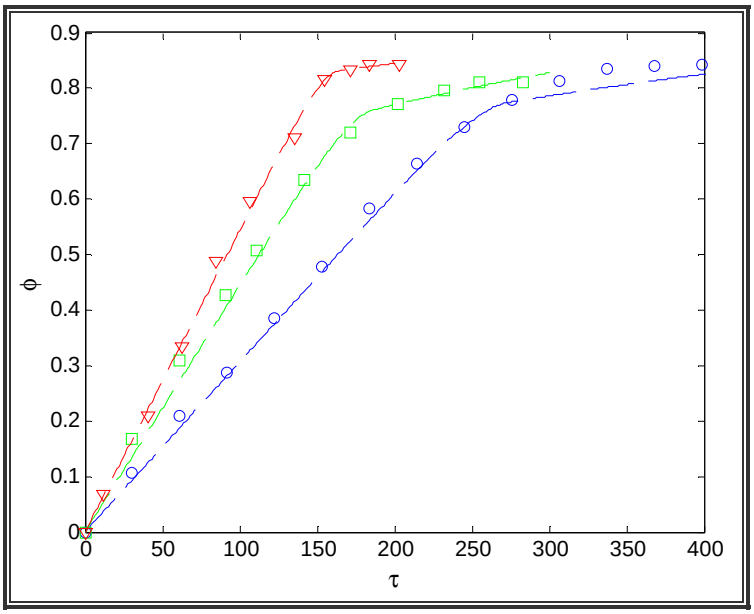

Figure 5.18 – Experimental and calculated dimensionless extraction curves of enzymatic pre-treated seed. Experimental Data: ○ (blue) - 160 bar/313.15 K; (green) – 180 bar/313.15 K; ∇ (red) - 200 bar/313.15 K.

Table 5.8 – Modelled parameters ($k_s a_s$, and r), enzymatically pre-treated *versus* untreated seed at 313.15 K.

P (bar)	Untreated seed			Enzymatically pre-treated seed		
	$k_s a_s$ (s^{-1})	r	AAD (%)	$k_s a_s$ (s^{-1})	r	AAD (%)
160	0.65E-06	0.56	5.14	3.51E-06	0.71	4.20
180	0.89E-06	0.55	1.96	4.89E-06	0.68	6.19
200	1.84E-06	0.54	4.05	1.41E-06	0.83	4.15

The volumetric convective mass transfer coefficients, $k_f a_0$, are independent of the pre-treatment applied, thus coincide with those of **Table 5.7**. Otherwise, $k_s a_s$ changes but exhibits analogous orders of magnitude. The optimize r values are clearly higher than those for untreated seed, i.e. 0.68-0.83 against 0.54-0.56 (see **Table 5.8**). Such fact is undoubtedly associated to the enzymatic pre-treatment, which increases the amount of broken cells, further increasing the global extraction yield by about 44%.

Concentration profiles. The concentration profiles have also been predicted to analyse the effect of seed pre-treatment in comparison to untreated seed. In **Figure 5.19** the concentration profiles at 160, 180, and 200 bar are presented for both treated and untreated seed. Because the experimental conditions are the same, the results show that when the pre-treatment is applied more oil is taken from intact cells, as X_2 is pronouncedly decreased in relation to untreated seed (see red and blue lines of X_2 in **Figure 5.19**).

With respect to the elution (or breakthrough) curves, results are not presented since the trends are similar to those discussed previously for untreated seed.

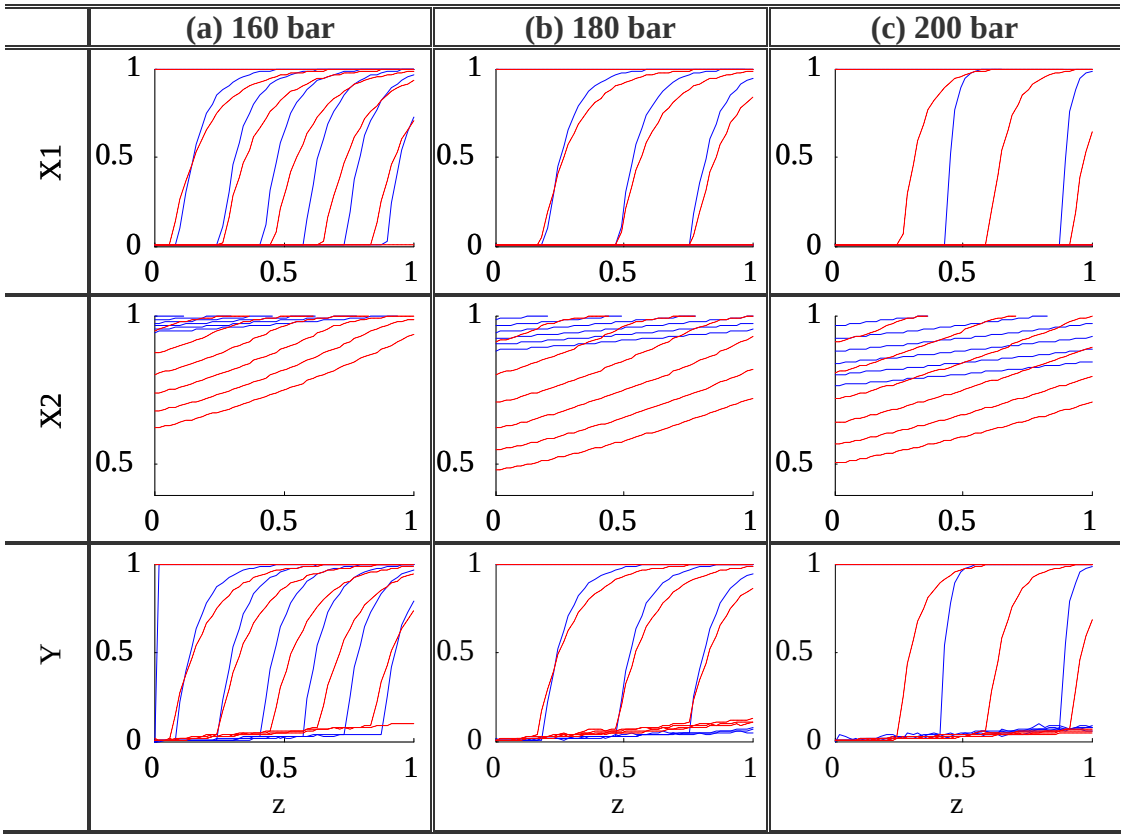

Figure 5.19 – Dimensionless concentration profiles predicted in the bed for $\Delta\tau = 50$ for: (a) 160 bar/313.15 K; (b) 180 bar/313.15 K; (c) 200 bar/313.15 K. Full (blue) lines: untreated seed; dashed (red) lines: enzymatically pre-treated seed.

SFE of high pressure pre-treated seed

The calculated and experimental SFE curves at 180 bar and 313.15 K are shown in **Figure 5.20** in dimensionless coordinates; the AAD achieved is only 2.08%. In **Table 5.9** the optimized parameters obtained for untreated, enzymatically pre-treated, and high pressure pre-treated seed are given for comparison. It is worth noting that the seed particle is larger in the last case, which results in an importantly lower grinding factor, r : 0.33 *versus* 0.55 and 0.68.

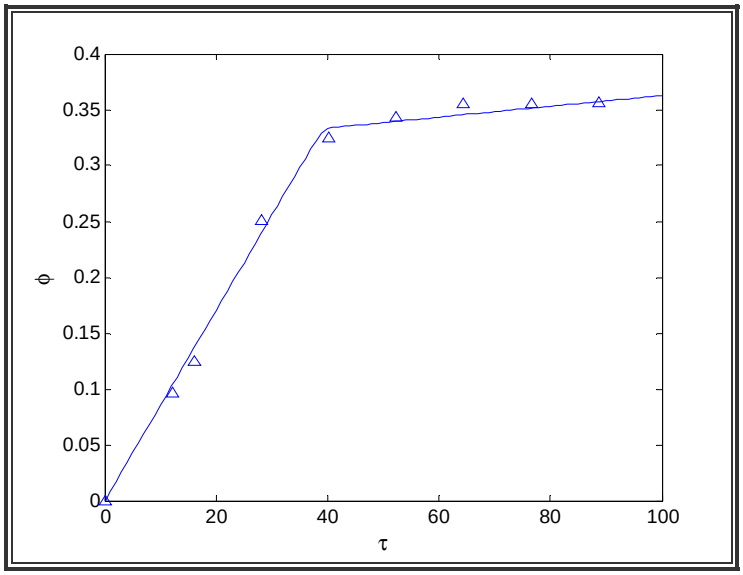

Figure 5.20 – Experimental and calculated dimensionless extraction curves of high pressure pre-treated seeds. Experimental Data: ∇ – 180 bar/313.15 K, d_p=0.85mm, ε=0.55. Full line –model results.

Table 5.9 – Fitted parameters for untreated *versus* pre-treated seed at 180 bar/313.15 K.

Pre-treatment	d_p (mm)	$k_s a_s$ (s^{-1})	r	AAD (%)
-	0.75	0.89E-06	0.55	1.96
Enzymatic		4.89E-06	0.68	6.19
HPP	0.85	0.47E-06	0.33	2.08

It is well known that parameter r depends on the particle diameter. From an approximate mass balance to the extractable oil it is possible to write:

$$\eta \times m_{seed} = r \times V_{seed} \times \rho_s \times x_u \quad \textbf{[5.34]}$$

this allows to compare data for different particle diameters as long as *P* and *T* are the same, by:

$$\eta_2 / \eta_1 = r_2 / r_1 \quad \textbf{[5.35]}$$

The calculated ratios of η and *r* are given in **Table 5.10** and obey the equality in **Equation 5.35** for the following pairs of experiments: Untreated/HPP and Untreated/Enzymatic.

Table 5.10 – Relationship between yield and grinding efficiency ratios at 180 bar/313.15 K for the different pre-treatments applied to the seed.

Pre-treatment	$\eta^{untreated} / \eta^{treated}$	$r^{untreated} / r^{treated}$
Untreated/HPP	1.7	1.7
Untreated/Enzymatic	0.7	0.8

6. Conclusions and Future Work

Every man's work, whether it be literature, or music or pictures or architecture or anything else, is always a portrait of himself.
[Samuel Butler]

6. Conclusions and Future Work

Conclusions.

In this work, the supercritical fluid extraction of grape seed oil and the effect of an enzymatic pre-treatment were carried out aiming to increase its extraction yield. The extraction curves obtained were related with grape seed oil quality. Additionally, the study of the extraction, fractionation, and structural characterization of grape seed procyanidins has been accomplished, as well as their antioxidant capacity was assessed.

Grape seed procyanidins are composed mainly by (+)-catechin, (-)-epicatechin, and (-)-epicatechin-*O*-gallate, and by the polymeric structures of the same monomers. (+)-Catechin occurred as the main terminal unit whereas (-)-epicatechin occurred as the main extension unit of procyanidins. The (-)-epicatechin-*O*-gallate unit accounted up to 20.3% of the total procyanidin residues. While maintaining a similar composition between red and white grape seeds, different average degrees of polymerization, ranging from 1.0 to 10.8, were assessed.

The extraction methodology using sequentially methanol and acetone/water, and then fractions of these extracts by graded precipitations in methanol/chloroform solutions allowed to collect a representative number of samples that endorsed to build calibration models to estimate the average degree of polymerization of grape seed procyanidins. The infrared spectra of the different fractions allowed to obtain a predictive O-PLS1 model with one latent variable. The results obtained with the model were comparable with those of HPLC-UV. Also, it was possible to observe that the solubility of these polymers in methanol/chloroform solutions are also inversely related with the degree of polymerization of the procyanidins.

The detailed analysis of grape seed procyanidins extracts by ESI-MS, ESI-MS/MS and LC–MS after thiolysis allowed to report, for the first time, the occurrence in grape seed of type-A galloylated procyanidin. Similar relative abundances and structural features were observed for the samples from white and red grape varieties. The ratio of abundance of type-A procyanidins to the correspondent type-B species was 60–80%, independent of the interflavanic linkage. The ratio of abundance of monogalloylated to nongalloylated ones was 20–60%. Type-A interflavanic linkages of grape seeds were found to be present mainly as terminal units.

Grape seed procyanidins-rich extracts revealed high antioxidant capacity (AOC), similar to that observed to the pure (+)-catechin standard. A slight increase in the AOC of most freeze-dried extracts was detected after one year of storage in the dark at room temperature, explained in the

literature by the higher AOC associated to higher oxidation states of partially oxidized polyphenolic compounds.

Since the yield of seed oil extraction may be enhanced by combining mechanical and/or enzymatic pre-treatments, the impact of such seed pre-treatments was considered. Experiments have shown that the global extraction yield of grape seed oil increased with increasing both reaction time and enzymatic cocktail concentration (cellulase, xylanase, pectinase, and protease). On the contrary, pH and temperature, gave rise to opposite behaviours when these enzymes are used. Concerning particle size, the enzymatic treatment had greater impact on larger particle diameters. On the whole, the following set of parameters for the grape seed enzymatic pre-treatment has been chosen for particles with diameters 1.0-1.4 mm: 24 h, pH 4, temperature range within 303.15-313.15 K, and an enzymatic cocktail with cellulase, xylanase, pectinase, and protease, whose concentrations are respectively 29, 1191, 21, and 569 U per gram of seed sample. Under these conditions, the extraction yield measured has been 13.7%, which represents an increment of 106.3% over untreated samples. Increasing two to three times the concentration of the enzymatic cocktail, the yield increment attained 136.5% over untreated samples.

The SFE of grape seed oil with carbon dioxide has been accomplished at 313.15 and 323.15 K, at 160, 180, 200 and 220 bar. The effects of the enzymatic pre-treatment upon SFE were studied at 313.15 K and 160, 180, and 200 bar. For untreated seeds, the maximum extraction yield obtained was 11.6%, whereas the enzymatic pre-treatment increased it by 43.5%, attaining η=16.4%. The yields obtained by SFE for both treated and untreated seeds were similar to those obtained by conventional Soxhlet with *n*-hexane. All cumulative extraction curves measured in this work exhibited a first linear part and a second asymptotic branch (which contributed with only 3-8% of the total oil removed) expected for edible oils (in opposition to essential oils).

With respect to the operating conditions, the mass transport increased with both increasing pressure and decreasing temperature, enhancing the extraction rate in both cases. The dependence of solubility on the operating conditions has proved to impart the strongest effect. A pressure increment of 20 bar has been proved to have the same effect as decreasing temperature by 10 K, as the cumulative curves for 180 bar/313.15 K and 200 bar/323.15 K overlapped. Furthermore, the mass of carbon dioxide necessary to reach 11.0% of yield – corresponding to the end of the 1st period of extraction – was only 2.4 kg per seeds batch at 220 bar/313.15 K against 8.0 kg at 160 bar/313.15 K, which means that 70% of solvent is saved.

In the case of the SFE of enzymatically pre-treated seeds, the cumulative curves exhibited the same trend reported above, with final yields similar to those determined by Soxhlet. If one considers the target yield of 11% cited above for untreated seeds, the CO_2 consumption needed is reduced by

44%, 33%, and 17% when the enzymatic pre-treatment was applied, for 160, 180, and 200 bar at 313.15 K, respectively.

With respect to the triacylglycerides content and oil composition, all extracts and final oil collected presented similar values, irrespective the SFE operating conditions for both untreated and pre-treated seed. The main compounds extracted were the unsaturated fatty acids linoleic (60-65%, 18:2 n-6) and oleic (14-17%, 18:1 n-9) acid, and the saturated palmitic (5-8%, 16:0) and stearic (4-6%, 18:0) acids. Very small amounts of linolenic (0.3-0.4%, 18:3 n-3) and traces of palmitoleic (less than 0.1%, 16:1 n-9) acids were also detected.

The antioxidant capacity of the global extracted oil, and of the individual extracts collected throughout the SFE, have been determined by the DPPH radical spectrophotometric method, and expressed as an equivalent tocopherol concentration. Results showed the AOC increases with increasing pressure and noticeably with rising temperature. Along extraction curves, the AOC is more pronounced on the oil collected during the first stages of the process, where 30-40% of the total oil is extracted.

The final stage of this work was devoted to the modelling of the SFE of grape seed oil and to the determination of their key parameters from the experimental data measured for both treated and untreated seed. With the aim to explain the sudden reduction of the extraction rate from the first to the second stage of the cumulative curve, the hypothesis of the existence of broken and intact cell fractions in the seed was considered. The equilibrium relationship adopted has a sigmoidal discontinuous trend. Accordingly, the 1st period of extraction is mainly associated to the depletion of free oil from the broken external cells to the solvent, and the 2nd period is determined by internal mass transfer from the intact inner cells to the broken ones at surface.

The model parameters to be optimized are the grinding efficiency of the seed (*r*), and an internal mass transfer coefficient multiplied by a specific surface area ($k_s a_s$). The convective mass transfer coefficient of the film ($k_f a_0$) was estimated by correlations from literature. The values of $k_f a_0$ were three to four order of magnitude superior to those of $k_s a_s$, which is in accordance with the convective and diffusional natures of the transport mechanisms. Analogous results were found for treated and untreated seed. Nonetheless, the same did not happen with parameter *r*, which was approximately 0.54 for untreated seed, and 0.68-0.83 for enzymatically pre-treated seed. On the whole, the model provided reliable representations of the experimental data with average absolute deviations lower than 6.19%.

Future Work.

Some suggestions for future work may be raised. It is important to enlarge the range of the operating conditions of the supercritical fluid extraction of grape seed oil, specially the solvent mass flow rate since only one value has been studied. Moreover, the effect of cosolvents upon global extraction yield and selectivity is a major point of investigation. In fact, the introduction of small quantities of polar modifiers, such as alcohols, may affect significantly the co-extraction of phenolic compounds, which ultimately will influence the antioxidant capacity of the final oil. Another topic to be developed is the identification and quantification of the compounds associated to the antioxidant properties of the oil, in a similar way to what have been accomplished in this work for the procyanidins extracts obtained from the defatted seeds. A final point of interest is the detailed study of the high pressure pre-treatment combined with grape seed oil extraction, namely its impact upon extraction yield, trend of cumulative curves, and oil quality, particularly its antioxidant capacity.

7. Bibliography

Inspiration comes of working every day.
[Charles Baudelaire]

7. Bibliography

Adachi, Y. and Lu, B. C. Y. (1983). Supercritical fluid extraction with carbon-dioxide and ethylene. *Fluid Phase Equilibria*, *14*, 147-156.

Akgun, M., Akgun, N. A. and Dincer, S. (2000). Extraction and modelling of lavender flower essential oil using supercritical carbon dioxide. *Industrial & Engineering Chemistry Research*, *39*(2), 473-477.

Antolovich, M., Prenzler, P., Robards, K. and Ryan, D. (2000). Sample preparation in the determination of phenolic compounds in fruits. *Analyst*, *125*(5), 989-1009.

Arai, Y., Sako, T. and Takebayashi, Y. Supercritical fluids molecular - interactions, physical properties and new applications. In *Materials Processing*, Springer Verlag, Berlin, Germany, 2002.

Bail, S., Stuebiger, G., Krist, S., Unterweger, H., and G. Buchbauer. (2008). Characterisation of various grape seed oils by volatile compounds, triacylglycerol composition, total phenols and antioxidant capacity, *Food Chemistry*, *108*(3), 1122-1132.

Barros, A. S. (1999). Contribution à la sélection et la comparaison de variables caractéristiques. Ph.D. Thesis. Institut National Agronomique Paris-Grignon, France.

Barros, A. S. and Rutledge, D. N. (2004). Principal components transform-partial least squares: a novel method to accelerate cross-validation in PLS regression. *Chemometrics and Intelligent Laboratory Systems*, *73*(2), 245-255.

Bartley, J. P. and Foley, P. (1994). Supercritical-fluid extraction of australian-grown ginger (*Zingiber-Officinale*). *Journal of the Science of Food and Agriculture*, *66*(3), 365-371.

Basile, A., Jimenez-Carmona, M. M. and Clifford, A. A. (1998). Extraction of rosemary by superheated water. *Journal of Agricultural and Food Chemistry*, *46*(12), 5205-5209.

Beckman, E. J. (2004). Supercritical and near-critical CO_2 in green chemical synthesis and processing. *Journal of Supercritical Fluids*, *28*(2-3), 121-191.

Berger, K. G. and Hamilton, R. J. (1995). Lipids and oxygen: is rancidity avoidable in practice? In *Developments in Oils and Fats*, Blackie Academic & Professional, Liverpool, England, 1995.

Berna, A., Tarrega, A., Blasco, M. and Subirats, S. (2000). Supercritical CO_2 extraction of essential oil from orange peel; effect of the height of the bed. *Journal of Supercritical Fluids*, *18*(3), 227-237.

Bernardo-Gil, G., Oneto, C., Antunes, P., Rodrigues, M. F. and Empis, J. M. (2001). Extraction of lipids from cherry seed oil using supercritical carbon dioxide. *European Food Research and Technology, 212*(2), 170-174.

Bernardo-Gil, M. G., Grenha, J., Santos, J. and Cardoso, P. (2002). Supercritical fluid extraction and characterisation of oil from hazelnut. *European Journal of Lipid Science and Technology*, *104*(7), 402-409.

Beveridge, T. H. J., Girard, B., Kopp, T. and Drover, J. C. G. (2005). Yield and composition of grape seed oils extracted by supercritical carbon dioxide and petroleum ether: varietal effects. *Journal of Agricultural and Food Chemistry*, *53*(5), 1799-1804.

Bravi, M., Spinoglio, F., Verdone, N., Adami, M., Aliboni, A., D'Andrea, A., De Santis, A. and Ferri, D. (2007). Improving the extraction of α-tocopherol-enriched oil from grape seeds by supercritical CO_2. Optimisation of the extraction conditions. *Journal of Food Engineering*, *78*(2), 488-493.

Brunner, G. Gas extraction - an introduction to fundamentals of supercritical fluids and the application to separation processes. In *Topics in Physical Chemistry, Vol. 4*, Steinkopff Darmstadt, Frankfurt, Germany, 1994.

Capuano, F., Beaudoin, F., Napier, J. A., Shewry, P. R. (2007). Properties and exploitation of oleosins. *Biotechnology Advances*, *25*(2), 203-206.

Cardoso, S. M., Guyot, S., Marnet, N., Lopes-da-Silva, J. A., Renard, C. M. G. C., Coimbra, M. A. (2005). Characterisation of phenolic extracts from olive pulp and olive pomace by electrospray mass spectrometry. *Journal of the Science of Food and Agriculture*, *81*, 21-32.

Carvalho, R. N., Moura, L. S., Rosa, P. T. V. and Meireles, M. A. A. (2005). Supercritical fluid extraction from rosemary (*Rosmarinus officinalis*): Kinetic data, extract's global yield, composition, and antioxidant activity. *Journal of Supercritical Fluids*, *35*(3), 197-204.

Castro, S. M., Van Loey, A., Saraiva, J. A., Smout, C. and Hendrickx, M. (2006). Inactivation of pepper (*Capsicum annuum*) pectin methylesterase by combined high-pressure and temperature treatments. *Journal of Food Engineering*, *75*(1), 50-58.

Catchpole, O. J., Bernig, R. and King, M. B. (1996a). Measurement and correlation of packed-bed axial dispersion coefficients in supercritical carbon dioxide. *Industrial & Engineering Chemistry Research*, *35*(3), 824-828.

Catchpole, O. J., Grey, J. B. and Smallfield, B. M. (1996b). Near-critical extraction of sage, celery, and coriander seed. *Journal of Supercritical Fluids*, *9*(4), 273-279.

Catchpole, O. J. and King, M. B. (1994). Measurement and correlation of binary diffusion coefficients in near critical fluids. *Industrial & Engineering Chemistry Research, 33*(7), 1828-1837.

Chrastil, J. (1982). Solubility of solids and liquids in supercritical gases. *Journal of Physical Chemistry, 86*(15), 3016-3021.

Christie, W. W. *High-performance liquid chromatography and lipids: a practical guide*, Pergamon Press cop., Oxford, England, 1987.

Christie, W. W. *Advances in lipid methodology – Two, Vol. 4*, The Oily Press Ltd., Dundee, England, 1993.

Constantinides, A. *Applied Numerical Methods with Personal Computers*, Chemical Engineering Series, McGraw-Hill International Editions, NY, USA, 1988.

Contreras-Domínguez, M., Guyot, S., Marnet, N., Le Petit, J., Perraud-Gaime, I., Roussos, S. and Augur, C. (2006). Degradation of procyanidins by *Aspergillus fumigatus*: identification of a novel aromatic ring cleavage product. *Biochimie, 88*(12), 1899-1908.

Copeland, L. O. and McDonald, M. B. *Principles of Seed Science and Tecnology*, 3rd Ed., Chapman & Hall, NY, USA, 1995.

Crews, C., Hough, P., Godward, J., Brereton, P., Lees, M., Guiet, S. and Winkelmann, W. (2006). Quantitation of the main constituents of some authentic grape-seed oils of different origin. *Journal of Agricultural and Food Chemistry, 54*(17), 6261-6265.

de Bruyne, T., Pieters, L., Witvrouw, M., de Clercq, E., Berghe, D. V. and Vlietinck, A. J. (1999). Biological evaluation of proanthocyanidins dimers and related polyphenols. *Journal of Natural Products, 62*(7), 954-958.

de Freitas, V. A. P., Glories, Y., Bourgeois, G. and Vitry, C. (1998). Characterisation of oligomeric and polymeric procyanidins from grape seeds by liquid secondary ion mass spectrometry. *Phytochemistry, 49*(5), 1435-1441.

de Gaulejac, N. S., Glories, Y. and Vivas, N. (1999). Free radical scavenging effect of anthocyanins in red wines. *Food Research International, 32*(5), 327-333.

del Valle, E. M. M. and Galan, M. A. (2005). Supercritical fluid technique for particle engineering: drug delivery applications. *Reviews in Chemical Engineering, 21*(1), 33-69.

del Valle, J. M. and Aguilera, J. M. (1988). An improved equation for predicting the solubility of vegetable oils in supercritical carbon dioxide. *Industrial & engineering chemistry research, 27*(8), 1551-1553.

del Valle, J. M., Bello, S., Thiel, J., Allen, A. and Chordia, L. (2000). Comparison of conventional and supercritical CO_2-extracted rosehip oil. *Brazilian Journal of Chemical Engineering, 17*(3), 335-348.

del Valle, J. M. and de la Fuente, J. C. (2006). Supercritical CO_2 extraction of oilseeds: Review of kinetic and equilibrium models. *Critical Reviews in Food Science and Nutrition, 46*(2), 131-160.

del Valle, J. M., de la Fuente, J. C. and Cardarelli, D. A. (2005). Contributions to supercritical extraction of vegetable substrates in latin America. *Journal of Food Engineering*, *67*(1-2), 35-57.

del Valle, J. M., Germain, J. C., Uquiche, E., Zetzl, C. and Brunner, G. (2006). Microstructural effects on internal mass transfer of lipids in prepressed and flaked vegetable substrates. *Journal of Supercritical Fluids*, *37*(2), 178-190.

del Valle, J. M., Godoy, C., Asencio, M. and Aguilera, J. M. (2004a). Recovery of antioxidants from boldo (*Peumus boldus* M.) by conventional and supercritical CO_2 extraction. *Food Research International*, *37*(7), 695-702.

del Valle, J. M., Rivera, O., Mattea, M., Ruetsch, L., Daghero, J. and Flores, A. (2004b). Supercritical CO2 processing of pretreated rosehip seeds: effect of process scale on oil extraction kinetics. *Journal of Supercritical Fluids*, *31*(2), 159-174.

Diaz-Reinoso, B., Moure, A., Dominguez, H. and Parajo, J. C. (2006). Supercritical CO_2 extraction and purification of compounds with antioxidant activity. *Journal of Agricultural and Food Chemistry*, *54*(7), 2441-2469.

Dominguez, H., Nunez, M. J. and Lema, J. M. (1994). Enzymatically pretreatment to enhance oil extraction from fruits and oilseeds - a Review. *Food Chemistry*, *49*(3), 271-286.

Dominguez, H., Nunez, M. J. and Lema, J. M. (1995). Enzyme-assisted hexane extraction of soya bean oil. *Food Chemistry*, *54*(2), 223-231.

Dourado, F., Barros, A., Mota, M., Coimbra, M. A. and Gama, F. M. (2004). Anatomy and cell wall polysaccharides of almond (*Prunus dulcis* D. A. Webb) seeds. *Journal of Agricultural and Food Chemistry*, *52*(5), 1364-1370.

Dourado, F., Vasco, P., Barros, A., Mota, M., Coimbra, M. A. and Gama, F. M. (2003). Characterisation of chilean hazelnut (*Gevuina avellana*) tissues: light microscopy and cell wall polysaccharides. *Journal of the Science of Food and Agriculture*, *83*(3), 158-165.

Dourado, F., Vasco, P., Gama, F. M., Coimbra, M. A. and Mota, M. (2000). Characterisation of rosa mosqueta seeds: cell wall polysaccharide composition and light microscopy observations. *Journal of the Science of Food and Agriculture*, *80*(13), 1859-1865.

Eder, K. (1995). Gas-chromatographic analysis of fatty-acid methyl-esters. *Journal of Chromatography B-Biomedical Applications*, *671*(1-2), 113-131.

Eggers, R., Ambrogi, A. and J., von Schnitzler (2000). Special features of SCF solid extraction of natural products: deoling of wheat gluten and extraction of rose hip oil. *Brazilian Journal of Chemical Engineering*, *17*(3), 329-346.

Escribano-Bailon, T., Gutierrez-Fernandez, Y., Rivas-Gonzalo, J. C. and Santos-Buelga, C. (1992). Characterization of procyanidins of *vitis vinifera* variety Tinta del Pais grape seeds. *Journal of Agricultural and Food Chemistry, 40*(10), 1794-1799.

Espín, J. C., Soler-Rivas, C. and Wichers, H. J. (2000). Characterization of the total free radical scavenger capacity of vegetable oils and oil fractions using 2,2-diphenyl-1-picrylhydrazyl radical. *Journal of Agricultural and Food Chemistry, 48*(3), 648-656.

Facino, R. M., Carini, M., Aldini, G., Calloni, M. T., Bombardelli, E. and Morazzoni, P. (1998). Sparing effect of procyanidins from *vitis vinifera* on vitamin E: In vitro studies. *Planta Medica, 64*(4), 343-347.

Fan, P. H. and Lou, H. X. (2004). Effects of polyphenols from grape seeds on oxidative damage to cellular DNA. *Molecular and Cellular Biochemistry, 267*(1-2), 67-74.

Ferreira, D., Guyot, S., Marnet, N., Delgadillo, I., Renard, C. M. G. C. and Coimbra, M. A. (2002). Composition of phenolic compounds in a portuguese pear (*pyrus communis* L. var. s. bartolomeu) and changes after sun-drying. *Journal of Agricultural and Food Chemistry, 50*(16), 4537-4544.

Ferreira de França, L., Reber, G., Meireles, M. A. A., Machado, N. T. and Brunner, G. (1999). Supercritical extraction of carotenoids and lipids from buriti (*mauritia flexuosa*), a fruit from the Amazon region. *The Journal of Supercritical Fluids 14*(3), 247-256.

Fiori, L. (2007). Grape seed oil supercritical extraction kinetic and solubility data: critical approach and modeling. *Journal of Supercritical Fluids, 43*(1), 43-54.

Flamini, R. (2003). Mass spectrometry in grape and wine chemistry. Part I: Polyphenols. *Mass Spectrometry Reviews, 22*(4), 218-250.

Freitas, V., Laguerre, M. and Glories, Y. Analyse conformationelle et propriétés physico-chimiques des procyanidines dimères. In *Proceedings of the Polyphenols Communication 96*, 75-76, Bordeaux, 1996.

Froment, G. F. and Bischoff, K. B. *Chemical Reactor - Analysis and Design*. John Wiley & Sons, Belgium, 1979.

Fuleki, T. and Ricardo-da-Silva, J. M. (1997). Catechin and procyanidin composition of seeds from grape cultivars grown in Ontario. *Journal of Agricultural and Food Chemistry, 45*(4), 1156-1160.

Fullbrook, P. D. (1983). The use of enzymes in the processing of oilseeds. *Journal of the American Oil Chemists Society, 60*(2), 476-478.

Gabetta, B., Fuzzati, N., Griffini, A., Lolla, E., Pace, R., Ruffilli, T. and Peterlongo, F. (2000). Characterization of proanthocyanidins from grape seeds. *Fitoterapia, 71*(2), 162-175.

Gaskell, S. J. (1997). Electrospray: principles and practice. *Journal of Mass Spectrometry*, *32*(7), 677-688.

Gomes, P. B., Mata, V. G. and Rodrigues, A. E. (2007). Production of rose geranium oil using supercritical fluid extraction. *Journal of Supercritical Fluids*, *41*(1), 50-60.

Gomez, A. M., Lopez, C. P. and De la Ossa, E. M. (1996). Recovery of grape seed oil by liquid and supercritical carbon dioxide extraction: A comparison with conventional solvent extraction. *The Chemical Engineering Journal and the Biochemical Engineering Journal*, *61*(3), 227-231.

Goto, M., Roy, B. C. and Hirose, T. (1996). Shrinking-core leaching model for supercritical-fluid extraction. *Journal of Supercritical Fluids*, *9*(2), 128-133.

Goto, M., Roy, B. C., Kodama, A. and Hirose, T. (1998). Modeling supercritical fluid extraction process involving solute-solid interaction. *Journal of Chemical Engineering of Japan*, *31*(2), 171-177.

Gu, L. W., Kelm, M. A., Hammerstone, J. F., Beecher, G., Holden, J., Haytowitz, D. and Prior, R. L. (2003a). Screening of foods containing proanthocyanidins and their structural characterization using LC-MS/MS and thiolytic degradation. *Journal of Agricultural and Food Chemistry*, *51*(25), 7513-7521.

Gu, L. W., Kelm, M. A., Hammerstone, J. F., Beecher, G., Cunningham, D., Vannozzi, S. and Prior, R. L. (2002). Fractionation of polymeric procyanidins from lowbush blueberry and quantification of procyanidins in selected foods with an optimized normal-phase HPLC-MS fluorescent detection method. *Journal of Agricultural and Food Chemistry*, *50*(17), 4852-4860.

Gu, L. W., Kelm, M. A., Hammerstone, J. F., Zhang, Z., Beecher, G., Holden, J., Haytowitz, D. and Prior, R. L. (2003b). Liquid chromatographic/electrospray ionization mass spectrometric studies of proanthocyanidins in foods. *Journal of Mass Spectrometry*, *38*(12), 1272-1280.

Guillen, D. A., Palma, M., Natera, R., Romero, R. and Barroso, C. G. (2005). Determination of the age of sherry wines by regression techniques using routine parameters and phenolic and volatile compounds. *Journal of Agricultural and Food Chemistry*, *53*(7), 2412-2417.

Gutnikov, G. (1995). Fatty-acid profiles of lipid samples. *Journal of Chromatography B-Biomedical Applications*, *671*(1-2), 71-89.

Guyot, S., Marnet, N. and Drilleau, J. F. (2001). Thiolysis-HPLC characterization of apple procyanidins covering a large range of polymerization states. *Journal of Agricultural and Food Chemistry*, *49*(1), 14-20.

Hancu, D. and Beckman, E. J. (2001). Generation of hydrogen peroxide directly from H_2 and O_2 using CO_2 as the solvent. *Green Chemistry*, *3*(2), 80-86.

Hangos, K. and Cameron, I. *Process modelling and model analysis, Vol. 4*, Process Systems Engineering series, Academic Press, London, England, 2001.

Hanmoungjai, P., Pyle, D. L. and Niranjan, K. (2002). Enzyme-assisted water-extraction of oil and protein from rice bran. *Journal of Chemical Technology and Biotechnology*, *77*(7), 771-776.

Hanmoungjai, P., Pyle, L. and Niranjan, K. (2000). Extraction of rice bran oil using aqueous media. *Journal of Chemical Technology and Biotechnology*, *75*(5), 348-352.

Hayasaka, Y., Waters, E. J., Cheynier, V., Herderich, M. J. and Vidal, S. (2003). Characterization of proanthocyanidins in grape seeds using electrospray mass spectrometry. *Rapid Communications in Mass Spectrometry*, *17*(1), 9-16.

Henning, J. A., Core, R. J. and Gardeatorresdey, J. L. (1994). Extracting volatile compounds from single plants using supercritical-fluid extraction. *Crop Science*, *34*(4), 1120-1122.

Huang, A. H. C. (1992). Oil bodies and oleosins in seeds. *Annual Review of Plant Physiology and Plant Molecular Biology*, 43, 177-200.

IUPAC. *Standard methods for Analysis of Oils, Fats and Derivatives*, 7th Ed., Blackwell Scientific Publications, Boston, USA, 1987.

IVV (2008). www.ivv.min-agricultura.pt (last time acceded: 14 May 2008).

Jensen, J.S., Egebo, M., Meyer, A.S. (2008). Identification of spectral regions for the quantification of red wine tannins with fourier transform mid-infrared spectroscopy. *Jounal of Agriculture and Food Chemistry*, *56*(10), 3493-3499.

Kaiser, C. S., Rompp, H. and Schmidt, P. C. (2004). Supercritical carbon dioxide extraction of chamomile flowers: extraction efficiency, stability, and in-line inclusion of chamomile-carbon dioxide extract in beta-cyclodextrin. *Phytochemical Analysis*, *15*(4), 249-256.

Karchesy, J. J., Hemingway, R. W., Foo, Y. L., Barofsky, E. and Barofsky, D. F. (1986). Sequencing procyanidin oligomers by fast-atom-bombardment mass-spectrometry. *Analytical Chemistry*, *58*(12), 2563-2567.

Kashyap, M. C., Agrawal, Y. C., Ghosh, P. K., Jayas, D. S., Sarkar, B. C., Singh, B. P. N. Oil extraction rates of enzymatically hydrolyzed soybeans. *Journal of Food Engineering, 81*(3) 611-617.

Kaur, C. and Kapoor, H. C. (2001). Antioxidants in fruits and vegetables - the millennium's health. *International Journal of Food Science and Technology*, *36*(7), 703-725.

King, M. B. and Bott, T. R. *Extraction of Natural Products using Near-critical Solvents*, Blackie Academic & Professional, Glasgow, England, 1993.

Knorr, D. (2003). Impact of non-thermal processing on plant metabolites. *Journal of Food Engineering*, *56*(2-3), 131-134.

Kondo, K., Kurihara, M., Fukuhara, K., Tanaka, T., Suzuki, T., Miyata, N. and Toyoda, M. (2000). Conversion of procyanidin B-type (catechin dimer) to A-type: evidence for abstraction of C-2 hydrogen in catechin during radical oxidation. *Tetrahedron Letters*, *41*(4), 485-488.

Kornsteiner, M., Wagner, K. H. and Elmadfa, I. (2006). Tocopherols and total phenolics in 10 different nut types. *Food Chemistry*, *98*(2), 381-387.

Krueger, C. G., Dopke, N. C., Treichel, P. M., Folts, J. and Reed, J. D. (2000). Matrix-assisted laser desorption/ionization time-of-flight mass spectrometry of polygalloyl polyflavan-3-ols in grape seed extract. *Journal of Agricultural and Food Chemistry*, *48*(5), 1663-1667.

Lang, Q. Y. and Wai, C. M. (2001). Supercritical fluid extraction in herbal and natural product studies - a practical review. *Talanta*, *53*(4), 771-782.

Latté, K. P. and Kolodziej, H. (2004). Antioxidant Properties of Phenolic Compounds from Pelargonium reniforme. *Journal of Agricultural and Food Chemistry, 52* (15), 4899-4902.

Le Bourvellec, C., Picot, M. and Renard, C. M. G. C. (2006). Size-exclusion chromatography of procyanidins: Comparison between apple and grape procyanidins and application to the characterization of fractions of high degrees of polymerization. *Analytica Chimica Acta*, *563*(1-2), 33-43.

Lopes, I. M. G. and Bernardo-Gil, M. G. (2005). Characterisation of acorn oils extracted by hexane and by supercritical carbon dioxide. *European Journal of Lipid Science and Technology*, *107*(1), 12-19.

Lucas, S., Alonso, E., Sanz, J. A. and Cocero, M. J. (2003). Safety study in a supercritical extraction plant. *Chemical Engineering & Technology*, *26*(4), 449-461.

Macheix, J. J., Fleuriet, A. and Billot, J. *Fruit Phenolics*. CRC Press, Boca Raton, FL, 1990.

Magalhães, A. L. (2008). Extracção de Óleo de Grainha de Uva com CO_2 Supercrítico. MSc. Thesis. Universidade de Aveiro, Aveiro.

Mansoori, G. A., Schulz, K. and Martinelli, E. E. (1988). Bioseparation using supercritical fluid extraction/retrograde condensation. *Biotechnology Advances*, *6*, 393-394.

Marrone, C., Poletto, M., Reverchon, E. and Stassi, A. (1998). Almond oil extraction by supercritical CO_2: experiments and modelling. *Chemical Engineering Science*, *53*(21), 3711-3718.

Martens, H. and Naes, T. *Multivariate Calibration*. Wiley, Chichester, England, 1994.

Mattusch, J., Cimpean, M. and Wennrich, R. (2006). Enzyme-assisted extraction of arsenic species from plant material. *International Journal of Environmental Analytical Chemistry*, *86*(9), 629-640.

Maxwell, R. J. *Supercritical Fluid Technology in Oil and Lipid Chemistry*, AOCS Press, Champaign, USA, 1996.

Meyer, A. S., Jepsen, S. M. and Sorensen, N. S. (1998). Enzymatically release of antioxidants for human low-density lipoprotein from grape pomace. *Journal of Agricultural and Food Chemistry*, *46*(7), 2439-2446.

Miller, J. N. and Miller, J. C. *Statistics and Chemometrics for Analytical Chemistry*, Person Education Ld, London, England, 2000.

Modey, W. K., Mulholland, D. A. and Raynor, M. W. (1996). Analytical supercritical fluid extraction of natural products. *Phytochemical Analysis*, *7*(1), 1-15.

Monagas, M., Gomez-Cordoves, C., Bartolome, B., Laureano, O. and Ricardo-Da-Silva, J. M. (2003). Monomeric, oligomeric, and polymeric flavan-3-ol composition of wines and grapes from *Vitis vinifera* L. cv. Graciano, Tempranillo, and Cabernet Sauvignon. *Journal of Agricultural and Food Chemistry*, *51*(22), 6475-6481.

Morin, O. (1996). Corn and grapeseed oil. *Oil and fats manual* 143-146, Hampshire.

Moyler, D. A. Extraction of flavours and fragrances with compressed CO_2. In *Extraction of Natural Products usinf Near-critical Solvents.* Blackie Academic & Professional, Glasgow, England, 1993.

Naczk, M. and Shahidi, F. (2004). Extraction and analysis of phenolics in food. *Journal of Chromatography A*, *1054*(1-2), 95-111.

Nicoli, M. C., Anese, M., Parpinel, M. (1999). Influence of processing on the antioxidant properties of fruit and vegetables, *Trends in Food Science and Technology*, *10*(3), 94-100.

O'Brien, R. D. Fats and oils - Formulating and processing for applications. Technomic Publishing Company Inc., Lancaster, England, 1998.

Ong, A. S. H. and Goh, S. H. (2002). Palm oil: A healthful and cost-effective dietary component. *Food and Nutrition Bulletin*, *23*, 11-22.

Otterbach, A. and Wenclawiak, B. W. (1999). Ultrasonic/soxhlet/supercritical fluid extraction kinetics of pyrethrins from flowers and allethrin from paper strips. *Fresenius Journal of Analytical Chemistry*, *365*(5), 472-474.

Palma, M., Taylor, L. T., Varela, R. M., Cutler, S. J. and Cutler, H. G. (1999). Fractional extraction of compounds from grape seeds by supercritical fluid extraction and analysis for antimicrobial and agrochemical activities. *Journal of Agricultural and Food Chemistry*, *47*(12), 5044-5048.

Palmer, M. V. and Ting, S. S. T. (1995). Applications for supercritical fluid technology in food processing. *Food Chemistry*, *52*(4), 345-352.

Papamichail, I., Louli, V. and Magoulas, K. (2000). Supercritical fluid extraction of celery seed oil. *The Journal of Supercritical Fluids*, *18*(3), 213-226.

Passos, C. P., Cardoso, S. M., Domingues, M. R. M., Domingues, P., Silva, C. M. and Coimbra, M. A. (2007). Evidence for galloylated type-A procyanidins in grape seeds. *Food Chemistry, 105*(4), 1457-1467.

Passos, C. P., Cardoso, S. M., Barros, A. S., Silva, C. M. and Coimbra, M. A. (2009a). Application of FT-IR spectroscopy and O-PLS/PLS1 regression for estimation of flavan-3-ols average degree of polymerization. *Analytica Chimica Acta*, doi:10.1016/j.aca.2009.12.028.

Passos, C. P., Silva, R. M., Da Silva, F. A., Coimbra, M. A. and Silva, C. M. (2009b). Enhancement of the supercritical fluid extraction of grape seed oil by using enzymatically pre-treated seed. *The Journal of Supercritical Fluids*, *48*, 225-229.

Passos, C. P., Yilmaz, S., Silva, C. M. and Coimbra, M. A. (2009c). Enhancement of grape seed oil extraction using a cell wall degrading enzyme cocktail. *Food Chemistry, 115*, 48-53.

Passos C. P., Silva, R. M., Da Silva, F. A., Coimbra, M. A. And Silva, C. M. (2010). Supercritical fluid extraction of grape seed (*vitis vinifera* L.) oil. Effect of the operating conditions upon oil composition and antioxidant capacity. *Chemical Engineering Journal*, In proof.

Peng, Z. K., Hayasaka, Y., Iland, P. G., Sefton, M., Hoj, P. and Waters, E. J. (2001). Quantitative analysis of polymeric procyanidins (tannins) from grape (*Vitis vinifera*) seeds by reverse phase high performance liquid chromatography. *Journal of Agricultural and Food Chemistry*, *49*(1), 26-31.

Perrut, M., Clavier, J. Y., Poletto, M. and Reverchon, E. (1997). Mathematical modeling of sunflower seed extraction by supercritical CO_2. *Industrial & Engineering Chemistry Research*, *36*(2), 430-435.

Peschel, W., Sánchez-Rabaneda, F., Diekmann, W., Plescher, A., Gartzía, I., Jiménez, D., Lamuela-Raventós, R., Buxaderas, S. and Codina, C. (2006). An industrial approach in the search of natural antioxidants from vegetable and fruit wastes. *Food Chemistry, 97*(1), 137-150.

Pincemail, J., Deby, C., Drieu, K., Anton, R. and Goutier, R. Flavonoids in Biology & Medicine. In *Proceedings of the 3rd International Symposium on Flavonoids in Biology & Medicine,* 161-179, Singapore, 1989.

Poling, B. E., Prausnitz, J. M. and O'Connell, J. P. *The properties of Gases and Liquids*. 5th Ed., MacGraw-Hill, NY, USA, 2001.

Povh, N. P., Marques, M. O. M. and Meireles, M. A. A. (2001). Supercritical CO_2 extraction of essential oil and oleoresin from chamomile (*Chamomilla recutita* L. Rauschert). *The Journal of Supercritical Fluids*, *21*(3), 245-256.

Quirin, K. W. (1982). Solubility behavior of fatty oils in dense carbon-dioxide in the pressure range up to 2600 bar. *Fette Seifen Anstrichmittel*, *84*(12), 460-468.

Ramos-Tejada, M. M., Durán, J. D. G., Ontiveros-Ortega, A., Espinosa-Jimenez, M., Perea-Carpio, R. and Chibowski, E. (2002). Investigation of alumina/(+)-catechin system properties. Part I: a study of the system by FTIR-UV-Vis spectroscopy. *Colloids and Surfaces B: Biointerfaces*, *24*(3-4), 297-308.

Rastogi, N. K., Raghavarao, K., Balasubramaniam, V. M., Niranjan, K. and Knorr, D. (2007). Opportunities and challenges in high pressure processing of foods. *Critical Reviews in Food Science and Nutrition*, *47*(1), 69-112.

Reed, J. D., Krueger, C. G. and Vestling, M. M. (2005). MALDI-TOF mass spectrometry of oligomeric food polyphenols. *Phytochemistry*, *66*(18), 2248-2263.

Reid, R. C., Prausnitz, J. M. and Poling, B. E. *The Properties of Gases and Liquids.* 4th Ed., Chemical Engineering Series, McGraw-Hill, N.Y., USA, 1988.

Reis, A., Domingues, M. R. M., Domingues, P., Ferrer-Correia, A. J., and Coimbra, M. A. (2003). Positive and negative electrospray ionisation tandem mass spectrometry as a tool for structural characterisation of acid released oligosaccharides from olive pulp glucuronoxylans. *Carbohydrate Research*, *338* (14), 1497-1505.

Reis-Vasco, E. M. C., Coelho, J. A. P., Palavra, A. M. F., Marrone, C. and Reverchon, E. (2000). Mathematical modelling and simulation of pennyroyal essential oil supercritical extraction. *Chemical Engineering Science*, *55*(15), 2917-2922.

Reverchon, E., Daghero, J., Marrone, C., Mattea, M. and Poletto, M. (1999). Supercritical fractional extraction of fennel seed oil and essential oil: Experiments and mathematical modeling. *Industrial & Engineering Chemistry Research*, *38*(8), 3069-3075.

Reverchon, E. and De Marco, I. (2006). Supercritical fluid extraction and fractionation of natural matter. *The Journal of Supercritical Fluids*, *38*(2), 146-166.

Reverchon, E., Kaziunas, A. and Marrone, C. (2000). Supercritical CO_2 extraction of hiprose seed oil: experiments and mathematical modelling. *Chemical Engineering Science*, *55*(12), 2195-2201.

Reverchon, E. and Marrone, C. (2001). Modeling and simulation of the supercritical CO_2 extraction of vegetable oils. *Journal of Supercritical Fluids*, *19*(2), 161-175.

Rezaei, K., Temelli, F. and Jenab, E. (2007). Effects of pressure and temperature on enzymatic reactions in supercritical fluids. *Biotechnology Advances*, *25*(3), 272-280.

Rice, A. C. (1976). Solid-waste generation and by-product recovery potential from winery residues. *American Journal of Enology and Viticulture*, *27* (1), 21-26.

Roberts, K. (2001). How the cell wall acquired a cellular context. *Plant Physiology*, *125*(1), 127-130.

Robb, C. S., Geldart, S. E., Seelenbinder, J. A., Brown, P. R. (2002). Analysis of green tea constituents by HPLC-FTIR. *Journal of Liquid Chromatography & Related Technologies*, *25*(5), 787-801.

Rosenthal, A., Pyle, D. L. and Niranjan, K. (1996). Aqueous and enzymatic processes for edible oil extraction. *Enzyme and Microbial Technology*, *19*(6), 402-420.

Rozzi, N. L., Phippen, W., Simon, J. E. and Singh, R. K. (2002). Supercritical fluid extraction of essential oil components from lemon-scented botanicals. *Lebensmittel-Wissenschaft Und-Technologie-Food Science and Technology*, *35*(4), 319-324.

Rozzi, N. L. and Singh, R. K. (2002). Supercritical fluids and the food Industry. *Comprehensive Reviews in Food Science and Food Safety*, *1*(1), 33-44.

Ryan, D. and Robards, K. (1998). Phenolic compounds in olives. *Analyst*, *123*(5), 31R-44R.

Sanders, N. Food legislation and the scope for increased use of near-critical fluid extraction operations in the food, flavouring and pharmaceutical industries. In *Extraction of Natural Products using Near-critical Solvents.* Blackie Academic & Professional, Glasgow, England, 1993.

Saraiva, J., Vitorino, R., Nunes, C. and Coimbra, M. A. (2002). Effect of high pressure treatments on protease and beta-galactosidase activities of table olives. *High Pressure Research*, *22*(3-4), 669-672.

Sarkar, B. C., Pandey, S., Kumbhar, B. K. and Agrawal, Y. C. (2004). Aqueous oil extraction from enzyme pretreated sesame seed and process parameters optimization. *Journal of Food Science and Technology-Mysore*, *41*(6), 604-608.

Saucier, C., Mirabel, M., Daviaud, F., Longieras, A. and Glories, Y. (2001). Rapid fractionation of grape seed proanthocyanidins. *Journal of Agricultural and Food Chemistry*, *49*(12), 5732-5735.

Schiesser, W. E. *The Numerical Method of Lines*, Academic Press, USA, 1991.

Silva, C. M., Passos, C. P., Coimbra, M. A. and da Silva, F. A. (2009). Numerical Simulation of Supercritical Extraction Processes. *Chemical Product and Process Modeling*, *4*(4).

Silva, M. V. and Barbosa, D. (2003). Fluidos supercríticos - uma nova classe de solventes. *Ingenium*, *78*, 79-82.

Silva, R. A. M. (2008). Projecto, Instalação e Modelação de uma Unidade de Extracção Supercrítica. MSc. Thesis. Universidade de Aveiro, Aveiro.

Sineiro, J., Dominguez, H., Nunez, M. J. and Lema, J. M. (1998a). Microstructural features of enzymatically treated oilseeds. *Journal of the Science of Food and Agriculture*, *78*(4), 491-497.

Sineiro, J., Dominguez, H., Nunez, M. J. and Lema, J. M. (1998b). Optimization of the enzymatic treatment during aqueous oil extraction from sunflower seeds. *Food Chemistry*, *61*(4), 467-474.

Soto, C., Chamy, R. and Zuniga, M. E. (2007). Enzymatic hydrolysis and pressing conditions effect on borage oil extraction by cold pressing. *Food Chemistry*, *102*(3), 834-840.

Sovová, H. (1994). Rate of the vegetable oil extraction with supercritical Co_2 .1. Modeling of extraction curves. *Chemical Engineering Science*, *49*(3), 409-414.

Sovová, H. (2005). Mathematical model for supercritical fluid extraction of natural products and extraction curve evaluation. *The Journal of Supercritical Fluids*, *33*(1), 35-52.

Sovová, H., Kucera, J. and Jez, J. (1994). Rate of the vegetable oil extraction with supercritical Co_2 .2. Extraction of grape oil. *Chemical Engineering Science*, *49*(3), 415-420.

Sovová, H., Sajfrtova, M., Bartlova, M. and Opletal, L. (2004). Near-critical extraction of pigments and oleoresin from stinging nettle leaves. *Journal of Supercritical Fluids*, *30*(2), 213-224.

Sovová, H., Zarevucka, M., Vacek, M. and Stransky, K. (2001). Solubility of two vegetable oils in supercritical CO_2. *Journal of Supercritical Fluids*, *20*(1), 15-28.

Subra, P., Castellani, S., Jestin, P. and Aoufi, A. (1998). Extraction of β-carotene with supercritical fluids: Experiments and modelling. *The Journal of Supercritical Fluids*, *12*(3), 261-269.

Talcott, S. T., Howard, L. R. and Brenes, C. H. (2000). Antioxidant changes and sensory properties of carrot puree processed with and without periderm tissue. *Journal of Agricultural and Food Chemistry*, *48*(4), 1315-1321.

Tan, C. S., Liang, S. K. and Liou, D. C. (1988). Fluid solid mass-transfer in a supercritical fluid extractor. *Chemical Engineering Journal and the Biochemical Engineering Journal*, *38*(1), 17-22.

Trygg, J. and Wold, S. (2002). *Journal of Chemometrics*, *16*(3) 119-128.

Tucker, G. A. Fundamentals of enzyme activity. In *Enzymes in Food Processing*, 2nd Ed., Blackie Academic & Professional, London, England, 1995.

Tzen, J. T. C., Cao, Y. Z., Laurent, P., Ratnayake, C., Huang, A. H. C. (1993). Lipids, Proteins, and Structure of Seed Oil Bodies from Diverse Species. *Plant Physiology*, *101*(1) 267-276.

Vasco, P., Gama, F.M., Coimbra, M.A. (2003). Caracterização dos polissacarídeos das paredes celulares da grainha de uva com vista à valorização do óleo por aplicação de enzimas exógenas. *Novas Perspectivas sobre Conservação, Processamento e Qualidade de*

Alimentos. Actas do 6º Encontro de Química dos Alimentos - Volume II. Sociedade Portuguesa de Química, Lisboa.

Vivas, N., Nonier, M. F., de Gaulejac, N. V., Absalon, C., Bertrand, A. and Mirabel, M. (2004). Differentiation of proanthocyanidin tannins from seeds, skins and stems of grapes (*Vitis vinifera*) and heartwood of quebracho (*Schinopsis balansae*) by matrix-assisted laser desorption/ionization time-of-flight mass spectrometry and thioacidolysis/liquid chromatography/electrospray ionization mass spectrometry. *Analytica Chimica Acta*, *513*(1), 247-256.

Wakao, N. and Kaguei, S. *Heat and Mass transfer in Packed Beds*, Gordon and Breach, NY, USA, 1982.

Wheeler, J. R. and McNally, M. E. (1989). supercritical fluid extraction and chromatography of representative agricultural products with capillary and microbore columns. *Journal of Chromatographic Science*, *27*(9), 534-539.

Whitaker, J. R., Voragen, A. G. J. and Wong, D. W. S. *Handbook of Food Enzymology*, Marcel Dekker Inc., NY, USA, 2003.

Wold, S., Martens, H. and Wold, H. The multivariate calibration problem in the chemistry solved by the PLS method. In *Proceedings of the Conference Matrix Pencils*, 286-293, Springer Verlag, 1983.

Wold, S., Sjostrom, M. and Eriksson, L. (2001a). PLS-regression: a basic tool of chemometrics. *Chemometrics and Intelligent Laboratory Systems*, *58*(2), 109-130.

Wold, S., Trygg, J., Berglund, A. and Antti, H. (2001b). Some recent developments in PLS modeling. *Chemometrics and Intelligent Laboratory Systems*, *58*(2), 131-150.

Yang, Y. and Chien, M. J. (2000). Characterization of grape procyanidins using high-performance liquid chromatography/mass spectrometry and matrix-assisted laser desorption/ionization time-of-flight mass spectrometry. *Journal of Agricultural and Food Chemistry*, *48*(9), 3990-3996.

Xu, Q. S. and Liang, Y. Z. (2001). Monte Carlo cross validation. *Chemometrics and Intelligent Laboratory Systems*, *56*(1), 1-11.

8. Appendix

When you cease to make a contribution, you begin to die.
[Eleanor Roosevelt]

Appendix A1 – Supercritical CO_2 related properties

Solubility, y_s

Chrastil (1982) established a linear log-log relationship between solute solubility and density of SC CO_2. Later, two empirical modifications have been introduced to improve its fitting capabilities, giving rise to the equations of Adachi and Lu (1983), and del Valle and Aguilera (1988). This last equation has been extensively used to correlate solubility data of vegetable oils in SC-CO_2 for pressures between 152-892 bar, temperatures between 293.15-353.15 K, and oil solubility below 100 kg.m^{-3}:

$$\ln y_s = 40.361 - \frac{18708}{T} + \frac{2186840}{T^2} + 10.7241 \ln \rho_{CO_2} \quad \textbf{[A1.1]}$$

Density, ρ

The carbon dioxide density was estimated as function of temperature and pressure by Bender's equation of state, whose parameters a_1 to a_{20} are listed in **Table A.1**:

$$P = T\rho\left[R + B\rho + C\rho^2 + D\rho^3 + E\rho^4 + F\rho^5 + \left(G + H\rho^2\right)\rho^2 \exp\left(-a_{20}\rho^2\right)\right] \quad \textbf{[A1.2]}$$

with:

$B = a_1 - a_2/T - a_3/T^2 - a_4/T^3 - a_5/T^4$; $C = a_6 + a_7/T - a_8/T^2$; $D = a_9 + a_{10}/T$;

$E = a_{11} + a_{12}/T$; $F = a_{13}/T$; $G = a_{14}/T^3 + a_{15}/T^4 + a_{16}/T^5$; $H = a_{17}/T^3 + a_{18}/T^4 + a_{19}/T^5$.

Table A1.1 – Coefficients of the Bender's equation of state for CO_2 (Brunner, 1994).

$a_1 = 0.22488558$	$a_8 = 0.40602371 \times 10^5$	$a_{15} = 0.19490511 \times 10^{11}$
$a_2 = 0.13717965 \times 10^3$	$a_9 = 0.40029509$	$a_{16} = -0.29186718 \times 10^{13}$
$a_3 = 0.14430214 \times 10^5$	$a_{10} = -0.39436077 \times 10^3$	$a_{17} = 0.24358627 \times 10^8$
$a_4 = 0.29630491 \times 10^7$	$a_{11} = 0.12115286$	$a_{18} = -0.37546530 \times 10^{11}$
$a_5 = 0.20606039 \times 10^9$	$a_{12} = 0.10783386 \times 10^3$	$a_{19} = 0.11898141 \times 10^{14}$
$a_6 = 0.45554393 \times 10^{-1}$	$a_{13} = 0.43962336 \times 10^2$	$a_{20} = 0.50000000 \times 10^1$
$a_7 = 0.77042840 \times 10^2$	$a_{14} = -0.36505545 \times 10^8$	

Binary diffusivity, D_{12}

The binary diffusion coefficient of the oil in supercritical carbon dioxide was estimated by correlation due to Catchpole and King (1994):

$$D_{12} = 5.152 D_{c_1} T_{r_1} \left(\rho_{r_1}^{-2/3} - 0.4510 \right) R \Big/ X \text{ , where } 1 < \rho_{r_1} < 2.5 \qquad \textbf{[A1.3]}$$

$$X = \left(1 + \left(V_{c2} / V_{c1} \right)^{1/3} \right)^2 \Big/ \left(1 + M_1 / M_2 \right) \qquad \textbf{[A1.4]}$$

where indexes 1 and 2 stand for solvent and solute, respectively. All data necessary for the calculations are listed in **Table A1.2.** For $2 < X$, $R = 1$; whereas if $2 < X < 10$, $R = X^{0.17}$. It is worth noting the solute (seed oil) is assumed to behave as a pseudo-component, specifically glycerol trioleate, whose properties have been collected.

Table A1.2 – Molar masses and critical properties of glycerol trioleate and carbon dioxide.

T_c (K)	P_c (bar)	V_c ($cm^3 mol^{-1}$)	M ($gmol^{-1}$)	D_c ($m^2 s^{-1}$)	ρ_c (kgm^{-3})
Carbon dioxide (Reid *et al.*, 1988; Catchpole and King, 1994)					
304.1	73.8	93.9	44.01	4.94E-08	468.7
Glycerol trioleate (Catchpole and King, 1994)					
-	-	3200	885.4	-	-

Appendix A2 – Correlations for the convective mass transfer and axial dispersion coefficients

Axial dispersion, D_{ax}

The axial dispersion coefficient has been estimated by the relationship presented by Catchpole *et al.* (1996a):

$$\frac{1}{N_{Pe,d}} = \frac{0.018}{N_{Re}} + \frac{10}{1+\left(0.7/N_{Re}\right)} \quad \text{, valid for } d_p < 1.0 \text{ mm} \qquad \textbf{[A2.1]}$$

where $N_{Pe,d} = u \cdot d_p \cdot D_{ax}^{-1}$ is the Peclet number based on the particle diameter, d_p.

Convective mass transfer coefficient, k_f

The convective mass transfer coefficients, k_f, were estimated by well known correlations involving the Sherwood, Reynolds and Schmidt numbers:

$$N_{Sh} = \alpha N_{Re}^{\beta} N_{Sc}^{\gamma} \qquad \textbf{[A2.2]}$$

In **Table A2** the correlations published by Wakao and Kaguei (1982), King and Bott (1993), and Tan *et al.* (1988) are listed.

Table A2 – Correlations for convective mass transfer coefficient, k_f.

Correlation	N_{Re}	N_{Sc}	Reference
$\frac{N_{Sh}}{\sqrt[3]{N_{Sc}}} = \frac{2}{\sqrt[3]{N_{Sc}}} + 1.1 N_{Re}^{0.6}$	3-3000	0.5-10000	Wakao and Kaguei (1982)
$N_{Sh} = 0.38 N_{Re}^{0.83} N_{Sc}^{0.33}$	2-4	2-20	Tan *et al.* (1988)
$N_{Sh} = 0.82 N_{Re}^{0.6} N_{Sc}^{0.33}$	1-70	3-11	King and Bott (1993)

$N_{Sh} = k_f \cdot d_p \cdot D_{12}^{-1}$: Sherwood number; $N_{Re} = \rho \cdot u \cdot d_p \cdot \mu^{-1}$: Reynolds number; $N_{Sc} = \mu\left(\rho \cdot D_{12}\right)^{-1}$: Schmidt number.